THE HORIZONTAL VELOCITY FIELD IN SOUTHERN CALIFORNIA FROM A COMBINATION OF TERRESTRIAL AND SPACE-GEODETIC DATA

by

DANAN DONG

Submitted to the Department of Earth, Atmospheric and
Planetary Sciences in partial fulfillment of the
requirements for the degree of

DOCTOR OF PHILOSOPHY

at the

MASSACHUSETTS INSTITUTE OF TECHNOLOGY

September, 1993

Signature of author _____
Department of Earth, Atmospheric and Planetary Sciences
July 23, 1993

Certified by _____
Professor Bradford H. Hager
Thesis supervisor

Certified by _____
Associate Professor Thomas A. Herring
Thesis supervisor

Certified by _____
Principal Research Scientist Robert W. King
Thesis supervisor

Accepted by _____
Professor Thomas H. Jordan, Department Head

THE HORIZONTAL VELOCITY FIELD IN SOUTHERN CALIFORNIA FROM A COMBINATION OF TERRESTRIAL AND SPACE-GEODETIC DATA

by

DANAN DONG

Submitted to the Department of Earth, Atmospheric and
Planetary Sciences on June 24, 1993 in partial fulfillment of
the requirements for the Degree of Doctor of Philosophy

ABSTRACT

The rapid development of space-geodesy has given an impetus to research on regional deformation, as well as to advancement in the methodology of geodetic analysis. Taking advantage of the 3-D vector measurement and the high accuracy of space-geodetic surveying over a large area, we develop the methodology to realize the combination of space-geodetic and terrestrial survey data. Our methodology has several important advantages:

(1) We adopt as our mathematical framework four-dimensional integrated geodesy, which embodies the intrinsic relation between Earth's shape and its gravity field. All formulations are expressed in a geocentric frame. Hence this methodology is rigorous and easy to connect with space-geodetic data.

(2) The methodology can handle various types of geodetic data.

(3) Our methodology uses quasi-observations obtained from loosely constrained intermediate solutions from subsets of the data, to which we apply general constraints at the final step. Hence it is efficient and flexible.

(4) We do not assume a spatially uniform velocity gradient. Hence this method is easy to apply to large areas.

(5) With our method, all three elements of a time-dependent reference frame – site coordinates, velocities, and episodic displacements – are estimated simultaneously.

(6) We establish the criteria to check the compatibility of data entering the solution. The criteria consider the correlation between the solutions before and after combination.

The second objective of our research is to combine VLBI, GPS, and terrestrial survey data to obtain the horizontal velocity field in southern California. Using this combination, in the region of the Big Bend, we can trace the transition from compression in the Santa Barbara Channel and the Ventura Basin to simple shear near the San Andreas fault. During the transition, about 5 mm/yr of fault-normal velocity is absorbed in the off-shore area, and another 5 mm/yr within a wedge-shaped area of the Ventura basin. Our residual velocity field indicates that the current multi-dislocation model needs to be refined in its transition between the creeping zone and the locking zone in Parkfield area.

Our analysis also reveals several unsolved problems. First, there is some incompatibility between USGS trilateration data and part of the VLBI/GPS solution, mainly in the Salton Trough area. The physical reason is still unknown and should be further investigated. Second, the current VLBI/GPS solution is still weak in the southern part of our network and east of the San Andreas fault. Third, in the San Luis trilateration network, the data from observations performed in 1970's by the California Division of Mines and Geology are not compatible with the USGS data after 1980. Using both data sets, the observed fault-normal velocity in the Southern Coast Ranges between Parkfield and the coast is not significantly different from zero.

Finally, two important byproducts stem from our analysis:

(1) Updated coordinates for the trilateration sites.

(2) Estimates of coseismic site displacements from 7 earthquakes: Superstition Hills (11/24/87, M_S = 6.2, 6.6), Westmoreland (04/26/81, M_L = 5.7), Mexicali (10/14/79, M_L = 6.6) and Victoria (06/09/80, M_L = 6.2), Homestead Valley (03/15/79, M_L = 5.6), North Palm Springs (07/08/86, M_S = 6.0), Joshua Tree (04/22/92, M_S = 6.2), and Landers and Big Bear (06/28/92, M_S = 7.5, 6.6).

Thesis Committe

Bradford H. Hager, Cecil and Ida Green Professor of Earth Sciences, MIT
Thomas A. Herring, Associate Professor of Geophysics, MIT
Thomas H. Jordan, Robert B. Shrock Professor of Earth, Atmospheric, and Planetary Sciences, MIT
Robert W. King, Principal Research Scientist, MIT
Michael Lisowski, Geophysicist, U. S. Geological Survey

ACKNOWLEDGMENTS

When I got the admission notice from MIT five years ago, I could not believe it: "Is it real?" Now I can convince myself: "Yes, it is." Study should be an equal right of human beings. To get such equal rights, however, I had to struggle for more than twenty years.

When I was a freshman at Beijing University in 1964, I was internally labeled as a "white specialist" (in China, "white" was the synonym for capitalist, compared to "red"—the synonym for communist) and was expelled from the University without being allowed to ask why. During the following Pandemonium period, deprived of all rights as a human being, my only dream was to survive. Finally, after fifteen years exiled in a remote desert area, I returned to the University and restarted my study. In 1985, when thousands of Chinese students went abroad to study advanced science and technology, I expressed the same desire. The response from my agency, however, was surprisingly negative: "Everybody can pursue his Ph.D. degree, but you cannot. We need you to work here." This time it was not political persecution. I had to struggle for another three years, just for the equal right to study. Then Tom Jordan and Bob King, resisting all kinds of pressure from China, accepted me as their graduate student.

Tom Jordan and his graduate students have been like a big family. It was at one of Tom's parties that I learned the difference between the hotness of cactus wine and red peppers. I sincerely thank Tom for his continuous concern, and for bringing Brad Hager and Tom Herring to our Department.

Bob King and Yehuda Bock led me in climbing the mountain of GPS techniques and the GAMIT software. I am deeply grateful to Bob and Yehuda for their generous support and help. It was surprising that my volley of questions never irritated them. Bob taught me not only the science, but also the morals and ethics. Unfortunately, I have exhausted all my English vocabulary and cannot find an appropriate word to express my special thanks to Bob.

Brad Hager, Tom Herring, and Bob King guided me in accomplishing this thesis. Brad taught me the tectonics. When I opened a can of worms, his keen instinct saved me from going astray. Tom taught me the rigor of science. His comments always sharpened my mind and enlarged my horizon. I am grateful for their grants from the National Science Foundation (EAR-86-18513 and EAR-89-05560), National Aeronautics and Space Administration (NAS-5-538 and NAS-5-737), Air Force Office of Scientific Research (AFOSR-90-0339), National Oceanic and Atmospheric

Administration (NA90AA-D-AC481), and Southern California Earthquake Center, which supported my research.

As companions, Mark Murray, Kurt Feigl and I learned GPS and started GPS field survey together. Whenever they showed up, fun showed up, either in the office or in the field. I was deeply impressed by Mark's patience. Kurt's magic functions made my computer work much more efficiently.

Special thanks to Mike Lisowski, Zhengkang Shen, Mark Murray, Dave Jackson, Richard Snay, Michael Cline, Will Prescott, Duncan Agnew, and Rob Reilinger for their generous support. Without their data, my velocity field would be a runaway horse. I am greatly indebted to Mike Lisowski for his e-mail lessons on the EDM technique. While I was wrestling with the range busts, Mike sacrificed several days to help me to track down these ruffians.

Thanks to Burch Oral for his magic *sh* family of shell scripts, to Rick Bennett for his results unearthed from the Imperial Valley, to Bob Ge for his story about the rupture at Landers, and to Don Grant and Hadley Johnson, who sent me their theses to provide detailed information. The maps and the figures of the thesis were generated using the Generic Mapping Tools (GMT) software, generously made public domain by Paul Wessel and Walter Smith [*EOS, Trans. Amer. Geophys. Un., 72*, 441, 1991].

I thank all of my English teachers: Bob King, Kurt Feigl, Mark Murray, Tonie vanDam, Andrea Donnellan, and Steve Shapiro. Without their help, it would be very hard to understand what I am saying.

Thanks to my officemates Steve Shapiro and Lana Panasyuk. They bring harmony into our office life. Steve (and his extremely nice father) showed me American humor. Lana never forgot to say "Dobroy vecherom" (Good night). I thank all of my student peers including my volleyball teammates. It is they who make my life colorful and joyful.

Thanks to Ben Chao, Ming Fang, and Zhengkang Shen for long discussions on the broad scope of sciences. I also thank Dawei Zheng, my former advisor, for his overall concern, and Madam Ye for her understanding my desire to study.

I sincerely thank my mother Yihui Dong. She was sent to labor camp for several months, just for her pleading justice for me. I hope my work will reward her. Thanks to my sister and brothers: Jin Wang, Damu Wang, Daxin Wang, and Dazhou Wang. It was they who encouraged me against decadence during my hardest time.

My wife Daxin Wu deserves all of my praises. She sacrificed herself to support my study. She tolerated my 12-hour work per day and 7-day work per week for 5 years. Please accept my promise: I will never do it again.

CURRICULUM VITAE

EXPERIENCE

Research Assistant, MIT Dept. of Earth, Atmospheric and Planetary Sciences, 1988 - 1993

Visiting scientist, Ashtech Incorporated, summer 1992

Visiting Scientist, MIT Dept. of Earth, Atmospheric and Planetary Sciences, 1987 - 1988

Research Associate, Shanghai Observatory, 1984 - 1987

M. S., Shanghai Observatory, 1982-1984

B. S., Dept. of Geophysics, Beijing University, 1979 - 1982

Teacher of Mathematics in high school, 1973 - 1979

HONORS

The second Excellent Essays for the young, Shanghai, 1984

The fourth Science and Technique Award, Seismology Bureau of China, 1984

The second Science and Technique Award, Academia Sinica, 1989

PUBLICATIONS

B. F. Chao, D. N. Dong, and T. A. Herring, Libration of the Earth's rotation, *Geophys. Res. Lett.*, 18, 11, 2007-2010, 1991

T. A. Herring, D. Dong, and R. W. King, Sub-milliarcsecond determination of pole position using Global Positioning System data, *Geophys. Res. Lett.*, 18, 10, 1893-1896, 1991

T. A. Herring and D. Dong, Current and future accuracy of Earth orientation measurements, *Proceedings of the AGU Chapman Conference on Geodetic VLBI: Monitoring Global Change,* NOAA Technical Report NOS 137 NGS 49, 306-324, 1991

Danan Dong and Yehuda Bock, Global Positioning System Network Analysis with Phase Ambiguity Resolution applied to Crustal Deformation Studies in California, *J. Geophys. Res.*, 94, 3949-3966,1989

Lin Banghui, Dong Danan, Lin Jizeng, Hu Xiaoxing, A study on the inversion of rupture process using the compound model method, *Acta Seismologica Sinica*, 10, No.4, 337-351, 1988

Zheng Dawei, Dong Danan, Marple Algorithm of Autoregressive Spectrum Estimate and its Application to Analyzing Astrometrical Data, *Acta Astronomica Sinica,* 28, No.4, 364-373, 1987

Dong Danan, Measurement of the Quality Factor Q of the Chandler Wobble, *Acta Astronomica Sinica,* 27, No.1, 16-22, 1986

Zhao Ming, Dong Danan, Chen Youfen, A new research for the secular drift of the Earth's pole, *Acta Astronomica Sinica*, 27, No.4, 352-359, 1986

Zhao Ming, Dong Danan, Chen Youfen, On the 30-year Scale Libration of the Earth's Pole, *Annals of Shanghai Observatory Academia Sinica*, 1986

Zheng Dawei, Dong Danan, Realization of Narrow-band Filtering of the Polar Motion Data with Multi-stage Filter, *Acta Astronomica Sinica,* 27, No.4, 368-376, 1986

Zheng Dawei, Dong Danan, research on the fine structure in polar motion with multi stage filter, *Proceedings of the International Conference on Earth Rotation and the Terrestrial Reference Frame*, Columbus, Ohio, 55-63, 1985

Dong Danan, Zheng Dawei, End Effects of the Vondrak Filter, *Annals of ShanghaiObservatory Academia sinica,* 7, 13-25, 1985

Yang Zhigen, Dong Danan, Computation of Displacement of Station Position caused by Tides using Spherical Harmonic Method, *Annals of Shanghai Observatory Academia Sinica,* 7, 41-50, 1985

Dong Danan, Simulation Test and Discussion on Q estimation of the Chandler Wobble by Spectral Analyses, *Annals of Shanghai Observatory Academia Sinica*, 6, 50-62, 1984

Lin Banghui, Dong Danan, A study of orthogonal and oblique rupture process with application to the 1966 Xingtai earthquakes, *A Collection of Papers of International Symposium on Continental Seismisity and Earthquake Prediction,* 736-750, 1984

TABLE OF CONTENTS

APPENDICES

FIGURES

CHAPTER 1

INTRODUCTION

Temporal deformations of the Earth's crust are induced by various sources. Some, such as solid tides, axial rotation, polar motion, ocean loading, and rigid plate motion, are comparatively well-understood. The deformations caused by the other sources, such as ice loading, tectonically induced stresses, thermal convection, fault interactions, volcanic eruptions, magma intrusions and earthquakes, are not as well constrained. In actively deforming regions, mostly located at plate boundaries, crustal movement demonstrates more complicated patterns than simply rigid-plate motion. These regions serve as the windows through which we gain insight into how the crust responds to various tectonic forces. Although the crustal movements no longer obey simple rigid motion in these regions, the deformation appears to be constant, except for short intervals around catastrophic events, such as earthquakes. Hence, recovering the interseismic velocity field would characterize the main features of regional deformation. Another important application of a regional velocity field is that it establishes the base for a dynamic geodetic reference system, which provides a powerful tool for predicting position as a function of time, documenting historical motion, detecting abnormal temporal deformation, and monitoring disasters [*Snay and Holdahl,* 1991].

In recent years, there have been increasing efforts to recover the horizontal velocity field in California, using either terrestrial survey data [*Lisowski et al.,* 1991; *Snay et al.*,1987] or space-geodetic data [*Clark et al.*,1984; *Ward* , 1990]. Combining Global Positioning System (GPS) data from 1986-1992 with Very Long Baseline Interferometry (VLBI) data from 1984-1991, investigators from Scripps, Caltech, UCLA and MIT have derived the horizontal velocity field of central and southern California with a precision of better than 2 mm/yr [*Feigl et al.* 1993]. In this thesis I further combine VLBI and GPS results with terrestrial survey data for this region. The aims of this work are to take advantage of more of the geodetic information currently available, to derive a more homogeneous solution with better spatial resolution, and to develop a methodology of combining different geodetic data in a way that optimally extracts the information appropriate for modeling deformation.

Chapter 2 will focus on the methodology. Chapter 3 will demonstrate the derived velocity field and its geophysical implications. Appendices will describe the details in specified areas.

CHAPTER 2

METHODOLOGY

We adopt four-dimensional integrated geodesy as our mathematical framework. This approach is powerful because it recognizes that most geodetic observations are functions of both position and gravity. The Earth's external gravity field is sensitive to crustal deformation, especially to vertical deformation. A general mathematical model of deformation analysis should embody the intrinsic correlation between the Earth's shape and its gravitational potential. Our formalization is based on the work of *Hein* [1986] and *Collier et al.* [1988], with some modifications. Site coordinate adjustments, site velocities, as well as episodic site displacements are expressed explicitly as the estimated parameters.

We perform our analysis in three steps. First, we obtain loosely constrained estimates of geodetic parameters from space-geodetic or terrestrial observations. Second, we combine the individual loosely constrained estimates into a uniform solution. Third, we impose general constraints to get a more robust estimate. This methodology allows us to 1) perform simultaneous reduction with various types of geodetic data, 2) estimate velocity directly without the assumption of a spatially uniform velocity gradient, 3) process efficiently and flexibly through general constraints and reparameterizations, and 4) obtain simultaneously two important byproducts – updated terrestrial network coordinates from the original poorly defined coordinates and earthquake-induced coseismic site displacements. We have implemented our analysis scheme using three preexisting software packages and a new one to incorporate terrestrial observations. The VLBI group delay observations were analyzed using the CALC/SOLVK software developed at the Goddard Space Flight Center (GSFC) and the Harvard Smithsonian Center for Astrophysics (CfA) [*Ma et al.*, 1992; *Herring et al.*, 1990]. The GPS phase observations were analyzed using the GAMIT software [*King and Bock*, 1993]. The combination of VLBI and GPS estimates is accomplished using the GLOBK software developed at CfA and MIT [*Herring*, 1993]. A new software package, designated FONDA (FOward modeling Network Deformation Analysis), was developed to process terrestrial survey data and to combine terrestrial and VLBI/GPS results.

Brief review of the methods currently available

A new methodology usually develops in response to new measurement techniques. Frank's method [*Frank,* 1966] of calculating angular shear strain γ_1 and γ_2 was applied to repeated triangulation observations, assuming strain is uniform in space. This method requires homogeneous data and an identically repeated network configurations; it is now rarely used. When repeated triangulation data with different networks became available, *Prescott* [1976] extended Frank's method to estimate angular shear strain rate $\dot{\gamma}_1$ and $\dot{\gamma}_2$, assuming that the strain is uniform in both space and time. The extended Frank's method permits multiple observation epochs and no longer requires identical networks. But this method still cannot handle directly heterogeneous data. In the new era of coexisting multiple geodetic techniques, *Bibby* [1982] developed the simultaneous reduction method, which estimates the velocity gradient with the assumption that the gradient is constant over the area network occupied. The DYNAP program developed at NGS [*Drew and Snay,* 1987] is the most widely used implementation of the simultaneous reduction algorithm. The advantage of these methods is that the estimated parameters are uniquely determined. For noisy data, these methods provide spatially averaged results to enhance the signal-to-noise ratio. But it is still not possible to derive the velocity field directly. Even by integrating the velocity gradient from a site with a well-constrained velocity, we only get the spatially averaged velocity field. Therefore, all these methods are most suitable for a small area, where the assumption of a spatially uniform velocity gradient is valid. A large or tectonically complicated area must be divided into smaller districts, based on a priori knowledge, in order to apply these methods. *Snay et al.* [1987] recognized the limitation of this approach and suggested that future improvements should "adjust California to a single model" and replace current expressions for secular motion with individual station velocity parameters".

An alternative approach is to remove the assumption of a spatially uniform velocity gradient and to estimate station velocity directly. If only trilateration or triangulation data are used, the translation and rotation of the entire network cannot be resolved. Thus, external constraints are required to eliminate the rank deficiency of such terrestrial survey data. The "inner coordinate solution" [*Brunner,* 1979] represents the minimum-norm generalized inverse of a singular normal matrix, and assumes no prior model. The "outer coordinate solution" [*Prescott,* 1981] adds a network rotation that minimizes velocities along a specified direction; the "model coordinate solution" [*Segall and Mathews,* 1988] applies the velocity field derived

from a geophysical model to constrain the solution. Hence, both of these solutions usually match well the known local tectonic features. They are especially useful when we want to calibrate or quantify the model parameters. Nevertheless, in a large or tectonically complicated area, it is very difficult to specify a single dominant direction to apply outer coordinate constraints or to construct a model velocity field. As a result, these methods are still applied to small areas. Furthermore, the solution is not unique and depends strongly on the model adopted. It is also difficult to judge the model accuracy directly.

Space geodesy has now arrived in the geodetic arena and can estimate 3-dimensional positions with unprecedented accuracy. Space-geodetic observations still have their own rank deficiency. For example, a globally distributed GPS network solution cannot resolve the longitudinal rotation of the whole network. However, the ambiguity of space geodesy is on a continental or global scale. If accompanied by a global network, the space-geodetic solution can be considered unambiguous on a regional scale. Combining terrestrial survey data with space geodetic data makes it possible not only to derive an unambiguous velocity field, but also to link observations of separated terrestrial networks to get a uniform solution. Several studies [*Snay and Drew* 1989; *Grant* 1990] have shown that such a combinational technique is feasible. Building on the previous studies, our work attempts to develop a theoretically rigorous, practically efficient, and usefully flexible methodology for combining heterogeneous data sets.

General observation equations in a geocentric Cartesian frame

The observations from different techniques are conventionally expressed in one of several possible frames: geocentric Cartesian, ellipsoidal geodetic, or topocentric planimetric. Considering the potential of space geodesy, we adopt the geocentric Cartesian frame as the internal coordinate system in which to construct the observation equations. The transformation between the Cartesian and the geodetic or topocentric frames, used conveniently for terrestrial observations, is given in Appendix 1. The geodetic measurement $l(t)$ can be expressed as

$$l(t) = F\{\mathbf{X}(\mathbf{a},t),W(\mathbf{X}(\mathbf{a},t),\mathbf{b},t),\mathbf{h}(t)\} \qquad (1)$$

where

$\mathbf{X}(\mathbf{a},t)$ is the position vector, whose time-dependence is described by the parameters $\mathbf{a}$.

$W(\mathbf{X}(\mathbf{a},t),\mathbf{b},t)$ is the gravitational potential, which can be decomposed into a reference potential U and a time-dependent disturbing potential π. The parameters **b** describe the temporal variation of the disturbing potential.

h(t) are the auxiliary parameters, such as rotation, translation, and satellite orbits.

F denotes a non-linear functional which operates upon **X**, W, and **h** to produce the scalar value of l (t).

The linearized observation equation is

$$\delta l = A\left(\Delta \mathbf{X}_0 + \Delta \mathbf{u}(\mathbf{a}_0,t)\right) + B\left(\Delta U(\mathbf{X}_0) + \pi(\mathbf{X}_0,\mathbf{b}_0,t)\right) + P\Delta\mathbf{a} + Q\Delta\mathbf{b} + C\Delta\mathbf{h} + \varepsilon \qquad (2)$$

where

δ represents the residual of observed minus calculated, based on the a priori model,

$\Delta \mathbf{X}_0$ is the adjustment of a priori position,

$\Delta U(\mathbf{X}_0)$ is the correction to the reference potential at a priori position $\mathbf{X}_0$,

$\pi(\mathbf{X}_0,\mathbf{b}_0,t)$ is the disturbing potential defined by a priori parameters,

$\Delta \mathbf{u}(\mathbf{a}_0,t)$ is the correction of displacement with a priori model parameter $\mathbf{a}_0$,

$\Delta\mathbf{a}$, $\Delta\mathbf{b}$ are corrections of the a priori model parameters $\mathbf{a}_0$ and $\mathbf{b}_0$,

$\Delta\mathbf{h}$ is the correction of the a priori auxiliary parameter $\mathbf{h}_0$, and

ε is the noise term.

$$A = \frac{\partial F}{\partial \mathbf{X}} + \frac{\partial F}{\partial W}\frac{\partial U}{\partial \mathbf{X}} \qquad B = \frac{\partial F}{\partial W}$$

$$P = \frac{\partial F}{\partial \mathbf{X}}\frac{\partial \Delta \mathbf{X}}{\partial \mathbf{a}} + \frac{\partial F}{\partial W}\frac{\partial U}{\partial \mathbf{X}}\frac{\partial \Delta \mathbf{X}}{\partial \mathbf{a}} \qquad Q = \frac{\partial F}{\partial W}\frac{\partial \pi}{\partial \mathbf{b}} \qquad (3)$$

$$C = \frac{\partial F}{\partial \mathbf{h}}$$

In the absence of an episodic event, we usually assume that crustal movement is uniform in time to the first order, so that **a** is simply the site velocity **V**. Site acceleration and high-order time-derivative terms are neglected. Additional parameters can be added when significant time-dependent signals are detected in the residuals. Time-dependent disturbing potentials π are not needed to estimate a horizontal velocity field. Thus the potential terms are used only to correct the raw observations. Readers interested in using 4-dimensional integrated geodesy to estimate potential parameters together with other parameters simultaneously are referred to *Milbert and Dewhurst* [1992]. Based on these simplifications, (2) becomes

$$\delta l = A\left(\Delta \mathbf{X}_0 + (t - t_0)\,\Delta \mathbf{V}\right) + B\,\Delta U(\mathbf{X}_0) + P\,\Delta \mathbf{V} + C\,\Delta \mathbf{h}_0 + \varepsilon \qquad (4)$$

Appendix 2 lists the linearized observation equations for various measurements.

Quasi-observation approach

Before introducing the trilogy of our analysis, we address the importance of using quasi-observations, employed by both GLOBK and FONDA. There are two approaches to estimating $\Delta\mathbf{X}_0$ and $\Delta\mathbf{V}$: i) estimate the position and velocity directly from the raw observations; ii) estimate intermediate solutions from the raw observations and use these intermediate solutions as quasi-observations to estimate $\Delta\mathbf{X}_0$ and $\Delta\mathbf{V}$. The final estimates of the parameters from the two approaches are equivalent (see Appendix 3). In data combination, the quasi-observation approach is more efficient and flexible. Here the term "combination" represents not only the combination of data from different techniques, but also the combination of measurements from different sessions using the same technique.

Computation time and memory space savings are the primary advantages of the quasi-observation approach. For example, data from a single GPS observation session consist typically of phase measurements of 6 satellites from 20 stations at 1000 epochs. The files required to store the residuals and the partial derivatives with respect to site coordinates and satellite parameters occupy about 20 Mb of storage. In the quasi-observation approach, we need to keep only the estimated station coordinates, satellite orbits, and their covariance matrix, easily stored in about 0.5 Mb. Computation time for the combination is typically reduced by about two orders of magnitude.

If we use the GLOBK output as quasi-observations to combine with the terrestrial survey data, only the parameters related to the sites in southern California and their covariance matrix are necessary. The parameters of the satellite orbits, VLBI radio-source positions, Earth rotation parameters, and the parameters relating to sites outside southern California need not be used directly to obtain a rigorous combination solution (see Appendix 3). This advantage of the quasi-observation approach cannot be easily realized by processing the raw data directly.

When the a priori coordinates for trilateration sites are poorly determined, we can compress the data into baseline length rates and baseline lengths at weighted mid epochs, at which the nominal baseline lengths and baseline length rates are uncorrelated. Then using only the resultant baseline length rates as quasi-observations, we can obtain reliable site velocity estimates. Such an approach is

insensitive to the poorly determined a priori coordinates and hence has been widely used to derive the velocity estimates in previous studies [*Lisowski et al.* 1991].

Estimation procedures

First step: the loosely constrained solutions

For each daily observation, we use GAMIT to analyze GPS phase data to obtain loosely constrained estimates of site coordinates and satellite orbits. Similarly, we use CALC/SOLVK to analyze the VLBI group delay data to obtain loosely constrained estimates of site coordinates and source positions. GLOBK treats these solutions as quasi-observations to obtain a homogeneous estimate of site coordinates at a reference epoch, site velocities, multi-session satellite orbits, and earth rotation parameters.

Using loose constraints is necessary to obtain a homogeneous solution in the combination. Directly using tightly constrained single-session solutions degrades the long-term repeatability, due mostly to the inconsistency of fiducial stations and insufficient orbital modeling [*Murray, 1991*; *Larson and Agnew,* 1991]. Loose constraints are necessary to prevent the normal matrix from becoming singular. On the other hand, these constraints should be loose enough that they do not bias the parameter estimates derived in later steps of the analysis. Our philosophy is to keep the loose constraints during most of the analysis, and to impose tight constraints at the final stage. Such an approach maintains a uniform frame and minimizes the effects from overconstraining [*Feigl et al,* 1993].

Second step: combining the data under a uniform reference frame

Suppose the observation equations for two subsets of the data are

$$\delta l_1 = A_1\,\delta \mathbf{X} + \varepsilon_1, \quad \text{with covariance matrix } C_1 \tag{5}$$

$$\delta l_2 = A_2\,\delta \mathbf{X} + \varepsilon_2, \quad \text{with covariance matrix } C_2 \tag{6}$$

Here **X** represents all parameters, not just the position adjustments. We assume that the observations in the two subsets are uncorrelated, and all observation uncertainties are purely Gaussian. Then the least squares solution of the combined system is given by

$$\delta\hat{\mathbf{X}}_{1+2} = C_{1+2}\left(A_1^T C_1^{-1}\,\delta l_1 + A_2^T C_2^{-1}\,\delta l_2\right) \tag{7}$$

where

$$C_{1+2} = \left(A_1^T C_1^{-1} A_1 + A_2^T C_2^{-1} A_2 + C_X\right)^{-1} \tag{8}$$

is the covariance matrix of the combined solution $\hat{\mathbf{X}}_{1+2}$ and C_X is the covariance matrix of the a priori values of the parameters **X**. The misfit is measured by "the weighted sum of squared residuals" (χ^2)

$$\chi^2_{1+2} = (\delta l_1 - A_1 \delta\hat{\mathbf{X}}_{1+2})^T C_1^{-1}(\delta l_1 - A_1 \delta\hat{\mathbf{X}}_{1+2}) + (\delta l_2 - A_2 \delta\hat{\mathbf{X}}_{1+2})^T C_2^{-1}(\delta l_2 - A_2 \delta\hat{\mathbf{X}}_{1+2}) \quad (9)$$

The above model is usually referred to as a Gauss-Markov model. In Appendix 4, we compare this formulation with the "model coordinate" approach.

In general, the reference frames implied by different techniques do not coincide. A uniform terrestrial reference frame is necessary for combining solutions. Since the original coordinates of terrestrial survey networks are very poor, we update the site coordinates of these networks to align them with the uniform frame (see Appendix 6).

In GLOBK, we solve only the rotation angles explicitly. For VLBI, which has almost no sensitivity to translation because of the nearly infinite distant quasar observation, the translation is constrained initially by the weak constraints. The translation of the frame can be specified later by fixing one site position and velocity or forcing the sum of the adjustments to the coordinates and velocities of several sites be zero. This latter procedure is used in GLOBK and is analogous to an inner coordinate solution. For GPS, there is no translational rank deficiency since the orbital dynamics is sensitive to the position and velocity of the Earth's center of mass, and no explicit translation is allowed. When the GPS network is not strong enough, we might adjust the velocity translation of the whole network at the final stage to stabilize the solution.

Third step: impose general constraints to obtain a robust solution

In the final step, we impose general constraints on the solution through conditional equations. Suppose that the original adjustments are $\mathbf{X}_L$ with covariance C_{XL} and misfit χ^2_L. The constraint observation equation is

$$l_c = A_c \mathbf{X} \quad \text{with covariance } C_c \quad (10)$$

Sequential least squares gives the updated solution:

$$\mathbf{X}_c = \mathbf{X}_L + C_{XL} A_c^T (C_c + A_c C_{XL} A_c^T)^{-1} \Delta l_c \quad (11)$$

$$C_{Xc} = C_{XL} - C_{XL} A_c^T (C_c + A_c C_{XL} A_c^T)^{-1} A_c C_{XL} \quad (12)$$

$$\chi^2_c = \chi^2_L + \Delta\mathbf{X}^T C_{XL}^{-1} \Delta\mathbf{X} + \Delta l_c^T C_c^{-1} \Delta l_c \quad (13)$$

where $\Delta l_c = l_c - A_c \mathbf{X}_L \quad (14)$

$$\Delta\mathbf{X} = \mathbf{X}_c - \mathbf{X}_L$$

There are several advantages in using a sequential least squares approach to impose the constraint. First, we can manipulate various constraints without reprocessing the original observation data. The savings in time and space are obvious. Second, the reasonableness of the constraints can be easily assessed by the increments of χ^2 from (13). Unrealistic constraints can be identified through abnormal χ^2 increments.

We have incorporated a variety of constraint equations in both GLOBK and FONDA. In order to provide flexibility in the analysis, most of these constraints are applied in a geodetic or topocentric frame. In the following equations, $\mathbf{x}(x,y,z)$ and $\mathbf{v}(u,v,w)$ denote the coordinate and velocity respectively.

1) Assign specified values to the coordinate adjustment or velocity for one or more sites:

$$\delta\mathbf{x}_i = \mathbf{x}_{spec}, \quad \delta\mathbf{v}_i = \mathbf{v}_{spec} \tag{15}$$

Although we have written the equations in the form of a vector, the constraint can be imposed separately for each component. The same will be true for other constraint equations. Specifying values to zero is equivalent to fixing the a priori coordinate or velocity for this site.

2) Tie the adjustments or total values of the coordinates or velocities:

$$\delta\mathbf{x}_i = \delta\mathbf{x}_j = \delta\mathbf{x}_k = ..., \quad \delta\mathbf{v}_i = \delta\mathbf{v}_j = \delta\mathbf{v}_k = ... \tag{16}$$

When the a priori coordinates of several sites have common errors, the coordinate tie may be used. The velocity tie is the most useful one. We can bind velocities of several closely located sites, for example a "main" mark and several "reference" marks, so that they move together, as if they were on the same rigid block. We can also bind the velocities at terrestrial survey sites to the velocities at the nearby GPS/VLBI sites, thereby resolving the translation and rotation of the whole network.

3) Assign the orientation of the velocity vector:

$$v_i+\delta v_i = k_v\left(u_i+\delta u_i\right) \tag{17}$$

where k_v is a specified constant.

4) Assign baseline or baseline-velocity orientation:

$$\begin{aligned}\left(y_j+\delta y_j\right) - \left(y_i+\delta y_i\right) &= k_x\left(\left(x_j+\delta x_j\right) - \left(x_i+\delta x_i\right)\right) \\ \left(v_j+\delta v_j\right) - \left(v_i+\delta v_i\right) &= k_v\left(\left(u_j+\delta u_j\right) - \left(u_i+\delta u_i\right)\right)\end{aligned} \tag{18}$$

where k_x, k_v are constants.

5) Freeze the baseline length:

$$\sum_{x,y,z}\left(dx_{ij} + \delta dx_{ij} + \left(dv_{ij}+ \delta dv_{ij}\right)(t - t_0)\right)^2 = \sum_{x,y,z}\left(dx_{ij} + dv_{ij}\,(t - t_0)\right)^2 \tag{19}$$

6) Fix the center of a sub-network or fix the motion of the sub-network center:

$$\sum_{i=1}^{k} \delta x_i = 0, \quad \sum_{i=1}^{k} (v_i + \delta v_i) = 0 \tag{20}$$

7) Fix horizontal or vertical rotation of a sub-network to zero:

$$\begin{aligned} &\sum_{i=1}^{k} (dx_i(v_i + \delta v_i) - dy_i(u_i + \delta u_i)) = 0 \\ &\sum_{i=1}^{k} (dy_i(w_i + \delta w_i) - dz_i(v_i + \delta v_i)) = 0 \\ &\sum_{i=1}^{k} (dz_i(u_i + \delta u_i) - dx_i(w_i + \delta w_i)) = 0 \end{aligned} \tag{21}$$

Here dx, dy, dz denote the distance from site i to the center of the sub-network. It should be noted that these constrained solutions of no-network-translation and no-network-rotation are different from the inner or outer coordinate solutions. In the inner coordinate solution, every parameter has the same weight, and the geometrical distance to the center is the dominant factor. A site with large uncertainty will affect the solutions and the covariance matrix of all other sites in the inner coordinate solution and hence should be eliminated in advance. In the constraints of (20) and (21), the parameter uncertainties affect the constrained solution, and the parameters with smaller uncertainties will be less changed. If the original solution is derived from only trilateration or triangulation data, the uncertainties depend on which site is chosen to be fixed.

8) Link velocity gradient:

Rotating the coordinate frame by a specified angle, in this frame

$$\frac{v_j + \delta v_j - v_i - \delta v_i}{x_j - x_i} = \frac{v_k + \delta v_k - v_i - \delta v_i}{x_k - x_i} \tag{22}$$

Formula (22) actually includes 4 independent constraints for horizontal velocities.

9) Inner, outer, and model coordinate constraints. The details of these constraints can be found in *Segall and Mathews* [1988].

Checking compatibility of the data sets

During the combination, compatibility checking is necessary to avoid misleading results due to systematic errors and blunders. Here our discussion focuses on the compatibility of velocity solutions.

For the same data but estimating additional parameters, the covariance matrix of the differences of the common parameters is given by Equation 15 of Appendix 3. *Davis et al.* [1985] have proved that for the same parameters with the addition of new data, the covariance matrix of differences of the parameter estimates has the relation:

$$C_{\tilde{x}-\hat{x}} = C_{\hat{x}} - C_{\tilde{x}} \qquad (23)$$

Here $\tilde{x}$ and $\hat{x}$ denote the estimated parameters with and without new data added respectively. The comparison between (23) and (3.15) shows that adding additional parameters enlarges the covariance of common parameters for the same data, whereas for the same parameters, adding new data reduces the estimated covariance. Equation (23) is often used to check the compatibility of new data with the original data or to test the sensitivity of parameter estimates to subsets of data.

In combining terrestrial survey data with space geodetic data, not only are new data added, but additional parameters are also added. In this extended case, we give the proof (see Appendix 5) that formula (23) is still valid provided that the new data are uncorrelated with the previous data. Our methodology uses (23) to check the compatibility between terrestrial survey data and space geodetic data. If the solution difference $\tilde{x}-\hat{x}$ exceeds the 95% confidence level, the terrestrial survey data are not compatible with the space geodetic data.

Terrestrial survey data have no sensitivity to the translation and rotation of the whole network. Hence the above compatibility test is unable to detect errors of network translation and rotation even though these errors exist in the space geodetic solution. If the common sites are concentrated in a small area of the terrestrial survey network, small errors of rotation in the space geodetic solution will be propagated and enlarged in the far sites of the terrestrial survey network. Therefore external compatibility checking based on prior geophysical information is also useful.

In the case of incompatible data, we have attempted to identify the sites with significant incompatibility and to avoid using them to impose constraints. If the first step does not improve the solution enough, we rescale the original covariance matrix to incorporate unknown systematic deviations.

Dealing with a large number of stations

The main shortcoming of our methodology is the computer resources necessary to store and use the large matrix required. Our methodology requires 6 parameters for each site plus episodic parameters and auxiliary parameters. In a typical solution for southern California involving 400 stations, this requires 30 megabytes of memory. For

our ambition of processing up to 10,000 sites, even a supercomputer is not large enough. A Helmert blocking approach [*Schwarz and Wade*, 1990] would reduce the size of space, allowing a large network to be handled with a sparse normal matrix. To perform Helmert blocking, all data should be arranged into multi-level blocks in advance. Each higher level block compresses the data from several lower level blocks. In combining the data from several lower blocks, this method implicitly estimates all the parameters, which then appear in only one block. The remaining common parameters are estimated explicitly and form the data at the higher level. Such a procedure is repeated until the last data set at the top of the block pyramid is used. Then this method backwards estimates explicitly all parameters of each block, which are previously solved implicitly. The Helmert blocking method is rigorous but requires complicated indexing and bookkeeping. We have not yet fully realized this method in our software since we have not yet experienced the pressure of processing a large number of sites.

Our philosophy is to realize the processing using a simpler method. We use the Helmert blocking approach to combine the VLBI/GPS quasi-observations with the USGS EDM trilateration data, which are the most accurate terrestrial surveys. Since that EDM data are observed in separated networks, we combine the VLBI/GPS solution with the trilateration data in each network sequentially. In each step, the parameters that are related to the EDM sites are estimated implicitly except at the sites collocated with VLBI/GPS sites. Thus, our block pyramid has only two levels. At the bottom level, the EDM data in each network form a block, and the VLBI/GPS quasi-observations are distributed in all blocks and are considered as common parameters. At the top level is the combined solution with only the parameters related to VLBI/GPS sites estimated explicitly. Thus we do not need additional indexing and bookkeeping. The shortcoming of this simplified Helmert blocking approach is that it does not work where the EDM network inclodes no VLBI/GPS sites.

We use the back solution approach described by*Herring*, [1983] to recover the parameters of the EDM network. At the last step the estimated parameters related to GPS/VLBI sites are $\hat{\mathbf{x}}_1$ and their covariance matrix is $C_{\hat{x}_1}$, derived from the normal equations:

$$\begin{pmatrix} N_{11}+C_{\tilde{x}_1}^{-1} & N_{12} \\ N_{21} & N_{22} \end{pmatrix}\begin{pmatrix} \hat{x}_1 \\ \hat{x}_2 \end{pmatrix}=\begin{pmatrix} B_1+C_{\tilde{x}_1}^{-1}\Delta\tilde{x}_1 \\ B_2 \end{pmatrix} \tag{24}$$

where

$\tilde{x}_1$ and $C_{\tilde{x}_1}$ denote the estimates and covariance matrix of x_1 from the previous step, used as quasi-observations, and

x_2 represent the parameters related to the sites of one EDM subnetwork.

The coefficients of the normal sub-matrices N_{11}, N_{12}, N_{21}, N_{22} and the right-hand terms B_1, B_2 are constructed from the data of the EDM subnetwork.

The back solutions are then

$$\hat{x}_2 = N_{22}^{-1} B_2 - E \hat{x}_1 \quad \text{and} \quad C_{\hat{x}_2} = N_{22}^{-1} + E C_{\hat{x}_1} E^T \tag{25}$$

where $E = N_{22}^{-1} N_{21}$.

Using formula (25) repeatedly, we can obtain the estimates and covariance matrices related to the sites of each EDM subnetwork.

For the less accurate triangulation data, our basic assumption is that these data cannot change the combined GPS/VLBI/EDM results significantly. Thus we can divide a whole region into several blocks. Within each block there are enough GPS/VLBI/EDM sites to control the movement of the whole block. We try only to obtain the velocities of triangulation sites relative to GPS/VLBI/EDM sites. As long as the velocities estimated from the entire GPS/VLBI/EDM network are self-consistant, the velocities at triangulation sites should be self-consistant also.

Conclusions

The developments of modern space geodesy have motivated the development of a rigorous and flexible methodology for combining terrestrial survey data with space geodetic data. The method presented in this chapter provides a useful tool for estimating the horizontal velocity field from a combination of terrestrial and space-geodetic survey data. Our methodology offers several important features: (1) The theoretical frame is rigorous and can easily incorporate leveling and gravity observations. (2) All three elements of a time-dependent reference frame – site coordinate, velocity, and episodic displacement – are estimated simultaneously. (3) Constraints can be applied in a general and flexible manner. (4) The compatibility criteria are relatively rigorous, taking into account the correlation between the solutions before and after combination.

Within a few years, space-geodetic data will be available for California and other regions with great spatial and temporal resolution. Given this rich data set, our methodology should be further developed to incorporate a large number of sites. How to handle time-dependent deformations in an optimal way will be an important extension of our current methodology. Although our current simplifications do not

inhibit our determination of a horizontal velocity field for southern California, the rapid development of space-geodesy will spur us to remove these simplifications in the near future.

REFERENCES

Bibby, H. M., Unbiased estimate of strain from triangulation data using the method of simultaneous reduction, *Tectonophysics*, 82, 161-174, 1982

Clark, M. M., K. K. Harms, J. J. Lienkaemper, D. S. Harwood, K. R. Lajoie, J. C. Matti, J. A. Perkins, M. J. Rymer, A. M. Sarna-Wojicki, R. V. Sharp, J. D. Sims, J. C. Tinsley III, and J. I. Ziony, Preliminary slip-rate table and map of late Quaternary faults of California, *U. S. Geol. Surv., Open file report* 84-106, 1984

Collier,P. A., B. Eissfeller, G. W. Hein and H. Landau, On a four-dimensional integrated geodesy, *Bull. Geod.*, 62, 71-91, 1988

Davis, J. L. et al., Geodesy by radio interferometry: effects of atmospheric modeling errors on estimates of baseline length, *Radio Sci.*, 20, 1593-1607, 1985

Drew, A. R. and R. A. Snay, DYNAP: software for estimating crustal deformation from geodetic data, *Tectonophysics*, 162, 331-343, 1989

Feigl, K. L., D. C. Agnew, Y. Bock, D. Dong, A. Donnellan, B. H. Hager, T. A. Herring, D. D. Jackson, T. H. Jordan, R. W. King, S. Larsen, K. M. Larson, M. Murray, Z. Shen, and F. H. Webb, Measurement of the velocity field of central and southern California, 1984-1992, *submitted to J. Geophys. Res.*, 1993

Frank, F. C., Deduction of earth strains from survey data, *Bull. Seismol. Soc. Am.*, 56, 35-42, 1966

Grant, D. B., Combination of terrestrial and GPS data for Earth deformation studies, Ph. D. Theses, *Unisurv report S-32*, 1990

Gu, G. H. and W. Prescott, Discussion on displacement analysis: detection of crustal deformation, *J. Geophys. Res.*, 91, 7439-7446, 1986

Hein, G. W., Integrated geodesy state-of-the-arc 1986 reference text, *Lecture Notes in Earth Sciences*, Vol. 7, 505-548, Edited by H. Sunkel, Springer-Verlag, 1986

Herring, T. A., Precision and accuracy of intercontinental distance determinations using radio interferometry, *Ph. D. Thesis*, Massachusetts Institute of Technology, 1983

Herring, T. A., J. L. Davis, and I. I. Shapiro, Geodesy by radio astronomy: the application of kalman filtering to very long baseline interferometry, *J. Geophys. Res.*, 95, 12561-12581, 1990

Herring, T. A., GLOBK: Global Kalman filter VLBI and GPS analysis program, unpublished documentation, MIT, 1993

King, R. W., and Y. Bock, Documentation for the MIT GPS analysis software: GAMIT, Massachusetts Institute of Technology, 1992

King, R. W., E. G. Masters, C. Rizos, A. Stolz, and J. Collins, Surveying with GPS, *Monogr. Ser.* , vol. 9, School of Surveying, University of New South Wales, New South Wales, Australia, 1985

Larson, K. M., and D. C. Agnew, Application of the Global Positioning System to crustal deformation measurement 1. precision and accuracy, *J. Geophys. Res.*, 96, 16547-16565, 1991

Lisowski, M., Recent Plate Motions and Crustal Deformation, *Reviews of Geophysics, supplement,* 162-171, 1991

Lisowski, M., J. C. Savage and W. H. Prescott, The velocity field along the San Andreas fault in central and Southern California, *J. Geophys. Res.*, 96, 8369-8389, 1991

Ma, C., J. W. Ruan, and D. S. Caprette, Crustal Dynamics Project Data Analysis-1991 VLBI geodetic results, *NASA Tech. Mem. 104552*, 1992

Milbert, D. G. and W. T. Dewhurst, The Yellowstone-Hebgen lake geoid obtained through the integrated geodesy approach, *J. Geophys. Res.*, 97, 545-558, 1992

Murray, M. H., Global Positioning System measurement of crustal deformation in Central California, Ph. D. Theses, *MIT*, 1991

Prescott, W. H., An extension of Frank's method for obtaining crustal shear strains from survey data, *Bull. Seismol. Soc. Am.*, 66, 1847-1853, 1976

Prescott, W. H., The determination of displacement field from geodetic data along a strike slip fault, *J. Geophys. Res.*, 86, 6067-6072, 1981

Savage, J. C. and W. H. Prescott, Precision of geodolite distance measurements for determining fault movements, *J. Geophys. Res.*, 78, 6001-6008 1973

Schwarz, C. R. and E. B. Wade, The North American Datum of 1983: project methodology and execution, *Bull. Geod.*, 64, 28-62, 1990

Segall, P. and M. V. Mattews, Displacement calculation from geodetic data and the testing of geophysical deformation models, *J. Geophys. Res.*, 93, 14954-14966, 1988

Snay, R. A. and Holdahl, S. R., The emergence of dynamical geodetic reference systems, *AGU Chapman Conference on Time Dependent Positioning: Modeling Crustal Deformation., Annapolis, Maryland*, 1-1, 1991

Snay, R. A. and A. R. Drew, Combining GPS and classical geodetic surveys for crustal deformation in the Imperial Valley, California, *High Precision Navigation -- Integration of Navigational and Geodetic Methods, Springer-Verlag, New York,* 225-236, 1989

Snay, R. A., M. W. Cline and E. L. Timmerman, Project REDEAM: Models for Historical Horizontal Deformation, *NOAA Technical Report NOS 125 NGS 42*, 1987

Ward, S. N., Pacific-North America plate motions: New results from very long baseline interferometry, *J. Geophys. Res.*, 95, 21965-21982, 1990

CHAPTER 3

RESULTS

Introduction

Southern California is located in the boundary zone between the North American and Pacific plates, where the crust shows more complicated behavior than simple rigid plate motion. Geological and geodetic evidence indicates that the slip rate of the San Andreas fault (SAF) accounts for less than three quarters of the velocity predicted by the NUVEL-1 model [*Demets et al.*, 1990]. The remaining motion, termed the "San Andreas discrepancy" [*Minster and Jordan,* 1984], is attributed to extension in the Basin and Range province and to the integrated rate of deformation in California [*Minster and Jordan,* 1987]. Quantifying the distribution of deformation in Southern California will provide important constraints on the geodynamical processes in this region. In Southern California, the main patterns of deformation are characterized by the horizontal velocity field, caused predominantly by strike-slip faults. Mapping this field directly from geodetic data has become feasible only in recent years [*Snay et al.*, 1987; *Lisowski et al.*, 1991; *Feigl et al.*, 1993].

Trilateration observations show that the deformation in a 100 km wide band near the main segments of the San Andreas fault is dominated by right-lateral shear, and can be modeled successfully by fault-slip motion on multiple dislocations [*Lisowski et al.*, 1991]. Recent results, however, based on a combination of VLBI and GPS (hereafter VG) data, find significant fault-normal velocities, which cannot be explained by a multi-fault dislocation model [*Feigl et al.*, 1993] (hereafter F93). Several questions arise: (1) Is the velocity field from terrestrial survey data compatible with the field derived from space geodetic data? (2) What is the distribution of the fault-normal velocity? (3) Can the deformation in the inland region of southern California absorb all of the San Andreas discrepancy? The trilateration networks have narrow apertures spanning short distances across the SAF, and hence cannot "see" the deformation far from the SAF. Most VG sites used by F93 are concentrated in the southern California borderland, with only a few sites across the SAF. Thus the current VG solution cannot "see" clearly the deformation transition from coastal areas to the SAF. The combination of terrestrial survey data with space geodetic data not only enhances the temporal and spatial coverage of the velocity

solution, but also provides the ability to preserve a homogeneous solution in a large area and to find the locations of the missing fault-normal velocity. Furthermore, the vector measurements of space-geodesy can resolve the rotation rate, to which terrestrial survey data are insensitive. The rotational tectonic features, such as block rotation [*Jackson and Molnar,* 1990], can therefore be determined directly.

Motivated by the benefits of combination, we attempt to derive the horizontal velocity field in southern California from both VG and terrestrial survey data, using the methodology developed in Chapter 2. Our results indicate that (1) deformation in the off-shore region contributes to the San Andreas fault discrepancy; (2) the fault-normal velocities are absorbed partly in the off-shore region, partly in the Ventura basin area, and partly east of the SAF; (3) some incompatibility between space-geodetic data and terrestrial survey data still exists. The causes of this incompatibility are not yet clear and can be resolved only with additional data.

Geodetic observations in southern California

Terrestrial survey data

The history of terrestrial survey data in southern California can be traced from 1850 [*Snay et al.*, 1987; *Hager et al.*, 1991]. Most nineteenth-century surveys were performed along the coast to support navigation. After 1930, survey networks were extended into the interior of California. Direction were the dominant measurements until the 1950's, when they were largely supplanted by electronic distance measurements (EDM). Regularly repeated length observations along the fault segments in California were performed by the California Department of Water Resources (CDWR) from 1959 to 1969, the California Division of Mines and Geology (CDMG) from 1969 to 1979, and the U. S. Geological Survey (USGS) since 1970. Nearly an order of magnitude improvement in accuracy was achieved in 1969 when the CDMG and USGS began using aircraft to measure the temperature and humidity along the line of sight, providing better calibration of atmospheric refractivity. Table 1 lists the accuracies of the terrestrial survey data.

Most of the trilateration data used in this chapter were obtained by the USGS between 1971 and 1991 (Table 1 and Figure 1). We also include data from USGS surveys in the Joshua network made just after the Joshua Tree earthquake (April 22,1992; M_s=6.1) and again after the Landers and Big Bear earthquakes (June 28, 1992; M_s=7.5; M_s=6.6). For the San Luis network, we added trilateration data surveyed by the California Division of Mines and Geology (CDMG) prior to 1979.

The earlier trilateration and triangulation measurements are also useful because of their long time span and dense spatial coverage. In order to reduce the computational burden, however, we have not yet included these data in our analysis. Among the 30 USGS trilateration networks in southern California, we have omitted from our analysis the Garlock, Coso, and Barstow networks because they are isolated from other networks and because there is no VG site within these three networks to provide control. We have also omitted the Mojave network because it was surveyed only once, in 1982. Finally, we have omitted 16 small-aperture networks, such as the Landers and Palmdale networks, since our current analysis is focused solely on broad-scale features of the velocity field. We group the remaining 10 networks into two separate sections. The northern section of 179 sites spans the SAF from Parkfield to Pearblossom and includes the San Luis, Carrizo, Los Padres, Tehachapi, San Gabriel networks, and most of the Monitor network. The southern section straddles the SA, San Jacinto and Elsinore faults from the southern end of the Big Bend to the Mexicali area, including total 144 sites of the Anza, Joshua, Salton, Mexicali networks, and a small part of Monitor network. Table 3 lists all of the trilateration sites used in this analysis.

VLBI/GPS data

In 1982, the first VLBI experiments were performed using both dual-frequency observations and the Mark III recording system. A regular program of observations at about 15 sites began in 1984. The first extensive GPS survey in southern California was made in 1986 [*Dixon et al.*, 1990]. During the first few years, the satellite constellation and the network of global tracking stations were limited. The permanent GPS Geodetic Array (PGGA) in southern California began operating in 1990 to continuously monitor the deformation and to provide a homogeneous reference series [*Bock & Leppard*, 1990]. The accuracies of the VG data in southern California are listed in Table 2. The location of the sites are shown in Figure 1.

Our VG data include VLBI experiments from 1984 to 1991, California GPS experiments from 1986 to 1992, and the global GPS experiments from 1991 to 1992. There are 94 VLBI sites and 147 GPS sites represented, with most of the California sites concentrated in the western Transverse Ranges and the southern California borderlands (Figure 1). East of the SAF, the distribution of sites is sparse. Only one site (FIBR_GPS) is in the Great Valley, three sites (MOJA, GOLDVENU, DEAD7267) are in the Mojave region, and one site (BLKB7269) is in the Salton Trough. Three VG sites share the same benchmarks as the USGS trilateration sites:

DEAD7267 with Sand Hill, SNP2_GPS with Santapau, and MPNS_GPS with Mt_pinos. All of the details concerning the data distribution, data analysis, and solution quality are described in F93. The software used for our analysis is described in Chapter 2. We take the VG solution and its covariance matrix as quasi-observations and make the following modifications:

1) We remove three subsets of sites: i) the sites outside of southern California because they are beyond the scope of our research; ii) the sites with fully correlated velocity solutions since they are redundant; and iii) the sites with poorly determined velocities because they cannot provide reliable constraints. In the end, 43 sites in southern California (including OVRO) enter our analysis (Table 4).

2) After conducting statistical tests and comparing different solutions, F93 concluded that the formal standard deviations should be doubled to reflect the realistic uncertainties in the solution. Therefore, we use the scaled covariance matrix, as did F93.

Analysis of the trilateration data

Choosing the observables

Previous analyses of the trilateration data have used baseline length rates as quasi-observables to derive the velocity field [*Lisowski et al.*, 1991]. The main advantage of this approach is that the baseline length rates are insensitive to site coordinates and contain most of the velocity information. But this approach discards two types of data: (1) baseline length with observations at only one epoch; and (2) compressed nominal baseline lengths at weighted mid epochs (See Appendix 5). These two types of data can provide meaningful velocity information, however, if the the site coordinates are well constrained. In Appendix 7, we give a quantitative assessment of the condition required for compressed nominal baseline lengths to make a significant contribution to the velocity solution. The length-observable approach utilizes all data, but requires external knowledge of the coordinates, e.g., from VG, when the original coordinates are poor. Although we were able to update the coordinates and to estimate the velocities simultaneously (Appendix 10), the few sites collocated by VG in our current data limit the accuracies of updated horizontal coordinates to the 1-3 meter level, which is not sufficient to provide a significant contribution to the velocity estimates.

Outer coordinate solutions for each trilateration subnetwork

Prioro to combining terrestrial and space-geodetic data, we divided the USGS trilateration data into 6 subnetworks (Table 5) and applied outer coordinate constraints [*Prescott*, 1981] to get the velocity field relative to the center of each subnetwork. The purpose of this analysis is threefold: (1) to scrutinize the local deformation pattern and its relation to local faults; (2) to compare the data quality of each subnetwork; (3) to diagnose outliers. The minimum-velocity directions for the outer coordinate solutions were chosen to be perpendicular to the local segment of the SAF. Based on our tests, the velocity solutions had no significant changes if the minimum-velocity direction changes were within ± 5°. We assessed the data quality of each subnetwork by the scatter in the length observations (Appendix 9). In order to avoid contamination from coseismic displacements, we estimated episodic displacement parameters for 7 recent earthquakes (Appendix 12). We have not, however, evaluated offsets due to errors in the eccentric ties at some of the sites [M. Lisowski, personal communication, 1993]. Our future research should examine the records of the local eccentric ties and correct the errors.

Our outer coordinate solutions of subnetworks are very similar to the results of *Lisowski et al.* [1991], so elaborating the solutions and their tectonic implications appears redundant. Figures 2 and 3 show the velocity fields and scatters corresponding to each subnetwork. We draw the following general conclusions:

(1) Simple shear is the dominant feature in all 6 subnetworks.

(2) No fault-normal velocities were found that are significantly different from zero. However, this conclusion should be further investigated for two reasons: i) Since the outer coordinate solution eliminates the translation and constrains the rotation of whole subnetwork, it is impossible to detect a common fault-normal velocity of an entire subnetwork. ii) For many sites far from the SAF the velocity uncertainties are large, so we cannot rule out the possibility that a fault-normal component of velocity exists at these sites.

(3) In the San Luis - Parkfield subnetwork, the USGS trilateration data from 1980 show different trends from the earlier CDMG data (Appendix 11). Thus the more recent data do not support *Harris and Segall* 's [1987] model of uniform fault-normal compression, which was based mostly on the CDMG data. Since neither the CDMG nor USGS data sets can be rejected, a conclusive statement awaits the analysis of recent GPS measurements in this region.

(4) Our scatter analysis indicates that the length measurements are not very homogeneous. The divergences from the scatter model curves are large. Using

Equation (9.1) in Appendix 9, we estimate the coefficients of the error model for the six subnetworks. Our estimated constant terms (3-6 mm) are larger than the term (3 mm) of *Savage and Prescott* [1973], while our estimated length-dependent terms are consistent with theirs (0.2 ppm). Recently, *Johnson* [1993] also rechecked the errors of the USGS trilateration data in the Anza, Joshua, and Salton networks, using a different approach. He reached the same conclusion as we did. Since the difference between our estimate and the estimate of *Savage and Prescott* is not too great and since most of the difference can be eliminated if we downweight a few apparent abnormal scatters with normalized rms larger than 1.0 (Figure 3), in this analysis we have adopted the error model of *Savage and Prescott* without modification.

Minimum-constraint solution

Two questions cannot be resolved by the outer coordinate solution: 1) What is the motion of the whole subnetwork? 2) Is there any inconsistency between the outer coordinate solutions of adjacent subnetworks? In a second analysis of the trilateration data alone, we attempted to obtain the velocity solution for the entire northern and southern sections using minimum constraints to control the rigid-body movement of a whole section. Our purpose is twofold: 1) to look at the relative movement between subnetworks, and 2) to explore the maximum capability of the current USGS trilateration data set to provide a homogeneous velocity solution. For a large network, there is usually no single dominant velocity direction for all sites. Hence the outer coordinate constraint is difficult to impose. In our analysis we fixed the velocity at one site and constrained one velocity orientation at another site. We chose sites to be close to the SAF since the near-fault sites most likely move parallel to the fault.

In the current USGS trilateration network, the connections between subnetworks are much weaker than the connections within subnetworks. In the southern section, the Anza-Joshua subnetwork and the Salton-Mexicali subnetwork are connected through only two sites, Mecca and Laquinta. The connections in the northern section are even weaker than those in the southern section. Two quadrilateral structures exist in the Los Padres - Tehachapi subnetwork. Further north, the Los Padres - Tehachapi subnetwork and the Carrizo subnetwork are connected by the nearly collinear sites Mckttrck, Crocker, and Caliente, making the Carrizo subnetwork very vulnerable to small rotational perturbations. The far northern San Luis - Parkfield subnetwork is connected to the southern part of the northern section only through site Simmler. In order to strengthen the connections between the northern networks, we added to the trilateration data the baseline rate vectors

between five sites (Black Hill, Almond, Red Hill, Gould, and FIBR) whose relative positions were measured in 1989 and 1992 by GPS (Z. Shen, Southern California Earthquake Center (SCEC), personal communication, 1993). For these GPS-derived baseline rates, we used uncertainties of about 7 mm/yr, over 10 times the uncertainties of the EDM baseline length rates in this region. Our constraints are listed in Table 6 and the solutions are plotted in Figure 4.

In order to examine the fine structures of the velocity field, which are hidden by the dominant feature of the simple shear, we remove a model velocity field, created from a multi-fault dislocation model [F93]. This model consists of the SAF, the San Jacinto fault, the Elsinore fault and the Garlock fault. The SAF is divided into seven segments The details of the model are described by F93. The residual velocity field is shown in Figure 5.

From the minimum constraint solution for the EDM data, we conclude the following:

(1) Simple shear is still the dominant pattern over both the northern and southern sections.

(2) The sizes of the error ellipses increase rapidly from the center to the edge of a section, due to the weak connections between subnetworks. At the edge sites, the error ellipses are so large that all information for these sites is obscured by the errors. Therefore the possibility of using trilateration data only to obtain a homogeneous solution for a large network is very limited.

(3) There is differential motion between subnetworks. The apparent west-east velocity divergence between the San Gabriel and the Los Padres subnetworks could be explained by the north-south compression in the Ventura basin region [*Donnellan et al.*, 1993].

Combination of the VG and EDM data

Besides the three VG sites that are collocated with EDM sites, there are six VG sites located less than 500 meters, and three VG sites located less than 2 km from nearby EDM sites. Assuming that the velocity varies little over a distance of 2 km, we can set the velocities at these EDM sites to match the velocities at the nearby VG sites. For an area with a strain rate of 10^{-7}/yr, such an assumption introduces 0.2 mm/yr error for each velocity component in a 2-km distance. With more GPS sites in Southern California being measured in recent years, we will eventually discard the velocity ties between sites more than 500 m apart. All of the constraints

that we tested in the combination are listed in Table 7, and the resultant velocity field using the velocity ties from the 12 VG sites is shown in Figure 6. In Figure 6, a common velocity is subtracted from all velocities. We find that after subtracting this common velocity from the F93 solution, the velocities of the VG sites in the northern section (except the VG sites in the Ventura basin and the off-shore islands) are almost parallel to the local SAF and close to a symmetric distribution across the SAF. Therefore Figure 6 can be considered as the velocity relative to the SAF.

This combined velocity solution fails to pass the compatibility criteria at the 95% confidence level (see Eqn. (23) of Chapter 2). We have tried to reduce the incompatibility by (1) identifying those velocity-constrained sites with the greatest apparent incompatibility and removing the velocity links from these sites, and (2) rescaling the covariance matrix of the VG solution and the EDM observation to account for the unmodeled systematic deviation. In the northern section, we remove the velocity links between JPLM_GPS and Jpl1_rm1 and between WHIT_GPS and Whitaker because the velocities at Jpl1_rm1 and WHIT_GPS are poorly determined and seem inconsistent with the velocities at nearby sites. The velocity link between SNP2_GPS and Santapau has also been removed because there are GPS observations for only three epochs, and the east velocity component of the combined solution at Santapau cannot pass our compatibility criterion.

In the southern section, there is a significant incompatibility between the velocities at VG sites NIGU_GPS, PINY_GPS and MONP7274. To single out which site is most responsible for the incompatibility, we tested three options: (1) Remove the constraint from the site NIGU_GPS (Figure 7a). The resultant apparent vortex (Figure 7a) is hard to interpret by the current dislocation model. (2) Remove the constraint from the site MONP7274 (Figure 7b). The resultant velocity field is similar to the EDM only solution (Figure 4). The velocity at the site DEAD7267 is changed by 0.6±2.7 mm/yr in west and 14.5±7.3 mm/yr in no[illegible] within the compatible range. (3) Remove the constraint from the site PINY_GPS (Figure 7c). The resultant relative velocity field is also similar to the EDM-only solution (Figure 4). The velocity at the site DEAD7267 is changed by 2.1±3.2 mm/yr in west and 6.6±7.2 mm/yr in north. It seems that option (3) gives the least change in the velocities of the VG sites in the southern section between the solutions before and after combination. However, both Figures 7b and 7c are the velocities relative to site Asbestos (close to PINY_GPS). If we use the common velocity (see Figure 6) as a reference, Figure 7b needs to have added about 1 mm/yr east velocity component to the velocity field of the whole southern section, and Figure 7c needs to have added

about 1 mm/yr west and 8 mm/yr south. This means that the velocity at MONP7274 is less in harmony with the velocities in the northern section than the velocity at PINY_GPS. For now, we choose to remove the velocity link between MONP7274 and Monu_res. How to judge the two cases (Figures 7b, 7c) is still an open question. Since removing these velocity links still does not help enough, we rescale the formal uncertainties of the VG solution by a factor of three instead of the factor of two suggested by F93 (see Table 8). The resultant velocity field and residuals are shown in Figures 8 and 9. It is clear that removing the velocity link at Monu_res leads to a poorly determined velocity field in the Salton-Mexicali subnetwork. Adding GPS data from the Salton Trough and Riverside County (STRC) surveys into the VG solution is critical to overcoming the poorly determined velocity field in Salton-Mexicali subnetwork, and to resolving the conflict of the velocity constraints at PINY_GPS and MONP7274.

Description of the derived velocity field

The most striking feature of the VG-derived velocity field is the fault-normal velocities. One could ask why such an obvious pattern has not been seen in the results obtained using USGS trilateration data? To answer this question, we must remove the dominant feature, i.e. a model velocity field describing the simple shear associated with the SAF system, from the observed velocity field. Where to put the reference point for the velocity residuals should also be considered. If the reference point is chosen in the stable interior of the North American plate, the velocity residuals will include contributions both east and west of the SAF. Since our data cover primarily the regions west of the SAF and the vicinity of the SAF, it is easier to discern the origins for the velocity residuals if we put the reference point at the stable interior of the Pacific plate. This approach requires us to transfer the observed velocity field from the North American frame to the Pacific frame using the NUVEL-1 model. Thus, using the Pacific frame introduces two error sources: the error from the multi-dislocation model and the error from the NUVEL-1 model. Nevertheless, we adopt the Pacific frame, as did F93, to analyze the residual velocity field.

Big Bend region

Viewed relative to the Pacific Plate (Figure 9a), the residuals at three off-shore island sites (TWIN, BLUF, and BRSH) are nearly zero. Thus we consider the movements at these three islands to be predominantly Pacific Plate motion. The

residuals at all coastal sites cannot be removed by simply modifying the parameters of the multi-dislocation model. Therefore, some deformation in the off-shore region must be incorporated to account for the velocity residuals at coastal sites. Modifying the parameters of the multi-dislocation model will change the fault-parallel velocities but will have little impact on the fault-normal velocities. Note that the velocity residuals at four coastal sites (PVER, CATO, SOLI, and LACU) are very similar (Figure 9a). Averaging the velocity residuals at these four sites and projecting this velocity vector onto the direction N17°E (perpendicular to the strike of the SAF in the Big Bend as given by *Eberhardt-Phillips et al.* [1990]), we obtain an estimate of 5±1 mm/yr for the fault-normal velocity, which is mostly attributed to the off-shore deformation. The faults most likely to contribute to the off-shore deformation are the Santa Cruz island fault in the Santa Barbara channel, and the Palos Verdes fault and the Newport-Inglewood fault near the coast from the Los Angeles basin to the border.

In order to better understand the residual velocities onshore, we replot the field relative to a site (MPNS) near the SAF at the northern end of the Big Bend (Figure 9b). For the western Transverse Ranges and Ventura basin region, we further zoom the velocity field and residual field relative to the site MPNS (Figure 10a, 10b). We find that the velocities at the sites near the SAF in the Big Bend area are basically parallel to the fault (Figure 10a). Thus we still use the average velocity at the four coastal sites (PVER, CATO, SOLI, and LACU) to estimate the rate of crustal shortening in the N17°E direction. The resultant rate of 5±1 mm/yr is very close to the estimate of *Donnellan et al.* [1993] for the shortening rate in the Ventura basin. But our estimate represents the crustal shortening rate from the coast to the SAF. Thus the area north of the Ventura basin makes nearly zero contribution to the crustal shortening (see Figure 10a). In the VG-alone solution, the velocity at MPNS is determined by observation at only two epochs and seems incongruous with the velocity at nearby site MUNS [*Donnellan et al.*,1993]. When we add the EDM data, the velocity at MPNS changes by 2.1 mm/yr in north with the uncertainty reduced by 1.5 mm/yr, and 0.6 mm/yr in the east with the uncertainty reduced by 1.7 mm/yr. The resultant velocity at MPNS appears more consistent with the velocities at other near-fault sites (Figure 10a). Also, nearly all of the velocity difference between MPNS and MUNS can be explained by the multi-dislocation model (Figure 10b). Figure 10a shows that the fault-normal velocities are confined to a wedge-shaped area, bounded to the northeast by the San Gabriel fault and to the northwest by the Santa Ynez fault.

West of the Ventura basin, the fault-normal velocities can be explained by the multi-dislocation model. In the Ventura basin itself, the significant fault-normal

residuals indicate that there must be other mechanisms to account for the crustal shortening [*Donnellan et al.*,1993]. The apparent east-west extension in the San Gabriel mountains and the region north of the Santa Ynez fault indicates that the vertical movement beneath the Ventura basin area does not absorb all of the extra material from the north-south compression. Hence the material in the San Gabriel mountains is pushed eastward, and the material in the region north of the Santa Ynez fault is pushed westward. A similar wedge-shaped region is the Los Angeles basin area, southeast of the Ventura basin area, which also undergoes north-south compression [*Shen*, 1991; *Davis et al.*, 1992]. Can we also see the east-west extension along both flanks of the wedge? We cannot answer this question without incorporating additional space-geodetic data and terrestrial survey data.

Southern Coast Ranges

In the Parkfield segment (north from 35°45'N), the cluster of large residuals indicates that our multi-dislocation model suffers from oversimplification (Figure 11). The current model uses a step-increase in locking depth from 1 km to 25 km at 35°58'N to approximate the transition from a locked to a creeping zone (see F93). In order to better represent the near-fault field deformation, a more realistic model, such as the "smooth transitional" model or "locked" model, should be used, as discussed by *Harris and Segall* [1987], *Sung and Jackson* [1988], *Segall and Harris* [1989], and *Sung and Jackson* [1989]. In the segment of the SAF from the northern end of the Big Bend to Parkfield, the residuals are basically fault-parallel. There is some indication that the locking depth may be shallower, as F93 inferred by comparing the velocity residuals at MADC and FIBR. At the current stage, we do not attempt to modify the multi-dislocation model for two reasons: 1) The residual uncertainties in the Parkfield region are too large. 2) As described in Appendix 11, the Parkfield dilemma has not yet resolved.

East of the SAF

Information about the deformation between the SAF and the East California Shear Zone (ECSZ) [*Travis and Dokka*, 1990; *Savage et al.*, 1990] is very limited. Comparing the velocity residual of MOJA with the velocity residuals of the sites east of SAF in the Big Bend area, the difference represents the accumulated deformation from east of the SAF to MOJA. Due to insufficient data coverage between east of SAF and ECSZ, we cannot discern if the deformation is uniformly distributed in this region or is concentrated in the ECSZ area.

Southern section

For the southern section, the VG data are insufficient to provide a useful constraint. The minimum constraint solution (Figure 4) shows that significant deformation occurs in a narrow corridor from the SAF to the San Jacinto fault, and probably extends to the Imperial fault. Such a "deformation corridor" is clearly seen in strain rate and rotation rate figures (Figure 12). *Larsen and Reilinger* [1992] also noticed a narrow deformation zone in the Imperial Valley. To explain the observed 1988-1989 GPS station displacements in the valley, they proposed a right-lateral shear plane at N40°W and a locking depth of 10 km across this area. *Lisowski et al.* [1991] interpreted the steep velocity gradient at the San Jacinto fault by a shallow locking depth of 5-6 km near Anza or by a broad fault zone with low rigidity. *Johnson* [1993] found the deformation corridor is dominated by the San Jacinto fault instead of the SAF. In this area, a series of parallel left-lateral faults trend northeast, nearly orthogonal to the main right-lateral faults [see Figure 1 of *Hudnut et al.*, 1989]. The seismicity time sequences indicate active interaction between the cross-faults and the main faults. Abnormal uplift in this area had been reported [*Reilinger*, 1985] but not resolved. In such a tectonically active area, a denser GPS network is likely to allow us to observe directly any block rotation.

Conclusions

We have taken advantage of the high accuracy of geodetic measurements over a large area and the spatial density of trilateration measurements to derive the horizontal velocity field for southern California. The strength of the combination for most of the region can be seen by comparing Figure 9b with the minimum constraint solution shown in Figure 5. The combination field allows us to explore the crustal deformation at the transition zone of the plate boundary from a wide-angle view. Our results can be described from three perspectives.

First, the combination solution reveals several important problems with the current data sets.

(1) The current VG site distribution cannot adequately constrain the trilateration data. Most sites which provide the velocity constraints are west of the SAF. Therefore our combined velocity solution is poorly constrained east of the SAF. The Joshua, Salton, Mexicali subnetworks in the southern section and the San Luis subnetwork in the northern section are also not well constrained.

(2) Our combination shows a significant conflict between the velocity solutions at PINY_GPS and MONP7274, both of which are very strong sites in the VG solution. There are also conflicts between the EDM and VG solution for some sites whose velocities are less reliably determined. These problems indicate that there are still some unsolved systematic differences between terrestrial and space-geodetic data, and between GPS and VLBI.

Second, in spite of the weakness in the current combination, we can still reach some useful conclusions about deformation in southern California.

(1) Through removing a model velocity field from a buried multi-dislocation [F93], we explore the distribution of the fault-normal velocities relative to the Big Bend segment of the SAF. We find that the narrow aperture of the EDM network may be the reason why the trilateration data cannot see the fault-normal velocity.

(2) Our current multi-dislocation model should be modified. In the Parkfield area, the step-function transition model should be replaced by the smooth transition model or more sophisticated model. In the southern end, the SAF probably changes its orientation and joins the Imperial fault along the Brawley seismic zone.

(3) In the San Luis subnetwork, The CDMG data from 1970 to 1979 are inconsistent with the USGS data from 1980 to 1990. The observed fault-normal velocity from the combined data set in this region is not significantly different from zero. Furthermore, the configuration of the San Luis subnetwork is weak for deriving a velocity solution (see Appendix 8). Hence inverting for fault slip parameters using the trilateration data in this region should be done with great caution.

Third, our approach also produces two important byproducts:

(1) Updated coordinates for the USGS trilateration sites (Table 2). The updated coordinates are not yet good enough to directly improve the velocity estimates, but they facilitate further research in combining the trilateration data and the space-geodetic data.

(2) Estimated coseismic site displacements (Appendix 12), which can be used to compare with the site displacements predicted by the seismic slip model.

Although the weakness of our current data set impedes us from deriving a strong horizontal velocity field in southern California, we are in a good position to realize such a dream for four reasons:

(1) We have developed a rigorous and flexible methodology to handle the combination.

(2) All software to perform the combination is ready and eager to work.

(3) We have acquired experience in combining terrestrial and space-geodetic data.

(4) Within a few years, data from a much denser network of GPS sites will be available (Figure 17).

REFERENCES:

Bock, Y. & Leppard, N. (eds), *Global Positioning System An Overview*, 40-56, Springer, New York, 40-56, 1990

Davis, J. L., W. E. Himwich, and W. H. Prescott, Space-geodetic determination of crustal deformation in the Los Angeles Basin, *Science*, submitted, 1992

Demets, C. R., R. G. Gordon, D. F. Argus, and S. Stein, Current plate motions, *Geophys. J. Intnl*, 101, 425-478, 1990

Dixon, T. H., G. Blewitt, K. Larson, D. Agnew, B. Hager, P. Kroker, L. Skrumeda, and W. Strange, GPS measurements of regional deformation in California: some constraints on performance, *Eos Trans. Amer. Geophys. Un.*, 71, 1051-1056, 1990

Dokka, R. K., and C. J. Travis, Role of Eastern California Shear Zone in accommodating Pacific-North America plate motion, *Geophys. Res. Lett.*, 17, 1323-1326, 1990

Donnellan, A., B. H. Hager, R. W. King, and T. A. Herring, Geodetic measurement of shortening across the Ventura basin, southern California, *submitted to J. Geophys. Res.*, 1993

Eberhardt-Phillips, D., M. Lisowski, and M. D. Zoback, Crustal strain near the Big Bend of the San Andreas fault: analysis of the Los Padres-Tehachapi trilateration networks, California, *J. Geophys. Res.*, 95, 1139-1153, 1990

Feigl, K. L., D. C. Agnew, Y. Bock, D. Dong, A. Donnellan, B. H. Hager, T. A. Herring, D. D. Jackson, T. H. Jordan, R. W. King, S. Larsen, K. M. Larson, M. Murray, Z. Shen, and F. H. Webb, Measurement of the velocity field of central and southern California, 1984-1992, *submitted to J. Geophys. Res.*, 1993

Hager, B. H., R. W. King, and M. H. Murray, Measurement of crustal deformation using the Global Positioning System, *Annu. Rev. Earth Planet. Sci.*, 19, 351-382, 1991

Harris, R. A. and P. Segall, Detection of a locked zone at depth on the Parkfield, California, segment of the San Andreas faul, *J. Geophys. Res.*, 92, 7945-7962, 1987

Herring, T. A., J. L. Davis, and I. I. Shapiro, Geodesy by radio astronomy: the application of kalman filtering to very long baseline interferometry, *J. Geophys. Res.*, 95, 12561-12581, 1990

Herring, T. A., GLOBK: Global Kalman filter VLBI and GPS analysis program, unpublished documentation, MIT, 1993

Hudnut, K. W., L. Seeber, and J. Pacheco, Cross-fault triggering in the November 1987 Superstition Hills earthquake sequence, southern California, *Geophys. Res. Lett.*, 16, 199-202, 1989

Hutton, L. K., and C. E. Johnson, Preliminary study of the Westmorland, California, earthquake swarm (abstract), *EOS Trans. AGU*, 62, 957, 1981

Jackson, J., and P. Molnar, Active faulting and block rotations in the western Transverse Ranges, California, *J. Geophys. Res.*, 95, 22073-22087, 1990

Johnson, H. O., Techniques and studies in crustal deformation, *Ph.D. Thesis*, Scripps Institution of Oceanography, University of California, San Diago, 1993

King, N. E., P. Segall, and W. Prescott, Geodetic Measurements near Parkfield, California, 1959-1984, *J. Geophys. Res.*, 92, 2747-2766, 1987

King, R. W., and Y. Bock, Documentation for the MIT GPS analysis software: GAMIT, Massachusetts Institute of Technology, 1992

Larsen, S., R. Reilinger, H. Neugebauer, and W. Strange, Global Positioning System Measurements of deformations associated with the 1987 Superstition Hills earthquake: evidence for conjugate faulting, *J. Geophys. Res.*, 97, 4885-4902, 1992

Larsen, S., and R. Reilinger, Global Positioning System Measurements of strain accumulation across the Imperial Valley, California: 1986-1989, *J. Geophys. Res.*, 97, 8865-8876, 1992

Larsen, S., D. C. Agnew, and B. H. Hager, Strain accumulation in the Santa Barbara channel: 1970-1988, *J. Geophys. Res.*, 98, 2119-2133, 1993

Li, V. C., and J. R. Rice, Crustal deformation in great California earthquake cycles, *J. G. R.*, 92, 11533-11551, 1987

Lisowski, M. and W. H. Prescott, Deformation near the epicenter of the 9 June 1980 M_L = 6.2 Victoria, Mexico, earthquake, Proceedings of the Fourth Symposium of the Cerro Prieto geothermal field, Baja California, Mexico, Guadalajora, Jalisco, Mexico, August 10-12, 1982

Lisowski, M., J. C. Savage and W. H. Prescott, The velocity field along the San Andreas fault in central and Southern California, *J. Geophys. Res.*, 96, 8369-8389, 1991

Minster, J. B., and T. H. Jordan, Vector constraints on quantenary deformation of the western United States east and west of the san Andreas fault, *Tectonics and Sedimentation along California Margin*, edited by J. K. Crouch and S. B. Bachman, *Pac. Sect. Soc. Econ. Paleontol. Mineral.*, 38, 1-16, 1984

Minster, J. B., and T. H. Jordan, Vector constraints on western U. S. deformation from space geodesy, neotectonics, and plate motions, *J. Geophys. Res.*, 92 4798-4804, 1987

Murray, M. H., J. C. Savage, M. Lisowski, and W. K. Gross, Coseismic displacements: 1992 Landers, California, earthquake, *Geophys. Res. Lett.*, 20, 623-626, 1993

Prescott, W. H., The determination of displacement field from geodetic data along a strike slip fault, *J. Geophys. Res.*, 86, 6067-6072, 1981

Reilinger, R., A strain anomaly near the southern end of the San Andreas fault, Imperial Valley, California, *Geophys. Res. Lett.*, 12, 561-564, 1985

Savage, J. C. and W. H. Prescott, Precision of geodolite distance measurements for determining fault movements, *J. Geophys. Res.*, 78, 6001-6008, 1973

Savage, J. C., W. H. Prescott and G. Gu, Strain accumulation in southern California, 1973-1984, *J. Geophys. Res.*, 91, 7455-7473, 1986

Savage, J. C., W. H. Prescott and M. Lisowski, Deformation along the San Andreas fault in 1982-1986 as indicated by frequent Geodolite measurements, *J. Geophys. Res.*, 92, 4785-4797, 1987

Savage, J. C., M. Lisowski, and W. H. Prescott , An apparent shear zone trending north-northwest across the Mojave desert into Owens Valley, eastern California, *Geophys. Res. Lett.*, 17, 2113-2116, 1990

Savage, J. C., M. Lisowski, and M. H. Murray, Deformation from 1973 through 1991 in the epicentral area of the 1992 Landers, California, earthquake (M_s = 7.5), *submitted to J. Geophys. Res.*, 1993

Schwarz, C. R. and E. B. Wade, The North American Datum of 1983: project methodology and execution, *Bull. Geod.*, 64, 28-62, 1990

Segall, P. and R. A. Harris, Comment on: 'Geodetic evidence for seismic potential at Parkfield, California' by L.-Y. Sung and D. D. Jackson, *Geophys. Res. Lett.*, 16, 101-104, 1989

Shen, Z. K, Regional tectonic deformation in southern California, inferred from terrestrial geodesy and the Global Positioning System, *Ph. D. thesis*, University of California, Los Angeles, 1991

Snay, R. A. and A. R. Drew, Combining GPS and classical geodetic surveys for crustal deformation in the Imperial Valley, California, *High Precision Navigation -- Integration of Navigational and Geodetic Methods, Springer-Verlag, New York*, 225-236, 1989

Snay, R. A., M. W. Cline and E. L. Timmerman, Project REDEAM: Models for Historical Horizontal Deformation, *NOAA Technical Report NOS 125 NGS 42*, 1987

Sung, L. Y., and D. D. Jackson, Geodetic evidence of the seismic potential at Parkfield, California, *Geophys. Res. Lett.*, 15, 820-823, 1988

Sung, L. Y., and D. D. Jackson, Reply, *Geophys. Res. Lett.*, 16, 105-107, 1989

Ward, S. N., Pacific-North America plate motions: New results from very long baseline interferometry, *J. Geophys. Res.*, 95, 21965-21982, 1990

Weldon, R., and E. Humphreys, A kinematic model of southern California, *Tectonics*, 5, 33-48, 1986

Appendices

Appendix 1: Coordinate frames

(a) Geocentric Cartesian coordinate (X, Y, Z)

We use the IERS Terrestrial Reference System (ITRS). The Z-axis is aligned with the pole of the ITRS, the X-axis is towards mean Greenwich zero meridian, and the Y-axis points east 90°.

(b) Geodetic coordinates (ϕ, λ, h)

This coordinate system includes geodetic latitude $\phi(t)$ with positive north, geodetic longitude $\lambda(t)$ with positive east, and geodetic height h(t) as its components.

(c) Local topocentric coordinates (x, y, z)

The x-axis is directed to local astronomical east, the y-axis is directed to local astronomical north, and the z-axis coincides with local zenith. Such a definition leads to a right-hand system which is the same that used by DYNAP [*Drew and Snay*, 1989] and different from that of *Collier et al.* [1988].

The conversion of (φ, λ, h) to (X, Y, Z) is:

$$\begin{aligned} X(t) &= (N + h(t)) \cos \varphi(t) \cos \lambda(t) \\ Y(t) &= (N + h(t)) \cos \varphi(t) \sin \lambda(t) \\ Z(t) &= (N(1-e^2) + h(t)) \sin \varphi(t) \end{aligned} \qquad (1.1)$$

where N is the radius of curvature in the prime vertical and e is the first eccentricity of the ellipsoid.

The vector in a local topocentric coordinate frame is transformed to a geocentric Cartesian frame via a time-variable rotation matrix R(t):

$$\mathbf{dx_{ij}}(t) = R(t)\, \mathbf{dX_{ij}}(t) \qquad (1.2)$$

where the bold character represents vector.

$dXij(t) = Xj(t) - Xi(t)$

$\mathbf{dx_{ij}}(t) = \mathbf{x_j}(t) - \mathbf{x_i}(t)$ is defined in a local topocentric frame at site i.

$$R(t) = \begin{bmatrix} -\sin \Lambda(t) & \cos \Lambda(t) & 0 \\ -\sin \Phi(t) \cos \Lambda(t) & -\sin \Phi(t) \sin \Lambda(t) & \cos \Phi(t) \\ \cos \Phi(t) \cos \Lambda(t) & \cos \Phi(t) \sin \Lambda(t) & \sin \Phi(t) \end{bmatrix} \qquad (1.3)$$

where

$\Phi(t)$ is astronomic latitude at site i.

$\Lambda(t)$ is astronomic longitude at site i.

The differences between astronomic (Φ, Λ) and geodetic (φ, λ) coordinates

$$\Phi - \varphi = \xi, \qquad \Lambda - \lambda = \frac{\eta}{\cos\varphi} \tag{1.4}$$

are called deflections of the vertical. ξ is the north-south component of deflection, with the downward vertical deviation towards the south being positive. η is the east-west component of deflection, with the downward vertical deviation towards the west being positive.

Appendix 2: Specific linearized observation equations

In this section, we present the linearized observation equations for the quasi-observations (site position and velocity) and for terrestrial observations. Observation equations for carrier beat phase and group delay can be found in *King et al.* [1985] and *Herring* [1983] respectively. Derivations of the terrestrial observation equations are similar to the work by *Collier et al.* [1988].

1) *Site displacement and velocity*

If the observables are in a geocentric Cartesian frame, the equations are

$$\begin{aligned}
\delta X &= L_x \begin{pmatrix} \delta X_0 \\ \delta V_0 \end{pmatrix} + L_x \begin{pmatrix} \mu & 0 \\ 0 & \mu \end{pmatrix} \begin{pmatrix} \omega_x \\ \omega_v \end{pmatrix} + L_x \begin{pmatrix} \tau_x \\ \tau_v \end{pmatrix} \\
\delta V &= L_v \begin{pmatrix} \delta X_0 \\ \delta V_0 \end{pmatrix} + L_v \begin{pmatrix} \mu & 0 \\ 0 & \mu \end{pmatrix} \begin{pmatrix} \omega_x \\ \omega_v \end{pmatrix} + L_v \begin{pmatrix} \tau_x \\ \tau_v \end{pmatrix}
\end{aligned} \tag{2.1}$$

where

$$L_x = \left(I_3 + \frac{\partial V_0}{\partial X_0}(t-t_0) \qquad I_3(t-t_0) \right), \qquad L_v = \left(\frac{\partial V_0}{\partial X_0} \qquad I_3 \right) \tag{2.2}$$

I_3 is the (3 x 3) identity matrix.

ω_x is the rotation angle, ω_v is the rotation angle rate.

τ_x is the translation, τ_v is the translation rate.

ω_x, ω_y, τ_x, τ_y are common for all sites.

$$\mu = \begin{pmatrix} 0 & -z_0 & y_0 \\ z_0 & 0 & -x_0 \\ -y_0 & x_0 & 0 \end{pmatrix} \tag{2.3}$$

x_0, y_0, z_0 are the a priori coordinates.

Currently, the term representing the velocity gradient is not used. One reason is that there is no detailed velocity contour of southern California at present. Another reason is that the value of this term is usually very small if the coordinate adjustments are at meter level or less.

If the observables are in a local topocentric frame, I_3 is replaced by the rotation matrix R_0, defined in Appendix 1 (1.3) as a function of the astronomic latitude Φ_0 and longitude Λ_0.

2) *Baseline and baseline rate vectors*:

If the observed vector is in a geocentric Cartesian frame,

$$\delta(dX_{ij}) = L_x\begin{pmatrix} \delta X_{0_j} - \delta X_{0_i} \\ \\ \delta V_{0_j} - \delta V_{0_i} \end{pmatrix}, \quad \delta(dV_{ij}) = L_v\begin{pmatrix} \delta X_{0_j} - \delta X_{0_i} \\ \\ \delta V_{0_j} - \delta V_{0_i} \end{pmatrix} \tag{2.4}$$

If the observed vector is in local frame, I_3 is again replaced by R_0 in L_x and L_v.

3) *Astronomic longitude Λ, latitude Φ, and gravity g*:

$$\begin{pmatrix} \delta\Lambda \\ \delta\Phi \\ \delta g \end{pmatrix} = -\begin{pmatrix} (g_0\cos\phi_0)^{-1} & 0 & 0 \\ 0 & g_0^{-1} & 0 \\ 0 & 0 & 1 \end{pmatrix} R_0 \left(M\, L_x\begin{pmatrix} \delta X_0 \\ \delta V_0 \end{pmatrix} + \frac{\partial(\Delta U_0(X_0))}{\partial X} \right) \tag{2.5}$$

where

g_0 is the apriori gravity, ϕ_0 is the apriori geodetic latitude, and

$$M = \frac{\partial^2 U}{\partial X^2}$$

is the Marussi tensor of second-order derivatives of U [*Hein*, 1986].

If the disturbing potential ΔU_0 is dominated by known mass anomalies, then the ΔU_0 term in (2.5) represents the deflections of the vertical for Λ and Φ, (Appendix 1), and the topographic gravity anomaly for g [*Hein*, 1986]. We prefer to absorb the deflections of the vertical and the topographic gravity anomaly correction into the residuals, so that (2.5) becomes

$$\begin{pmatrix} \delta\Lambda \\ \delta\Phi \\ \delta g \end{pmatrix} = -\begin{pmatrix} (g_0\cos\phi_0)^{-1} & 0 & 0 \\ 0 & g_0^{-1} & 0 \\ 0 & 0 & 1 \end{pmatrix} R_0\, M\, L_x\begin{pmatrix} \delta X_0 \\ \delta V_0 \end{pmatrix} \tag{2.6}$$

If the quasi-observable rates of Λ, Φ and g are used, L_x is replaced by L_v in (2.6).

4) *Horizontal and vertical angles and mark-to-mark distances*

From local site i to site j, the distance is $l(t)$, the azimuth is $\alpha(t)$, and the vertical angle is $\beta(t)$. The linearized observation equations of triangulation, leveling, and trilateration are expressed as:

$$\begin{pmatrix} \delta\alpha \\ \delta\beta \\ \delta l \end{pmatrix} = \begin{pmatrix} (l_0\cos\beta_0)^{-1} & 0 & 0 \\ 0 & l_0^{-1} & 0 \\ 0 & 0 & 1 \end{pmatrix} \left(S^T R_0 L_x \begin{pmatrix} \delta X_{0_j} - \delta X_{0_i} \\ \delta V_{0_j} - \delta V_{0_i} \end{pmatrix} - \frac{K R_0 M L_x}{g_0} \begin{pmatrix} \delta X_{0_i} \\ \delta V_{0_i} \end{pmatrix} \right) \quad (2.7)$$

where

$$S = \begin{pmatrix} \cos\alpha_0 & -\sin\alpha_0 \sin\beta_0 & \sin\alpha_0 \cos\beta_0 \\ -\sin\alpha_0 & -\cos\alpha_0 \sin\beta_0 & \cos\alpha_0 \cos\beta_0 \\ 0 & \cos\beta_0 & \sin\beta_0 \end{pmatrix} \quad (2.8)$$

$$K = \begin{pmatrix} l_0(\tan\phi_0 \cos\beta_0 - \cos\alpha_0 \sin\beta_0) & l_0 \sin\alpha_0 \sin\beta_0 & 0 \\ l_0 \sin\alpha_0 & l_0 \cos\alpha_0 & 0 \\ 0 & 0 & 0 \end{pmatrix} \quad (2.9)$$

and the zero subscript indicates values calculated from a priori coordinates and velocities.

As mentioned before, the residual terms of (2.7) include the terms for the deflection of the vertical. For direction observations, FONDA adopts auxiliary parameters to account for the unknown arbitrary azimuth of the first "pointing" in each "zero". This approach is equivalent to the angle difference method, but the latter must construct a full instead of a diagonal covariance matrix to describe the correlations among observations [*Prescott*, 1976].

The observation equations of quasi-observable rates of α, β and l are similar to (2.7), with L_x replaced by L_v .

5) *Episodic site displacement vector*

Episodic deformations, such as coseismic displacements, are estimated as step functions in site position. If the displacements occupy only a limited area of the whole network, it is possible to resolve them simultaneously with other parameters. The time-dependent positions can then be expressed as

$$\delta X(t) = L_x \begin{pmatrix} \delta X_0 \\ \delta V_0 \end{pmatrix} + \sum_k r_k(t,t_k)\, \delta\xi_k \quad (2.10)$$

$$r_k(t,t_k) = \begin{cases} -1 & \text{if } t < t_k < t_0 \\ 0 & \text{if } t > t_k, t_k < t_0 \text{ or } t < t_k, t_k > t_0 \\ 1 & \text{if } t > t_k > t_0 \end{cases} \quad (2.11)$$

Where t_k is the occurrence epoch of the k-th event, and $\delta\xi_k$ is the site displacement vector from the k-th event.

In the case of known episodic events, all the above equations should be modified by adding the episodic site displacement terms. We note that the estimated

episodic site displacement vector does not always represent the actual displacement of the benchmark. For example, in trilateration observations if one site has only one distance observation around the earthquake epoch, the estimated ξ_k is the projection of the benchmark displacement vector onto the baseline vector. If a whole network is shifted by an earthquake, the estimated site displacements from trilateration or triangulation data will contain the ambiguities of network translation and rotation.

We choose not to estimate fault-slip parameters directly in order to avoid biasing our velocity estimates through an inadequacy in the fault-slip model. Our estimated episodic displacement field is independent of the fault model. Therefore the geodetically estimated coseismic displacement field provides a useful comparison to the seismically derived fault-slip model. Another advantage is that this approach can estimate the site displacement caused by other sources, such as benchmark instability.

Appendix 3: Reparameterization

Let $x(m_x)$ and $y(m_y)$ be two different parameterizations of the same observations, $l(n)$

$$l = A_x x + \varepsilon_x \quad \text{with covariance } C_l \tag{3.1}$$

$$l = A_y y + \varepsilon_y \quad \text{with covariance } C_l \tag{3.2}$$

The least square estimates are well-known:

$$\hat{x} = \left(A_x^T C_l^{-1} A_x\right)^{-1} A_x^T C_l^{-1} l \tag{3.3}$$

$$C_{\hat{x}} = \left(A_x^T C_l^{-1} A_x\right)^{-1} \tag{3.4}$$

$$\hat{y} = \left(A_y^T C_l^{-1} A_y\right)^{-1} A_y^T C_l^{-1} l \tag{3.5}$$

$$C_{\hat{y}} = \left(A_y^T C_l^{-1} A_y\right)^{-1} \tag{3.6}$$

Research on the general relations between the two solutions is beyond the scope of this thesis. Here we discuss only the applications of reparameterization related to our methodology.

1) *Use $\hat{y}$ and $C_{\hat{y}}$ as quasi-observations to obtain the final solution (3.3) and (3.4)*

It is easy to prove that if we construct a quasi-observation equation

$$\hat{y} = B x \qquad \text{with covariance matrix } C_{\hat{y}} \tag{3.7}$$

The solution is:

$$\hat{x} = \left(B^T C_{\hat{y}}^{-1} B\right)^{-1} B^T C_{\hat{y}}^{-1} \hat{y} = (3.3) \tag{3.8}$$

$$C_{\hat{x}} = \left(B^T C_{\hat{y}}^{-1} B\right)^{-1} = (3.4) \tag{3.9}$$

The great benefit is that we do not need to keep and reprocess the original observation data. We keep only the intermediate solution (3.5) and its covariance matrix (3.6). Furthermore, we can choose to test different final parameter sets x, adding stochastic parameters, for example, to get the optimal solution.

2) *Use* $\hat{y}$ *and* $C_{\hat{y}}$ *as quasi-observations and add extra parameters* x_a *to* x

The quasi-observation equation is

$$y = (B_x \quad B_{x_a}) \begin{pmatrix} x \\ x_a \end{pmatrix} \tag{3.10}$$

To distinguish from (3.8) and (3.9), we use $\tilde{x}$ and $C_{\tilde{x}}$ to denote the estimated subsolutions of (3.10). After some manipulations, we obtain the relations

$$\tilde{x} = \hat{x} + Q_{12}\, Q_{22}^{-1}\, \tilde{x}_a \tag{3.11}$$

$$C_{\tilde{x}} = C_{\hat{x}} + Q_{12}\, Q_{22}^{-1}\, Q_{21} \tag{3.12}$$

where

$$\begin{aligned} &C_{\hat{x}} = N_{11}^{-1}\,, \quad C_{\tilde{x}} = Q_{11}\,, \quad Q_{12} = -\,N_{11}^{-1}\, N_{12}\; Q_{22} = Q_{21}^{T} \\ &N_{12} = A_x^T\, C_l^{-1}\, A_{x_a}\,, \quad N_{22} = A_{x_a}^T\, C_l^{-1}\, A_{x_a}, \quad A_{x_a} = A_y\, B_{x_a} \\ &Q_{22} = \left(N_{22} - N_{21}\, N_{11}^{-1}\, N_{12}\right)^{-1} = C_{\tilde{x}_a} \end{aligned} \tag{3.13}$$

From (3.11), it is straightforward to get

$$C_{\tilde{x}-\hat{x}} = Q_{12}\, Q_{22}^{-1}\, Q_{21} \tag{3.14}$$

Then

$$C_{\tilde{x}} = C_{\hat{x}} + C_{\tilde{x}-\hat{x}} \tag{3.15}$$

If the parameters x_a actually do not exist, the expectation of the observation is

$$E\{l\} = A_x\, \bar{x} \tag{3.16}$$

From (3.11) and using (3.16)

$$\begin{aligned} E\{\tilde{x}\} &= E\{\hat{x}\} + Q_{12}\, Q_{22}^{-1} \left(Q_{21}\, A_x^T\, C_l^{-1} + Q_{22}\, A_{x_a}^T\, C_l^{-1}\right) E\{l\} \\ &= \bar{x} + Q_{12}\, Q_{22}^{-1} \left(Q_{21}\, N_{11} + Q_{22}\, N_{21}\right) \bar{x} = \bar{x} \end{aligned} \tag{3.17}$$

That means that even if the additional parameters x_a do not exist, $\tilde{x}$ is still an unbiased estimate of x. But its covariance is enlarged (see (3.15)). On the other hand, if the additional parameters x_a do exist, the omission of x_a will underestimate the variance of x and lead to a biased estimate $\tilde{x}$ unless the expectation of x_a is zero.

3) *Two data sets related to two sets of parameters with only part of the parameters in common*

Assume the first data set is related to parameters x_1 and x_2 and the second data set is related to parameters x_2 and x_3. The typical example is to consider space-geodetic data as the first data set, with x_1 satellite orbit, polar motion, UT1, quasar position, etc., and x_2 station coordinates and velocities; and terrestrial survey data as

the second data set with x_3 new station coordinates and velocities. We still treat the solution of space-geodetic data as quasi-observations. In this case the quasi-observation equations are

$$\begin{pmatrix}\hat{x}_1\\ \hat{x}_2\end{pmatrix}=\begin{pmatrix}I & 0\\ 0 & E_2\end{pmatrix}\begin{pmatrix}x_1\\ x_2\end{pmatrix} \qquad \text{with covariance matrix } C=\begin{pmatrix}C_{11} & C_{12}\\ C_{21} & C_{22}\end{pmatrix} \tag{3.18}$$

The combined normal equations are

$$\begin{pmatrix}N_{11} & N_{12}E_2 & 0\\ E_2^TN_{21} & E_2^TN_{22}E_2+A_{22} & A_{23}\\ 0 & A_{32} & A_{33}\end{pmatrix}\begin{pmatrix}x_1\\ x_2\\ x_3\end{pmatrix}=\begin{pmatrix}N_{11}\hat{x}_1+N_{12}\hat{x}_2\\ B_2+E_2^TN_{21}\hat{x}_1+E_2^TN_{22}\hat{x}_2\\ B_3\end{pmatrix} \tag{3.19}$$

Here $N = C^{-1}$.

Solving x_1 implicitly and using the matrix partition formula, we obtain

$$\begin{pmatrix}E_2^TC_{22}^{-1}E_2+A_{22} & A_{23}\\ A_{32} & A_{33}\end{pmatrix}\begin{pmatrix}x_2\\ x_3\end{pmatrix}=\begin{pmatrix}B_2+E_2^TC_{22}^{-1}\hat{x}_2\\ B_3\end{pmatrix} \tag{3.20}$$

This important result shows that if we do not care about the estimate of x_1, we can use only the common parameters x_2 and their covariance submatrix C_{22} as the quasi-observations. The result is as rigorous as using all parameters.

4) *Use part of the solutions to estimate another set of parameters*

Assuming the solutions include parameters x_1 and x_2, we attempt to use x_2 to estimate another parameter set u_2. A typical example is to estimate fault slips from episodic site displacement solutions.

$$\begin{pmatrix}\hat{x}_1\\ \hat{x}_2\end{pmatrix}=\begin{pmatrix}I & 0\\ 0 & E_2\end{pmatrix}\begin{pmatrix}x_1\\ u_2\end{pmatrix} \qquad \text{with covariance matrix } C=\begin{pmatrix}C_{11} & C_{12}\\ C_{21} & C_{22}\end{pmatrix} \tag{3.21}$$

As has been proved above, if we use x_2 and its covariance submatrix C_{22} as the quasi-observations, we can obtain the same estimates by directly estimating x_1 and u_2 from the raw data. But this time we do not update the solutions of x_1, since we know that the episodic site displacements more accurately describe the real episodic deformation field than the fault slip parameters. We want to leave the model errors in the residuals instead of distorting the estimate of x_1. Here the quasi-observation approach gives us the flexibility to obtain the optimal choice.

Appendix 4: Comparison between the Gauss–Markov model and other approaches

If we consider the velocity derived from space geodesy as a model velocity, both the Gauss–Markov model and model coordinate method can be summarized as minimizing

$$\lambda\left(\delta l_1 - A_1\,\delta X\right)^T C_1^{-1}\left(\delta l_1 - A_1\,\delta X\right) + \left(\delta l_2 - A_2\,\delta X\right)^T C_2^{-1}\left(\delta l_2 - A_2\,\delta X\right) \qquad (4.1)$$

where l_1 represents the terrestrial observation with covariance C_1 and design matrix A_1, and l_2 represents the space-geodetic solution with covariance C_2 and design matrix A_2.

The Lagranian multiplier λ is equivalent to an externally imposed relative weighting factor between l_1 and l_2. The choice of λ is rather philosophical, and reflects the balance between believing the formal uncertainties of the estimated velocities and imposing the prior model on the final solution. The Gauss-Markov model represents the case of $\lambda = 1$, which means the estimated formal covariance matrices are accepted. The model coordinate method corresponds to the case of $\lambda = \infty$, placing maximum weight on fitting the terrestrial survey data. Finally $\lambda = 0$ represents the case of fixing the velocities to the model i.e., space-geodetically derived velocities. For our analysis, we choose the Gauss-Markov model to perform the combination. Because the space-geodetically derived velocities are from the real data, not from a "pure" model, neither $\lambda = \infty$ nor $\lambda = 0$ correctly represents the statistical character of the space-geodetically derived velocities.

Appendix 5: Solution changes in the case of adding new data and new parameters

Assume the original data l_1 relate to the parameters x, and the new data l_2 relate to parameters x and y. $\hat{x}_1$ are the original estimate and $\hat{x}_{1+2}, \hat{y}_{1+2}$ are estimates from data l_1+l_2.

$$l_1 = A_1\,x + \varepsilon_1 \text{ with covariance } C_{l1} \qquad (5.1)$$

$$l_2 = B_1\,x + B_2\,y + \varepsilon_2 \text{ with covariance } C_{l2} \qquad (5.2)$$

The covariance matrices are

$$C_{\hat{x}_1} = \left(A_1^T C_{l1}^{-1} A_1\right)^{-1} \qquad (5.3)$$

$$C_{\begin{pmatrix}\hat{x}_{1+2}\\ \hat{y}_{1+2}\end{pmatrix}} = \begin{pmatrix} A_1^T C_{l1}^{-1} A_1 + B_1^T C_{l2}^{-1} B_1 & B_1^T C_{l2}^{-1} B_2 \\ B_2^T C_{l2}^{-1} B_1 & B_2^T C_{l2}^{-1} B_2 \end{pmatrix}^{-1} = \begin{pmatrix} N_{11} & N_{12} \\ N_{21} & N_{22} \end{pmatrix}^{-1} = \begin{pmatrix} Q_{11} & Q_{12} \\ Q_{21} & Q_{22} \end{pmatrix} \qquad (5.4)$$

$$C_{\hat{x}_{1+2}} = Q_{11} \qquad (5.5)$$

The solution change of parameters x can be derived as

$$\hat{x}_{1+2} - \hat{x}_1 = \left(Q_{11} - \left(A_1^T C_{11}^{-1} A_1\right)^{-1}\right) A_1^T C_{11}^{-1} l_1 + \left(Q_{11} B_1^T + Q_{12} B_2^T\right) C_{12}^{-1} l_2 \qquad (5.6)$$

Since the two data sets are uncorrelated,

$$C_{\hat{x}_{1+2}-\hat{x}_1} = \left(Q_{11} - \left(A_1^T C_{11}^{-1} A_1\right)^{-1}\right) A_1^T C_{11}^{-1} A_1 \left(Q_{11} - \left(A_1^T C_{11}^{-1} A_1\right)^{-1}\right) + \left(Q_{11} B_1^T + Q_{12} B_2^T\right) C_{12}^{-1} \left(B_1 Q_{11} + B_2 Q_{21}\right)$$

$$= \left(Q_{11} N_{11} + Q_{12} N_{21} - I\right) Q_{11} - Q_{11} + C_{\hat{x}_1} + \left(Q_{11} N_{12} + Q_{12} N_{22}\right) Q_{21}$$

From the well-known relations,

$$Q_{11} N_{11} + Q_{12} N_{21} = I \qquad \text{and} \qquad Q_{11} N_{12} + Q_{12} N_{22} = 0$$

We derive the very simple result

$$C_{\hat{x}_{1+2}-\hat{x}_1} = C_{\hat{x}_1} - C_{\hat{x}_{1+2}} \qquad (5.7)$$

Appendix 6: Procedures for updating poorly known coordinates in a terrestrial network

In order to update the coordinates of a terrestrial survey network, there must be at least three non-collinear sites that have also been observed by space-geodetic techniques. Theoretically, two space-geodetic sites can control the translation and rotation of the network provided there is no figure defect. The third site is necessary to avoid divergence during the iteration. If this condition is satisfied, then a bootstrapping strategy may be applied to update the poorly known terrestrial coordinate system. For simplicity, we use a trilateration network as an example. We adopt the following procedures:

1) Perform a transformation to align the original trilateration coordinate system to the space-geodetic reference frame. The parameters are estimated from the coordinate differences of the common sites. Currently, we estimate only the translation and rotation, and neglect the scale factor. Due to an error in the velocity of light used to convert the EDM measurements to ranges, they are too long by 0.14 ppm [M. Lisowski, personal communication, 1993], causing about 4 mm error for a 30 km baseline. We have not applied this (relatively small) correction to our estimates of site coordinates.

2) Compress the trilateration data into baseline lengths related to weighted mid epochs and baseline length rates. Use baseline length rates as quasi-observations to estimate site velocities.

3) Using the compressed data, tight outlier identification criteria, and tightly constrained coordinates at the common sites, estimate and update the remaining site coordinates.

4) Repeat step 3) with updated coordinates, gradually loosening the outlier identification criteria. This procedure continues until no more data fail to pass the criteria.

5) Using the initial raw data and realistic constraints on the coordinates and velocities of all sites, estimate coordinates and velocities simultaneously.

There are limits on the ability of terrestrial survey data to update coordinates. For example, trilateration data is not sensitive to height change. In this case, the heights should be tightly constrained in steps 3) and 4) and estimated only in the last step to get limited improvement.

In the final step, the estimated coordinates and velocities are in general correlated. We prefer to obtain updated coordinates that are approximately uncorrelated with velocities. To realize this, we modify the reference epoch for each site coordinate.

Assume that the estimated coordinates and velocities for one site are **X** and **V**. Their covariance matrix is C and the reference epoch is t_0.

$$C = \begin{pmatrix} C_{xx} & C_{xv} \\ C_{vx} & C_{vv} \end{pmatrix} \tag{6.1}$$

The uncorrelated coordinate is **X'** and the modified reference epoch is t_0'.

$$\begin{pmatrix} \mathbf{X}' \\ \mathbf{V} \end{pmatrix} = \begin{pmatrix} 1 & \Delta t \\ 0 & 1 \end{pmatrix} \begin{pmatrix} \mathbf{X} \\ \mathbf{V} \end{pmatrix} = J \begin{pmatrix} \mathbf{X} \\ \mathbf{V} \end{pmatrix} \tag{6.2}$$

The epoch offset Δt is selected so that the off-diagonal terms of C' are close to zero. Where $C' = J\,C\,J^T$. We use the weighted average estimate

$$\Delta t = -\frac{\dfrac{C_{x_x v_x}}{C_{x_x x_x} C_{v_x v_x}} + \dfrac{C_{x_y v_y}}{C_{x_y x_y} C_{v_y v_y}} + \dfrac{C_{x_z v_z}}{C_{x_z x_z} C_{v_z v_z}}}{\dfrac{1}{C_{x_x x_x}} + \dfrac{1}{C_{x_y x_y}} + \dfrac{1}{C_{x_z x_z}}} \tag{6.3}$$

Then $t_0' = t_0 + \Delta t$ (6.4)

$\mathbf{X}' = \mathbf{X} + \mathbf{V}\,\Delta t$, $C' = J\,C\,J^T$ (6.5)

Appendix 7: Contribution of nominal lengths to the estimate of velocity

A time series of distance measurements can be compressed into one baseline length rate and one length at a weighted mid epoch, for which the length and its rate are uncorrelated. Using all nominal lengths and their rates to estimate site coordinate adjustments and site velocities, the linearized observation equations are

$$\begin{pmatrix} \Delta L \\ \dot{\Delta L} \end{pmatrix} = \begin{pmatrix} A_{11} & A_{12} \\ 0 & A_{22} \end{pmatrix} \begin{pmatrix} \delta X \\ \delta V \end{pmatrix} \quad \text{with } C = \begin{pmatrix} C_L & 0 \\ 0 & C_{\dot{L}} \end{pmatrix} \tag{7.1}$$

The normal equations are:

$$\begin{pmatrix} A_{11}^T C_L^{-1} A_{11} + \sigma_X^{-2} & A_{11}^T C_L^{-1} A_{12} \\ A_{12}^T C_L^{-1} A_{11} & A_{12}^T C_L^{-1} A_{12} + A_{22}^T C_{\dot{L}}^{-1} A_{22} + \sigma_V^{-2} \end{pmatrix} \begin{pmatrix} \delta X \\ \delta V \end{pmatrix} = \begin{pmatrix} A_{11}^T C_L^{-1} \Delta L \\ A_{12}^T C_L^{-1} \Delta L + A_{22}^T C_{\dot{L}}^{-1} \dot{\Delta L} \end{pmatrix} \tag{7.2}$$

where

σ_X is the apriori uncertainty on X.

σ_V is the apriori uncertainty on V.

L and $\dot{L}$ are the compressed baseline length and baseline length rate respectively. Solving for δX implicitly, (7.2) becomes:

$$\left[A_{22}^T C_{\dot{L}}^{-1} A_{22} + \sigma_V^{-2} + A_{12}^T \left(C_L + A_{11}^T \sigma_X^2 A_{11}\right)^{-1} A_{12}\right] \delta V = A_{22}^T C_{\dot{L}}^{-1} \dot{\Delta L} + A_{12}^T \left(C_L + A_{11}^T \sigma_X^2 A_{11}\right)^{-1} \Delta L \tag{7.3}$$

Equation (7.3) reveals the following:

1. Using only rates is equivalent to the case of $\sigma_X \to \infty$.
2. The maximum contribution of L to V is the case of $\sigma_X \to 0$.
3. If the misfit of L (ΔL) is too large, it can bias significantly the velocity estimate. Hence poor a priori coordinates should be updated before estimating velocities.
4. Consider the simplest case of 1-d. Given the scalar values:

   $A_{11}, A_{22} \approx 1$, $A_{12} \approx \Delta t$, $C_L \approx (4 \text{ mm})^2$, $C_{\dot{L}} \approx (1 \text{ mm/year})^2$, $\sigma_V \approx 200$ mm/year

   Δt is the difference between the reference epoch and the weighted mid epoch.

The maximum contribution of L to V ($\sigma_X \to 0$) can be determined by $\hat{\delta V} \approx \frac{16\,\dot{\Delta L} + \Delta t\,\Delta L}{16 + (\Delta t)^2}$. The formal uncertainty of the estimated velocity from original 1 (considering only the length rates) to $1 - \frac{(\Delta t)^2}{(16 + (\Delta t)^2)}$.

5. The current updated USGS trilateration site coordinates (σ_X) are considered as accurate as 1 to 10 meters. For most baselines, $\Delta t < 5$ years. Therefore the contribution of L to V is very small. To get a meaningful contribution to V from L, the accuracies of a priori coordinates should reach the centimeter level. Using the above example with σ_x = 1 cm and Δt = 5 year, the compressed baseline lengths L can reduce the formal uncertainty by about 30%.

Appendix 8: Sensitivity testing

Network configuration affects the sensitivity of the adjustments to the signal to be detected. In this Appendix, we do not discuss the theory of optimal network design. Rather, we use a simplified methodology to estimate the sensitivity of a given network.

Let the signal be the velocity field induced by a dislocation model of an infinitely long strike-slip fault in a half-space. Take the fault orientation to be along the y-axis in a local 2-D reference frame. The baseline makes an angle of θ to the y-axis. The observable is the baseline length rate dL/dt. The linearized observation equation can be simplified to

$$\frac{dL}{dt} = \frac{\partial L}{\partial x_1}(t-t_0)\,\delta v_{x1} + \frac{\partial L}{\partial x_2}(t-t_0)\,\delta v_{x2} + \frac{\partial L}{\partial y_1}(t-t_0)\,\delta v_{y1} + \frac{\partial L}{\partial y_2}(t-t_0)\,\delta v_{y2}$$
$$= \sin\theta\,(t-t_0)\left(\delta v_{x1} - \delta v_{x2}\right) + \cos\theta\,(t-t_0)\left(\delta v_{y1} - \delta v_{y2}\right) \qquad (8.1)$$

In this special case, all velocities are expected to be parallel to the y-axis. If the baselines are parallel to the fault orientation ($\theta = 0°$), there is no sensitivity since all measurements are always zero. If the baselines are perpendicular to the fault ($\theta = 90°$), there is also no sensitivity, because $\cos\theta = 0$, and all measurements are still zero to first order. However, if the baselines are nearly perpendicular to the fault, the solution is sensitive to small perturbations. If v_y has a constant gradient in the x direction, the optimal baseline orientation is $\theta = 45°$. For a narrow network nearly perpendicular to a strike-slip fault, the solution is sensitive to small changes in the observations even if some diagonal baselines in the network have the optimal angle of $\theta = 45°$.

To quantify the above statement, the observable L is described as $L = L(\mathbf{x}, \mathbf{s})$, where $\mathbf{x}$ and $\mathbf{s}$ are adjusted and unadjusted parameters respectively. The difference $\delta\mathbf{s}$ between the true value of $\mathbf{s}$ and the a priori value, $\mathbf{s_0}$, represents the systematic error.

$$\delta\mathbf{s} = \mathbf{s} - \mathbf{s}_0 \qquad (8.2)$$

The computed linearized observation equation is

$$l(t) = L(\mathbf{x}, \mathbf{s}, t) - L(\mathbf{x}_0, \mathbf{s}_0, t_0) = A_x(t)\,\delta\mathbf{x} + \varepsilon_x(t) \qquad (8.3)$$

with observation covariance C_l and model covariance C_{x0}.

The estimated adjustments are

$$\delta\hat{\mathbf{x}} = C_{\hat{x}}\left(A_x^T C_l^{-1}\, l + C_{x0}^{-1}(\mathbf{x}_m - \mathbf{x}_0)\right) \qquad (8.4)$$

with $$C_{\hat{x}} = \left(A_x^T C_l^{-1} A_x + C_{x0}^{-1}\right)^{-1} \qquad (8.5)$$

Usually we choose the parameter model as its a priori value $\mathbf{x}_m = \mathbf{x}_0$; equation (8.4) then becomes

$$\delta\hat{\mathbf{x}} = C_{\hat{x}}\, A_x^T\, C_l^{-1}\, l \tag{8.6}$$

Due to the systematic error, the estimate (8.6) is biased. The true linearized observation equation should be

$$l_t(t) = L(\mathbf{x}, \mathbf{s}, t) - L(\mathbf{x}_0, \mathbf{s}, t_0) = l(t) + A_s(t)\,\delta\mathbf{s} \tag{8.7}$$

Therefore, the true solution should be

$$\delta\hat{\mathbf{x}}_t = C_{\hat{x}}\left(A_x^T\, C_l^{-1}\, l + A_x^T\, C_l^{-1}\, A_s\, \delta\mathbf{s}\right) \tag{8.8}$$

The perturbation from systematic error can be written

$$p_x = \delta\hat{\mathbf{x}} - \delta\hat{\mathbf{x}}_t = S\,\delta\mathbf{s} \tag{8.9}$$

where

$$S = -\,C_{\hat{x}}\, A_x^T\, C_l^{-1}\, A_s \tag{8.10}$$

is known as the sensitivity matrix.

In this chapter, we use (8.9) and (8.10) to test the perturbation from each isolated systematic change of baseline length rate.

Appendix 9: Error model

The commonly accepted model for the errors in EDM observations has the form

$$\sigma = \sqrt{a^2 + b^2\, L^2} \tag{9.1}$$

where L is the baseline length. For USGS EDM data with line-of-sight atmospheric calibration, a = 3 mm and b = 0.2 ppm [*Savage and Prescott* 1973], which includes the systematic errors with a = 0.5 mm and b = 0.14 ppm [*Savage et al.*, 1986]. Systematic errors occur in individual surveys due to improper calibration of the meteorological probes. This kind of systematic errors affects all measurements in a particular survey but is related randomly to the systematic errors of other surveys due to frequent recalibrations. Therefore the systematic component of errors can be treated as random errors in the analysis of multiple survey data. Since our analysis attempts to estimate the velocity field from multiple trilateration networks simultaneously, it is important to check whether the different networks have different data quality due to different topography, instrumentation, or operators. The data quality of each network is assessed by the scatters about the best-fit linear trend of the baseline length observations. For each baseline, the scatter is defined as

$$s_i = \sqrt{\frac{\sum_{j=1}^{n} w_j \left(L_i(t_j) - L_i(t_0) - \dot{L}_i\,(t_j - t_0)\right)^2}{\frac{n-2}{n}\sum_{j=1}^{n} w_j}} \tag{9.2}$$

where

$L_i(t)$ is the observed baseline length.

$L_i(t_0)$, $\dot{L}_i$ are the estimated length at epoch t_0 and the length rate, respectively.

i is the baseline index.

j is the observation index for this baseline.

$w_j = \frac{1}{\sigma_j^2}$

The squares of the residuals obey the χ^2 distribution with degrees of freedom *n-2*, providing that all residuals are independent and follow a normal distribution. Therefore the upper and lower bounds of each scatter are obtained from the χ^2 distribution with a specified confidence level α. Choosing α=0.68 and averaging the distances from the upper and lower bounds, the result is assigned as the uncertainty for the scatter. Thus for each network, we obtain a series of scatters from the baselines with three or more observations. Performing a least squares adjustment to these scatters by fitting the error model (9.1), we get the estimated values of *a* and *b* for each network. Note that these scatters reflect not only the quality of the observations, but also the appropriateness of the linear trend. Therefore, any time-varying deformation will be treated as noise.

The systematic differences between VG and EDM data should be discussed. Based on the GPS and EDM measurements performed at Loma Prieta, California, and Hebgen Lake, Montana, *Davis et al.* [1989] modeled the differences of baseline lengths between the two techniques using the equation

$$\Delta L = a + b\,L \qquad (9,3)$$

where L is the baseline length. Their results show that both *a* (0.6 ± 0.5 mm) and *b* (0.1 ± 0.1 ppm) do not significantly differ from zero. Thus we neglect the effects of the systematic differences between VG and EDM data in this analysis.

Appendix 10: Procedures for updating coordinates

To update the coordinates of the USGS trilateration sites, we used several collocated VG site coordinates from the solution of F93. The relative horizontal positions of these VG sites have accuracies better than 2 cm. We also used coordinates determined for several collocated GPS sites from GPS observations made by USGS in the Parkfield area and by SCEC in the Gorman region. Analysis of these coordinates gives an accuracy of about a decimeter. While updating coordinates, we

also encountered the problem with errors in the integer-wavelength ambiguities in EDM measurements. These errors are known as "coarse range busts" and it is possible, although uncommon, to have 10-ft, 100-ft, and 1000-ft range busts. After checking part of the original survey log sheets, we identified and corrected 12 range busts, as small as 10 feet and as large as 1100 feet. However, we are still suspicious of hidden range busts in the corrected data set, because we have not performed an exhaustive search. Assuming that there are no undiscovered range busts, the updated horizontal coordinates can reach 1-3 meter accuracy for the sites with observations of multiple baselines. The vertical coordinates keep their original accuracy because baseline length observables have little sensitivity to vertical changes.

Appendix 11: Parkfield dilemma

In the San Luis network, using the CDWR measurements from 1959 to 1969, the CDMG observations in the 1970's, and the USGS Geodolite data from 1980 to 1984, *Harris and Segall* [1987] (hereafter as HS) found that there was a normal strain perpendicular to the SAF, representing about 6.1 ± 1.7 mm/yr of shortening for the 80-km wide network. Including such a normal strain, the derived site velocity field fit their model velocity field better, decreasing χ^2 by 25%. It is surprising that such a convergent pattern does not show up in the same network when using the USGS data from 1980 to 1991 (Figure 13a). Instead, Figure 13a implies that some dilation occurs along both sides of the SAF, although the error ellipses indicate that such a dilation is not significantly different from zero. This discrepancy between our solution and HS's needs to be explored. Because this discrepancy exists not only in the fault-normal velocity component, but also in the fault-parallel velocity component, both aspects affect an inversion for a fault slip model.

We use the Geodolite data from 1980 to 1984 and the CDMG survey data between 1971 and 1979 to derive an outer coordinate velocity solution with a minimum velocity direction of N50°E (Figure 13b). Omitting the CDWR data from 1959 to 1969 does not change the solution significantly, since we nearly reproduce the HS solution (Figure 9 of HS). It is the different data sets that cause the discrepancy. This conclusion can be further confirmed by looking at the observation data series directly (see Appendix 13). The baselines Almond-Bench, Kenger-Mason, Bench-Bonnie, and Bonnie-Cotton are the main sources for the divergence. All four baselines show different trends before and after 1980.

Which data set should be adopted in this analysis, the CDMG data set, the USGS data set, both, or neither? Both the CDMG data set and the USGS data set are strong and self-consistent, and neither can be rejected on the basis of its internal statistics. We also cannot attribute the discrepancy to the change of measuring instruments or survey agency since not all observations show such a dramatic change. Furthermore, the change of instruments could introduce a discontinuity in the measured baseline lengths, but not their rate of change. Is it time-dependent deformation? Other groups have also noticed this discrepancy. *Shen* [1991] estimated -0.08 ± 0.02 μrad/yr compression from the HS trilateration data set, but 0.03 ± 0.02 μrad/yr strain normal to the SAF from the combination of GPS observations with much earlier triangulation data. Time-dependent deformation is a possible interpretation. However, it is premature to reach this conclusion just based on these data. For now, we adopt both data sets with a constant-velocity model in our analysis. Additional GPS data for this area are critical to resolving the dilemma.

Appendix 12: Coseismic site displacements

We estimated the coseismic site displacements simultaneously with site coordinate adjustments and site velocities (Chapter 2). From this analysis, we obtained estimates of displacements induced by 7 earthquakes (Figure 14). In addition, we also estimated episodic site displacements related to other origins: aftershocks and steam well extractions from 1981 to 1991 in the eastern part of the Mexicali network (Figure 14); and apparent offsets from the eccentric tie deductions at the site Hopper of the San Luis network in 1981 and 1986.

The 1987 Superstition Hills earthquake consisted of two main shocks: an M_s=6.2 event occurred along the northeast-trending Elmore Ranch fault, and twelve hours later, an M_s=6.6 event was triggered along the northwest-trending Superstition Hills fault. *Larsen et al.* [1992] estimated coseismic displacements using GPS measurements made in 1986 and 1988. In Figure14a, we present our estimates using the USGS trilateration data, and we also compare ours with their GPS estimates at three collocated sites (Kane, Dixie, and Alamo). For the three common sites, there are differences of 5-10 cm, suggesting a rotational or translational offset. There are four possibilities to account for this offset: (i) We missed some sites which had significant coseismic displacements. (ii) All EDM sites have been rotated or translated by the Superstition Hills earthquake. (iii) Site OCTI, which was used as the reference site by *Larsen et al.*, has coseismic displacement. (iv) The estimate of

Larsen et al. has some systematic errors. It is unlikely that we missed any significantly affected site since the EDM measurements in the Salton subnetwork were strong, and the survey after the Superstition Hills earthquake covered a large area. We do not see any other significant discontinuities in the length series (see Appendix 12). Possibilities (ii) and (iii) do not help since if all of the EDM sites had common coseismic displacements, so did the site OCTI. Therefore both the estimates will shift, and the offset between them will remain. We suspect that systematic errors from *Larsen et al.*'s estimate are the main source for the offset. There were several differences between their analysis of the 1986 and 1988 GPS data sets, each one of which could cause systematic errors. For the 1986 data, they adopted satellite orbits calculated by broadcast ephemerides, which had an accuracy of about 1 ppm. For the 1988 data, they adjusted the orbits of satellites using tracking data from three CIGNET fiducial sites in North America. For the 1986 data, several California sites were fixed to adjust coordinates at other sites, but for the 1988 data, the coordinates of one site in California (Mojave) and two sites in eastern North America (Westford, Massachusetts, and Richmond, Florida) were fixed. Finally, for the 1986 data, all ambiguities were fixed to their nearest integers, but for the 1988 data, all ambiguities were estimated. It may worthwhile to reprocess these GPS data with a uniform scheme (see Chapter 2), in order to discern the origin of the offset.

The Westmoreland earthquake (M_L=5.7; April 26, 1981) was nucleated by a left-lateral slip along a northeast-trending fault [*Hutton and Johnson*, 1981]. This earthquake induced baseline discontinuities related to site Alamo [*Savage et al.*, 1986]. *Lisowski et al.* [1991] presumed that the anomalous velocity at Alamo in their map was associated with the Westmoreland earthquake. We estimate the coseismic displacement at Alamo (Figure 14b) and our results (Figure 4) confirm their statement.

The Mexicali earthquake (M_L=6.6; October 14, 1979) ruptured in the eastern vicinity of the Mexicali network. The Victoria earthquake (M_L=6.2; June 9, 1980) occurred along the Cerro Prieto fault southeast of the Mexicali subnetwork. Because no survey was conducted in this area between these two earthquakes, the trilateration data recorded the superimposed effects of the two strike-slip earthquakes (Figure 14c). Sites Puerta, Prieto, Bnp 10065, 24, 8, 9, and 10 were most affected by the Mexicali earthquake, and sites 17 and 3 were most affected by the Victoria earthquake and its aftershocks [*Lisowski and Prescott*, 1982].

All of the remaining four earthquakes (Homestead Valley, March 15, 1979, M_s = 5.6; North Palm Springs, July 8, 1986, M_s = 6.0; Joshua Tree, April 22, 1992, M_s =

6.1; Landers and Big Bear, June 28, 1992, M_s = 7.5, M_s = 6.6) occurred in the Joshua network. Because the northern part of the Joshua network was not established before the Homestead Valley earthquake, only at site Sandhill do we obtain a significant estimate of coseismic displacements for the Homestead Valley earthquake (Figure 14d). The coseismic site displacements from the North Palm Springs earthquake are the most poorly determined. Only four sites (Edom, Dome, Beacon, and Stubbe) are significantly affected by this earthquake. Except Edom, these sites have only one or two baseline observation. The large error ellipses (Figure 14e) reflect the weakness. The estimated coseismic site displacements from the Joshua Tree earthquake are poorly constrained (Figure 14f). The estimated coseismic displacements are significant at the 95% confidence level at only four sites (Edom 2, Inspncer, Pax_ncer, and Warren). The Landers earthquake displored the entire Joshua subnetwork. We use the USGS GPS survey results from before and after the Landers earthquake to set up an external control on the movement of the entire network. All GPS-derived site discontinuities are relative to the site Resort. Hence the estimated coseismic displacements may have a common offset from the coseismic displacement at the site Resort. We nearly reproduce the result of *Murray et al.* [1993] (see our Figure 14g and Fig. 2 of *Murray et al.*, 1993). This is not surprising because we use most of their data and impose the same external constraints. However, there is one exception: we triple the formal errors of the GPS results. Therefore our error ellipses of estimated coseimic site displacements are larger. We find that if we impose the GPS constraints with their formal errors, the velocity field of the Joshua network is distorted significantly. It is not yet clear whether this inconsistency comes from the two-epoch GPS surveys, or from the outliers of the trilateration survey made after the Landers earthquake, or both.

After 1981, there was only one survey in 1991 in the Mexicali network. The 10-year interval seems too long to identify the geophysical events in a tectonically active region. Significant discontinuities in the baseline lengths are seen in the eastern part of the Mexicali subnetwork between the 1981 and 1991 surveys (Figure 15). Thus the estimated site displacements are a mixture of secular motion, aftershock effects, possible survey blunders, and steam extraction in this geothermal area. We leave the interpretation of these displacements for future study.

The estimated coseismic site displacements show that if the data cover a large area both before and after the earthquake, our approach obtains satisfactory results (see the coseismic site displacements induced by Superstition Hills earthquake (Figure 14a) and Landers earthquake (Figure 14g). In the case of poor data coverage,

our estimated site displacements do not fully reflect the coseismic displacements. In this case, the better way is probably to combine our approach and with an a priori rupture model to remove the coseismic offsets induced by small earthquakes [*Savage et al.*, 1993].

Appendix 13: List of all baseline length observations

In this Appendix, we present the plots of all baseline length data used in this analysis (Figure 16). Outliers have been identified and removed from the measurement series based on a three-sigma (standard deviation off the linear trend) criterion [*Savage et al.*, 1986]. However, if the anomalies are associated with a known earthquake, we leave these data and estimate episodic site displacements, together with other unknowns to absorb the coseismic positional offsets. The solid lines in the plots represent the least squares fits for all of the data from each line independently. The dashed lines are the postfit from our analysis. The statistics of the fit are printed at the top of each plot. When there is coseismic displacement, the fit statistics do not reflect the real quality of the baseline observations.

For several series of measurements, we downweight the data:

(1) In the Carrizo subnetwork, we double the formal errors of all 1977 observations.

(2) In the Salton subnetwork, we double the formal errors of the measurements in 1983 and 1984 related to site Dixie (Carri_sa to Dixie, Dixie to Sup, Dixie to Fish, Dixie to Off_225, and Dixie to Off_229). There were apparent jumps in these baseline data series at 1983. But we cannot attribute the jumps to an episodic site displacement at Dixie.

(3) In the Joshua subnetwork, we double the formal error of the Keys–Sandhill baseline observation in 1988. It seems inconsistent with previous observations.

Savage et al. [1987] reported a systematic error in the measurements of the Monitor subnetwork from 1984 due to the change of survey group. We do not find a significant difference between these series and others, so we did not treat it in a special way.

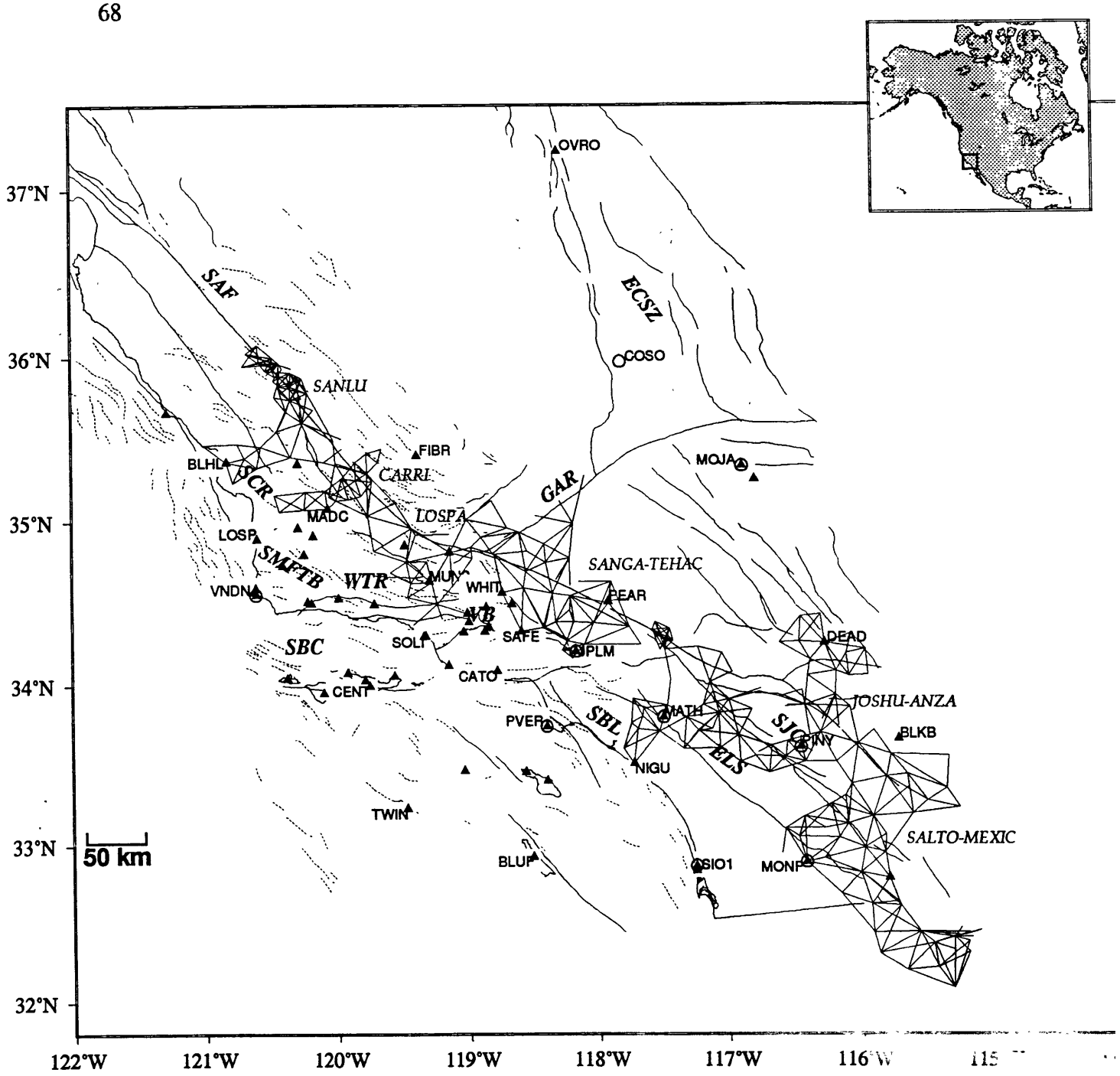

Figure. 1. Map of southern California showing the VLBI/GPS (VG) stations (triangles) and USGS trilateration networks (named with italics and linked with solid lines). The names of the main VG sites are labeled with four-character codes. The sites of the Permanent GPS Geodetic Array (PGGA) are marked with circles. The main tectonic domains are labeled with italics: the eastern California shear zone (ECSZ), the southern Coast Ranges (SCR), the Santa Maria Fold and Trust Belt (SMFTB), the western Transverse Ranges (WTR), the Ventura Basin (VB), the Santa Barbara Channel (SBC), and the southern Borderlands (SBL). Major faults include the San Andreas (SAF), San Jacinto (SJC), the Elsinore (ELS), and the Garlock (GAR).

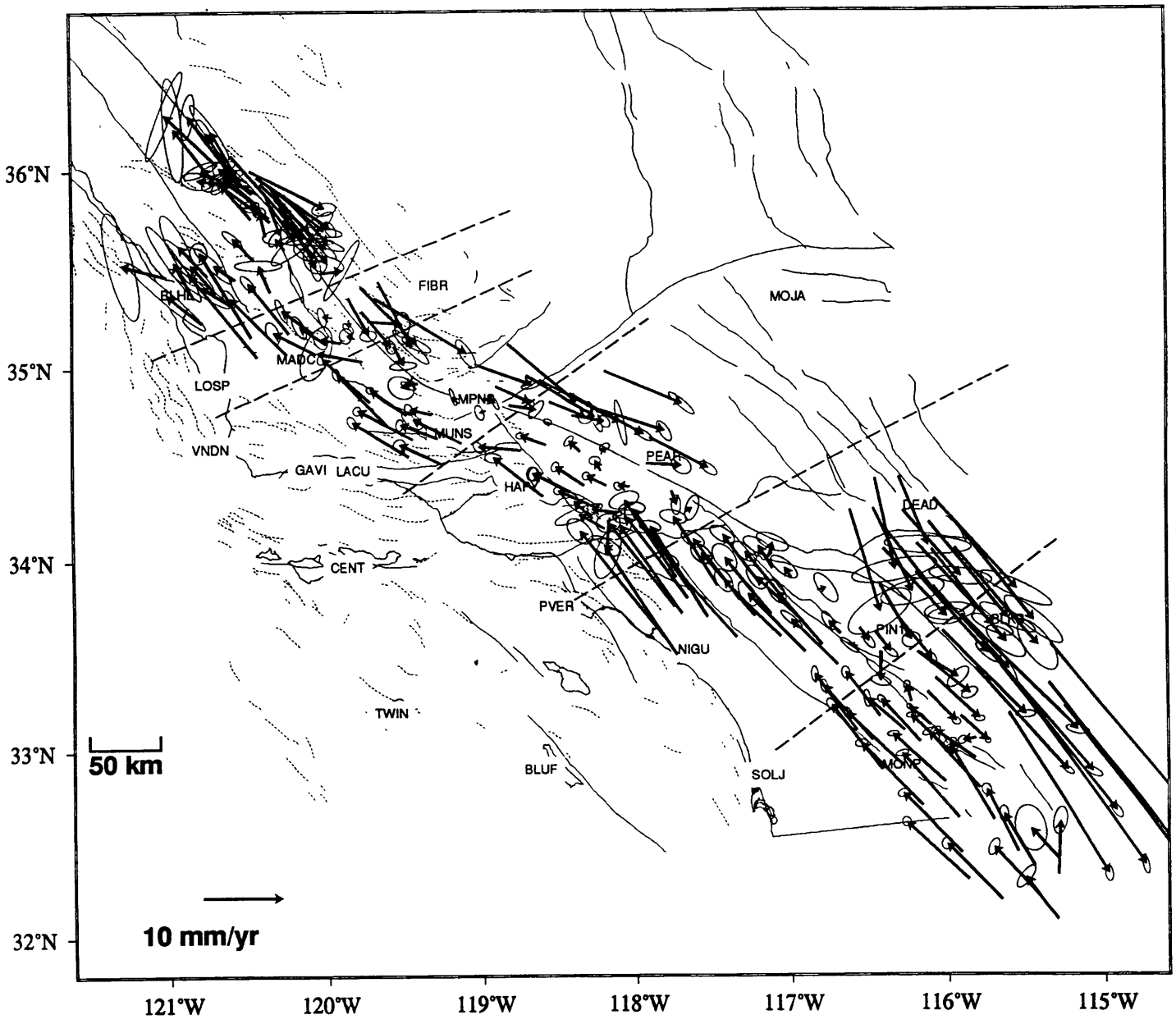

Figure 2. Outer coordinate solutions of the six USGS trilateration subnetworks (from north to south: San Luis – Parkfield, Carrizo – San Luis, Los Padres – Tehachapi, San Gabriel – Tehachapi, Anza – Joshua, Salton – Mexicali). The subnetworks and their minimum velocity directions to constrain the outer coordinate solutions are listed in Table 5. The six outer coordinate solutions are independent and are separated by heavy dashed lines. The ellipses represent one-sigma errors (i.e. 39% confidence in two-dimension). All tectonic features shown in this figure are the same as in Figure 1.

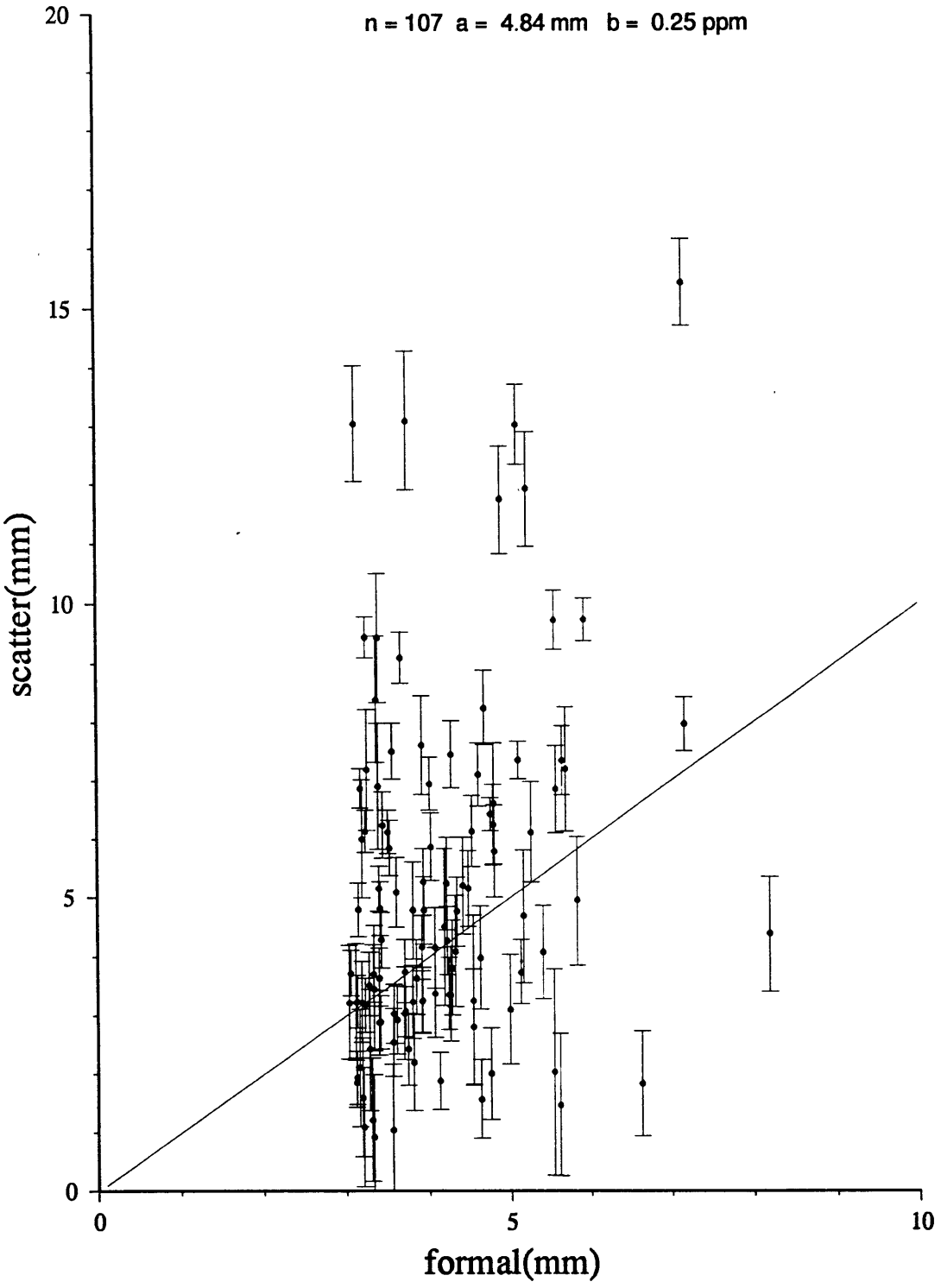

Figure 3a. Scatters of the trilateration data of the USGS San Luis – Parkfield trilateration network. The formal errors are calculated from the model $\sigma^2 = a^2 + b^2\ L^2$ with a = 3 mm, b = 0.2 ppm [*Savage and Prescott*, 1973]. The scatters are estimated by the procedures described in Appendix 9. The estimated coefficients of a and b are printed at the top of the figure. The straight line of unity slope represents agreement with assumed model.

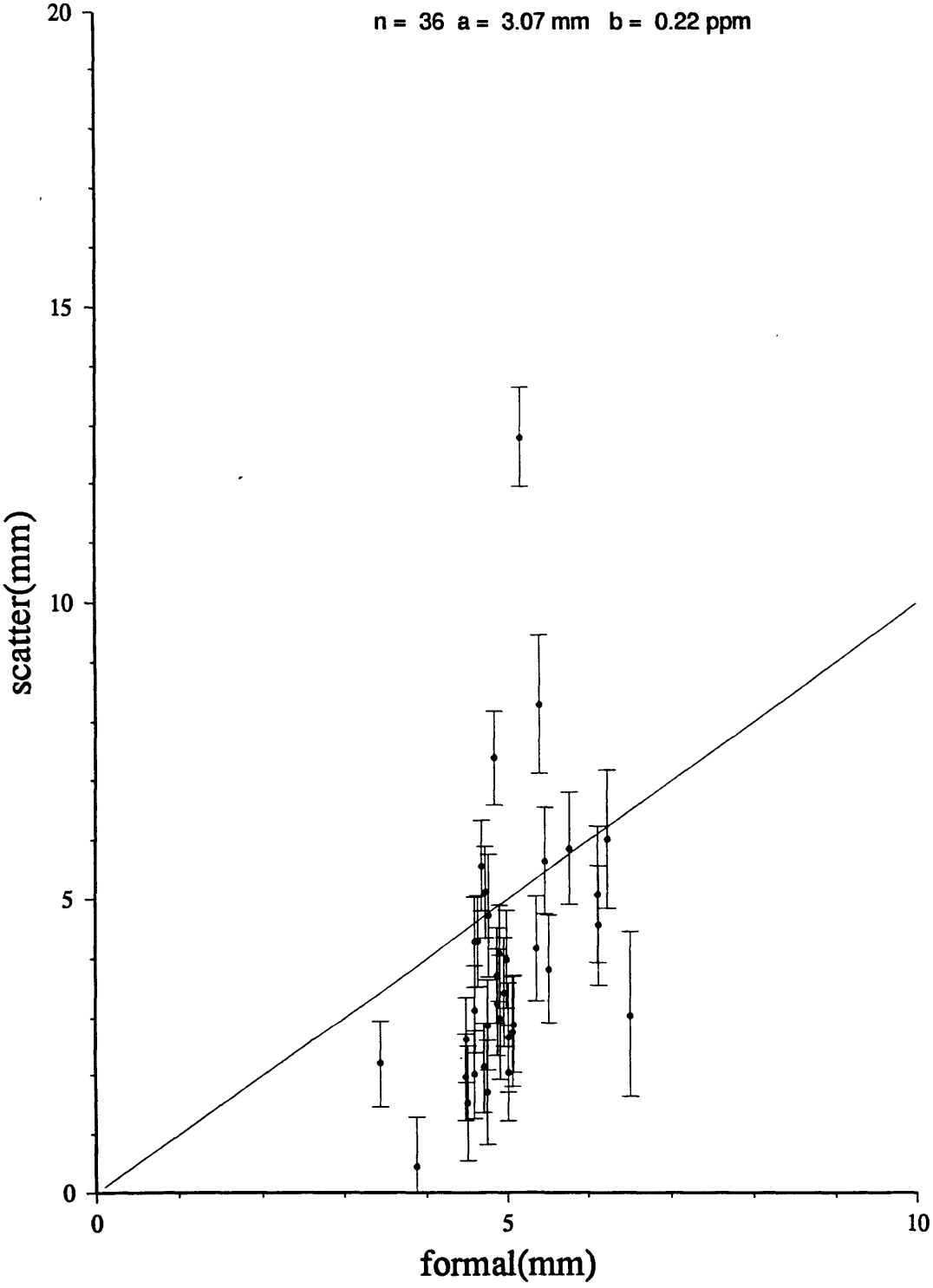

Figure 3b. Scatters of the trilateration data of the USGS Carrizo – San Luis trilateration network. The formal errors and best-fit coefficients are as described in Figure 3a.

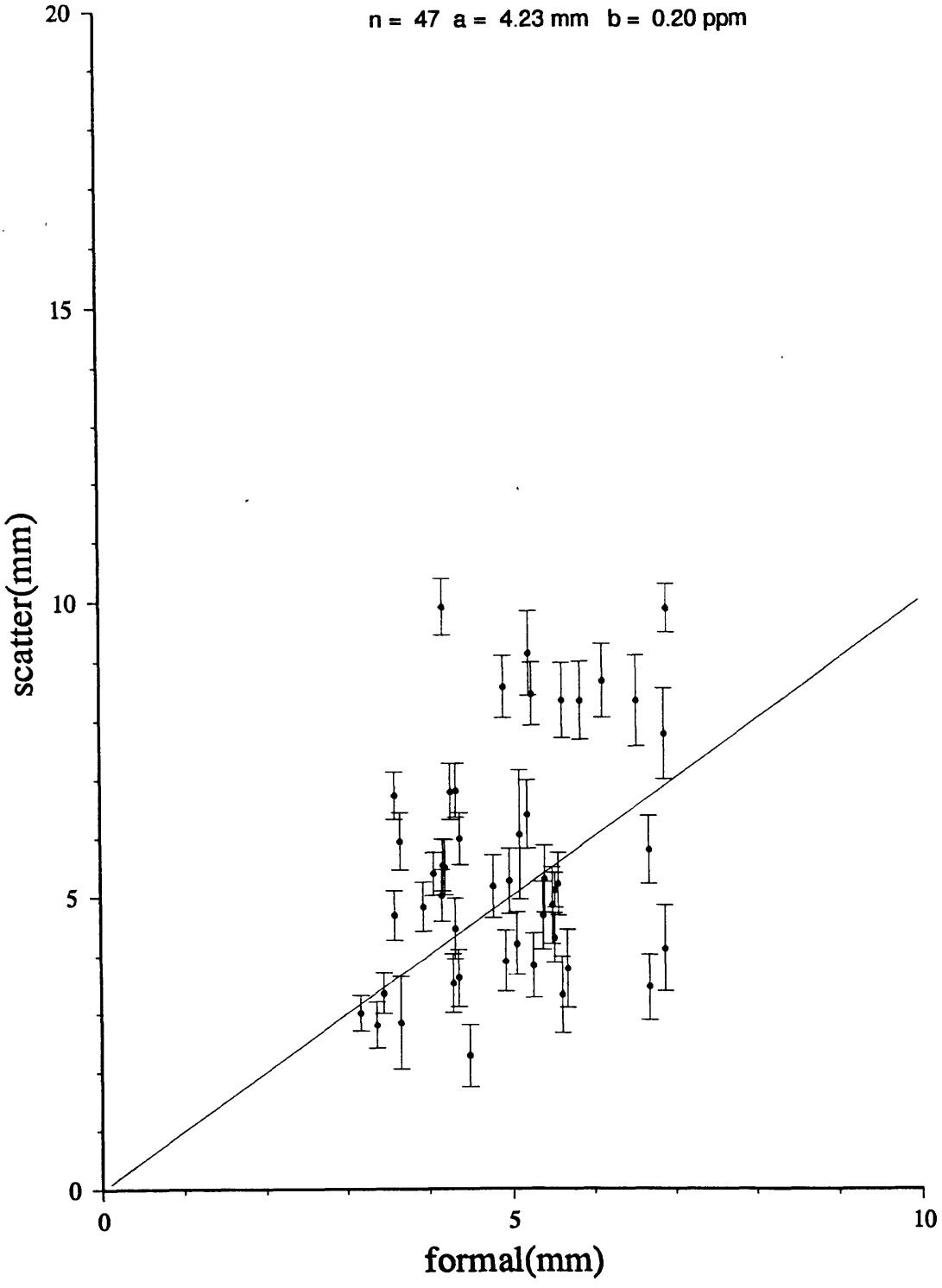

Figure 3c. Scatters of the trilateration data of the USGS Los Padres - Tehachapi trilateration network. The formal errors and best-fit coefficients are as described in Figure 3a.

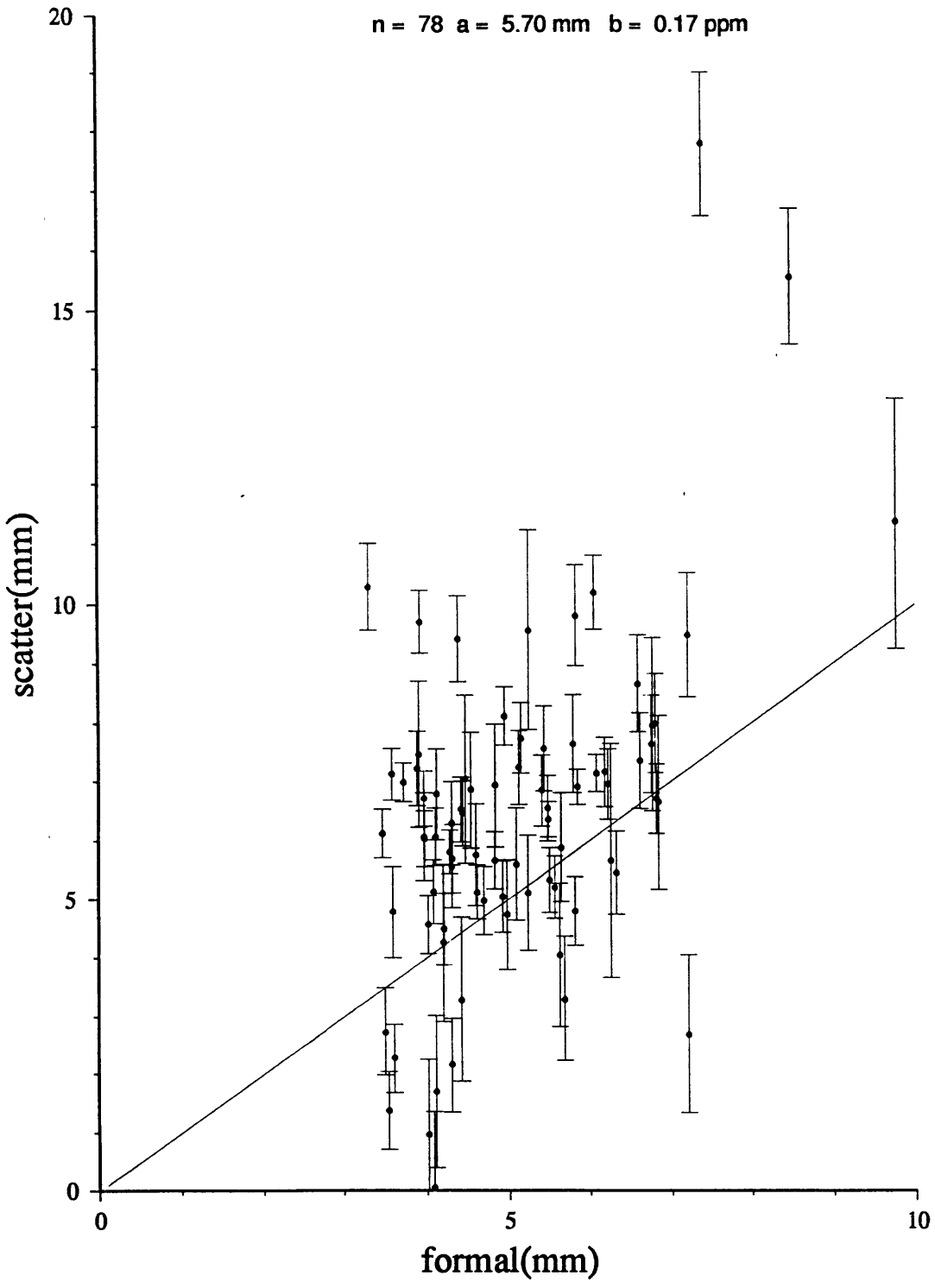

Figure 3d. Scatters of the trilateration data of the USGS San Gabriel - Tehachapi trilateration network. The formal errors and best-fit coefficients are as described in Figure 3a.

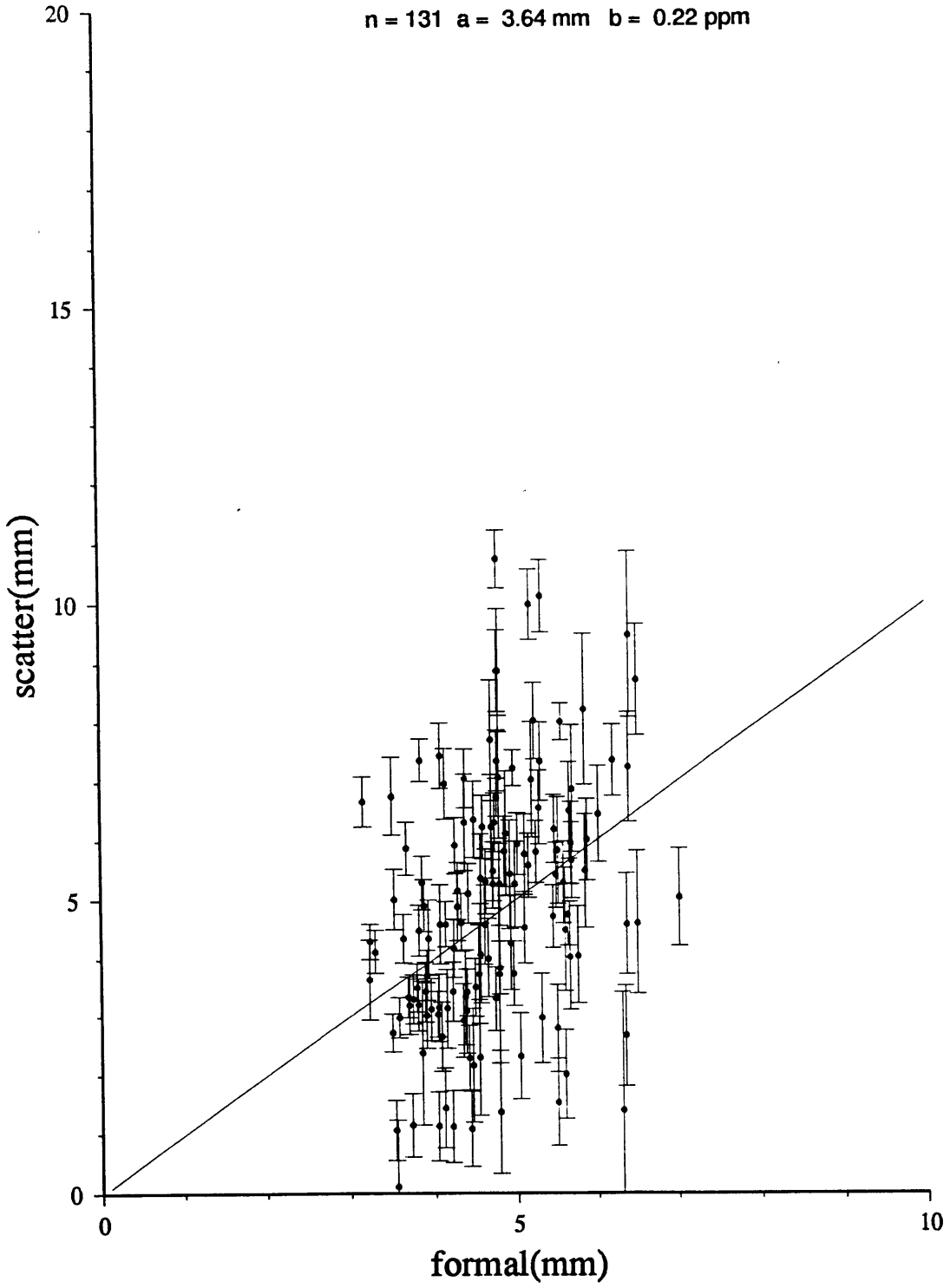

Figure 3e. Scatters of the trilateration data of the USGS Anza - Joshua trilateration network. The formal errors and best-fit coefficients are as described in Figure 3a.

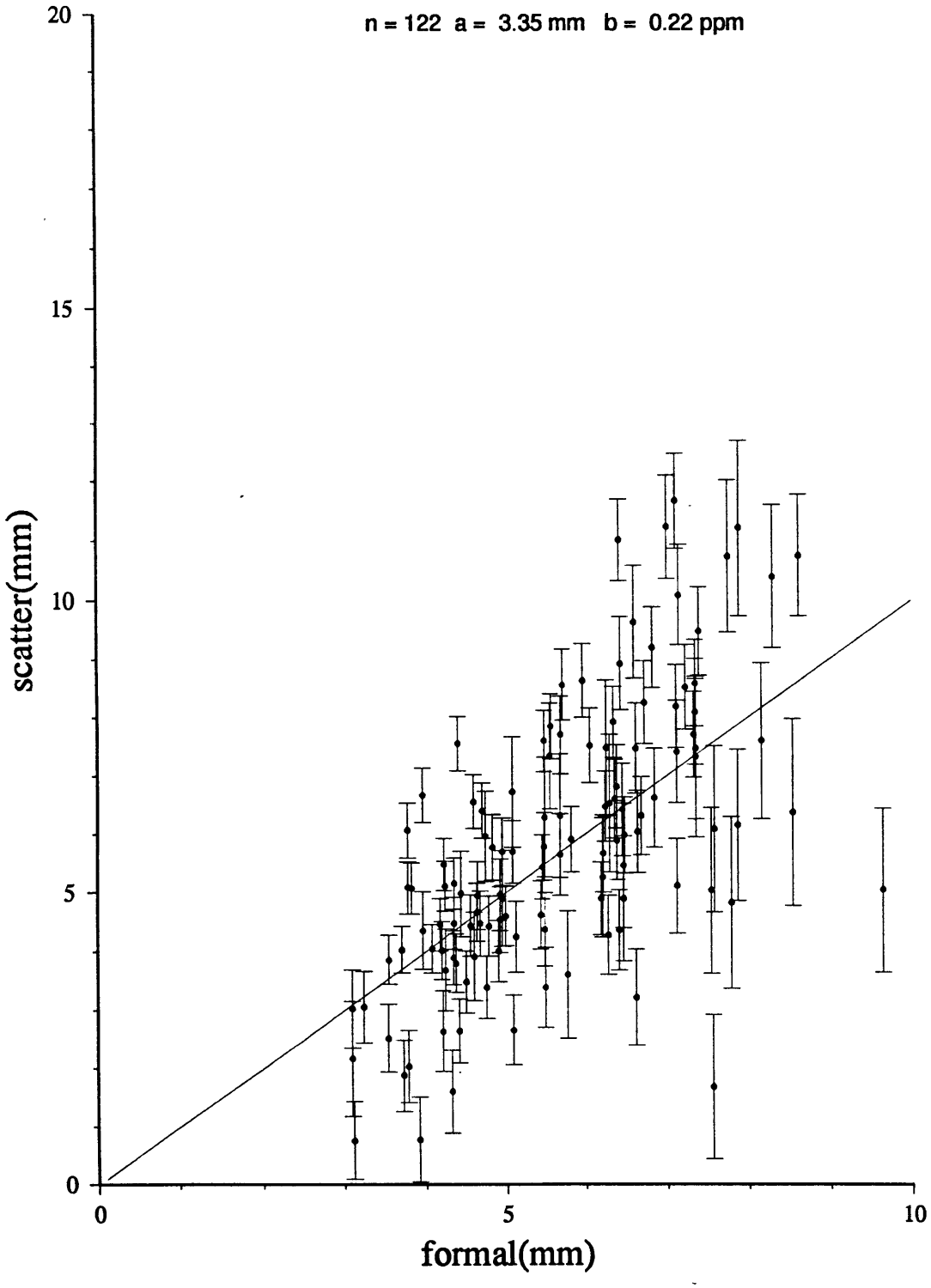

Figure 3f. Scatters of the trilateration data of the USGS Salton - Mexicali trilateration network. The formal errors and best-fit coefficients are as described in Figure 3a.

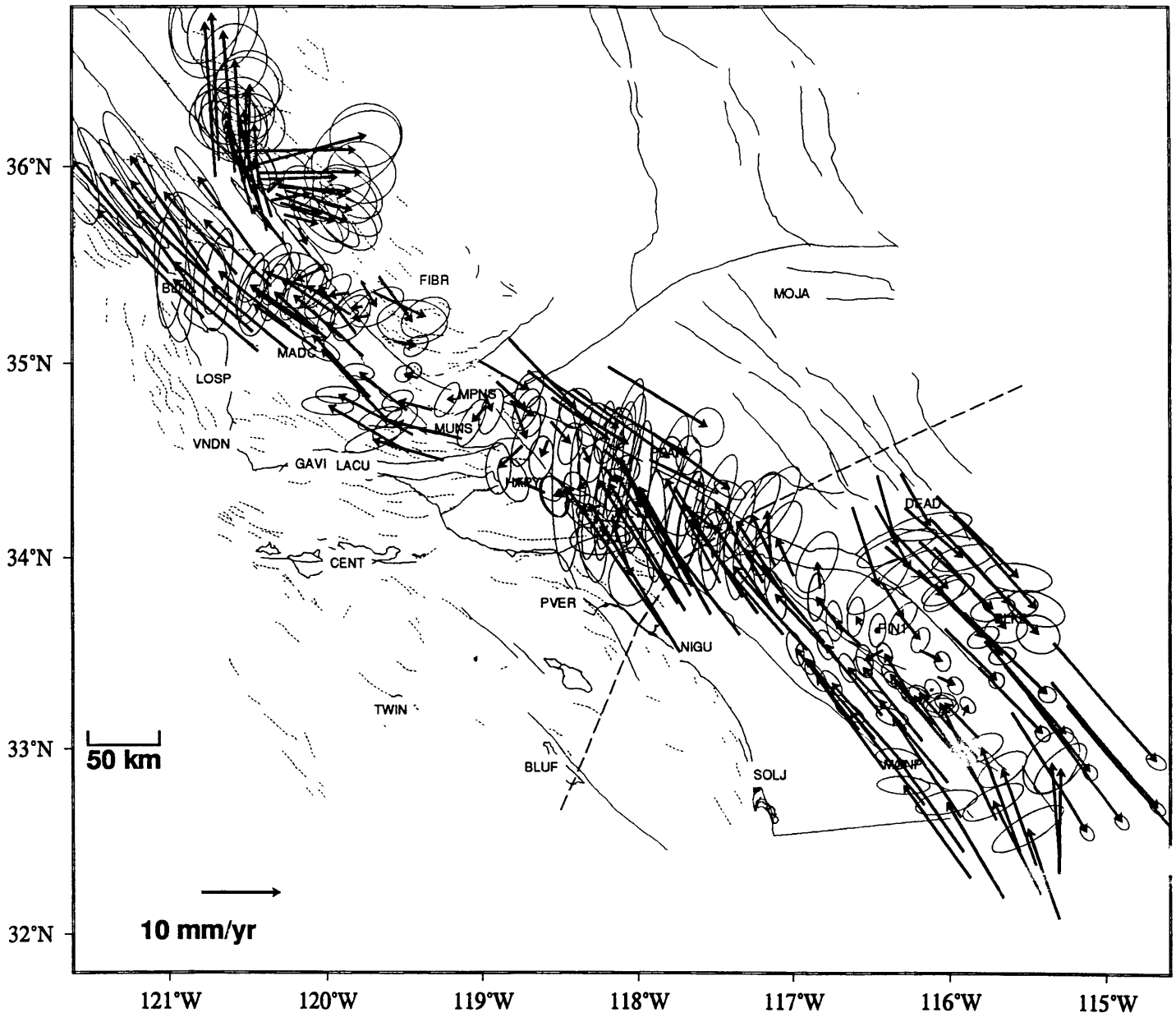

Figure 4. Constrained velocity solutions of the northern and southern sections. All imposed constraints are listed in Table 6. The two solutions are independent, and are separated by a heavy dashed line in this plot. The error ellipses represent 39% confidence level. In the northern section, the velocities are relative to the site Pattiway (N37° 58', W119° 26'). In the southern section, the velocities are relative to site Asbestos (N33° 38', W116° 28').

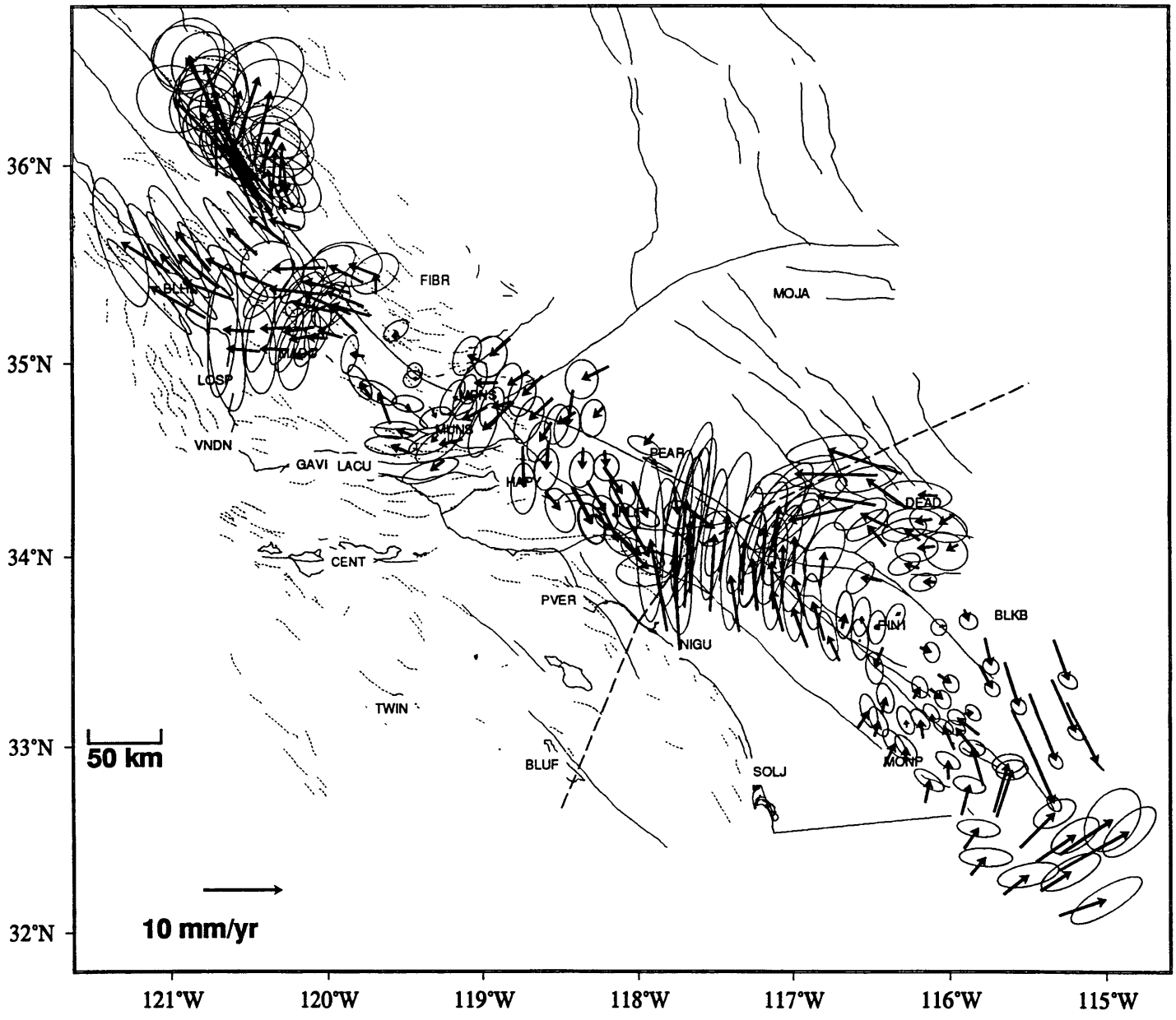

Figure 5. Same as Figure 4 but with the multi-dislocation model of *Feigl et al.* [1993] subtracted from the velocities for all sites.

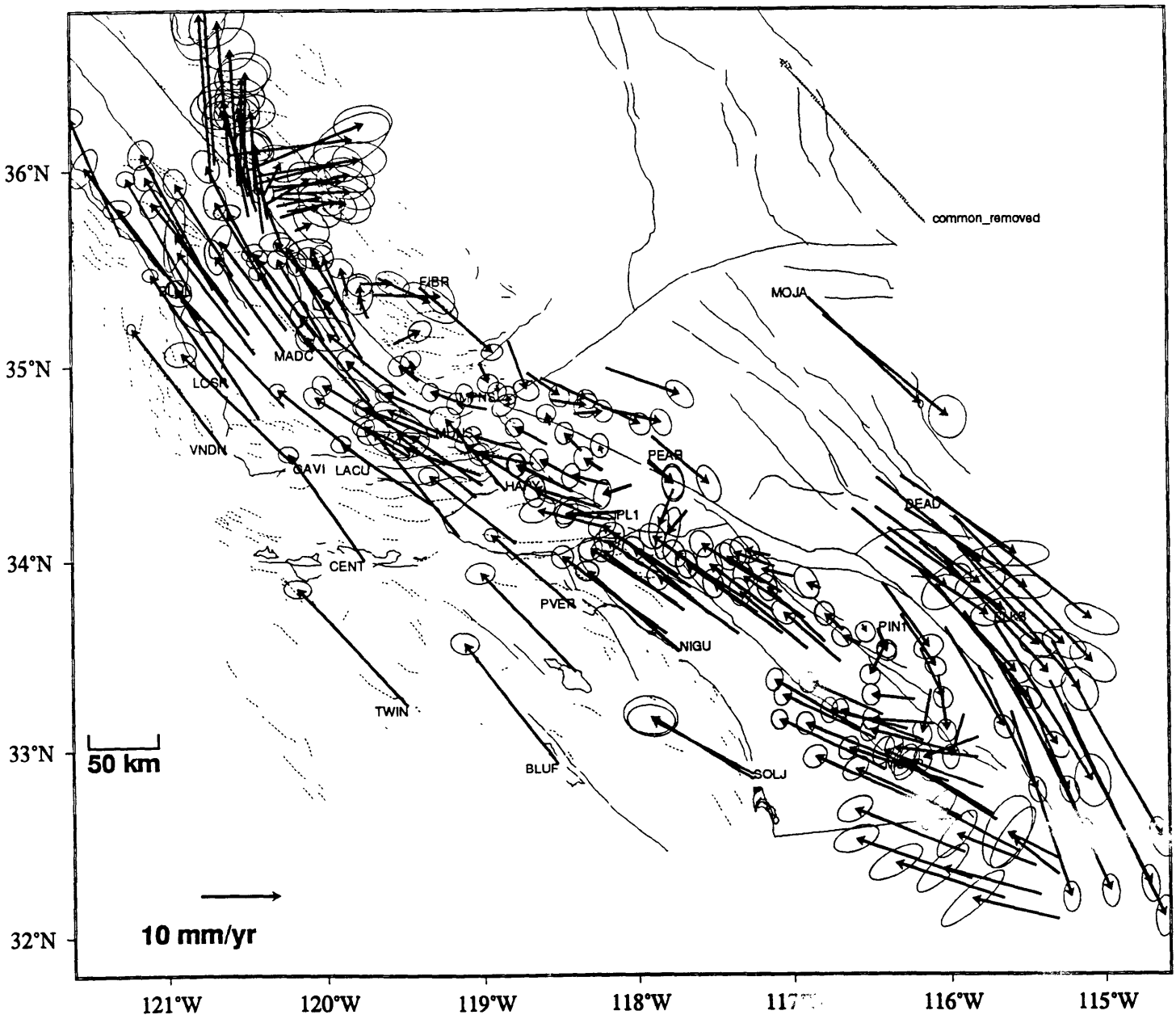

Figure 6. Velocity field of the combined solution with the velocity constraints on common sites listed in Table 7. The estimated velocity field is relative to the North America plate. In this plot, a common velocity (Ve = -18.2 mm/yr, Vn = 20.8 mm/yr) is subtracted from the velocities at all sites. This commonly subtracted velocity is plotted with a gray arrow at the northeastern corner of the figure. The error ellipses represent 39% confidence level.

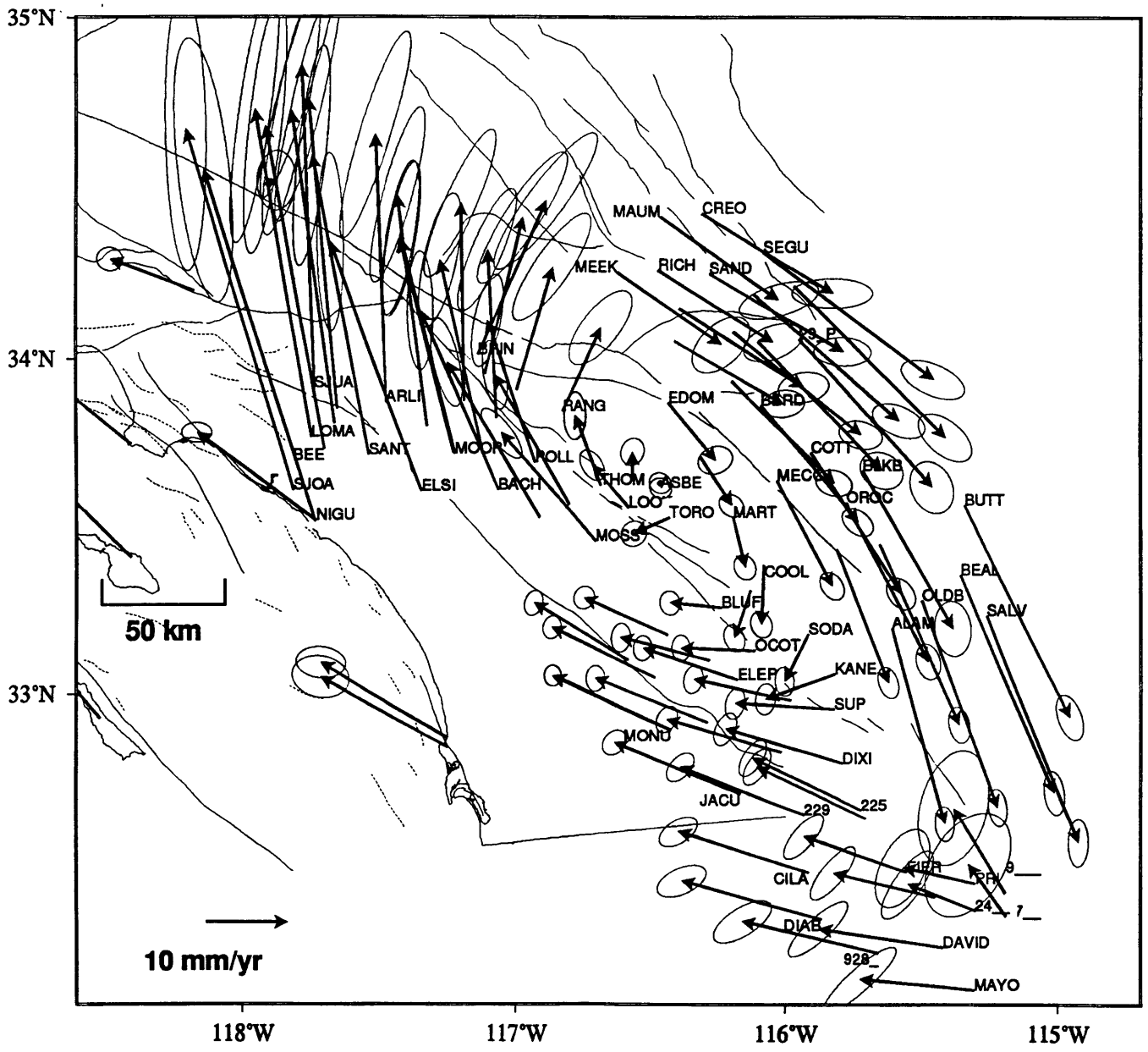

Figure 7a. Velocity fields of the combined solution in the southern section with the velocity constraint between Niguel and NIGU_GPS removed. The velocities are relative to site Asbestos (N33° 38', W116° 28').

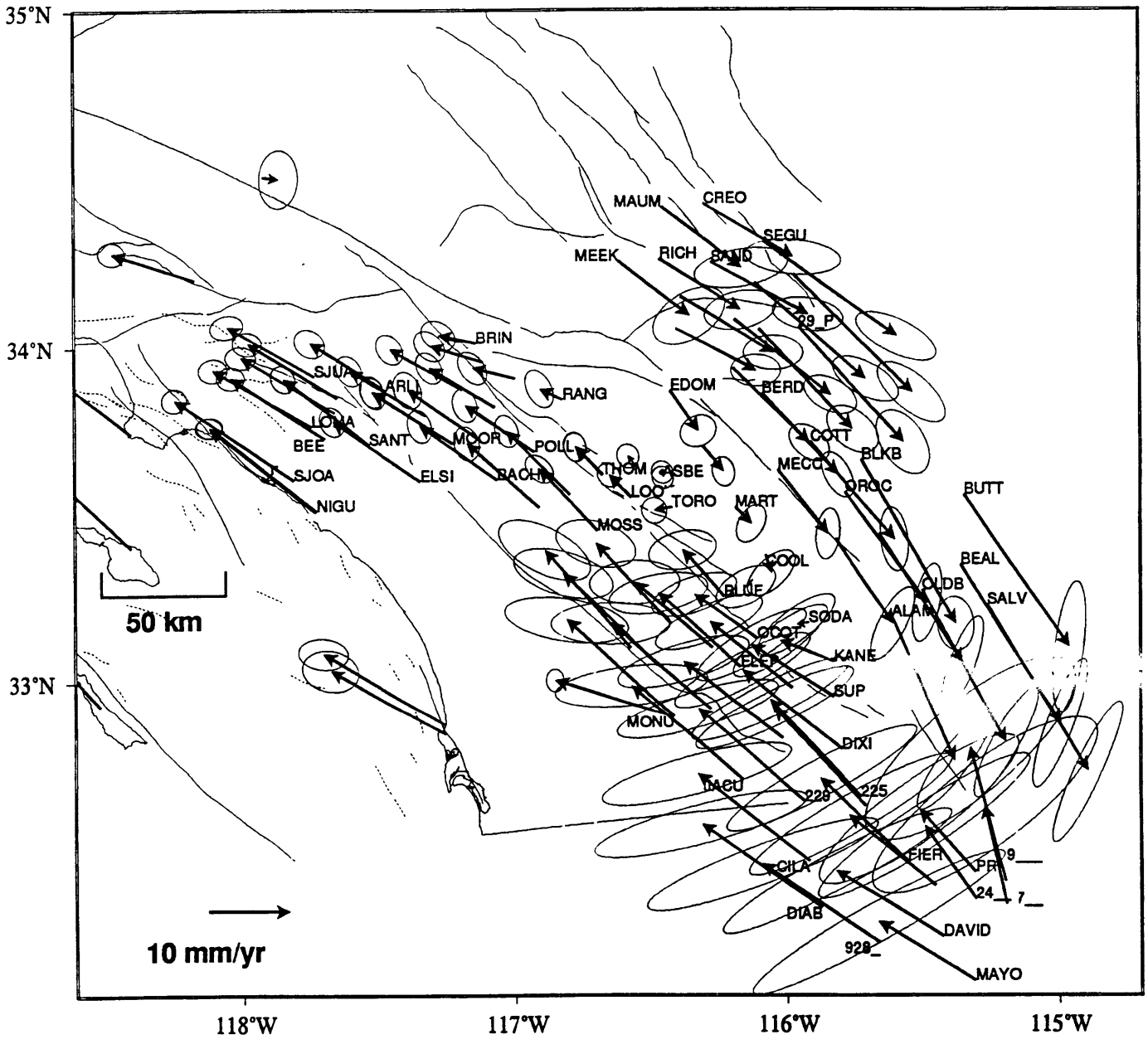

Figure 7b. Velocity fields of the combined solution in the southern section with the velocity constraint between Monu_res and MONP7274 removed. The velocities are relative to site Asbestos (N33° 38', W116° 28').

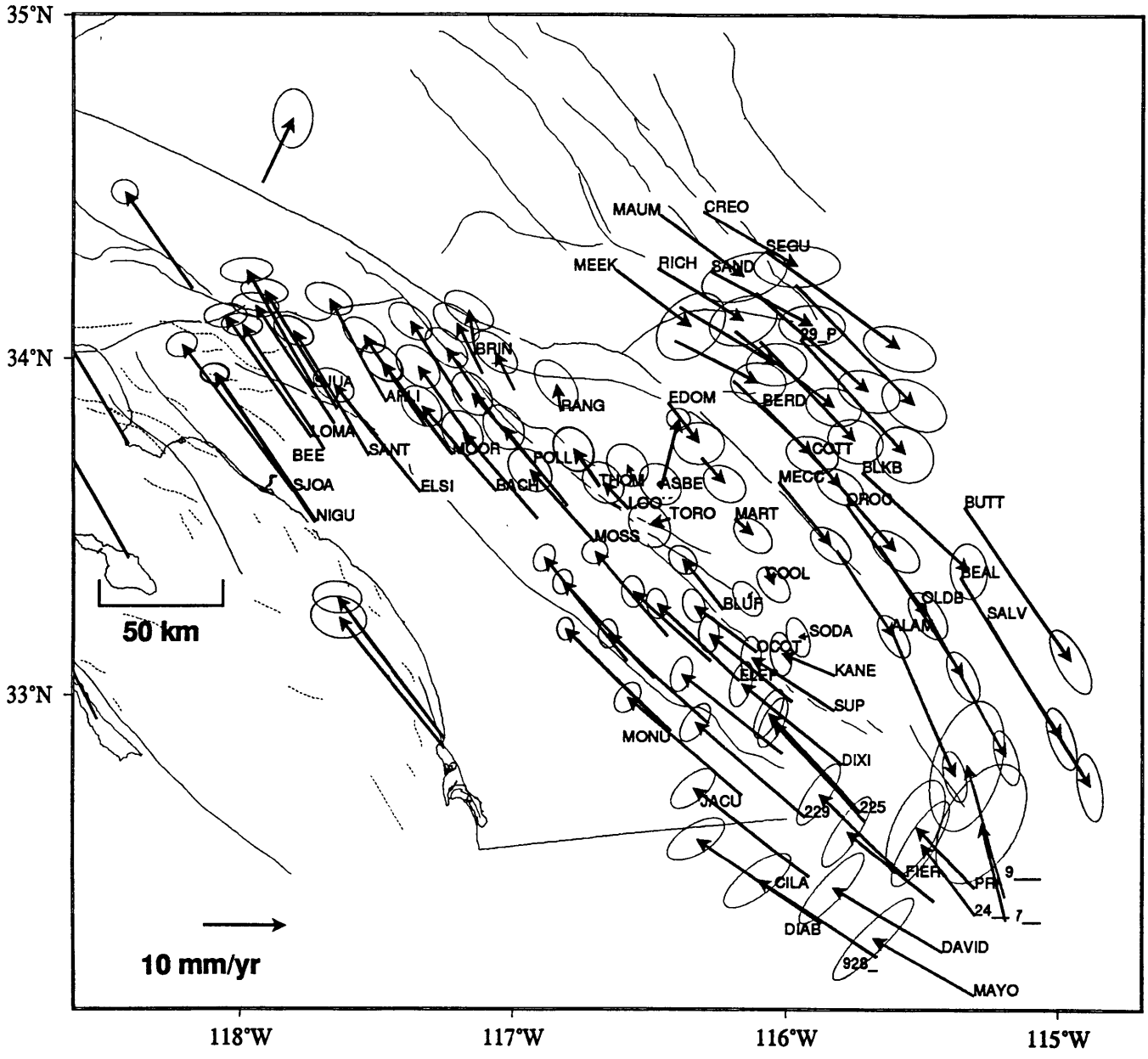

Figure 7c. Velocity fields of the combined solution in the southern section with the velocity constraint between Asbestos and PINY_GPS removed. The velocities are relative to site Asbestos (N33° 38', W116° 28').

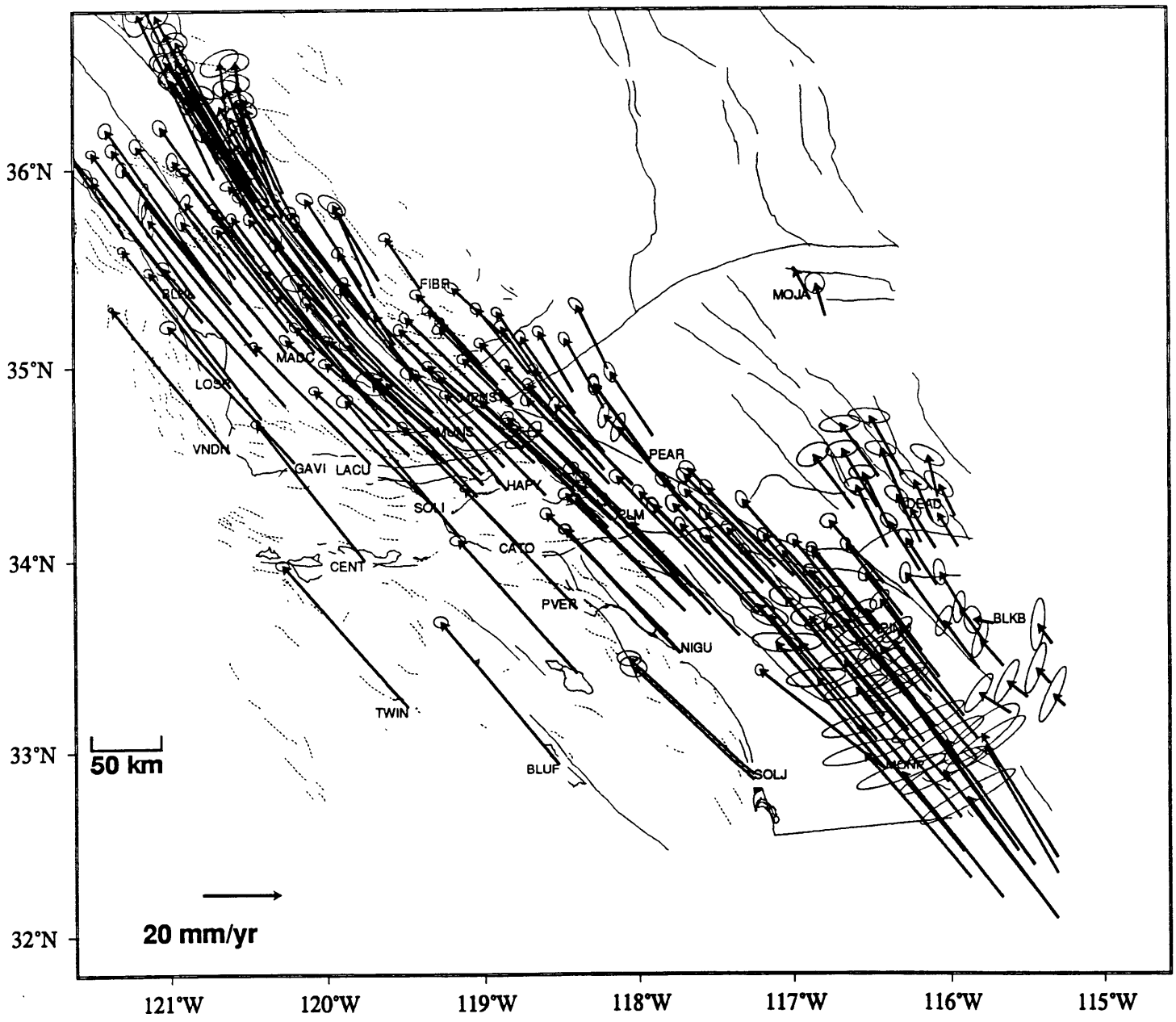

Figure 8a. Velocity field relative to the North American plate of the combined solution with the velocity constraints listed in Table 7 (final status: used). The error ellipses represent 39% confidence level.

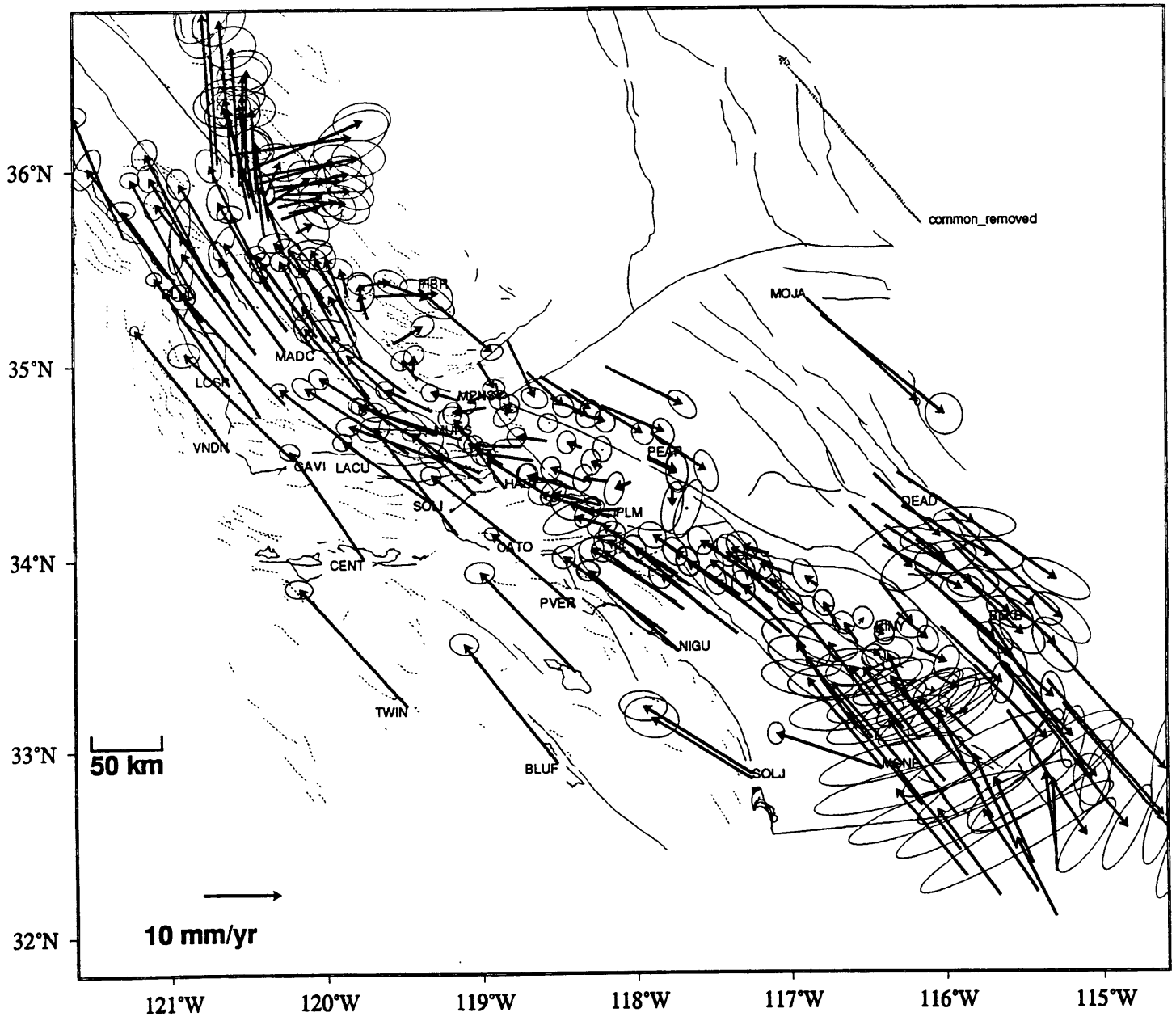

Figure 8b. Same as Figure 8a but with a common velocity (Ve = -18.2 mm/yr, Vn = 20.8 mm/yr) subtracted from the velocities at all sites. This commonly subtracted velocity is plotted with gray arrow at the northeastern corner of the figure.

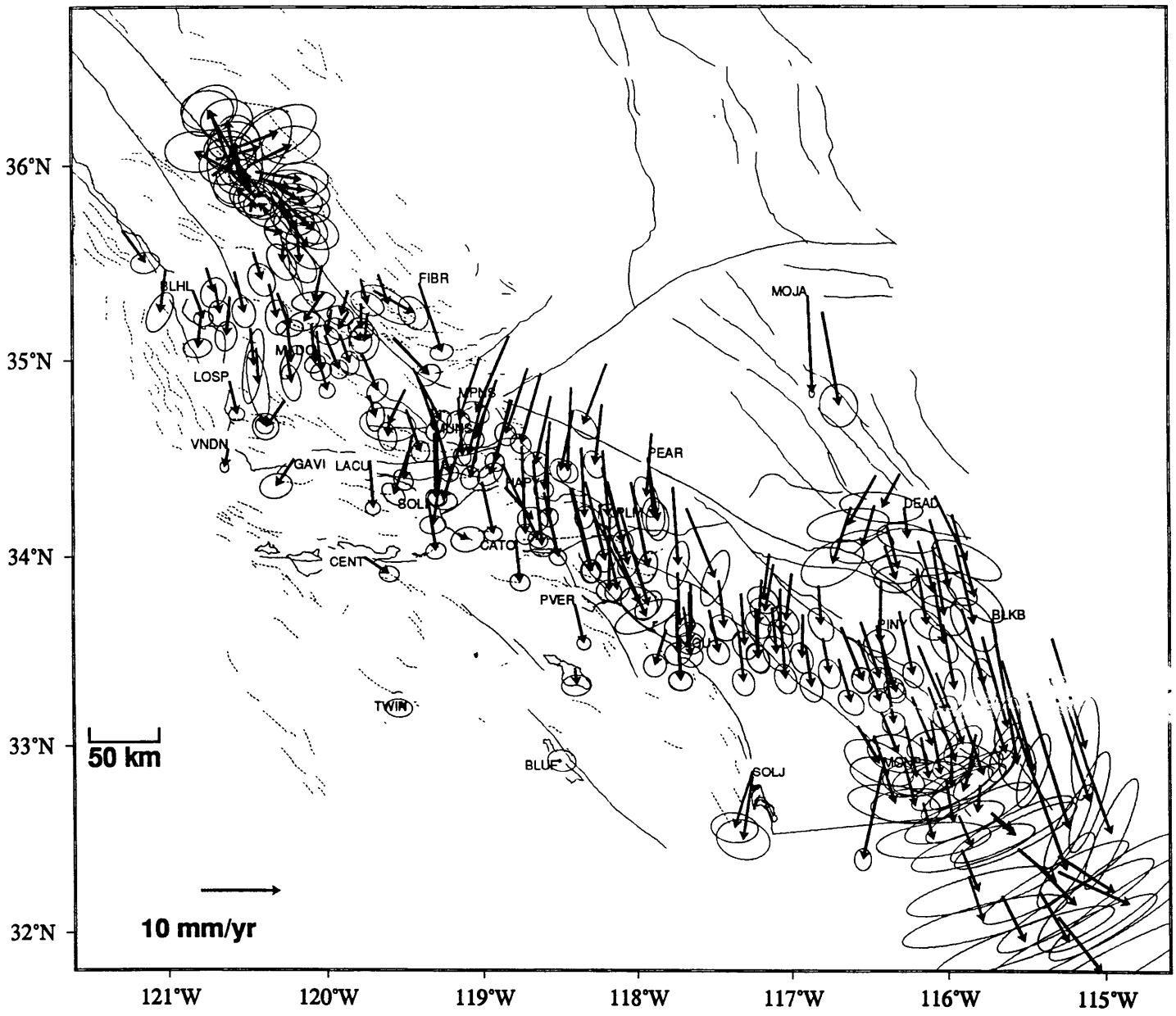

Figure 9a. Velocity residuals with respect to the Pacific Plate of the combined solution with the multi-dislocation model of *Feigl et al* [1993] removed. The error ellipses represent 39% confidence.

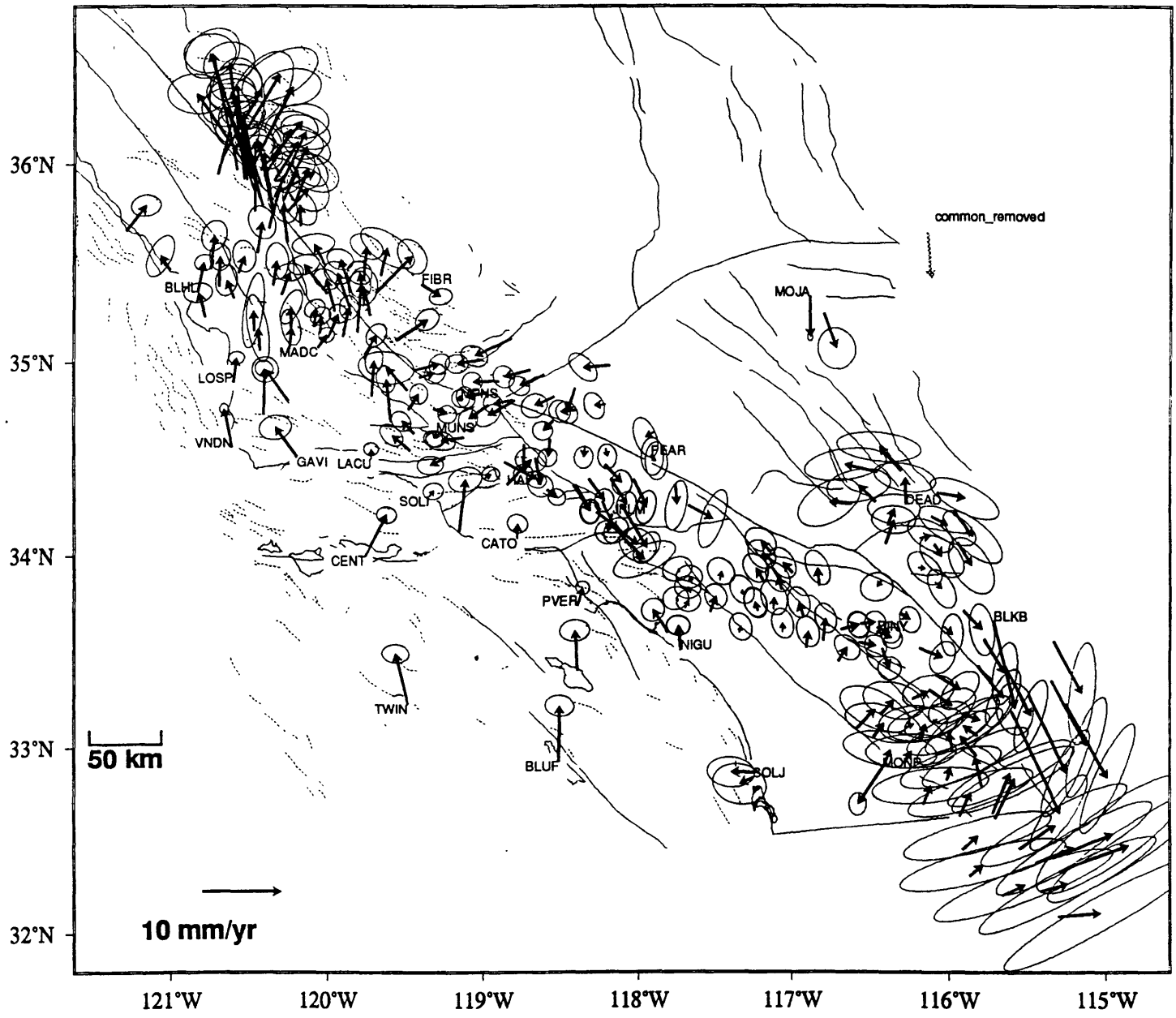

Figure 9b. Same as Figure 9a but with a common velocity residual relative to Pacific plate (Ve = 0.5 mm/yr, Vn = -7.1 mm/yr) subtracted from the velocities at all sites. This commonly subtracted velocity residual is plotted with a gray arrow at the northeastern corner of the figure. The velocity residuals are shown relative to site MPNS_GPS near the SAF.

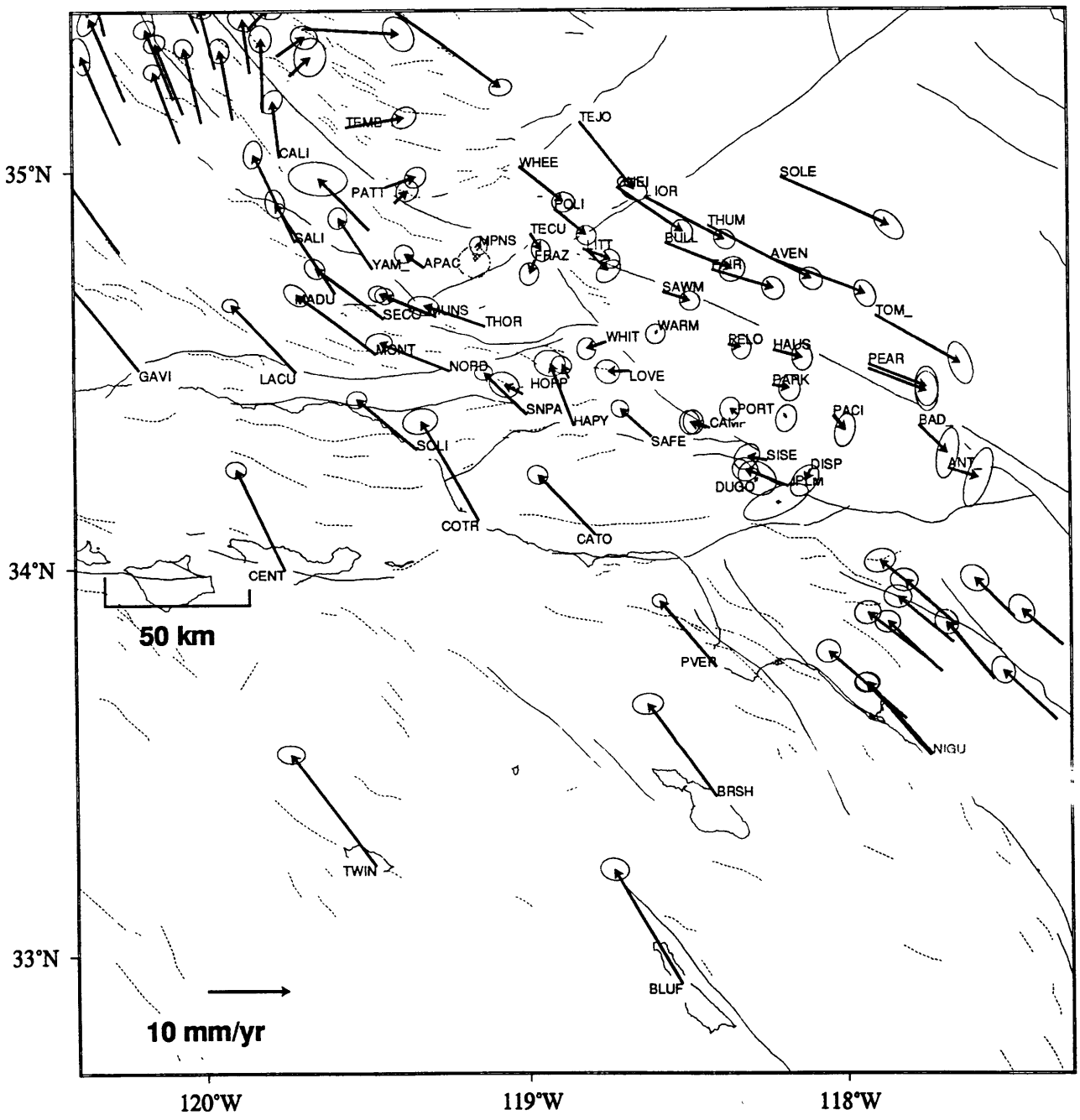

Figure 10a. Enlargement of the combined velocity field for the Big Bend area. relative to site MPNS. The error ellipses represent 39% confidence level.

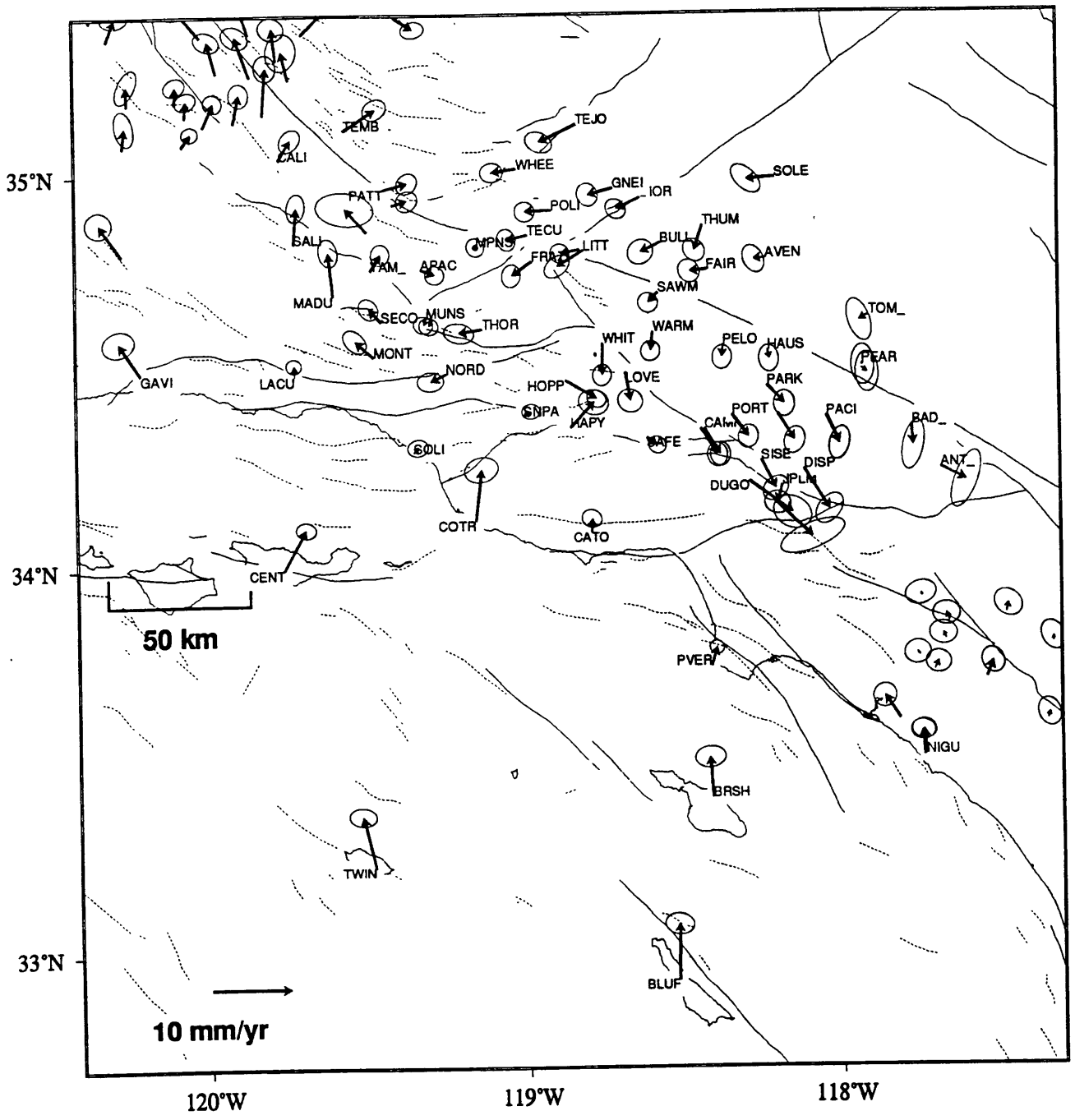

Figure 10b. Same as Figure 10a but with the dislocation model of *Feigl et al.* [1993] removed.

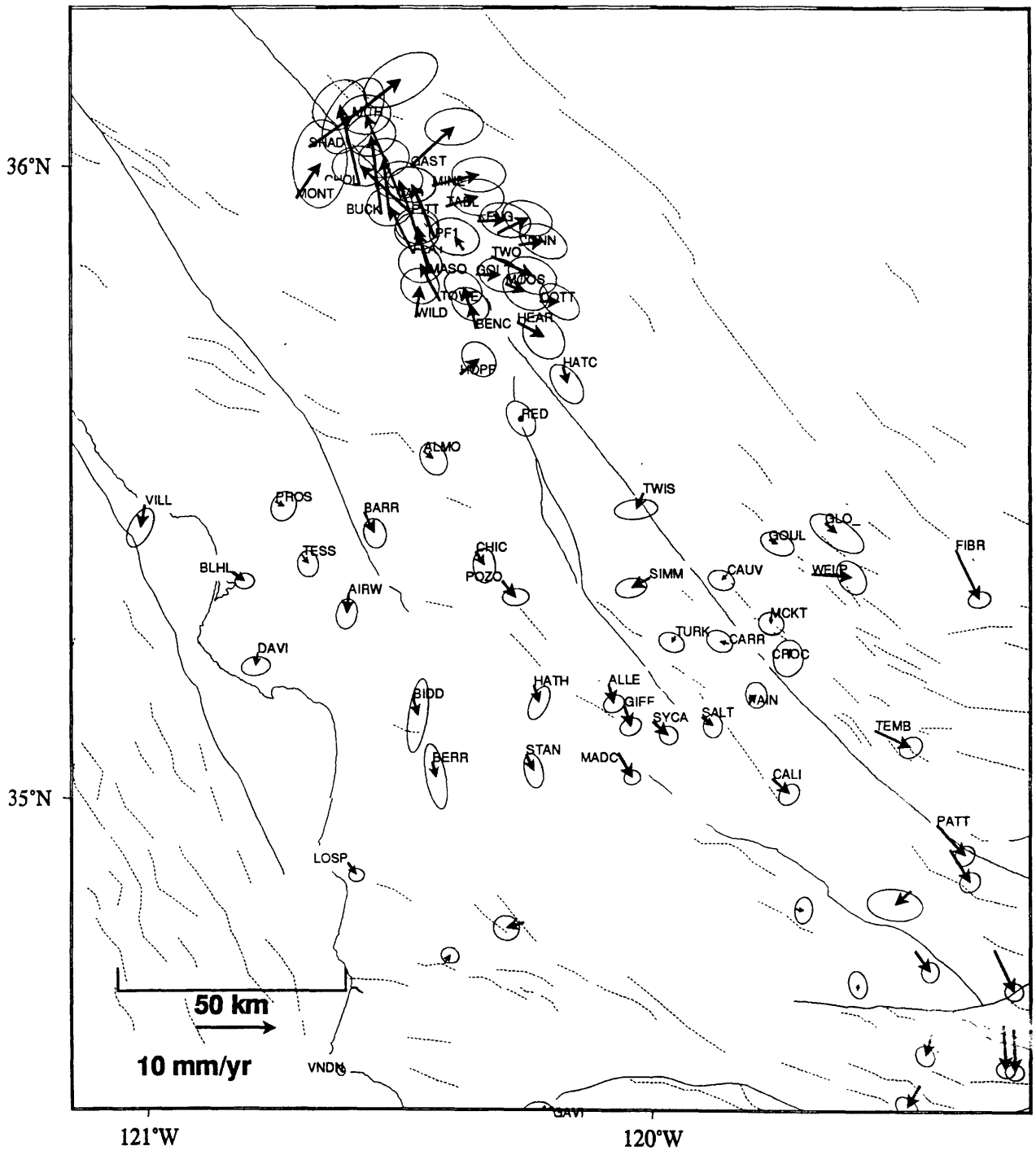

Figure 11. Residual velocities relative to site Red Hill in the San Luis network.

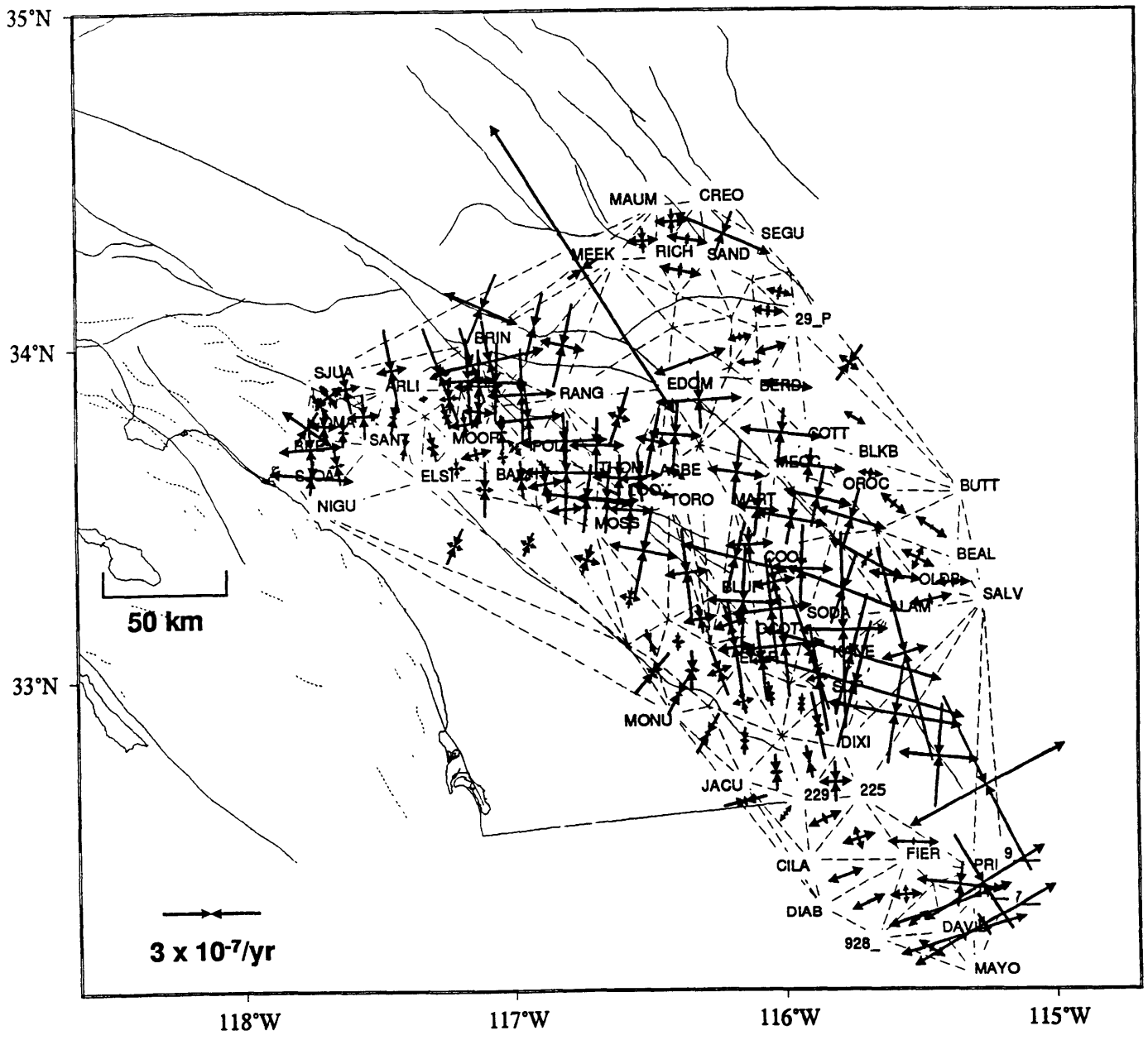

Figure 12a. Principal axes of the horizontal strain rate tensors in each Delaunay triangle of the southern section, calculated from the constrained velocity solution of Figure 4. The inward pointing arrows represent compression, outward pointing arrows represent extension. In each Delaunay triangle, if both principal strain rates are smaller in magnitude than their uncertainties, or if the sum of the magnitudes of the two principal strain rates is larger than 2×10^{-6}, the axes are not plotted.

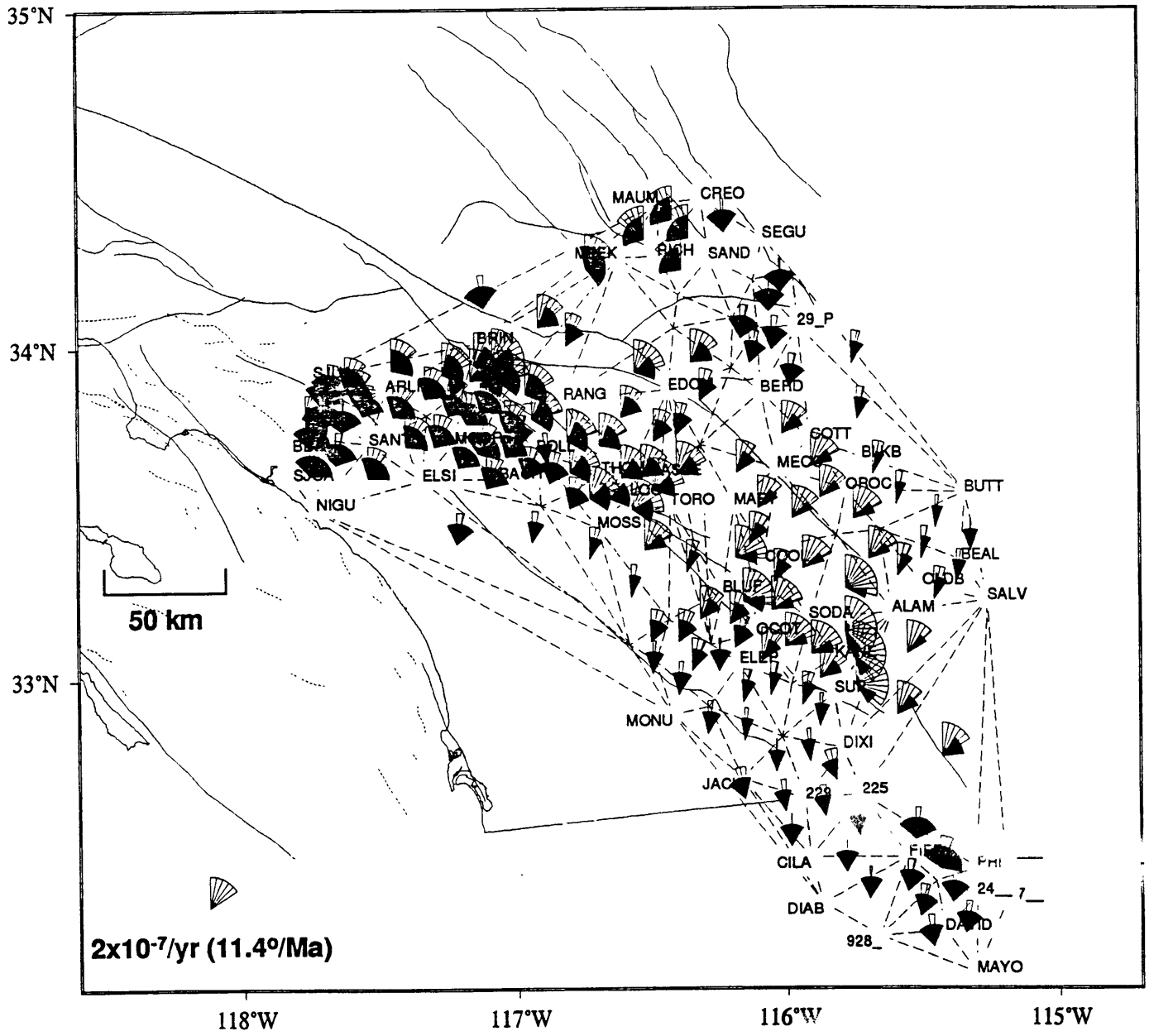

Figure 12b. Rotation rates in each Delaunay triangle of the southern section, calculated from the constrained velocity solution of Figure 4. The fans display clockwise or anticlockwise rotations from north. In each Delaunay triangle, if the uncertainty on the rotation rate exceeds 10°/Ma, the rotation rate is not plotted.

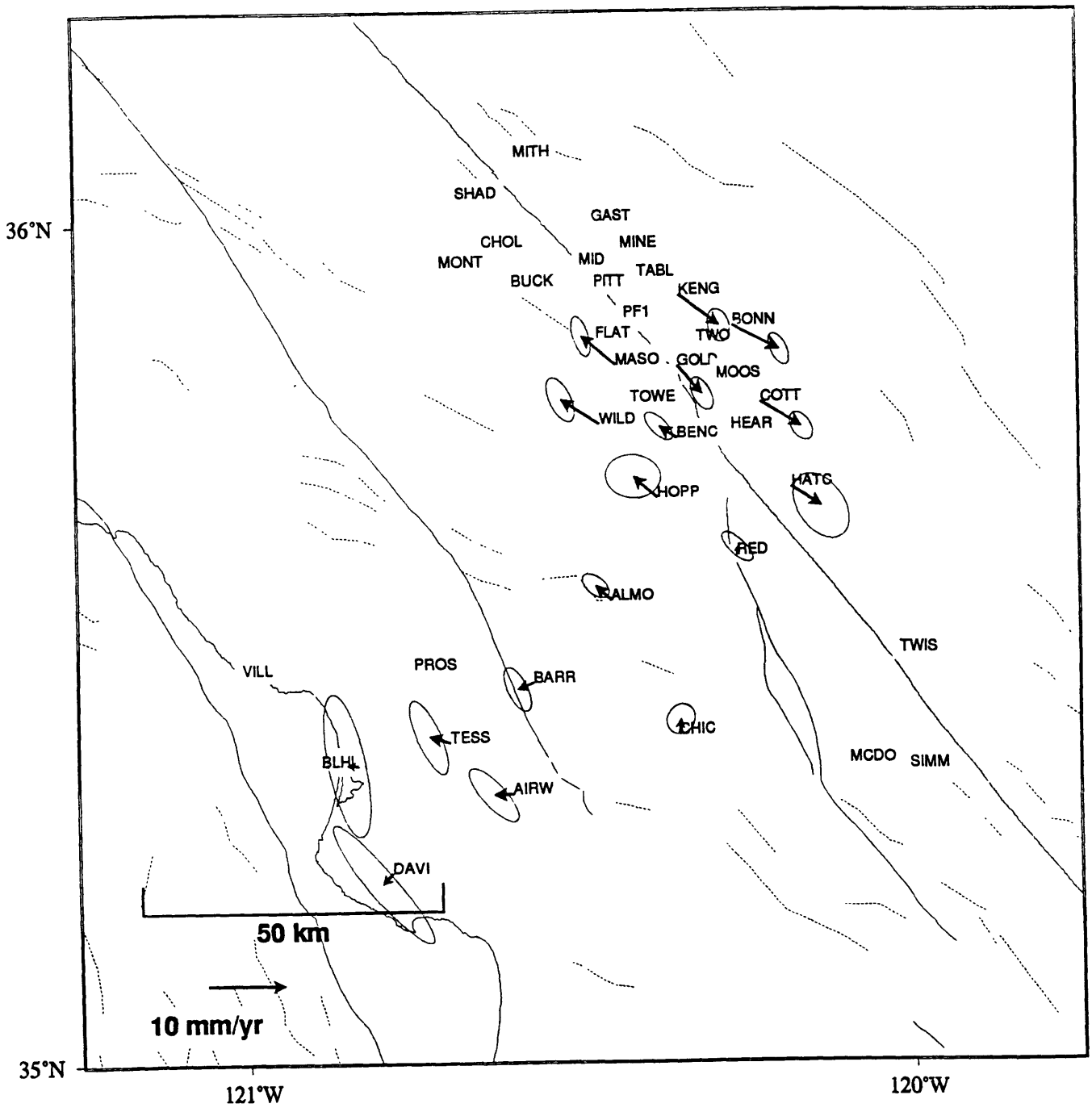

Figure 13a. Outer coordinate solution for the San Luis subnetwork using the USGS EDM data from 1980 to 1991. The sites are the same as used by *Harris and Segall* [1987]. The error ellipses represent 39% confidence level.

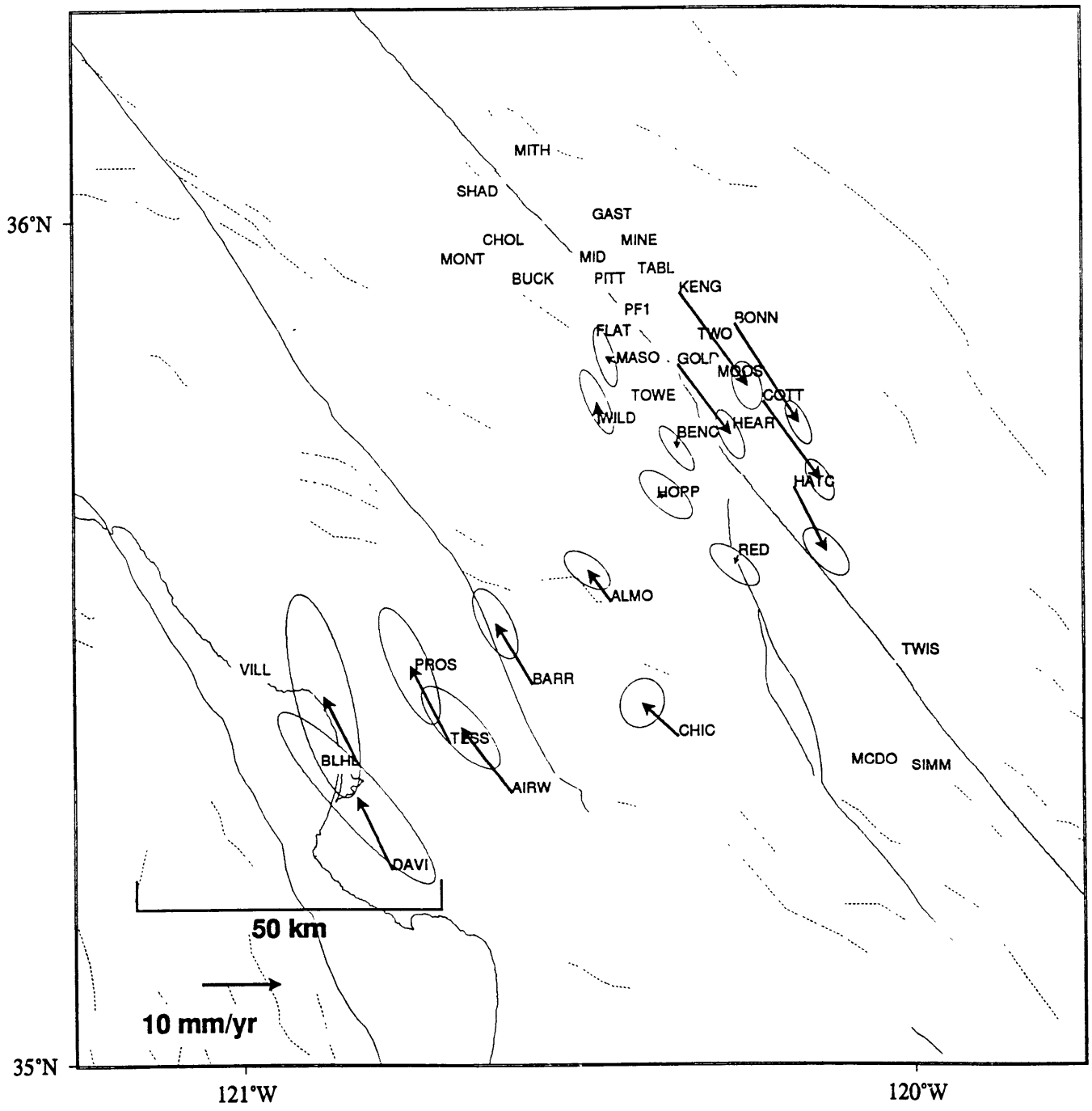

Figure 13b. Same as Figure 13a but using the CDMG data from the 1970's and the USGS from only 1980 to 1984.

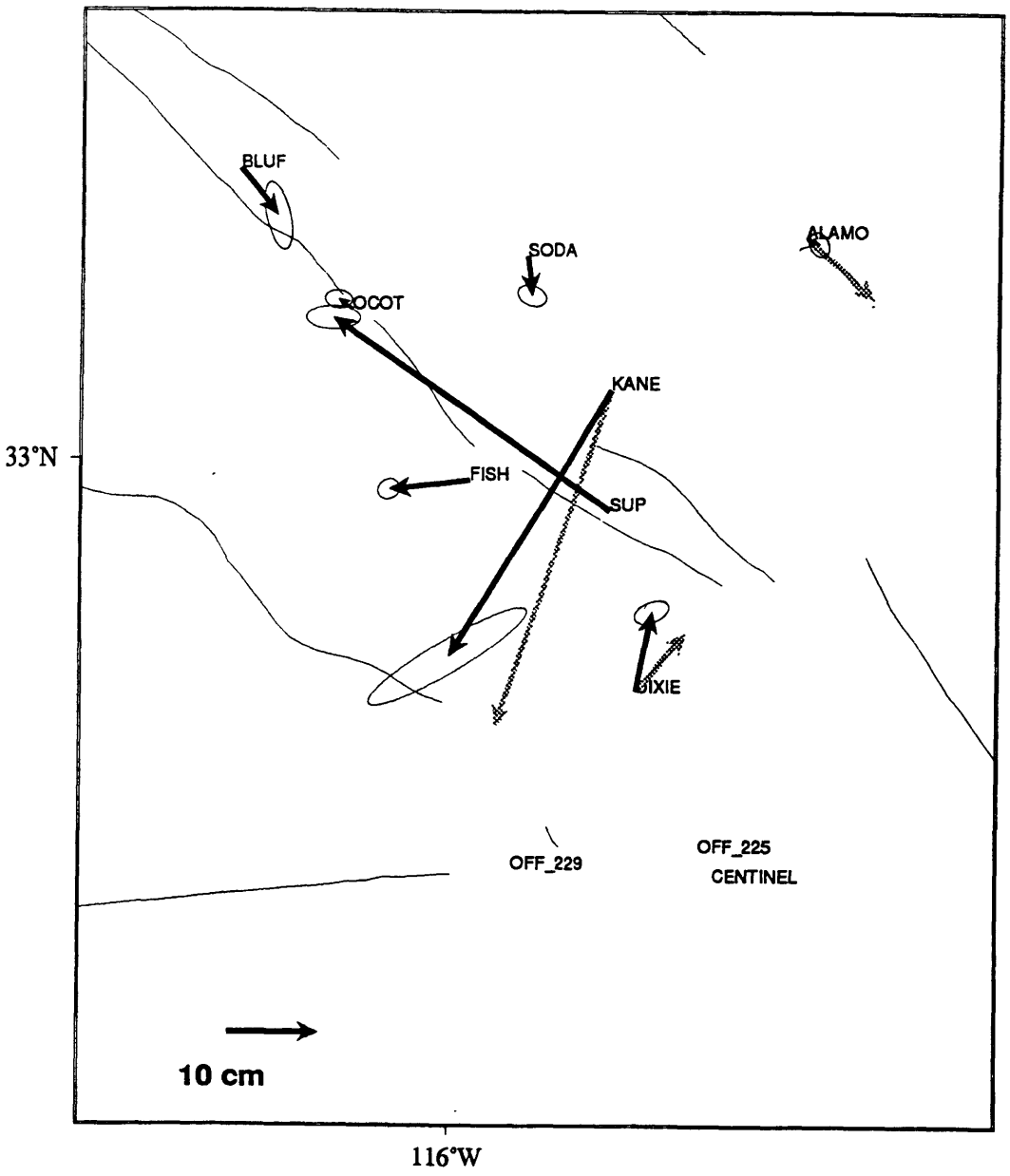

Figure 14a. Estimated coseismic site displacements from the combined solution (Figure 8) for the 11/24/87 Superstition Hills earthquake sequence (M_s = 6.2, 6.6). The gray arrows at three sites (Kane, Dixie, and Alamo) represent the 1986-1988 displacements estimated by *Larsen et al.* [1992] but with the secular motion from our velocity solution removed. The error ellipses represent 95% confidence. The scaling arrows are shown in the lower left corner of the plot.

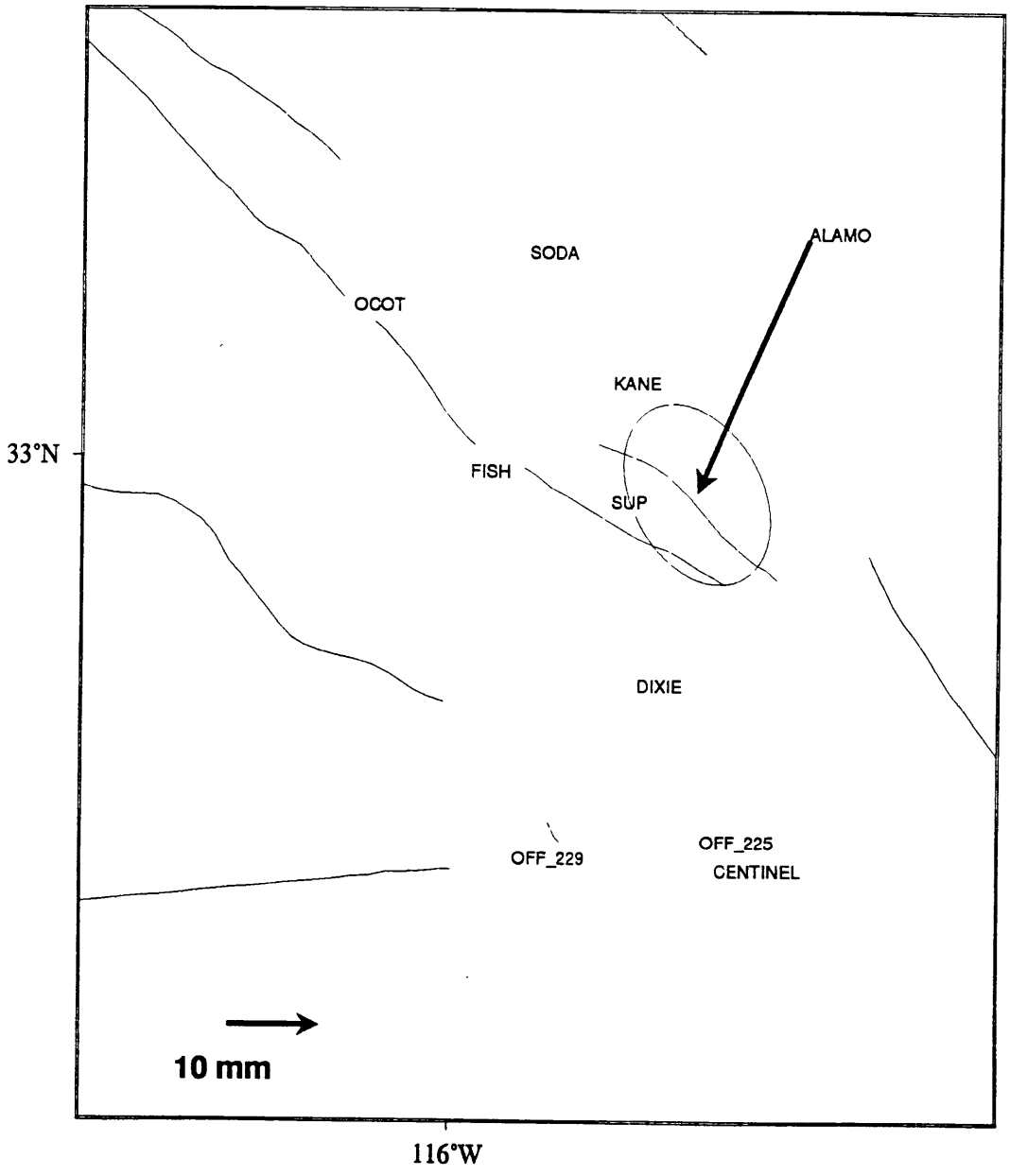

Figure 14b. Estimated coseismic site displacements from the combined solution (Figure 5) for the 04/26/81 Westmoreland earthquake (M_L = 5.7). The error ellipses represent 95% confidence. The scaling arrows are shown in the lower left corner of the plot.

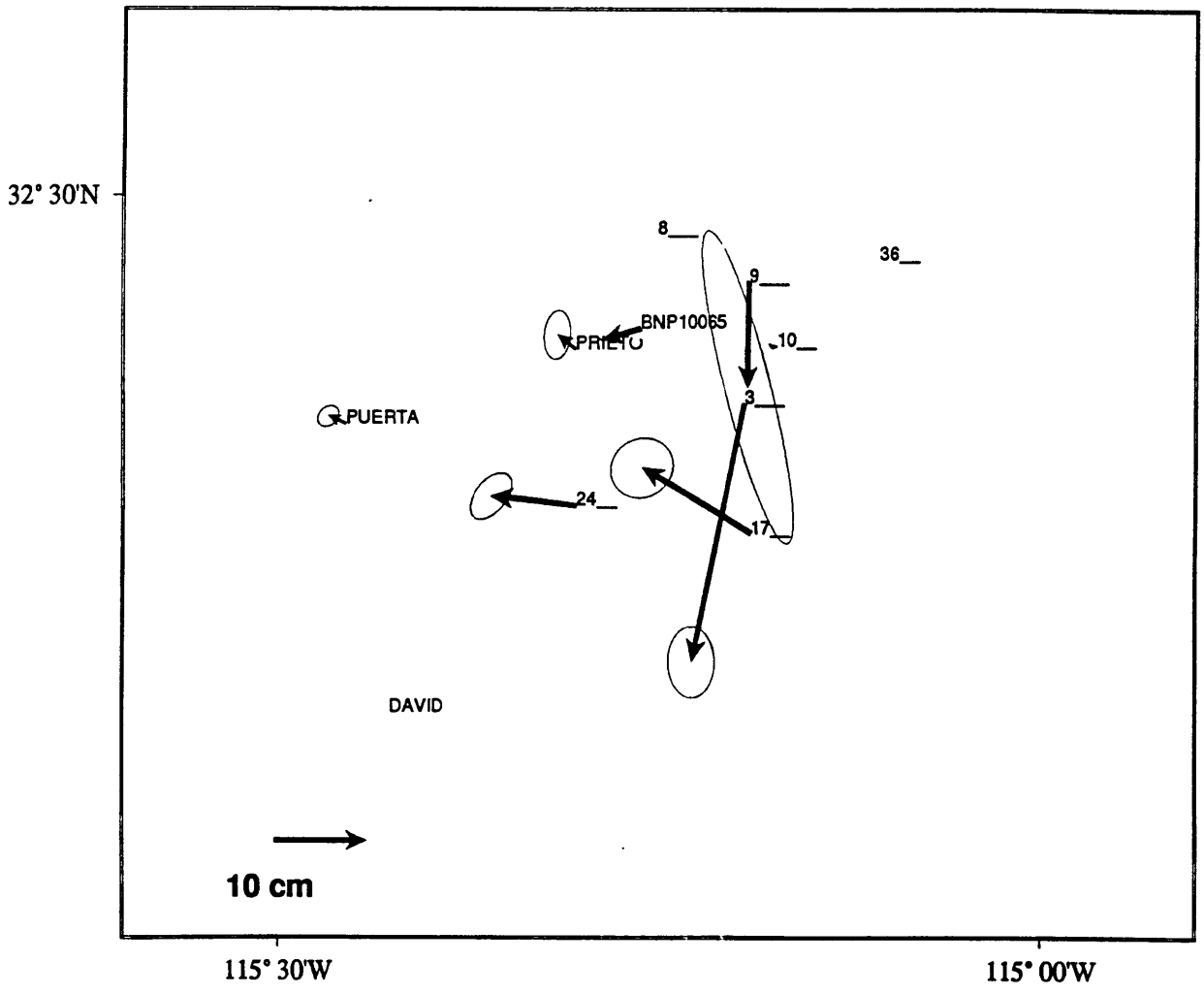

Figure 14c. Estimated coseismic site displacements from the combined solution (Figure 8) for the 10/14/79 Mexicali earthquake (M_L = 6.6) and 06/09/80 Victoria earthquake (M_L = 6.2). The error ellipses represent 95% confidence. The scaling arrows are shown in the lower left corner of the plot.

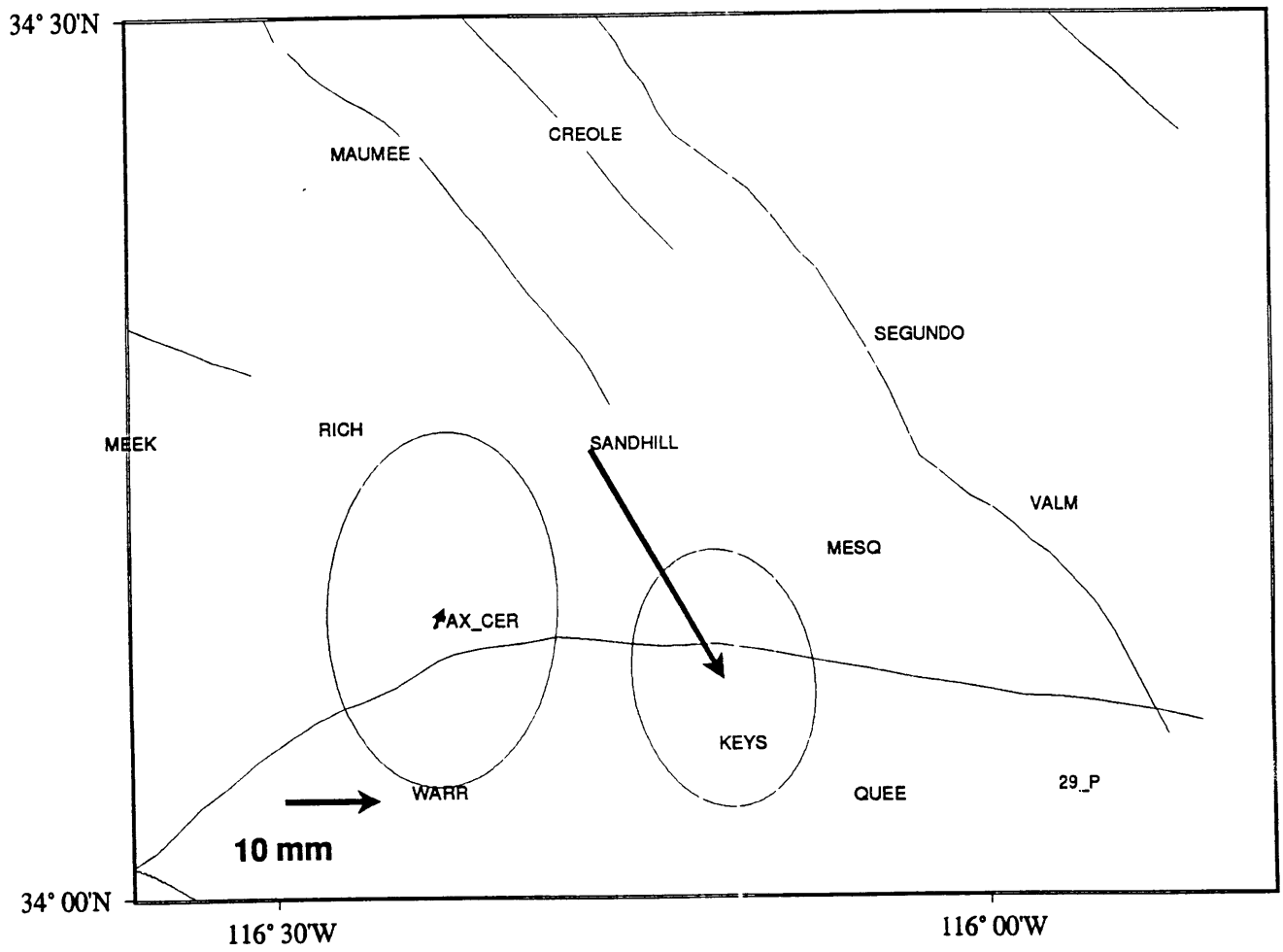

Figure 14d. Estimated coseismic site displacements from the combined solution (Figure 8) for the 03/15/79 Homestead Valley earthquake (M_s = 5.6). The error ellipses represent 95% confidence. The scaling arrows are shown in the lower left corner of the plot.

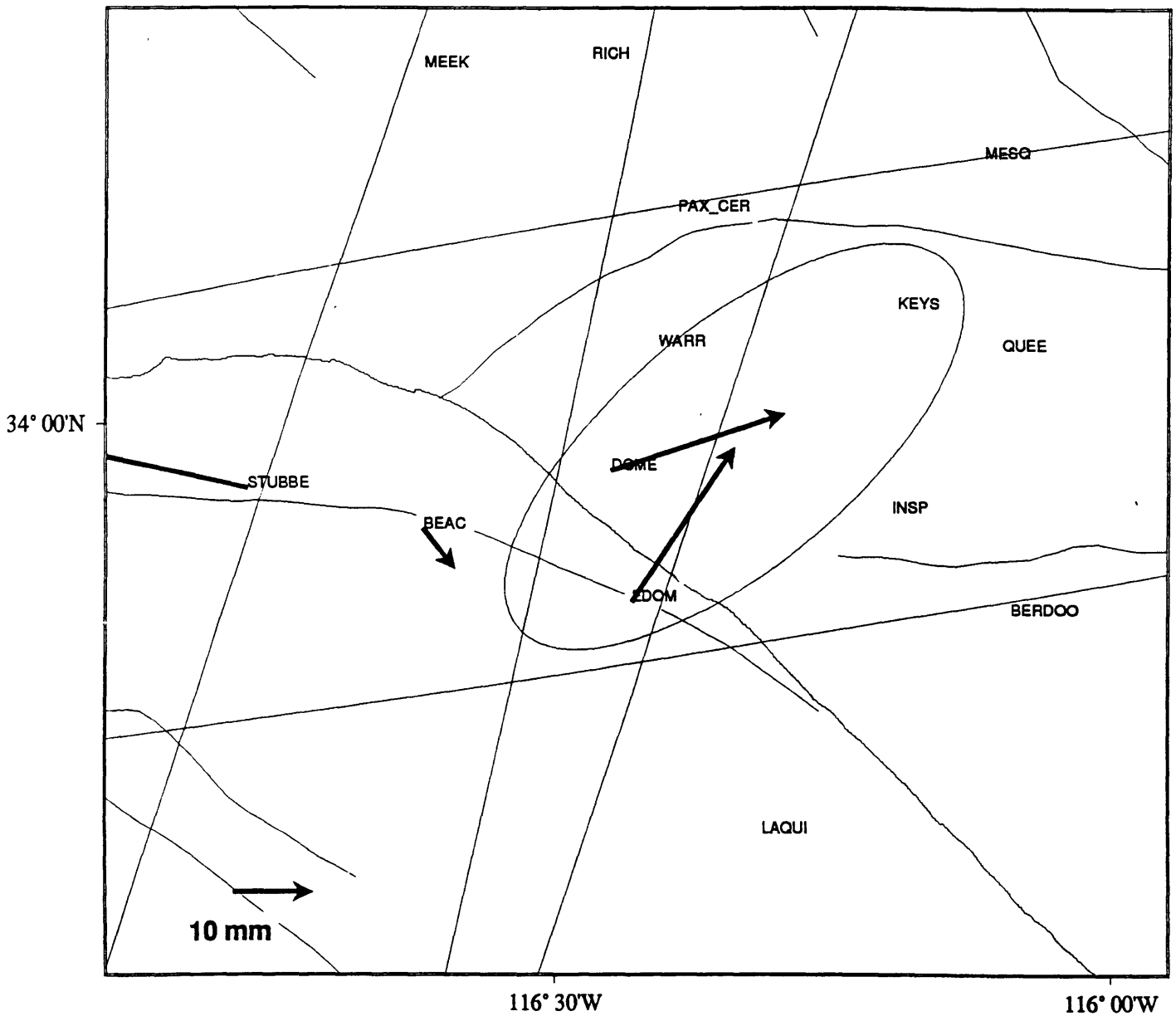

Figure 14e. Estimated coseismic site displacements from the combined solution (Figure 8) for the 07/08/86 North Palm Springs earthquake (M_s = 6.0). The error ellipses represent 95% confidence. The scaling arrows are shown in the lower left corner of the plot.

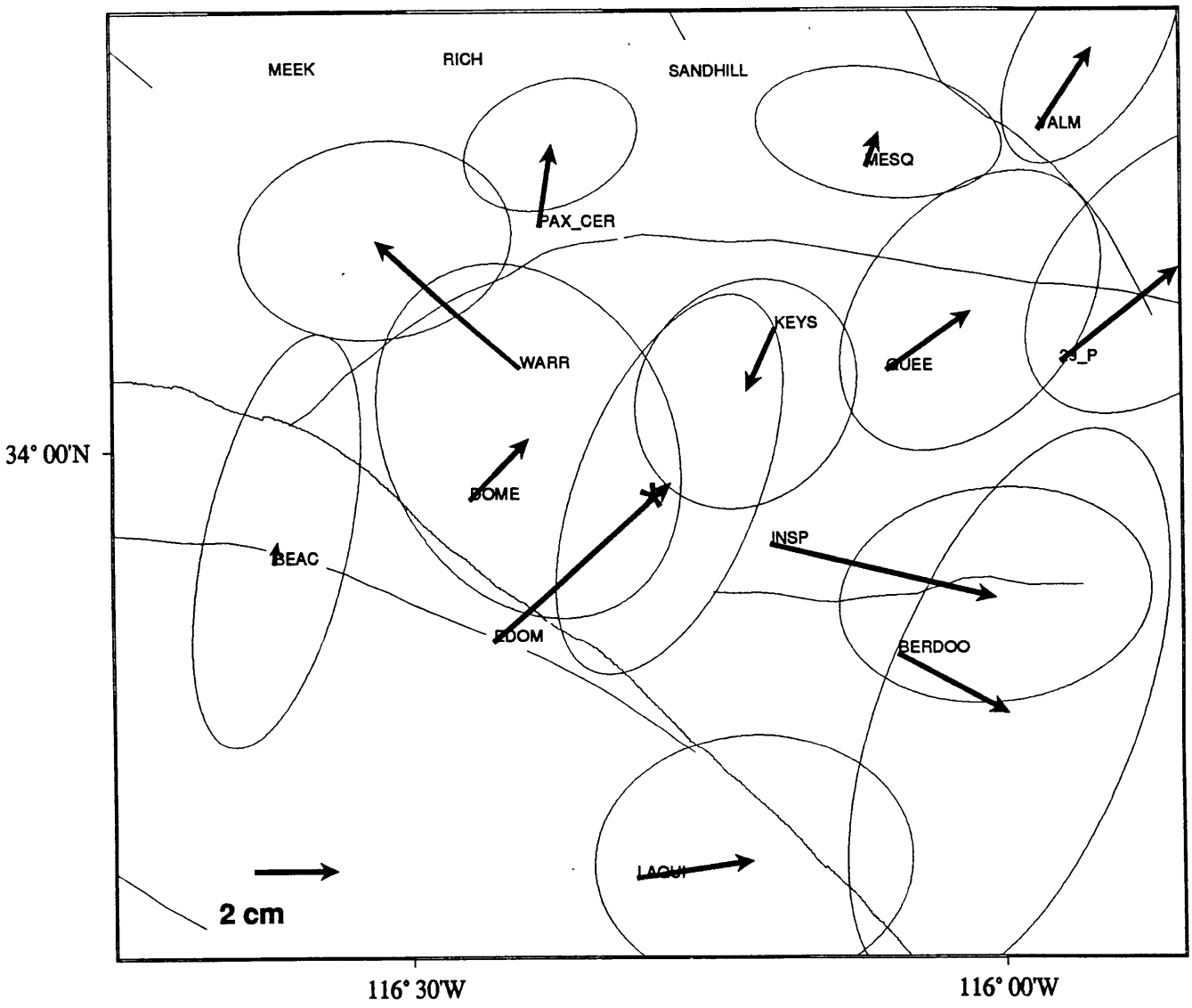

Figure 14f. Estimated coseismic site displacements from the combined solution (Figure 8) for the 04/22/92 Joshua Tree earthquake (M_s = 6.1). The star symbol represents the epicenter. The error ellipses represent 95% confidence. The scaling arrows are shown in the lower left corner of the plot.

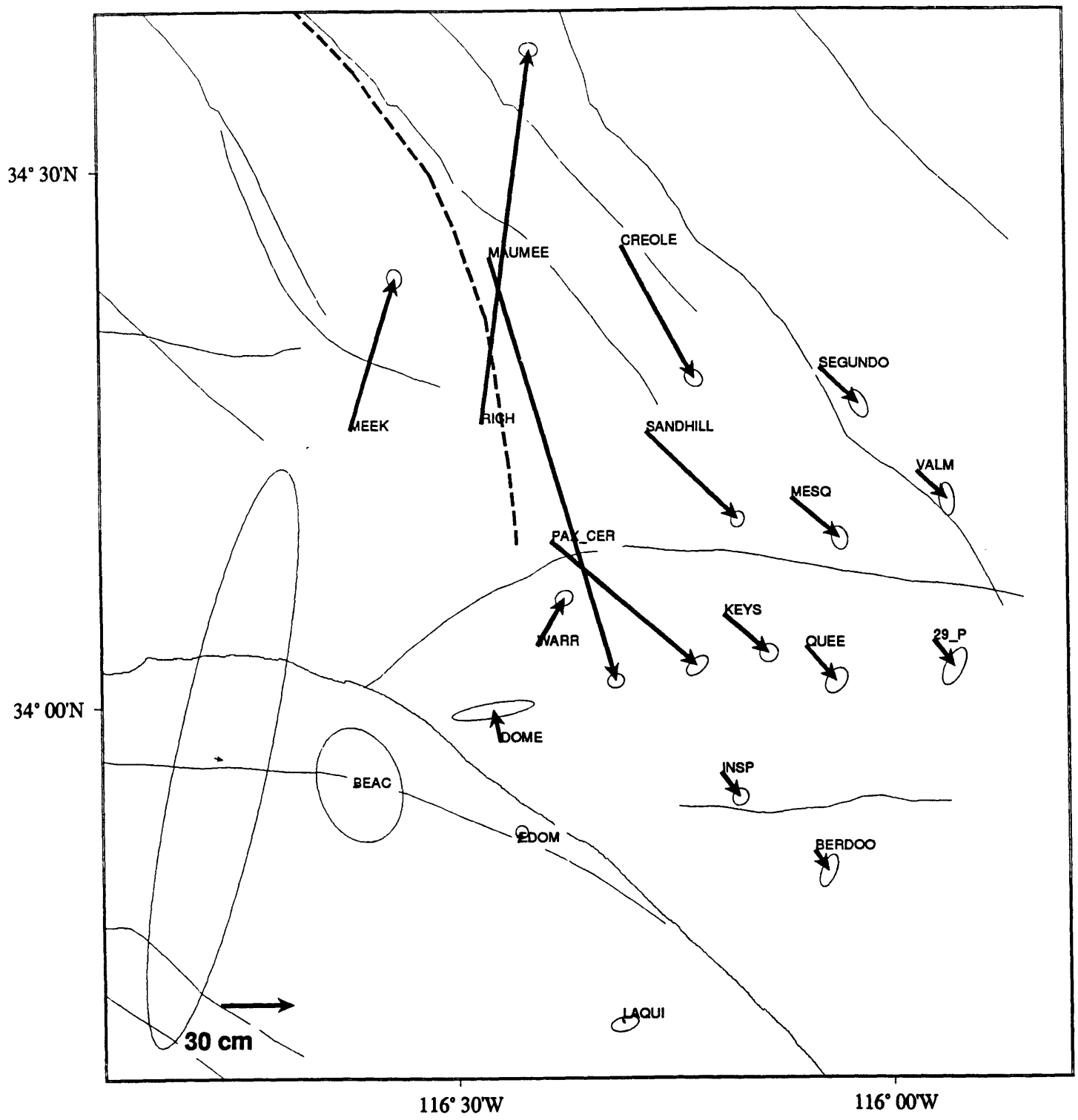

Figure 14g. Estimated coseismic site displacements from the combined solution (Figure 8) for the 06/28/92 Landers (M_s = 7.5) and Big Bear (M_s = 6.6) earthquakes. The surface trace of the rupture (heavy dash line) is from *Bock et al.*, [1993].04/22/92. The error ellipses represent the 95% confidence The scaling arrows are shown in the lower left corner of the plot.

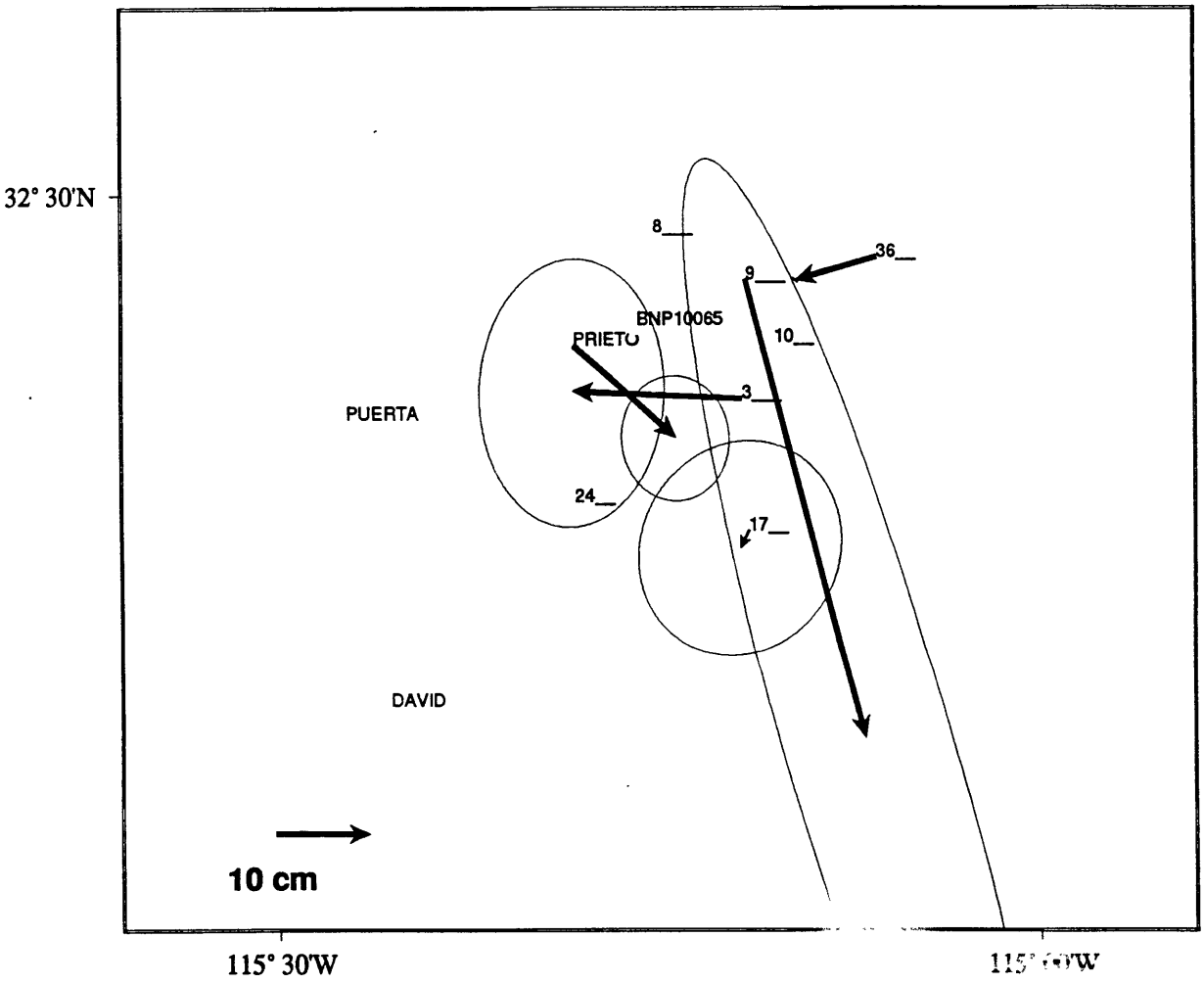

Figure 15. Estimated site displacements in the Mexicali network from 1981 to 1991. The error ellipses represent 95%.confidence.

Figures 16. Time series of the EDM observations. The error bars represent one-sigma formal uncertainties. The solid lines represent the best weighted-least-squares fit to each time series, considered independently; the dashed lines represent the estimated values from our combined (VG+EDM) analysis. The first group of plots, shown 15 per page, are for those lines experiencing no co-seismic displacements. Any discontinuities in the dashed lines represent our attempt to account for breaks due to destruction of sites or changes in instrumentation. The second group of sites, shown 6 per page, are for those lines with co-seismic displacements, shown by discontinuities in the dashed lines. Note the change of scale.

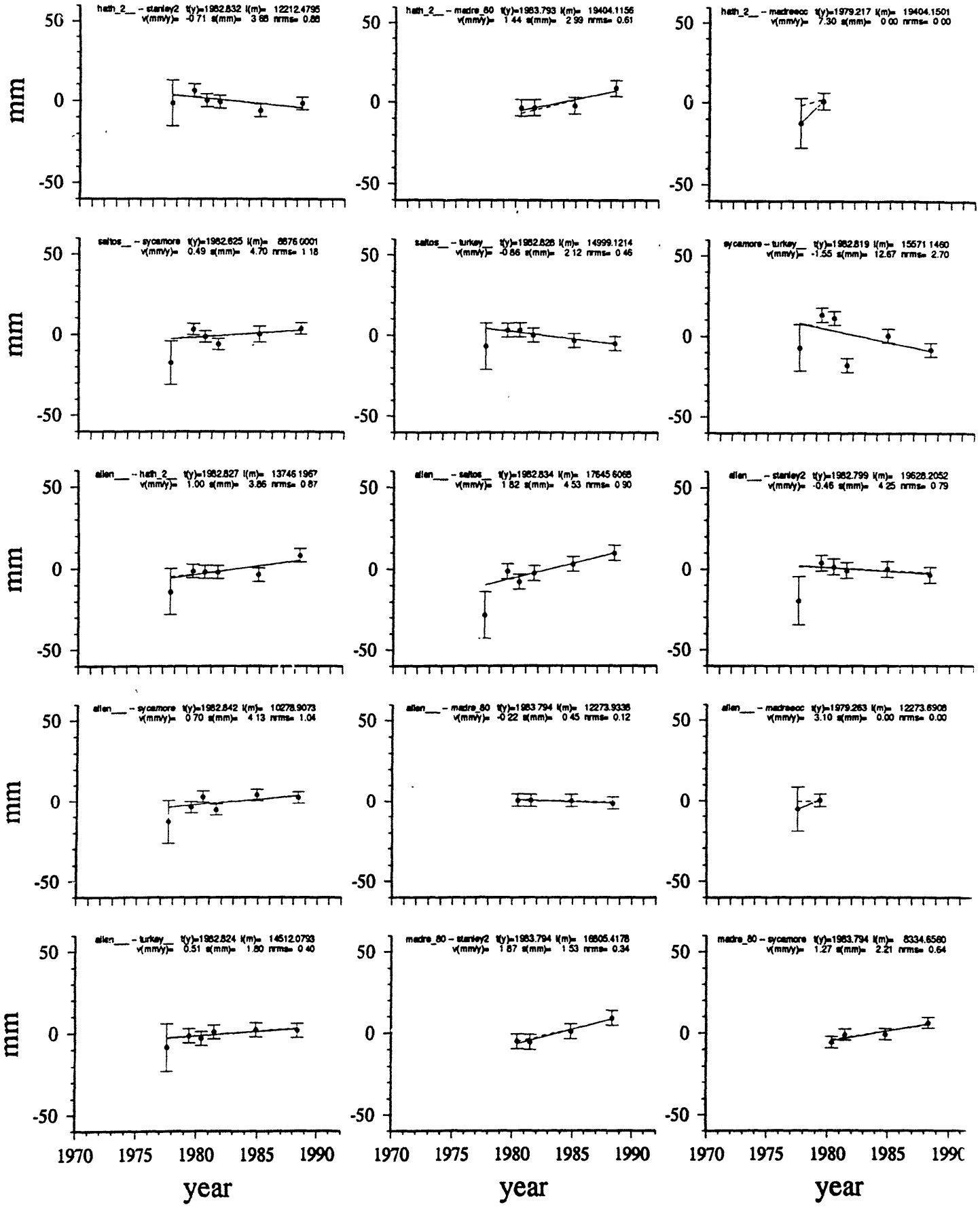
heth_2__ – stanley2 t(y)=1982.832 l(m)= 12212.4795
v(mm/y)= -0.71 s(mm)= 3.66 nrms= 0.66
heth_2__ – madre_80 t(y)=1983.793 l(m)= 19404.1156
v(mm/y)= 1.44 s(mm)= 2.99 nrms= 0.61
heth_2__ – madreecc t(y)=1979.217 l(m)= 19404.1501
v(mm/y)= 7.30 s(mm)= 0.00 nrms= 0.00
saltos__ – sycamore t(y)=1982.625 l(m)= 8676.0001
v(mm/y)= 0.49 s(mm)= 4.70 nrms= 1.18
saltos__ – turkey__ t(y)=1982.828 l(m)= 14999.1214
v(mm/y)= -0.66 s(mm)= 2.12 nrms= 0.46
sycamore – turkey__ t(y)=1982.819 l(m)= 15571.1460
v(mm/y)= -1.55 s(mm)= 12.67 nrms= 2.70
alien___ – heth_2__ t(y)=1982.827 l(m)= 13746.1967
v(mm/y)= 1.00 s(mm)= 3.86 nrms= 0.87
alien___ – saltos__ t(y)=1982.834 l(m)= 17645.6068
v(mm/y)= 1.82 s(mm)= 4.53 nrms= 0.90
alien___ – stanley2 t(y)=1982.799 l(m)= 19628.2052
v(mm/y)= -0.46 s(mm)= 4.25 nrms= 0.79
alien___ – sycamore t(y)=1982.842 l(m)= 10278.9073
v(mm/y)= 0.70 s(mm)= 4.13 nrms= 1.04
alien___ – madre_80 t(y)=1983.794 l(m)= 12273.9336
v(mm/y)= -0.22 s(mm)= 0.45 nrms= 0.12
alien___ – madreecc t(y)=1979.263 l(m)= 12273.6908
v(mm/y)= 3.10 s(mm)= 0.00 nrms= 0.00
alien___ – turkey__ t(y)=1982.824 l(m)= 14512.0793
v(mm/y)= 0.51 s(mm)= 1.80 nrms= 0.40
madre_80 – stanley2 t(y)=1983.794 l(m)= 16805.4178
v(mm/y)= 1.87 s(mm)= 1.53 nrms= 0.34
madre_80 – sycamore t(y)=1983.794 l(m)= 8334.6560
v(mm/y)= 1.27 s(mm)= 2.21 nrms= 0.64
mm
50
0
-50
1970
1975
1980
1985
1990
year

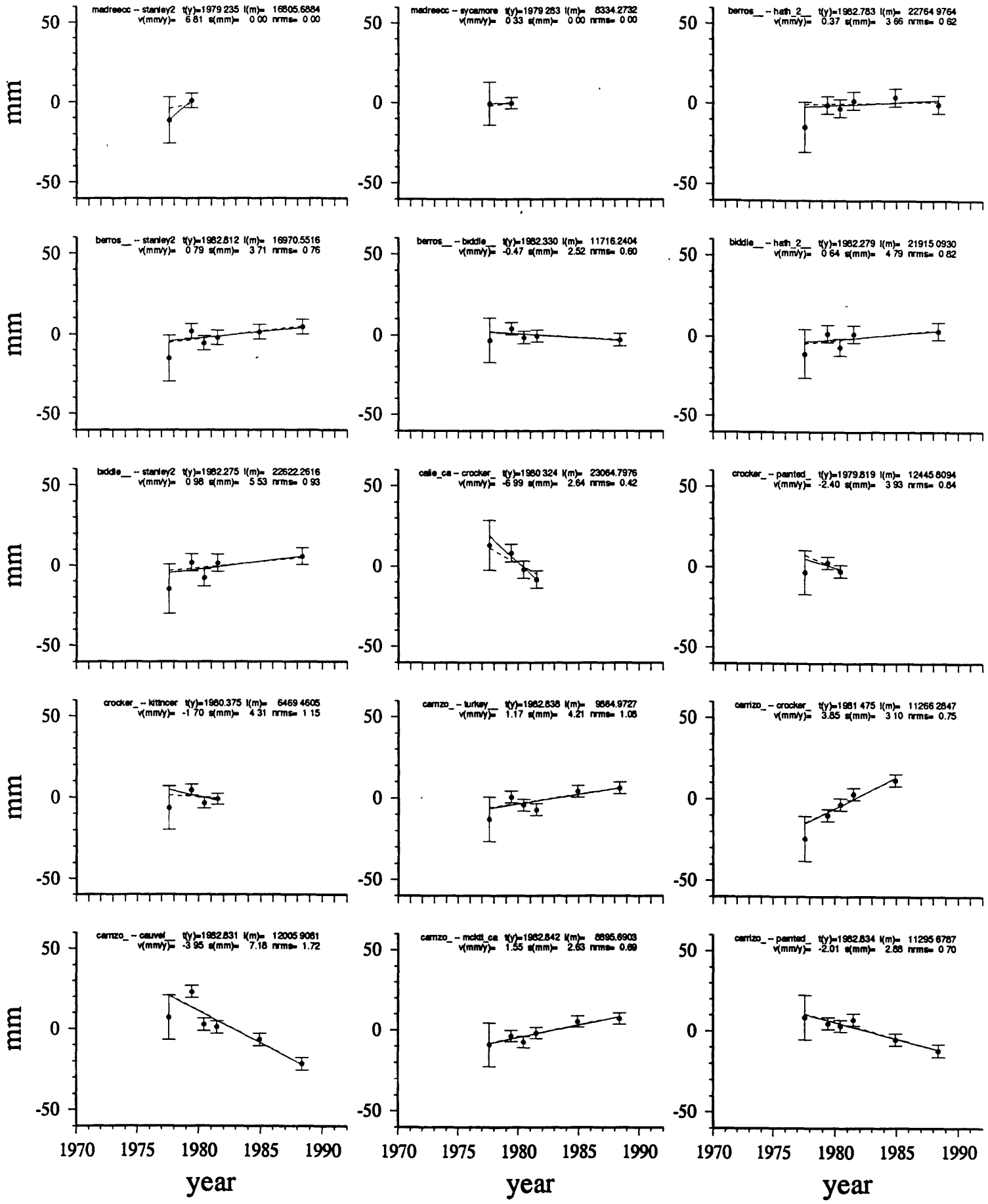
madreecc -- stanley2 t(y)=1979.235 l(m)= 16805.6884
v(mm/y)= 6.81 s(mm)= 0.00 nrms= 0.00
madreecc -- sycamore t(y)=1979.283 l(m)= 8334.2732
v(mm/y)= 0.33 s(mm)= 0.00 nrms= 0.00
berros__ -- hath_2__ t(y)=1982.783 l(m)= 22764.9764
v(mm/y)= 0.37 s(mm)= 3.66 nrms= 0.62
berros__ -- stanley2 t(y)=1982.812 l(m)= 16970.5516
v(mm/y)= 0.79 s(mm)= 3.71 nrms= 0.76
berros__ -- biddle__ t(y)=1982.330 l(m)= 11716.2404
v(mm/y)= -0.47 s(mm)= 2.52 nrms= 0.60
biddle__ -- hath_2__ t(y)=1982.279 l(m)= 21915.0930
v(mm/y)= 0.64 s(mm)= 4.79 nrms= 0.82
biddle__ -- stanley2 t(y)=1982.275 l(m)= 22622.2616
v(mm/y)= 0.98 s(mm)= 5.53 nrms= 0.93
calle_ca -- crocker_ t(y)=1980.324 l(m)= 23064.7976
v(mm/y)= -6.99 s(mm)= 2.64 nrms= 0.42
crocker_ -- painted_ t(y)=1979.819 l(m)= 12445.8094
v(mm/y)= -2.40 s(mm)= 3.93 nrms= 0.84
crocker_ -- kittncer t(y)=1980.375 l(m)= 6469.4605
v(mm/y)= -1.70 s(mm)= 4.31 nrms= 1.15
carrizo_ -- turkey__ t(y)=1982.838 l(m)= 9564.9727
v(mm/y)= 1.17 s(mm)= 4.21 nrms= 1.06
carrizo_ -- crocker_ t(y)=1981.475 l(m)= 11266.2847
v(mm/y)= 3.85 s(mm)= 3.10 nrms= 0.75
carrizo_ -- cauvel__ t(y)=1982.831 l(m)= 12005.9061
v(mm/y)= -3.95 s(mm)= 7.18 nrms= 1.72
carrizo_ -- mckit_ca t(y)=1982.842 l(m)= 8695.6903
v(mm/y)= 1.55 s(mm)= 2.63 nrms= 0.69
carrizo_ -- painted_ t(y)=1982.834 l(m)= 11295.6787
v(mm/y)= -2.01 s(mm)= 2.88 nrms= 0.70
mm
50
0
-50
1970
1975
1980
1985
1990
year

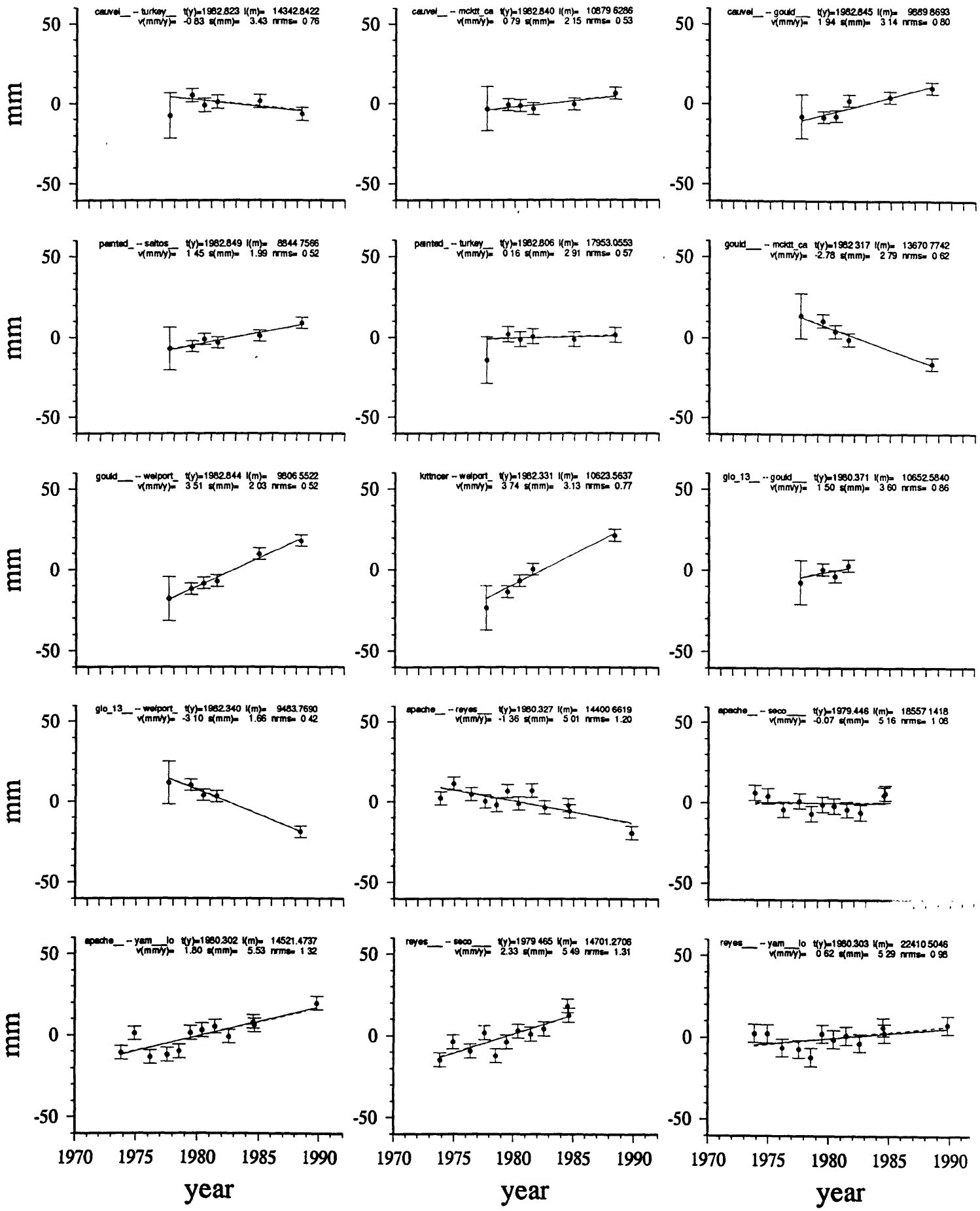
cauvel__ -- turkey__ t(y)=1982.823 l(m)= 14342.8422
v(mm/y)= -0.83 s(mm)= 3.43 nrms= 0.76
cauvel__ -- mckit_ca t(y)=1982.840 l(m)= 10879.6286
v(mm/y)= 0.79 s(mm)= 2.15 nrms= 0.53
cauvel__ -- gould___ t(y)=1982.845 l(m)= 9889.8693
v(mm/y)= 1.94 s(mm)= 3.14 nrms= 0.80
painted_ -- saltos__ t(y)=1982.849 l(m)= 8844.7566
v(mm/y)= 1.45 s(mm)= 1.99 nrms= 0.52
painted_ -- turkey__ t(y)=1982.806 l(m)= 17953.0553
v(mm/y)= 0.16 s(mm)= 2.91 nrms= 0.57
gould___ -- mckit_ca t(y)=1982.317 l(m)= 13670.7742
v(mm/y)= -2.78 s(mm)= 2.79 nrms= 0.62
gould___ -- welport_ t(y)=1982.844 l(m)= 9806.5522
v(mm/y)= 3.51 s(mm)= 2.03 nrms= 0.52
kittnicer -- welport_ t(y)=1982.331 l(m)= 10623.5637
v(mm/y)= 3.74 s(mm)= 3.13 nrms= 0.77
glo_13__ -- gould___ t(y)=1980.371 l(m)= 10652.5840
v(mm/y)= 1.50 s(mm)= 3.60 nrms= 0.86
glo_13__ -- welport_ t(y)=1982.340 l(m)= 9483.7690
v(mm/y)= -3.10 s(mm)= 1.66 nrms= 0.42
apache__ -- reyes___ t(y)=1980.327 l(m)= 14400.6619
v(mm/y)= -1.36 s(mm)= 5.01 nrms= 1.20
apache__ -- seco____ t(y)=1979.446 l(m)= 18557.1418
v(mm/y)= -0.07 s(mm)= 5.16 nrms= 1.08
apache__ -- yam___lo t(y)=1980.302 l(m)= 14521.4737
v(mm/y)= 1.80 s(mm)= 5.53 nrms= 1.32
reyes___ -- seco____ t(y)=1979.465 l(m)= 14701.2706
v(mm/y)= 2.33 s(mm)= 5.49 nrms= 1.31
reyes___ -- yam___lo t(y)=1980.303 l(m)= 22410.5046
v(mm/y)= 0.62 s(mm)= 5.29 nrms= 0.98
50
0
-50
mm
1970
1975
1980
1985
1990
year

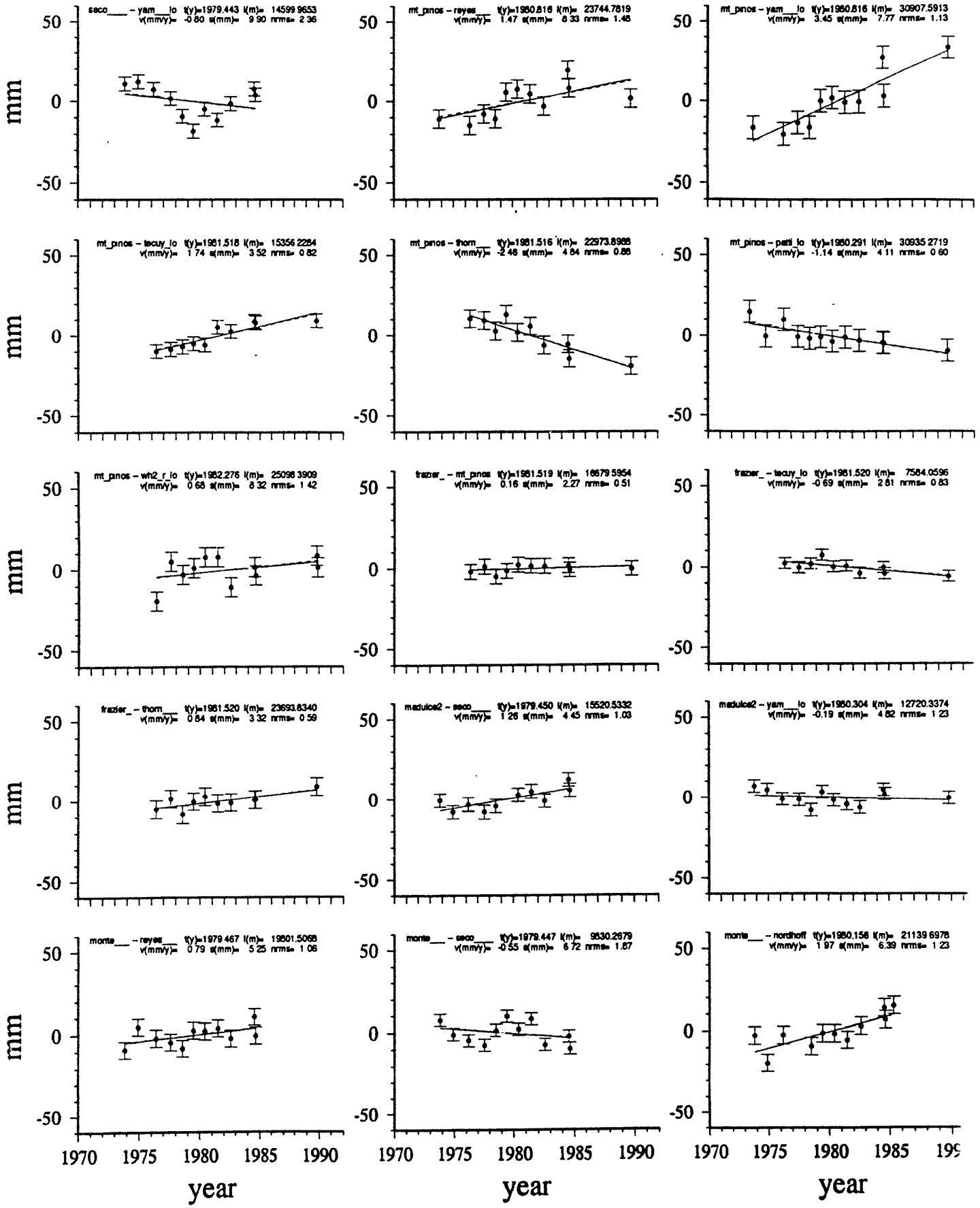
seco___ – yam___lo t(y)=1979.443 l(m)= 14599.9653
v(mm/y)= -0.80 s(mm)= 9.90 nrms= 2.36
mt_pinos – reyes___ t(y)=1980.816 l(m)= 23744.7819
v(mm/y)= 1.47 s(mm)= 8.33 nrms= 1.48
mt_pinos – yam___lo t(y)=1980.816 l(m)= 30907.5913
v(mm/y)= 3.45 s(mm)= 7.77 nrms= 1.13
mt_pinos – tecuy_lo t(y)=1981.518 l(m)= 15356.2284
v(mm/y)= 1.74 s(mm)= 3.52 nrms= 0.82
mt_pinos – thorn___ t(y)=1981.516 l(m)= 22973.6968
v(mm/y)= -2.46 s(mm)= 4.84 nrms= 0.86
mt_pinos – patti_lo t(y)=1980.291 l(m)= 30935.2719
v(mm/y)= -1.14 s(mm)= 4.11 nrms= 0.60
mt_pinos – wh2_r_lo t(y)=1982.276 l(m)= 25098.3909
v(mm/y)= 0.68 s(mm)= 8.32 nrms= 1.42
frazier_ – mt_pinos t(y)=1981.519 l(m)= 16679.5954
v(mm/y)= 0.16 s(mm)= 2.27 nrms= 0.51
frazier_ – tecuy_lo t(y)=1981.520 l(m)= 7584.0596
v(mm/y)= -0.69 s(mm)= 2.81 nrms= 0.83
frazier_ – thorn___ t(y)=1981.520 l(m)= 23693.6340
v(mm/y)= 0.84 s(mm)= 3.32 nrms= 0.59
madulce2 – seco___ t(y)=1979.450 l(m)= 15520.5332
v(mm/y)= 1.26 s(mm)= 4.45 nrms= 1.03
madulce2 – yam___lo t(y)=1980.304 l(m)= 12720.3374
v(mm/y)= -0.19 s(mm)= 4.82 nrms= 1.23
monte___ – reyes___ t(y)=1979.467 l(m)= 19501.5068
v(mm/y)= 0.79 s(mm)= 5.25 nrms= 1.06
monte___ – seco___ t(y)=1979.447 l(m)= 9530.2679
v(mm/y)= -0.55 s(mm)= 6.72 nrms= 1.87
monte___ – nordhoff t(y)=1980.156 l(m)= 21139.6978
v(mm/y)= 1.97 s(mm)= 6.39 nrms= 1.23
mm
50
0
-50
1970
1975
1980
1985
1990
year

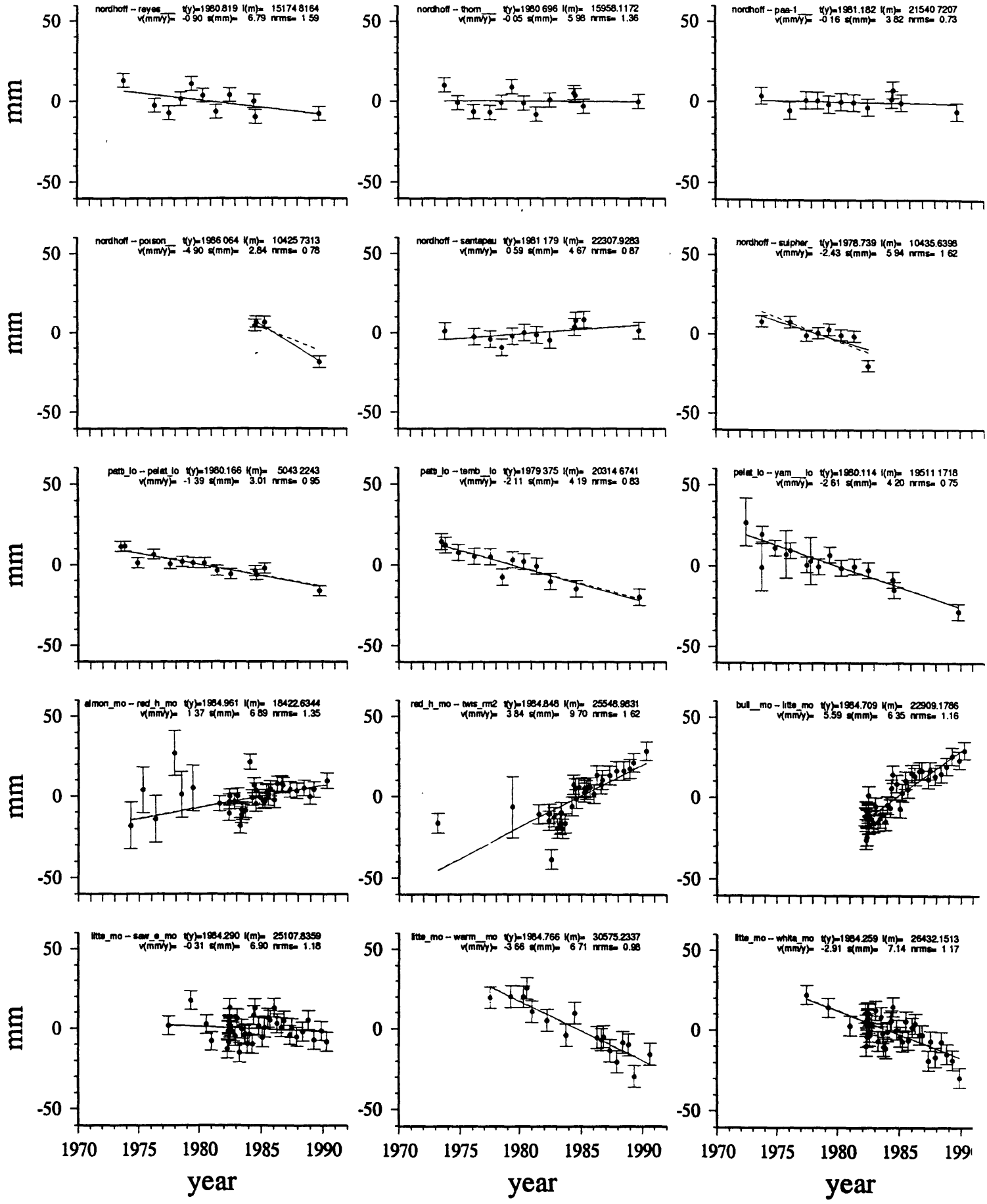
nordhoff – reyes t(y)=1980.819 l(m)= 15174.8164
v(mm/y)= -0.90 s(mm)= 6.79 nrms= 1.59
nordhoff – thorn t(y)=1980.696 l(m)= 15958.1172
v(mm/y)= -0.05 s(mm)= 5.98 nrms= 1.36
nordhoff – paa-1 t(y)=1981.182 l(m)= 21540.7207
v(mm/y)= -0.16 s(mm)= 3.82 nrms= 0.73
nordhoff – poison t(y)=1986.064 l(m)= 10425.7313
v(mm/y)= -4.90 s(mm)= 2.84 nrms= 0.78
nordhoff – santapau t(y)=1981.179 l(m)= 22307.9283
v(mm/y)= 0.59 s(mm)= 4.67 nrms= 0.87
nordhoff – sulpher t(y)=1978.739 l(m)= 10435.6398
v(mm/y)= -2.43 s(mm)= 5.94 nrms= 1.62
patb_lo – pelat_lo t(y)=1980.166 l(m)= 5043.2243
v(mm/y)= -1.39 s(mm)= 3.01 nrms= 0.95
patb_lo – temb_lo t(y)=1979.375 l(m)= 20314.6741
v(mm/y)= -2.11 s(mm)= 4.19 nrms= 0.83
pelat_lo – yam_lo t(y)=1980.114 l(m)= 19511.1718
v(mm/y)= -2.61 s(mm)= 4.20 nrms= 0.75
almon_mo – red_h_mo t(y)=1984.961 l(m)= 18422.6344
v(mm/y)= 1.37 s(mm)= 6.89 nrms= 1.35
red_h_mo – tws_rm2 t(y)=1984.848 l(m)= 25548.9631
v(mm/y)= 3.84 s(mm)= 9.70 nrms= 1.62
bull_mo – litte_mo t(y)=1984.709 l(m)= 22909.1786
v(mm/y)= 5.59 s(mm)= 6.35 nrms= 1.16
litte_mo – saw_e_mo t(y)=1984.290 l(m)= 25107.8359
v(mm/y)= -0.31 s(mm)= 6.90 nrms= 1.18
litte_mo – warm_mo t(y)=1984.766 l(m)= 30575.2337
v(mm/y)= -3.66 s(mm)= 6.71 nrms= 0.98
litte_mo – white_mo t(y)=1984.259 l(m)= 26432.1513
v(mm/y)= -2.91 s(mm)= 7.14 nrms= 1.17
mm
50
0
-50
1970
1975
1980
1985
1990
year

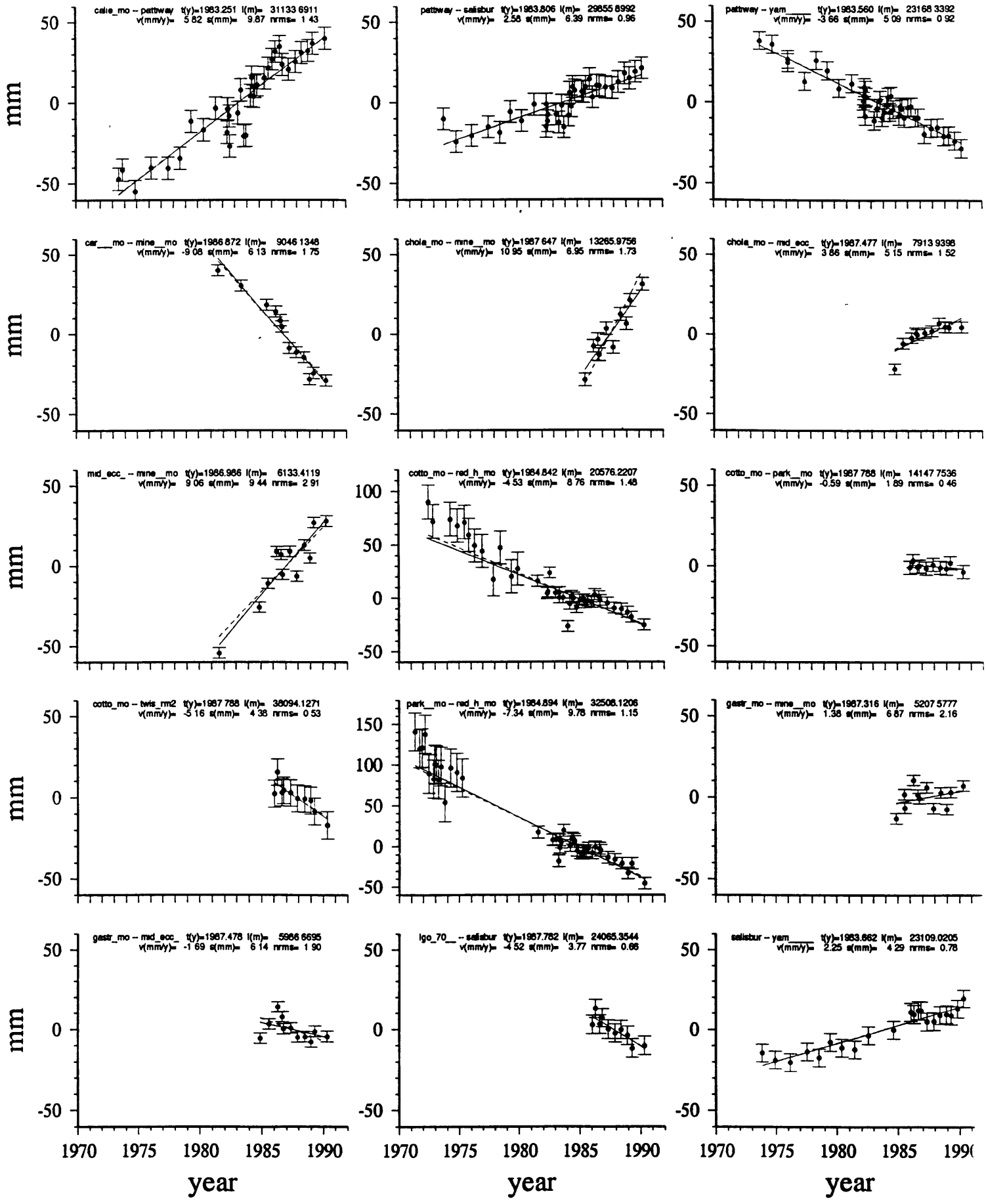
calle_mo – pattway t(y)=1983.251 l(m)= 31133.6911
v(mm/y)= 5.82 s(mm)= 9.87 nrms= 1.43
pattway – salisbur t(y)=1983.806 l(m)= 29855.8992
v(mm/y)= 2.58 s(mm)= 6.39 nrms= 0.96
pattway – yam____ t(y)=1983.560 l(m)= 23168.3392
v(mm/y)= -3.66 s(mm)= 5.09 nrms= 0.92
car___mo – mine__mo t(y)=1986.872 l(m)= 9046.1348
v(mm/y)= -9.08 s(mm)= 6.13 nrms= 1.75
chola_mo – mine__mo t(y)=1987.647 l(m)= 13265.9756
v(mm/y)= 10.95 s(mm)= 6.95 nrms= 1.73
chola_mo – mid_ecc_ t(y)=1987.477 l(m)= 7913.9398
v(mm/y)= 3.86 s(mm)= 5.15 nrms= 1.52
mid_ecc_ – mine__mo t(y)=1986.986 l(m)= 6133.4119
v(mm/y)= 9.06 s(mm)= 9.44 nrms= 2.91
cotto_mo – red_h_mo t(y)=1984.842 l(m)= 20576.2207
v(mm/y)= -4.53 s(mm)= 8.76 nrms= 1.48
cotto_mo – park__mo t(y)=1987.788 l(m)= 14147.7536
v(mm/y)= -0.59 s(mm)= 1.89 nrms= 0.46
cotto_mo – twis_rm2 t(y)=1987.788 l(m)= 38094.1271
v(mm/y)= -5.16 s(mm)= 4.38 nrms= 0.53
park__mo – red_h_mo t(y)=1984.894 l(m)= 32506.1206
v(mm/y)= -7.34 s(mm)= 9.78 nrms= 1.15
gastr_mo – mine__mo t(y)=1987.316 l(m)= 5207.5777
v(mm/y)= 1.38 s(mm)= 6.87 nrms= 2.16
gastr_mo – mid_ecc_ t(y)=1987.478 l(m)= 5966.6695
v(mm/y)= -1.69 s(mm)= 6.14 nrms= 1.90
lgo_70__ – salisbur t(y)=1987.782 l(m)= 24065.3544
v(mm/y)= -4.52 s(mm)= 3.77 nrms= 0.66
salisbur – yam____ t(y)=1983.662 l(m)= 23109.0205
v(mm/y)= 2.25 s(mm)= 4.29 nrms= 0.78
mm
year
1970
1975
1980
1985
1990

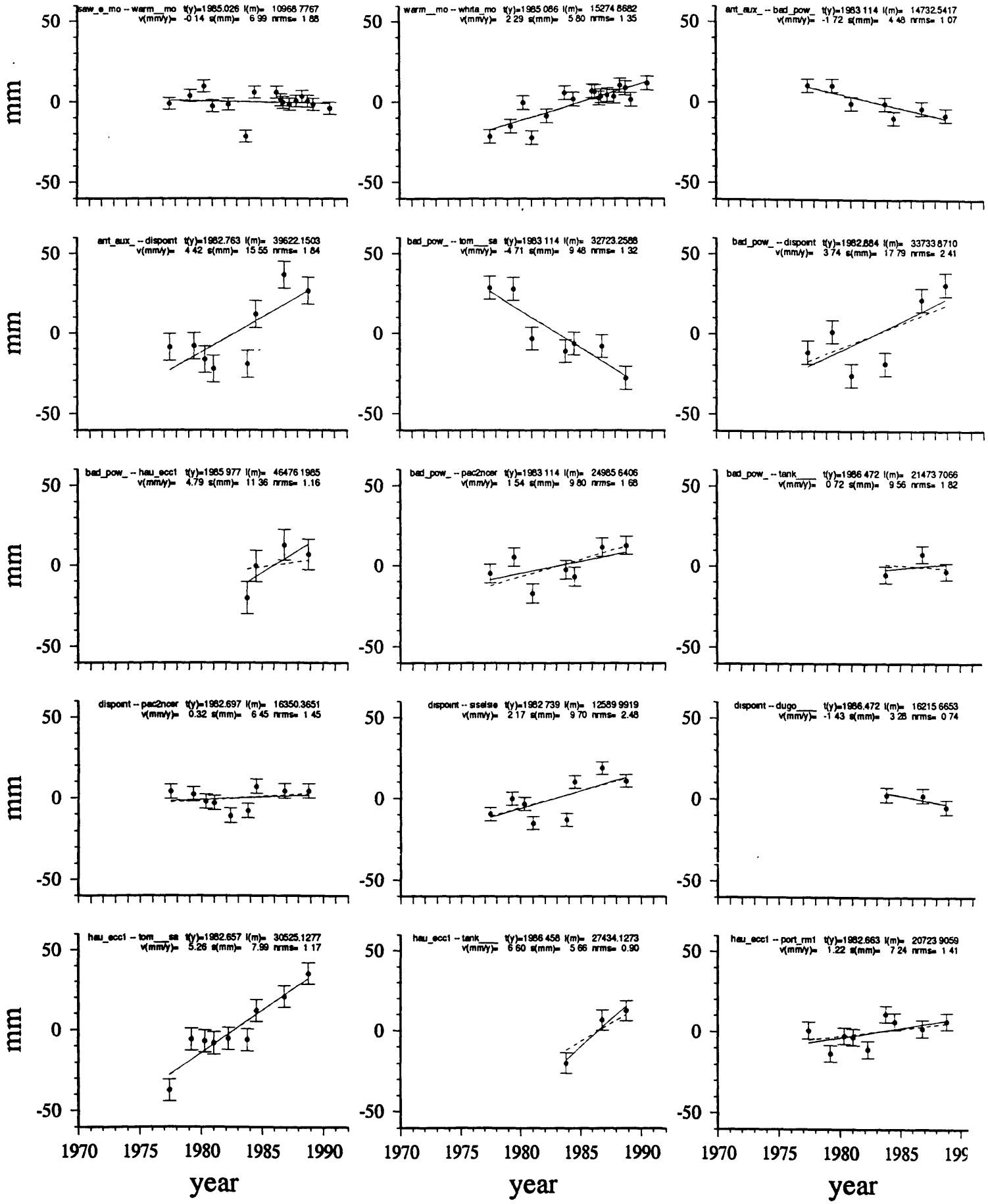
saw_e_mo -- warm__mo t(y)=1985.026 l(m)= 10968.7767
v(mm/y)= -0.14 s(mm)= 6.99 nrms= 1.88
warm__mo -- whrta_mo t(y)=1985.086 l(m)= 15274.8682
v(mm/y)= 2.29 s(mm)= 5.80 nrms= 1.35
ant_aux_ -- bad_pow_ t(y)=1983.114 l(m)= 14732.5417
v(mm/y)= -1.72 s(mm)= 4.48 nrms= 1.07
ant_aux_ -- dispont t(y)=1982.763 l(m)= 39622.1503
v(mm/y)= 4.42 s(mm)= 15.55 nrms= 1.84
bad_pow_ -- tom___sa t(y)=1983.114 l(m)= 32723.2588
v(mm/y)= -4.71 s(mm)= 9.48 nrms= 1.32
bad_pow_ -- dispont t(y)=1982.884 l(m)= 33733.8710
v(mm/y)= 3.74 s(mm)= 17.79 nrms= 2.41
bad_pow_ -- hau_ecc1 t(y)=1985.977 l(m)= 46476.1985
v(mm/y)= 4.79 s(mm)= 11.36 nrms= 1.16
bad_pow_ -- pac2ncer t(y)=1983.114 l(m)= 24985.6406
v(mm/y)= 1.54 s(mm)= 9.80 nrms= 1.68
bad_pow_ -- tank____ t(y)=1986.472 l(m)= 21473.7066
v(mm/y)= 0.72 s(mm)= 9.56 nrms= 1.82
dispont -- pac2ncer t(y)=1982.697 l(m)= 16350.3651
v(mm/y)= 0.32 s(mm)= 6.45 nrms= 1.45
dispont -- sisalse t(y)=1982.739 l(m)= 12589.9919
v(mm/y)= 2.17 s(mm)= 9.70 nrms= 2.48
dispont -- dugo____ t(y)=1986.472 l(m)= 16215.6653
v(mm/y)= -1.43 s(mm)= 3.28 nrms= 0.74
hau_ecc1 -- tom___sa t(y)=1982.657 l(m)= 30525.1277
v(mm/y)= 5.26 s(mm)= 7.99 nrms= 1.17
hau_ecc1 -- tank____ t(y)=1986.458 l(m)= 27434.1273
v(mm/y)= 6.60 s(mm)= 5.66 nrms= 0.90
hau_ecc1 -- port_rm1 t(y)=1982.663 l(m)= 20723.9059
v(mm/y)= 1.22 s(mm)= 7.24 nrms= 1.41
mm
50
0
-50
1970
1975
1980
1985
1990
199
year

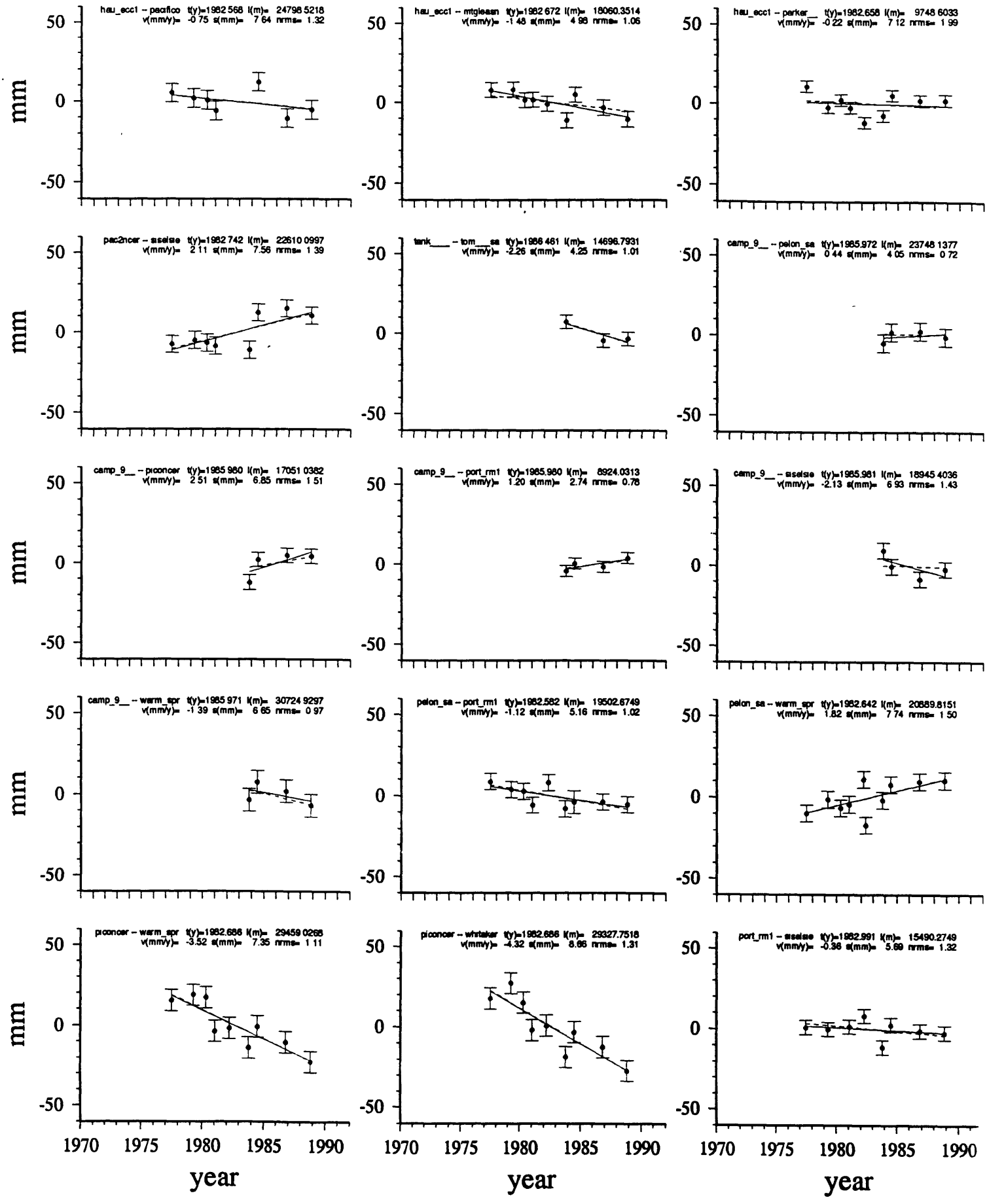
hau_ecc1 – pacifico t(y)=1982.568 l(m)= 24798.5218
v(mm/y)= -0.75 s(mm)= 7.64 nrms= 1.32
hau_ecc1 – mtgleasn t(y)=1982.672 l(m)= 18060.3514
v(mm/y)= -1.48 s(mm)= 4.98 nrms= 1.06
hau_ecc1 – parker__ t(y)=1982.658 l(m)= 9748.6033
v(mm/y)= -0.22 s(mm)= 7.12 nrms= 1.99
pac2ncer – sseise t(y)=1982.742 l(m)= 22610.0997
v(mm/y)= 2.11 s(mm)= 7.56 nrms= 1.39
tank____ – tom___sa t(y)=1986.461 l(m)= 14696.7931
v(mm/y)= -2.26 s(mm)= 4.25 nrms= 1.01
camp_9__ – pelon_sa t(y)=1985.972 l(m)= 23748.1377
v(mm/y)= 0.44 s(mm)= 4.05 nrms= 0.72
camp_9__ – piconcer t(y)=1985.980 l(m)= 17051.0382
v(mm/y)= 2.51 s(mm)= 6.85 nrms= 1.51
camp_9__ – port_rm1 t(y)=1985.980 l(m)= 8924.0313
v(mm/y)= 1.20 s(mm)= 2.74 nrms= 0.78
camp_9__ – sseise t(y)=1985.981 l(m)= 18945.4036
v(mm/y)= -2.13 s(mm)= 6.93 nrms= 1.43
camp_9__ – warm_spr t(y)=1985.971 l(m)= 30724.9297
v(mm/y)= -1.39 s(mm)= 6.65 nrms= 0.97
pelon_sa – port_rm1 t(y)=1982.582 l(m)= 19502.6749
v(mm/y)= -1.12 s(mm)= 5.16 nrms= 1.02
pelon_sa – warm_spr t(y)=1982.642 l(m)= 20889.8151
v(mm/y)= 1.82 s(mm)= 7.74 nrms= 1.50
piconcer – warm_spr t(y)=1982.686 l(m)= 29459.0268
v(mm/y)= -3.52 s(mm)= 7.35 nrms= 1.11
piconcer – whitaker t(y)=1982.686 l(m)= 29327.7518
v(mm/y)= -4.32 s(mm)= 8.66 nrms= 1.31
port_rm1 – sseise t(y)=1982.991 l(m)= 15490.2749
v(mm/y)= -0.36 s(mm)= 5.69 nrms= 1.32
mm
50
0
-50
1970
1975
1980
1985
1990
year

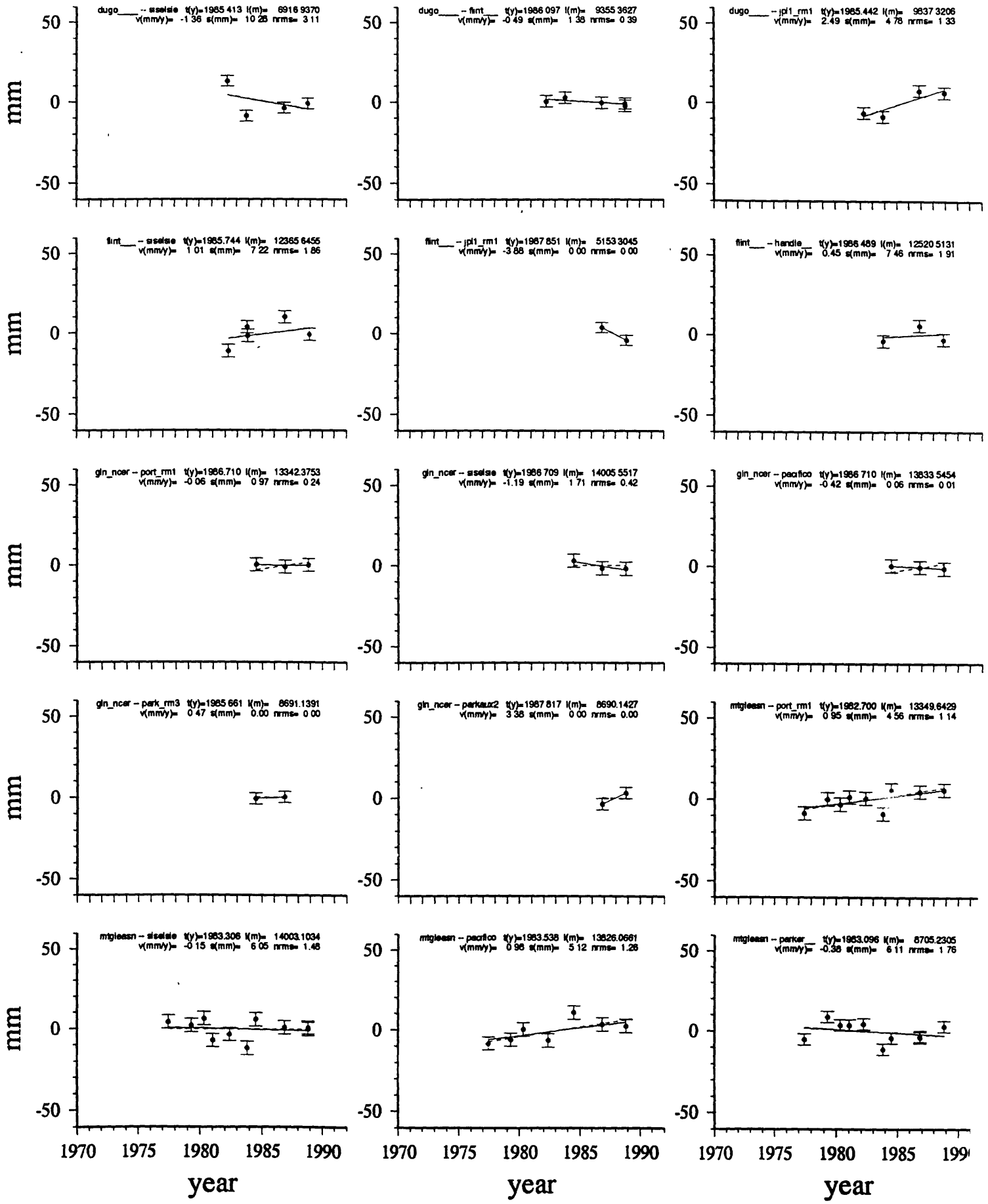
dugo___ -- siselsie t(y)=1985.413 l(m)= 6916.9370
v(mm/y)= -1.36 s(mm)= 10.25 nrms= 3.11
dugo___ -- flint___ t(y)=1986.097 l(m)= 9355.3627
v(mm/y)= -0.49 s(mm)= 1.35 nrms= 0.39
dugo___ -- jpl1_rm1 t(y)=1985.442 l(m)= 9837.3206
v(mm/y)= 2.49 s(mm)= 4.78 nrms= 1.33
flint___ -- siselsie t(y)=1985.744 l(m)= 12365.6455
v(mm/y)= 1.01 s(mm)= 7.22 nrms= 1.86
flint___ -- jpl1_rm1 t(y)=1987.851 l(m)= 5153.3045
v(mm/y)= -3.88 s(mm)= 0.00 nrms= 0.00
flint___ -- handle___ t(y)=1986.489 l(m)= 12520.5131
v(mm/y)= 0.45 s(mm)= 7.46 nrms= 1.91
gln_ncer -- port_rm1 t(y)=1986.710 l(m)= 13342.3753
v(mm/y)= -0.06 s(mm)= 0.97 nrms= 0.24
gln_ncer -- siselsie t(y)=1986.709 l(m)= 14005.5517
v(mm/y)= -1.19 s(mm)= 1.71 nrms= 0.42
gln_ncer -- pacifico t(y)=1986.710 l(m)= 13833.5454
v(mm/y)= -0.42 s(mm)= 0.06 nrms= 0.01
gln_ncer -- park_rm3 t(y)=1985.661 l(m)= 8691.1391
v(mm/y)= 0.47 s(mm)= 0.00 nrms= 0.00
gln_ncer -- parkaux2 t(y)=1987.817 l(m)= 8690.1427
v(mm/y)= 3.38 s(mm)= 0.00 nrms= 0.00
mtgleasn -- port_rm1 t(y)=1982.700 l(m)= 13349.6429
v(mm/y)= 0.95 s(mm)= 4.56 nrms= 1.14
mtgleasn -- siselsie t(y)=1983.306 l(m)= 14003.1034
v(mm/y)= -0.15 s(mm)= 6.05 nrms= 1.48
mtgleasn -- pacifico t(y)=1983.538 l(m)= 13826.0661
v(mm/y)= 0.96 s(mm)= 5.12 nrms= 1.26
mtgleasn -- parker___ t(y)=1983.096 l(m)= 8705.2305
v(mm/y)= -0.38 s(mm)= 6.11 nrms= 1.76
50
0
-50
mm
1970
1975
1980
1985
1990
year

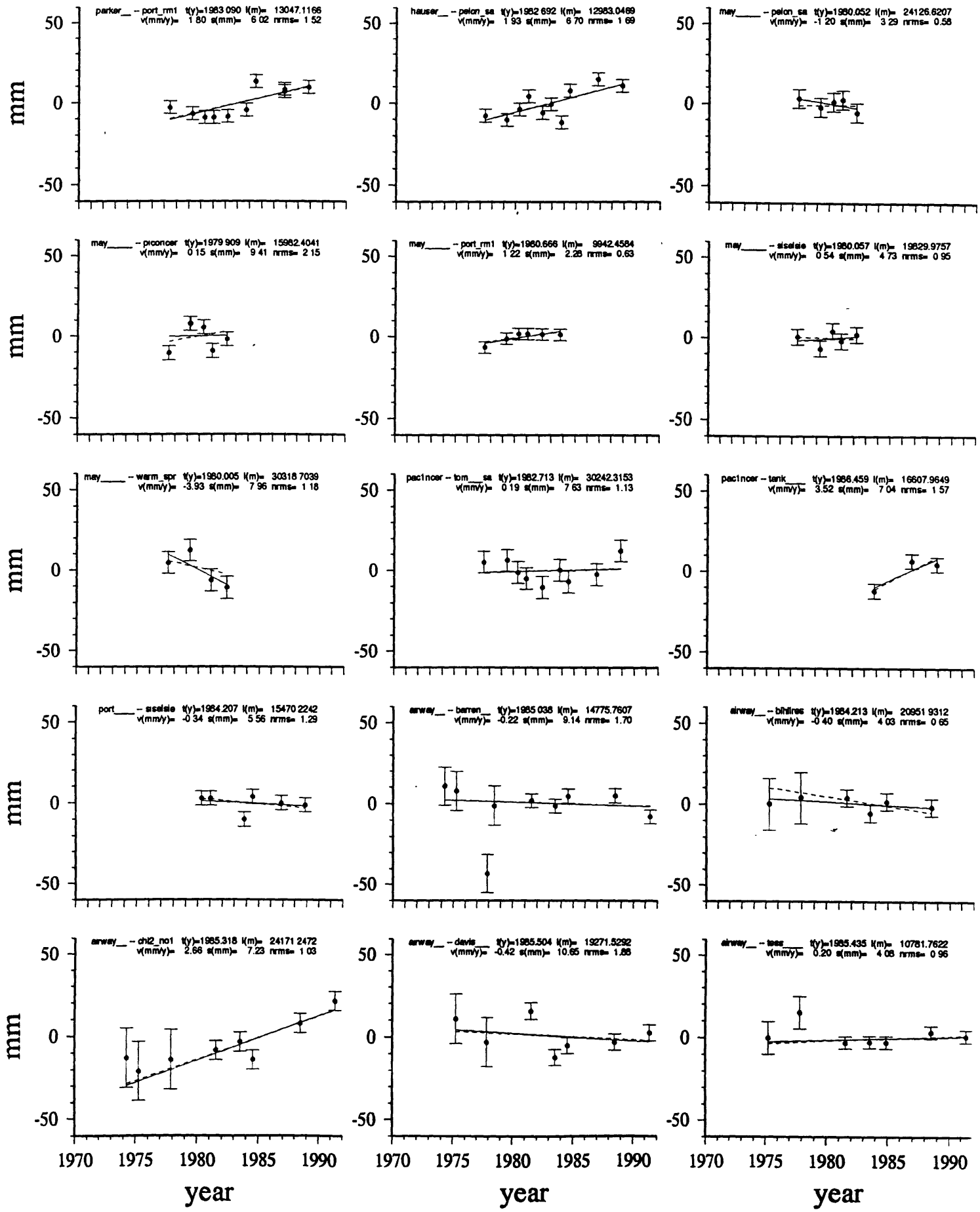
parker__ – port_rm1 t(y)=1983.090 l(m)= 13047.1166
v(mm/y)= 1.80 s(mm)= 6.02 nrms= 1.52
hauser__ – pelon_sa t(y)=1982.692 l(m)= 12983.0469
v(mm/y)= 1.93 s(mm)= 6.70 nrms= 1.69
may_____ – pelon_sa t(y)=1980.052 l(m)= 24126.6207
v(mm/y)= -1.20 s(mm)= 3.29 nrms= 0.58
may_____ – piconcer t(y)=1979.909 l(m)= 15982.4041
v(mm/y)= 0.15 s(mm)= 9.41 nrms= 2.15
may_____ – port_rm1 t(y)=1980.666 l(m)= 9942.4584
v(mm/y)= 1.22 s(mm)= 2.28 nrms= 0.63
may_____ – siselsie t(y)=1980.057 l(m)= 19829.9757
v(mm/y)= 0.54 s(mm)= 4.73 nrms= 0.95
may_____ – warm_spr t(y)=1980.005 l(m)= 30318.7039
v(mm/y)= -3.93 s(mm)= 7.96 nrms= 1.18
pac1ncer – tom___sa t(y)=1982.713 l(m)= 30242.3153
v(mm/y)= 0.19 s(mm)= 7.63 nrms= 1.13
pac1ncer – tank____ t(y)=1986.459 l(m)= 16607.9649
v(mm/y)= 3.52 s(mm)= 7.04 nrms= 1.57
port____ – siselsie t(y)=1984.207 l(m)= 15470.2242
v(mm/y)= -0.34 s(mm)= 5.56 nrms= 1.29
airway__ – barren__ t(y)=1985.038 l(m)= 14775.7607
v(mm/y)= -0.22 s(mm)= 9.14 nrms= 1.70
airway__ – bihilres t(y)=1984.213 l(m)= 20951.9312
v(mm/y)= -0.40 s(mm)= 4.03 nrms= 0.65
airway__ – chl2_no1 t(y)=1985.318 l(m)= 24171.2472
v(mm/y)= 2.66 s(mm)= 7.23 nrms= 1.03
airway__ – davis___ t(y)=1985.504 l(m)= 19271.5292
v(mm/y)= -0.42 s(mm)= 10.65 nrms= 1.85
airway__ – tess____ t(y)=1985.435 l(m)= 10781.7622
v(mm/y)= 0.20 s(mm)= 4.08 nrms= 0.96
mm
50
0
-50
1970
1975
1980
1985
1990
year

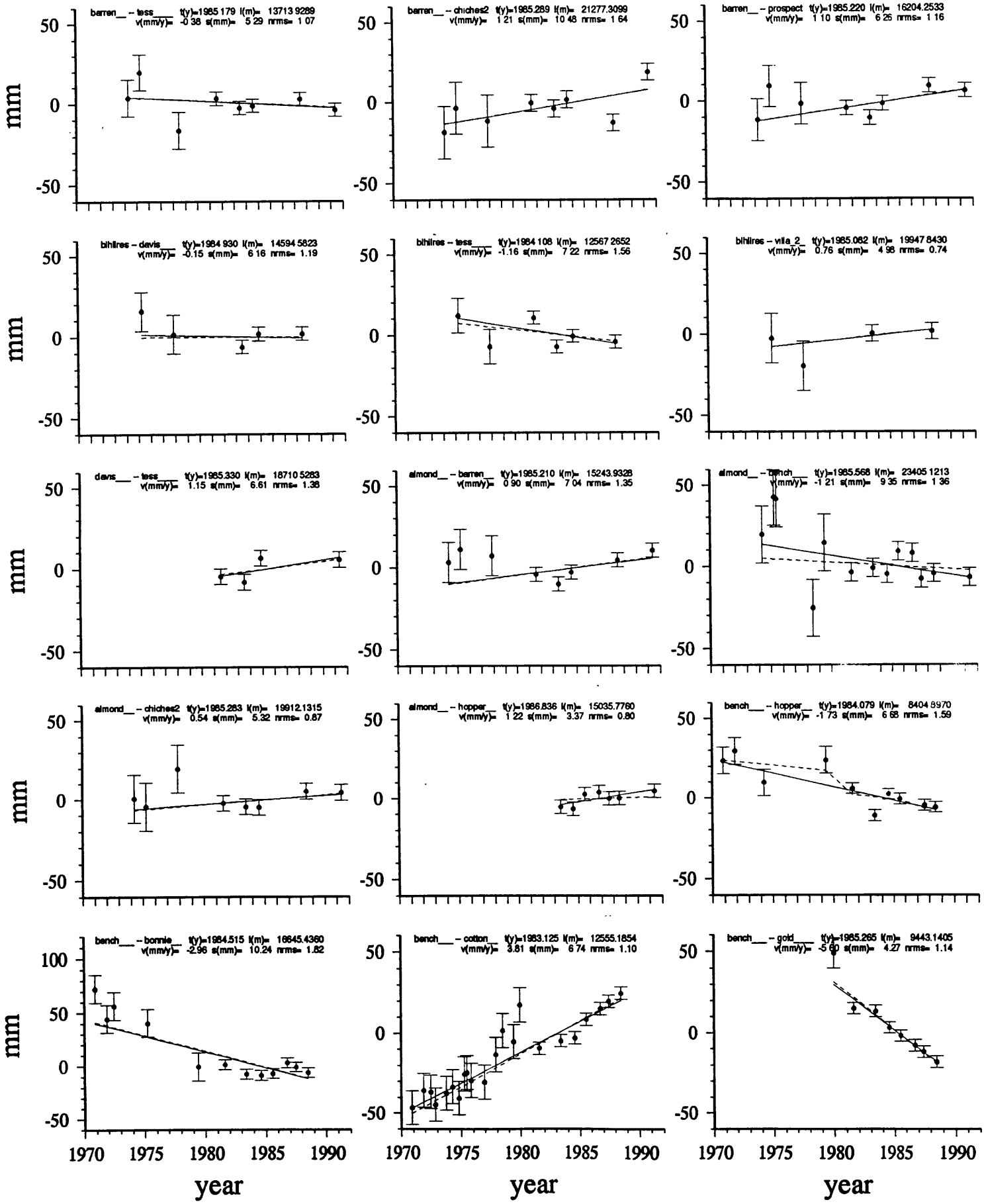
barren__ – tess___ t(y)=1985.179 l(m)= 13713.9289
v(mm/y)= -0.38 s(mm)= 5.29 nrms= 1.07
barren__ – chiches2 t(y)=1985.289 l(m)= 21277.3099
v(mm/y)= 1.21 s(mm)= 10.48 nrms= 1.64
barren__ – prospect t(y)=1985.220 l(m)= 16204.2533
v(mm/y)= 1.10 s(mm)= 6.26 nrms= 1.16
bihlres – davis___ t(y)=1984.930 l(m)= 14594.5823
v(mm/y)= -0.15 s(mm)= 6.16 nrms= 1.19
bihlres – tess___ t(y)=1984.108 l(m)= 12567.2652
v(mm/y)= -1.16 s(mm)= 7.22 nrms= 1.56
bihlres – villa_2 t(y)=1985.062 l(m)= 19947.8430
v(mm/y)= 0.76 s(mm)= 4.98 nrms= 0.74
davis___ – tess___ t(y)=1985.330 l(m)= 18710.5283
v(mm/y)= 1.15 s(mm)= 6.61 nrms= 1.38
almond__ – barren__ t(y)=1985.210 l(m)= 15243.9328
v(mm/y)= 0.90 s(mm)= 7.04 nrms= 1.35
almond__ – bench___ t(y)=1985.568 l(m)= 23405.1213
v(mm/y)= -1.21 s(mm)= 9.35 nrms= 1.36
almond__ – chiches2 t(y)=1985.283 l(m)= 19912.1315
v(mm/y)= 0.54 s(mm)= 5.32 nrms= 0.87
almond__ – hopper__ t(y)=1986.836 l(m)= 15035.7760
v(mm/y)= 1.22 s(mm)= 3.37 nrms= 0.80
bench___ – hopper__ t(y)=1984.079 l(m)= 8404.8970
v(mm/y)= -1.73 s(mm)= 6.68 nrms= 1.59
bench___ – bonnie__ t(y)=1984.515 l(m)= 16645.4360
v(mm/y)= -2.96 s(mm)= 10.24 nrms= 1.82
bench___ – cotton__ t(y)=1983.125 l(m)= 12555.1854
v(mm/y)= 3.81 s(mm)= 6.74 nrms= 1.10
bench___ – gold___ t(y)=1985.265 l(m)= 9443.1405
v(mm/y)= -5.60 s(mm)= 4.27 nrms= 1.14
mm
year
1970
1975
1980
1985
1990

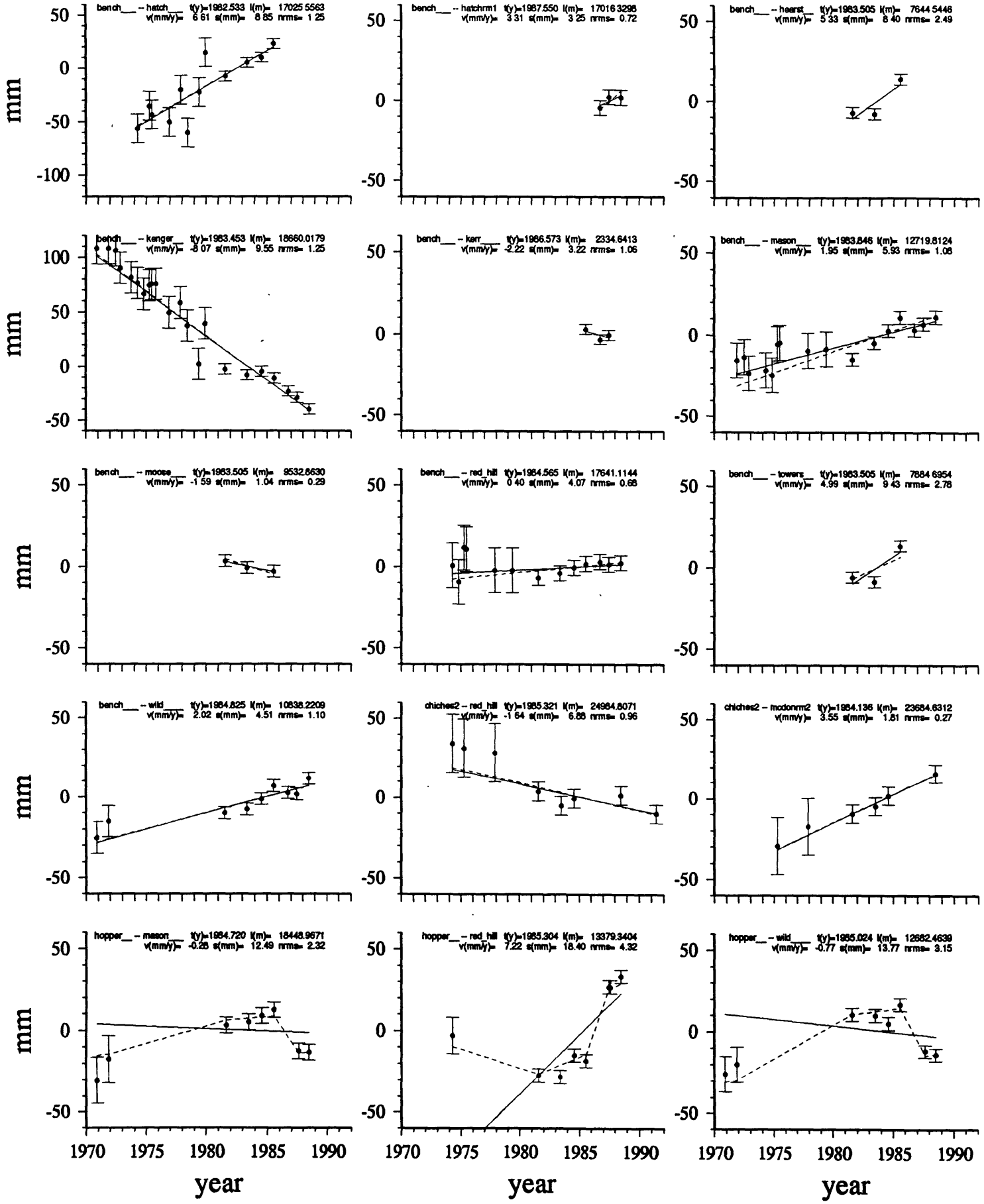
bench___ – hatch___ t(y)=1982.533 l(m)= 17025.5563
v(mm/y)= 6.61 s(mm)= 8.85 nrms= 1.25
bench___ – hatchrm1 t(y)=1987.550 l(m)= 17016.3298
v(mm/y)= 3.31 s(mm)= 3.25 nrms= 0.72
bench___ – hearst___ t(y)=1983.505 l(m)= 7644.5446
v(mm/y)= 5.33 s(mm)= 8.40 nrms= 2.49
bench___ – kenger___ t(y)=1983.453 l(m)= 18660.0179
v(mm/y)= -8.07 s(mm)= 9.55 nrms= 1.25
bench___ – kerr___ t(y)=1986.573 l(m)= 2334.6413
v(mm/y)= -2.22 s(mm)= 3.22 nrms= 1.06
bench___ – mason___ t(y)=1983.846 l(m)= 12719.8124
v(mm/y)= 1.95 s(mm)= 5.93 nrms= 1.08
bench___ – moose___ t(y)=1983.505 l(m)= 9532.6630
v(mm/y)= -1.59 s(mm)= 1.04 nrms= 0.29
bench___ – red_hill t(y)=1984.565 l(m)= 17641.1144
v(mm/y)= 0.40 s(mm)= 4.07 nrms= 0.68
bench___ – towers___ t(y)=1983.505 l(m)= 7684.6954
v(mm/y)= 4.99 s(mm)= 9.43 nrms= 2.78
bench___ – wild___ t(y)=1984.825 l(m)= 10838.2209
v(mm/y)= 2.02 s(mm)= 4.51 nrms= 1.10
chiches2 – red_hill t(y)=1985.321 l(m)= 24984.8071
v(mm/y)= -1.64 s(mm)= 6.88 nrms= 0.96
chiches2 – modonrm2 t(y)=1984.136 l(m)= 23684.8312
v(mm/y)= 3.55 s(mm)= 1.81 nrms= 0.27
hopper___ – mason___ t(y)=1984.720 l(m)= 18448.9671
v(mm/y)= -0.28 s(mm)= 12.49 nrms= 2.32
hopper___ – red_hill t(y)=1985.304 l(m)= 13379.3404
v(mm/y)= 7.22 s(mm)= 16.40 nrms= 4.32
hopper___ – wild___ t(y)=1985.024 l(m)= 12682.4639
v(mm/y)= -0.77 s(mm)= 13.77 nrms= 3.15
mm
year
1970
1975
1980
1985
1990

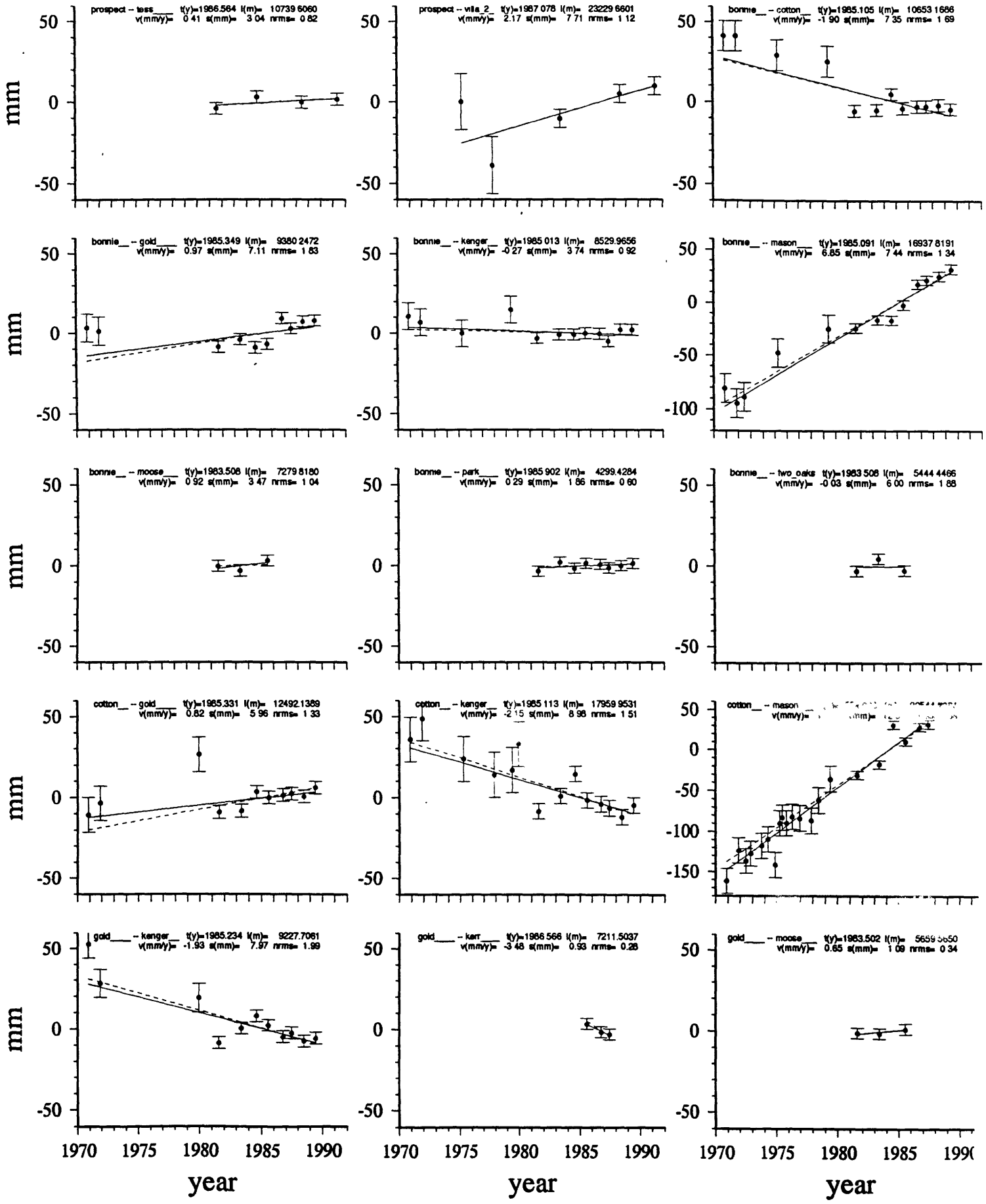
prospect -- tass___ t(y)=1986.564 l(m)= 10739.6060
v(mm/y)= 0.41 s(mm)= 3.04 nrms= 0.82
prospect -- vila_2_ t(y)=1987.078 l(m)= 23229.6601
v(mm/y)= 2.17 s(mm)= 7.71 nrms= 1.12
bonnie__ -- cotton__ t(y)=1985.105 l(m)= 10653.1686
v(mm/y)= -1.90 s(mm)= 7.35 nrms= 1.69
bonnie__ -- gold___ t(y)=1985.349 l(m)= 9380.2472
v(mm/y)= 0.97 s(mm)= 7.11 nrms= 1.83
bonnie__ -- kenger__ t(y)=1985.013 l(m)= 8529.9656
v(mm/y)= -0.27 s(mm)= 3.74 nrms= 0.92
bonnie__ -- mason___ t(y)=1985.091 l(m)= 16937.8191
v(mm/y)= 6.85 s(mm)= 7.44 nrms= 1.34
bonnie__ -- moose___ t(y)=1983.506 l(m)= 7279.8180
v(mm/y)= 0.92 s(mm)= 3.47 nrms= 1.04
bonnie__ -- park___ t(y)=1985.902 l(m)= 4299.4284
v(mm/y)= 0.29 s(mm)= 1.86 nrms= 0.60
bonnie__ -- two_oaks t(y)=1983.508 l(m)= 5444.4466
v(mm/y)= -0.03 s(mm)= 6.00 nrms= 1.88
cotton__ -- gold___ t(y)=1985.331 l(m)= 12492.1389
v(mm/y)= 0.82 s(mm)= 5.96 nrms= 1.33
cotton__ -- kenger__ t(y)=1985.113 l(m)= 17959.9531
v(mm/y)= -2.15 s(mm)= 8.98 nrms= 1.51
cotton__ -- mason___
gold___ -- kenger__ t(y)=1985.234 l(m)= 9227.7061
v(mm/y)= -1.93 s(mm)= 7.97 nrms= 1.99
gold___ -- kerr___ t(y)=1986.566 l(m)= 7211.5037
v(mm/y)= -3.48 s(mm)= 0.93 nrms= 0.28
gold___ -- moose___ t(y)=1983.502 l(m)= 5659.3650
v(mm/y)= 0.65 s(mm)= 1.09 nrms= 0.34
mm
year
50
0
-50
-100
-150
1970
1975
1980
1985
1990

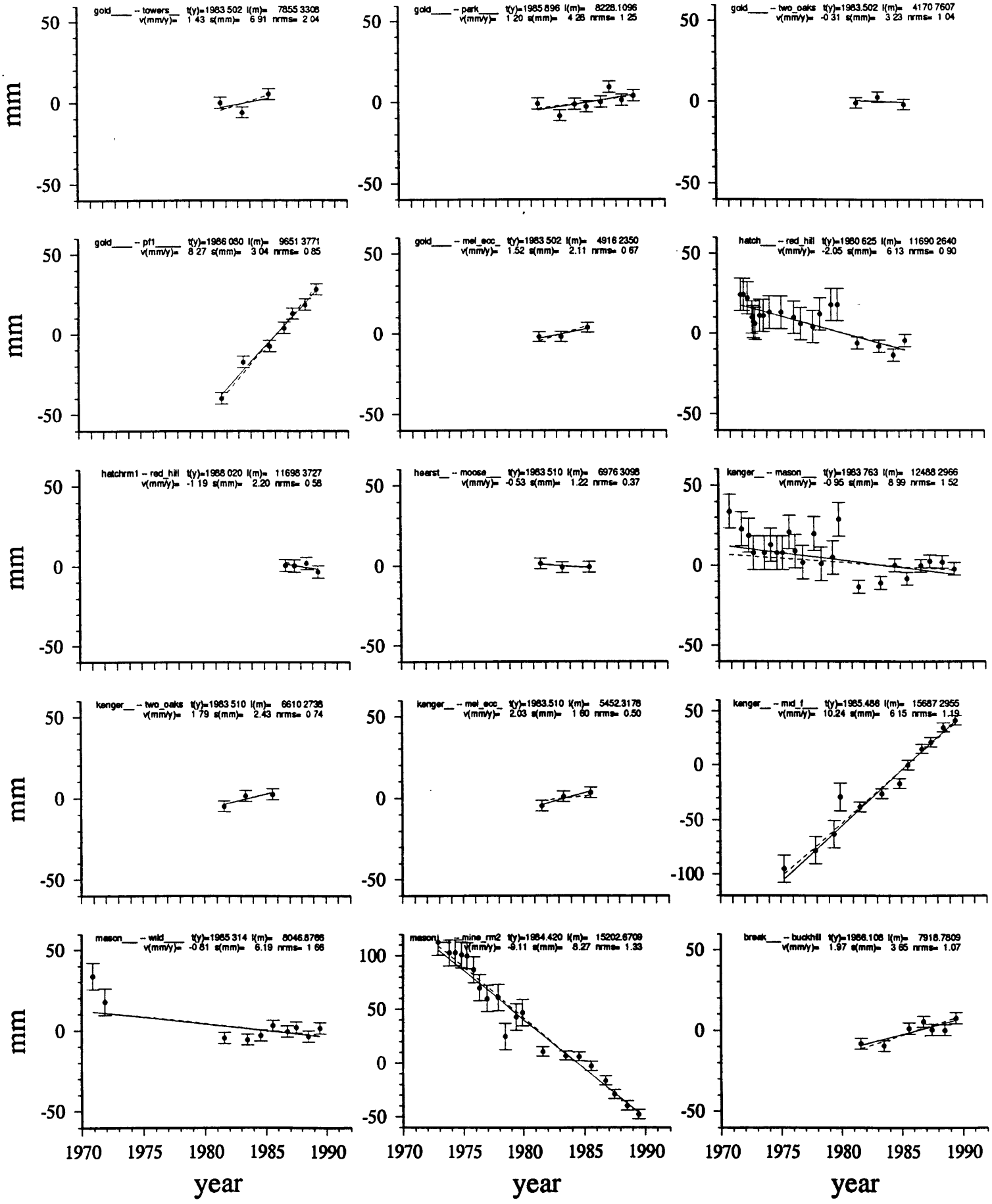
gold___ -- towers_ t(y)=1983.502 l(m)= 7855.3308
v(mm/y)= 1.43 s(mm)= 6.91 nrms= 2.04
gold___ -- park___ t(y)=1985.896 l(m)= 8228.1096
v(mm/y)= 1.20 s(mm)= 4.28 nrms= 1.25
gold___ -- two_oaks t(y)=1983.502 l(m)= 4170.7607
v(mm/y)= -0.31 s(mm)= 3.23 nrms= 1.04
gold___ -- pf1____ t(y)=1986.080 l(m)= 9651.3771
v(mm/y)= 8.27 s(mm)= 3.04 nrms= 0.85
gold___ -- mel_ecc_ t(y)=1983.502 l(m)= 4916.2350
v(mm/y)= 1.52 s(mm)= 2.11 nrms= 0.67
hatch___ -- red_hill t(y)=1980.625 l(m)= 11690.2640
v(mm/y)= -2.05 s(mm)= 6.13 nrms= 0.90
hatchrm1 -- red_hill t(y)=1988.020 l(m)= 11698.3727
v(mm/y)= -1.19 s(mm)= 2.20 nrms= 0.58
hearst__ -- moose___ t(y)=1983.510 l(m)= 6976.3098
v(mm/y)= -0.53 s(mm)= 1.22 nrms= 0.37
kenger__ -- mason___ t(y)=1983.763 l(m)= 12488.2966
v(mm/y)= -0.95 s(mm)= 8.99 nrms= 1.52
kenger__ -- two_oaks t(y)=1983.510 l(m)= 6610.2736
v(mm/y)= 1.79 s(mm)= 2.43 nrms= 0.74
kenger__ -- mel_ecc_ t(y)=1983.510 l(m)= 5452.3178
v(mm/y)= 2.03 s(mm)= 1.60 nrms= 0.50
kenger__ -- mid_f___ t(y)=1985.486 l(m)= 15687.2955
v(mm/y)= 10.24 s(mm)= 6.15 nrms= 1.19
mason___ -- wild____ t(y)=1985.314 l(m)= 8046.8766
v(mm/y)= -0.81 s(mm)= 6.19 nrms= 1.66
mason___ -- mine_rm2 t(y)=1984.420 l(m)= 15202.6709
v(mm/y)= -9.11 s(mm)= 8.27 nrms= 1.33
break___ -- buckhill t(y)=1986.106 l(m)= 7916.7809
v(mm/y)= 1.97 s(mm)= 3.65 nrms= 1.07
mm
year
1970
1975
1980
1985
1990

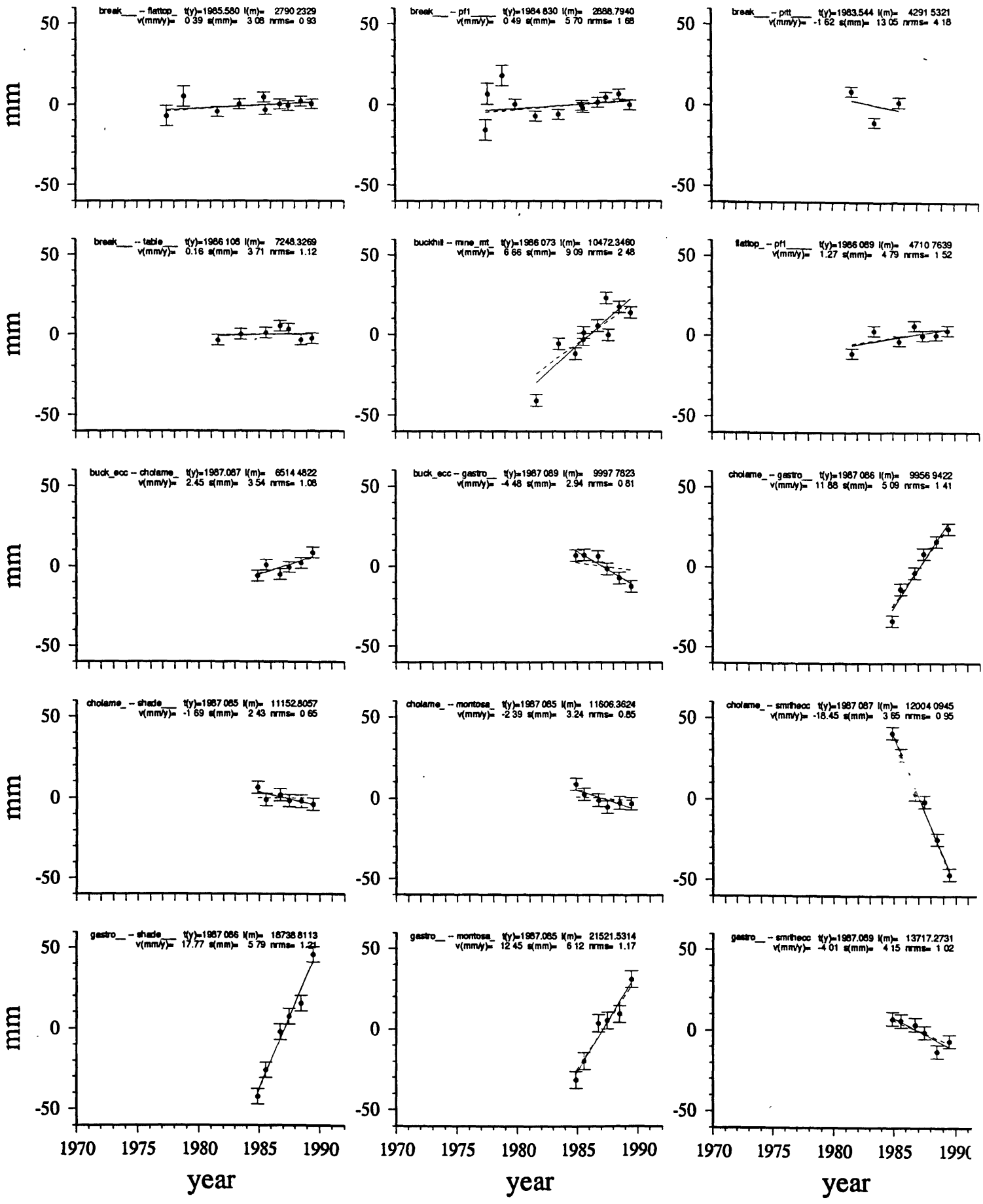
break___ – flattop_ t(y)=1985.580 l(m)= 2790.2329
v(mm/y)= 0.39 s(mm)= 3.06 nrms= 0.93
break___ – pf1____ t(y)=1984.830 l(m)= 2888.7940
v(mm/y)= 0.49 s(mm)= 5.70 nrms= 1.68
break___ – prtt____ t(y)=1983.544 l(m)= 4291.5321
v(mm/y)= -1.62 s(mm)= 13.05 nrms= 4.18
break___ – table___ t(y)=1986.106 l(m)= 7248.3269
v(mm/y)= 0.16 s(mm)= 3.71 nrms= 1.12
buckhill – mine_mt_ t(y)=1986.073 l(m)= 10472.3460
v(mm/y)= 6.66 s(mm)= 9.09 nrms= 2.48
flattop_ – pf1____ t(y)=1986.089 l(m)= 4710.7639
v(mm/y)= 1.27 s(mm)= 4.79 nrms= 1.52
buck_ecc – cholame_ t(y)=1987.087 l(m)= 6514.4822
v(mm/y)= 2.45 s(mm)= 3.54 nrms= 1.08
buck_ecc – gastro__ t(y)=1987.089 l(m)= 9997.7823
v(mm/y)= -4.48 s(mm)= 2.94 nrms= 0.81
cholame_ – gastro__ t(y)=1987.086 l(m)= 9956.9422
v(mm/y)= 11.88 s(mm)= 5.09 nrms= 1.41
cholame_ – shade___ t(y)=1987.085 l(m)= 11152.8057
v(mm/y)= -1.69 s(mm)= 2.43 nrms= 0.65
cholame_ – montosa_ t(y)=1987.085 l(m)= 11606.3624
v(mm/y)= -2.39 s(mm)= 3.24 nrms= 0.85
cholame_ – smrthecc t(y)=1987.087 l(m)= 12004.0945
v(mm/y)= -18.45 s(mm)= 3.65 nrms= 0.95
gastro__ – shade___ t(y)=1987.086 l(m)= 18738.8113
v(mm/y)= 17.77 s(mm)= 5.79 nrms= 1.21
gastro__ – montosa_ t(y)=1987.085 l(m)= 21521.5314
v(mm/y)= 12.45 s(mm)= 6.12 nrms= 1.17
gastro__ – smrthecc t(y)=1987.089 l(m)= 13717.2731
v(mm/y)= -4.01 s(mm)= 4.15 nrms= 1.02
50
0
-50
mm
1970
1975
1980
1985
1990
year

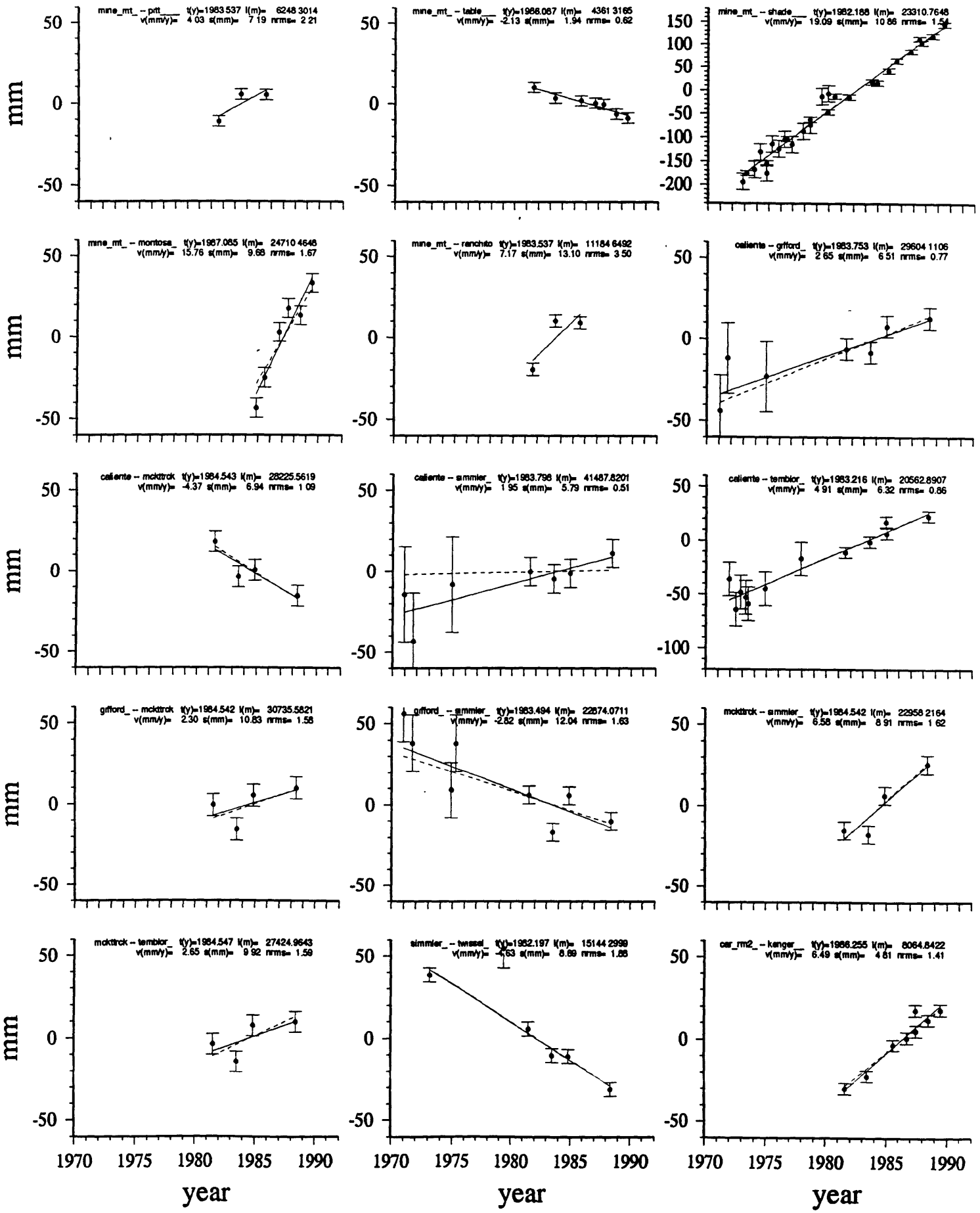
mine_mt_ – prtt____ t(y)=1983.537 l(m)= 6248.3014
v(mm/y)= 4.03 s(mm)= 7.19 nrms= 2.21
mine_mt_ – table___ t(y)=1986.067 l(m)= 4361.3165
v(mm/y)= -2.13 s(mm)= 1.94 nrms= 0.62
mine_mt_ – shade___ t(y)=1982.188 l(m)= 23310.7648
v(mm/y)= 19.09 s(mm)= 10.86 nrms= 1.54
mine_mt_ – montosa_ t(y)=1987.065 l(m)= 24710.4646
v(mm/y)= 15.76 s(mm)= 9.68 nrms= 1.67
mine_mt_ – ranchito t(y)=1983.537 l(m)= 11184.6492
v(mm/y)= 7.17 s(mm)= 13.10 nrms= 3.50
caliente – grfford_ t(y)=1983.753 l(m)= 29604.1106
v(mm/y)= 2.65 s(mm)= 6.51 nrms= 0.77
caliente – mckttrck t(y)=1984.543 l(m)= 28225.5619
v(mm/y)= -4.37 s(mm)= 6.94 nrms= 1.09
caliente – simmier_ t(y)=1983.798 l(m)= 41487.8201
v(mm/y)= 1.95 s(mm)= 5.79 nrms= 0.51
caliente – temblor_ t(y)=1983.216 l(m)= 20562.8907
v(mm/y)= 4.91 s(mm)= 6.32 nrms= 0.86
grfford_ – mckttrck t(y)=1984.542 l(m)= 30735.5821
v(mm/y)= 2.30 s(mm)= 10.83 nrms= 1.58
grfford_ – simmier_ t(y)=1983.494 l(m)= 22874.0711
v(mm/y)= -2.82 s(mm)= 12.04 nrms= 1.63
mckttrck – simmier_ t(y)=1984.542 l(m)= 22958.2164
v(mm/y)= 6.58 s(mm)= 8.91 nrms= 1.62
mckttrck – temblor_ t(y)=1984.547 l(m)= 27424.9643
v(mm/y)= 2.65 s(mm)= 9.92 nrms= 1.59
simmier_ – twssel_ t(y)=1982.197 l(m)= 15144.2998
v(mm/y)= -4.63 s(mm)= 8.69 nrms= 1.86
cer_rm2_ – kenger_ t(y)=1986.255 l(m)= 8064.8422
v(mm/y)= 6.49 s(mm)= 4.81 nrms= 1.41
mm
year
1970
1975
1980
1985
1990

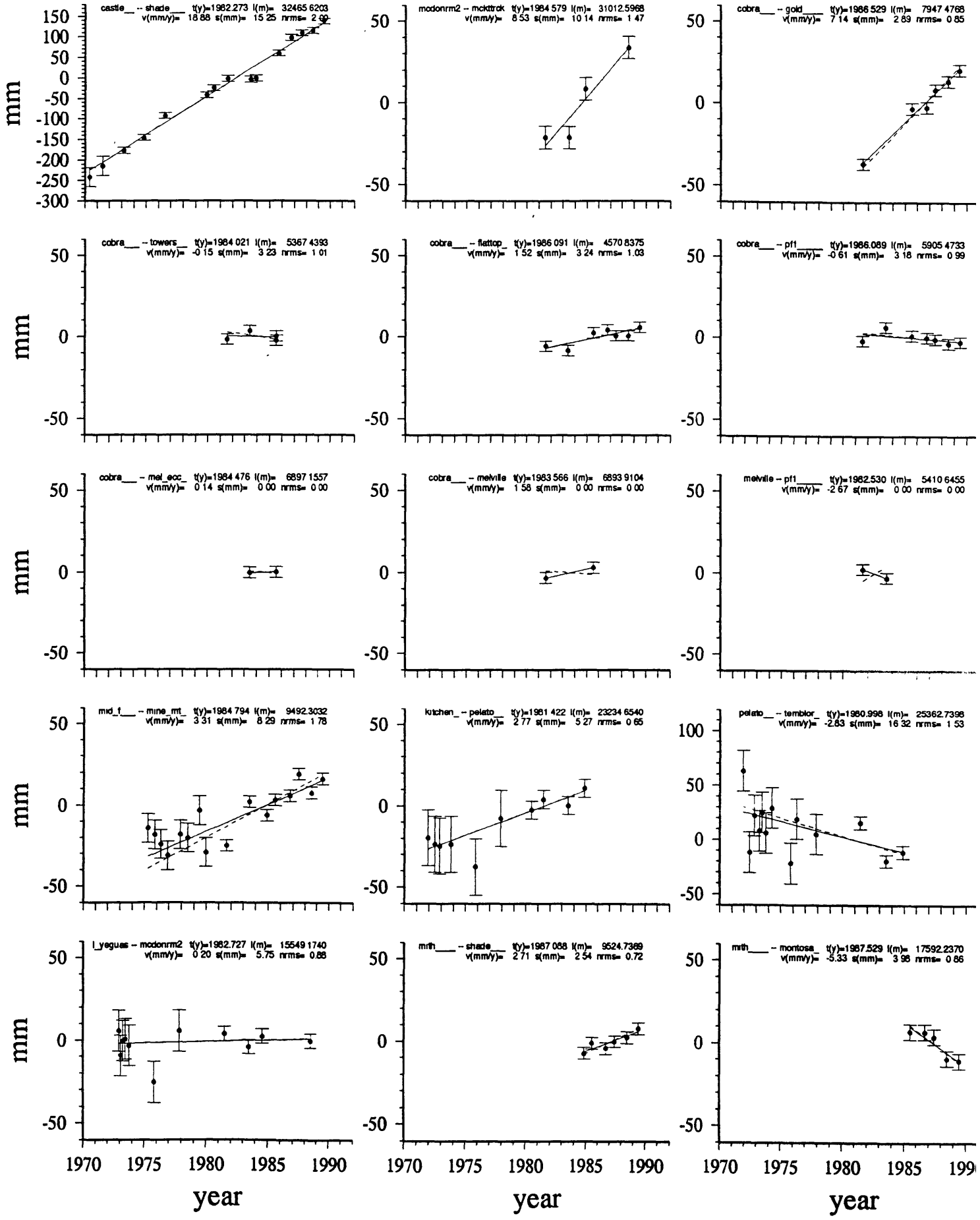
castle__ -- shade___ t(y)=1982.273 l(m)= 32465.6203
v(mm/y)= 18.68 s(mm)= 15.25 nrms= 2.99
modonrm2 -- mcktrck t(y)=1984.579 l(m)= 31012.5968
v(mm/y)= 8.53 s(mm)= 10.14 nrms= 1.47
cobra___ -- gold____ t(y)=1986.529 l(m)= 7947.4768
v(mm/y)= 7.14 s(mm)= 2.89 nrms= 0.85
cobra___ -- towers__ t(y)=1984.021 l(m)= 5367.4393
v(mm/y)= -0.15 s(mm)= 3.23 nrms= 1.01
cobra___ -- flattop_ t(y)=1986.091 l(m)= 4570.8375
v(mm/y)= 1.52 s(mm)= 3.24 nrms= 1.03
cobra___ -- pf1_____ t(y)=1986.089 l(m)= 5905.4733
v(mm/y)= -0.61 s(mm)= 3.18 nrms= 0.99
cobra___ -- mel_ecc_ t(y)=1984.476 l(m)= 6897.1557
v(mm/y)= 0.14 s(mm)= 0.00 nrms= 0.00
cobra___ -- melville t(y)=1983.566 l(m)= 6893.9104
v(mm/y)= 1.58 s(mm)= 0.00 nrms= 0.00
melville -- pf1_____ t(y)=1982.530 l(m)= 5410.6455
v(mm/y)= -2.67 s(mm)= 0.00 nrms= 0.00
mid_f___ -- mine_mt_ t(y)=1984.794 l(m)= 9492.3032
v(mm/y)= 3.31 s(mm)= 8.29 nrms= 1.78
kitchen_ -- pelato__ t(y)=1981.422 l(m)= 23234.6540
v(mm/y)= 2.77 s(mm)= 5.27 nrms= 0.65
pelato__ -- temblor_ t(y)=1980.998 l(m)= 25362.7398
v(mm/y)= -2.83 s(mm)= 16.32 nrms= 1.53
l_yeguas -- modonrm2 t(y)=1982.727 l(m)= 15549.1740
v(mm/y)= 0.20 s(mm)= 5.75 nrms= 0.88
mth____ -- shade___ t(y)=1987.088 l(m)= 9524.7389
v(mm/y)= 2.71 s(mm)= 2.54 nrms= 0.72
mth____ -- montosa_ t(y)=1987.529 l(m)= 17592.2370
v(mm/y)= -5.33 s(mm)= 3.98 nrms= 0.86
mm
year
1970
1975
1980
1985
1990

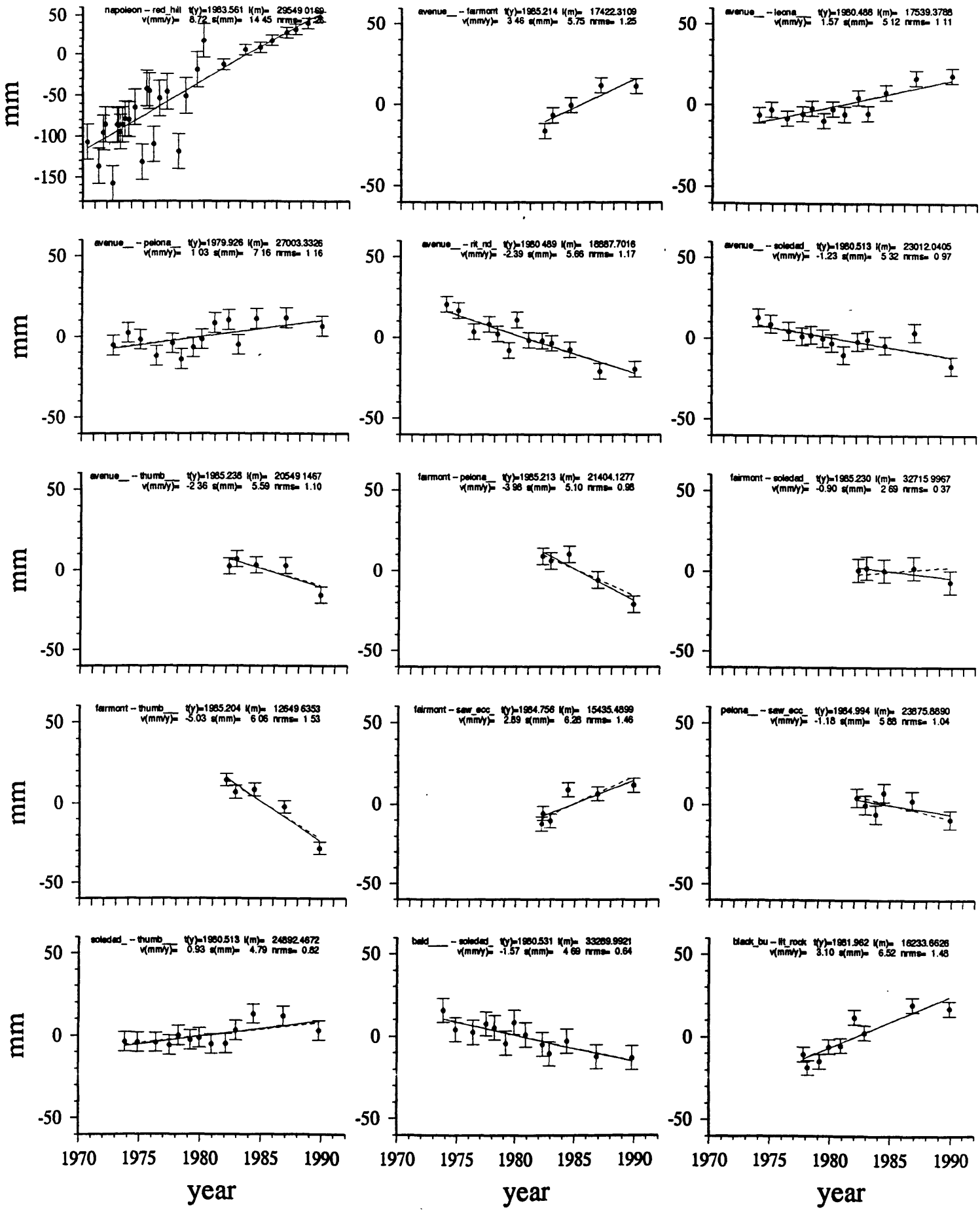
napoleon – red_hill t(y)=1983.561 l(m)= 29549.0169
v(mm/y)= 8.72 s(mm)= 14.45 nrms= 1.28
avenue__ – fairmont t(y)=1985.214 l(m)= 17422.3109
v(mm/y)= 3.46 s(mm)= 5.75 nrms= 1.25
avenue__ – leona__ t(y)=1980.488 l(m)= 17539.3788
v(mm/y)= 1.57 s(mm)= 5.12 nrms= 1.11
avenue__ – pelona__ t(y)=1979.926 l(m)= 27003.3326
v(mm/y)= 1.03 s(mm)= 7.16 nrms= 1.16
avenue__ – rit_rd_ t(y)=1980.489 l(m)= 18687.7016
v(mm/y)= -2.39 s(mm)= 5.66 nrms= 1.17
avenue__ – soledad_ t(y)=1980.513 l(m)= 23012.0405
v(mm/y)= -1.23 s(mm)= 5.32 nrms= 0.97
avenue__ – thumb___ t(y)=1985.238 l(m)= 20549.1467
v(mm/y)= -2.36 s(mm)= 5.59 nrms= 1.10
fairmont – pelona__ t(y)=1985.213 l(m)= 21404.1277
v(mm/y)= -3.98 s(mm)= 5.10 nrms= 0.98
fairmont – soledad_ t(y)=1985.230 l(m)= 32715.9967
v(mm/y)= -0.90 s(mm)= 2.69 nrms= 0.37
fairmont – thumb___ t(y)=1985.204 l(m)= 12649.6353
v(mm/y)= -5.03 s(mm)= 6.06 nrms= 1.53
fairmont – saw_ecc_ t(y)=1984.756 l(m)= 15435.4899
v(mm/y)= 2.89 s(mm)= 6.28 nrms= 1.46
pelona__ – saw_ecc_ t(y)=1984.994 l(m)= 23875.8890
v(mm/y)= -1.18 s(mm)= 5.85 nrms= 1.04
soledad_ – thumb___ t(y)=1980.513 l(m)= 24892.4672
v(mm/y)= 0.93 s(mm)= 4.79 nrms= 0.82
bald____ – soledad_ t(y)=1980.531 l(m)= 33269.9921
v(mm/y)= -1.57 s(mm)= 4.69 nrms= 0.64
black_bu – lit_rock t(y)=1981.962 l(m)= 16233.6626
v(mm/y)= 3.10 s(mm)= 6.52 nrms= 1.48
mm
50
0
-50
-100
-150
1970
1975
1980
1985
1990
year

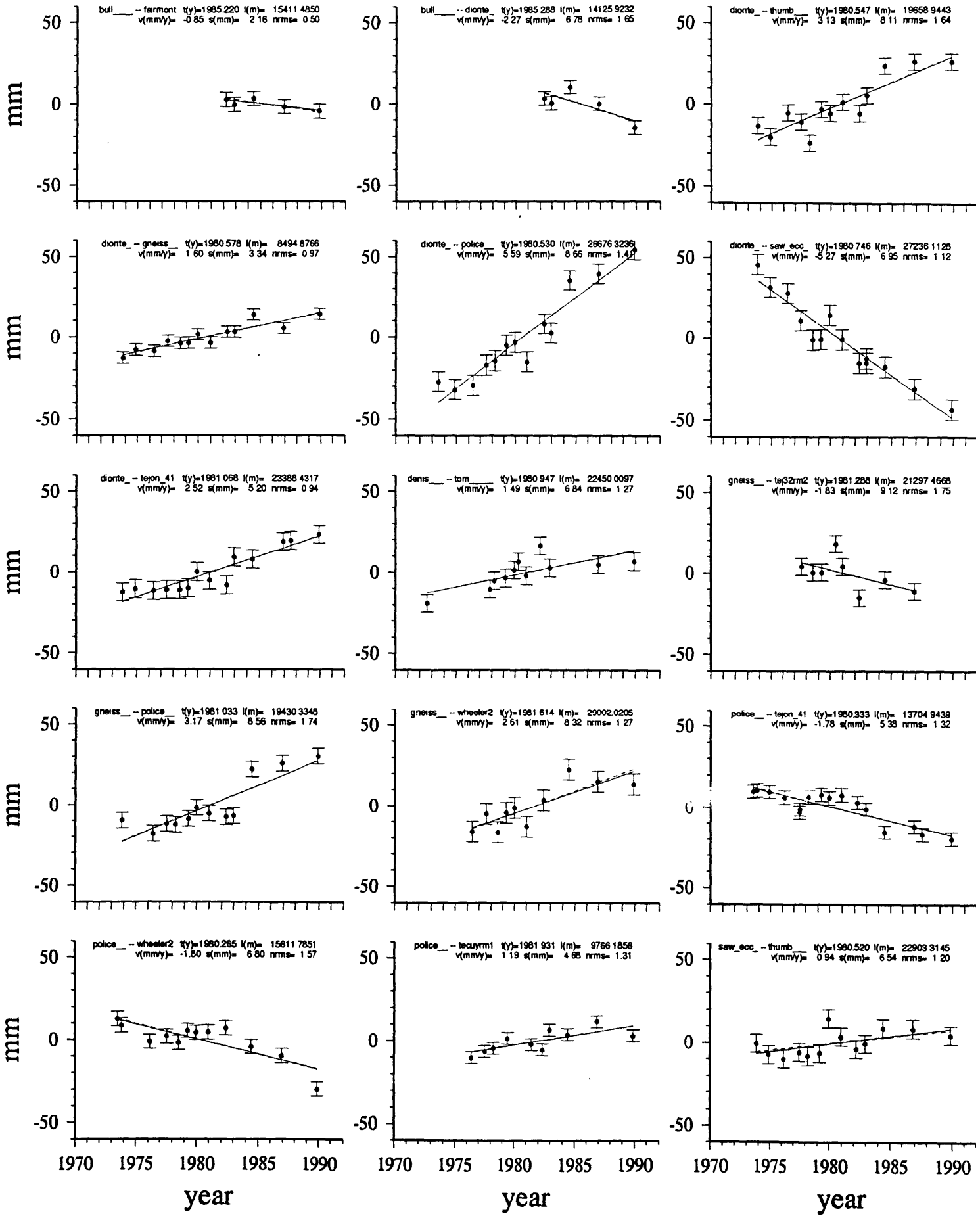
bull___ -- fairmont t(y)=1985.220 l(m)= 15411.4850
v(mm/y)= -0.85 s(mm)= 2.16 nrms= 0.50
bull___ -- diorite_ t(y)=1985.288 l(m)= 14125.9232
v(mm/y)= -2.27 s(mm)= 6.78 nrms= 1.65
diorite_ -- thumb___ t(y)=1980.547 l(m)= 19658.9443
v(mm/y)= 3.13 s(mm)= 8.11 nrms= 1.64
diorite_ -- gneiss__ t(y)=1980.578 l(m)= 8494.8766
v(mm/y)= 1.60 s(mm)= 3.34 nrms= 0.97
diorite_ -- police__ t(y)=1980.530 l(m)= 26676.3236
v(mm/y)= 5.59 s(mm)= 8.66 nrms= 1.41
diorite_ -- saw_ecc_ t(y)=1980.746 l(m)= 27236.1128
v(mm/y)= -5.27 s(mm)= 6.95 nrms= 1.12
diorite_ -- tejon_41 t(y)=1981.068 l(m)= 23388.4317
v(mm/y)= 2.52 s(mm)= 5.20 nrms= 0.94
denis___ -- tom_____ t(y)=1980.947 l(m)= 22450.0097
v(mm/y)= 1.49 s(mm)= 6.84 nrms= 1.27
gneiss__ -- tej32rm2 t(y)=1981.288 l(m)= 21297.4668
v(mm/y)= -1.83 s(mm)= 9.12 nrms= 1.75
gneiss__ -- police__ t(y)=1981.033 l(m)= 19430.3348
v(mm/y)= 3.17 s(mm)= 8.56 nrms= 1.74
gneiss__ -- wheeler2 t(y)=1981.614 l(m)= 29002.0205
v(mm/y)= 2.61 s(mm)= 8.32 nrms= 1.27
police__ -- tejon_41 t(y)=1980.333 l(m)= 13704.9439
v(mm/y)= -1.78 s(mm)= 5.38 nrms= 1.32
police__ -- wheeler2 t(y)=1980.265 l(m)= 15611.7851
v(mm/y)= -1.80 s(mm)= 6.80 nrms= 1.57
police__ -- tecuyrm1 t(y)=1981.931 l(m)= 9766.1856
v(mm/y)= 1.19 s(mm)= 4.68 nrms= 1.31
saw_ecc_ -- thumb___ t(y)=1980.520 l(m)= 22903.3145
v(mm/y)= 0.94 s(mm)= 6.54 nrms= 1.20
50
0
-50
mm
1970
1975
1980
1985
1990
year

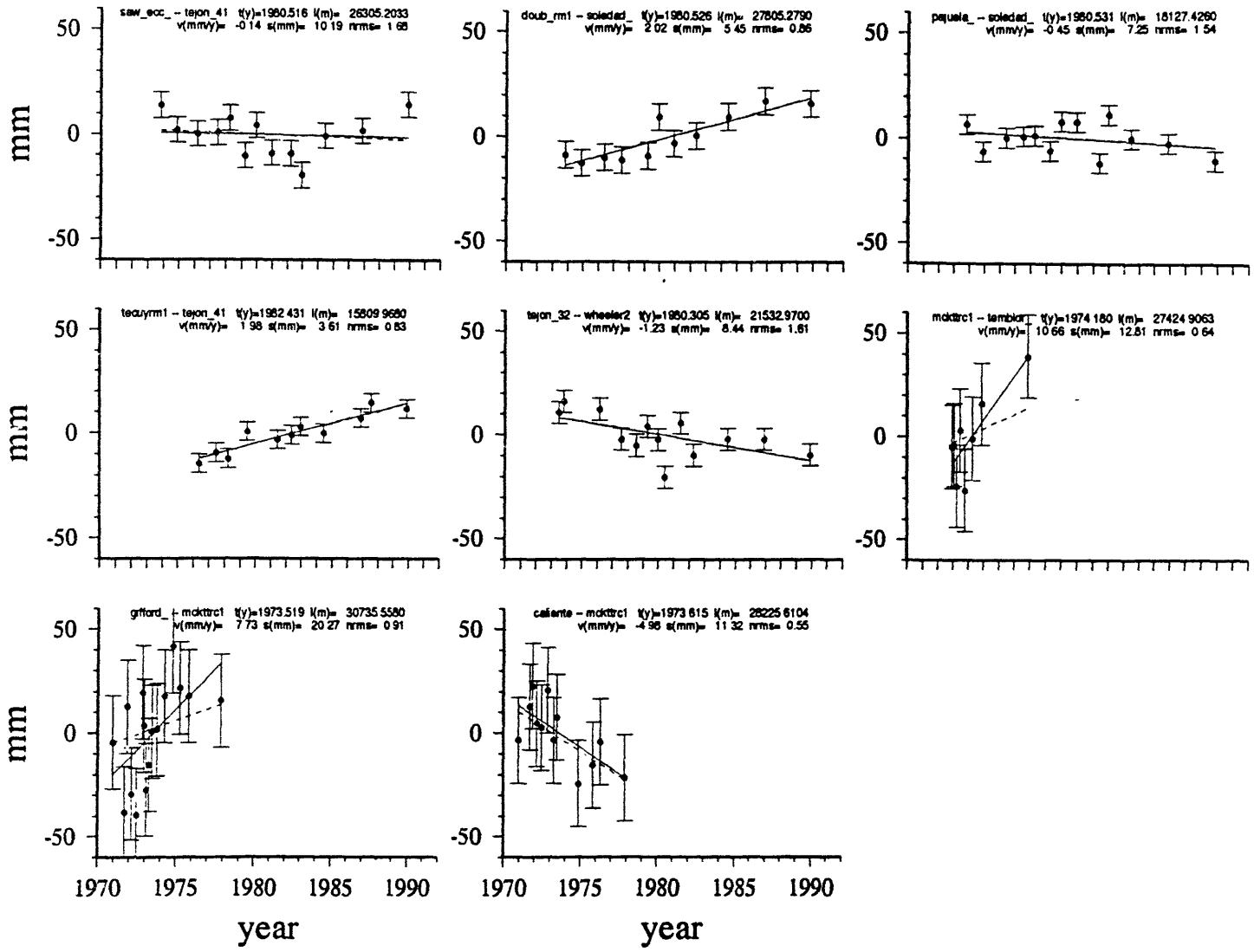
saw_ecc_ – tejon_41 t(y)=1980.516 l(m)= 26305.2033
v(mm/y)= -0.14 s(mm)= 10.19 nrms= 1.68
doub_rm1 – soledad_ t(y)=1980.526 l(m)= 27805.2790
v(mm/y)= 2.02 s(mm)= 5.45 nrms= 0.86
pajuela_ – soledad_ t(y)=1980.531 l(m)= 18127.4260
v(mm/y)= -0.45 s(mm)= 7.25 nrms= 1.54
tecuyrm1 – tejon_41 t(y)=1982.431 l(m)= 15809.9680
v(mm/y)= 1.98 s(mm)= 3.61 nrms= 0.83
tejon_32 – wheeler2 t(y)=1980.305 l(m)= 21532.9700
v(mm/y)= -1.23 s(mm)= 8.44 nrms= 1.61
mcktrc1 – temblor_ t(y)=1974.180 l(m)= 27424.9063
v(mm/y)= 10.66 s(mm)= 12.81 nrms= 0.64
grflord_ – mcktrc1 t(y)=1973.519 l(m)= 30735.5580
v(mm/y)= 7.73 s(mm)= 20.27 nrms= 0.91
caliente – mcktrc1 t(y)=1973.615 l(m)= 28225.6104
v(mm/y)= -4.96 s(mm)= 11.32 nrms= 0.55
mm
50
0
-50
1970
1975
1980
1985
1990
year

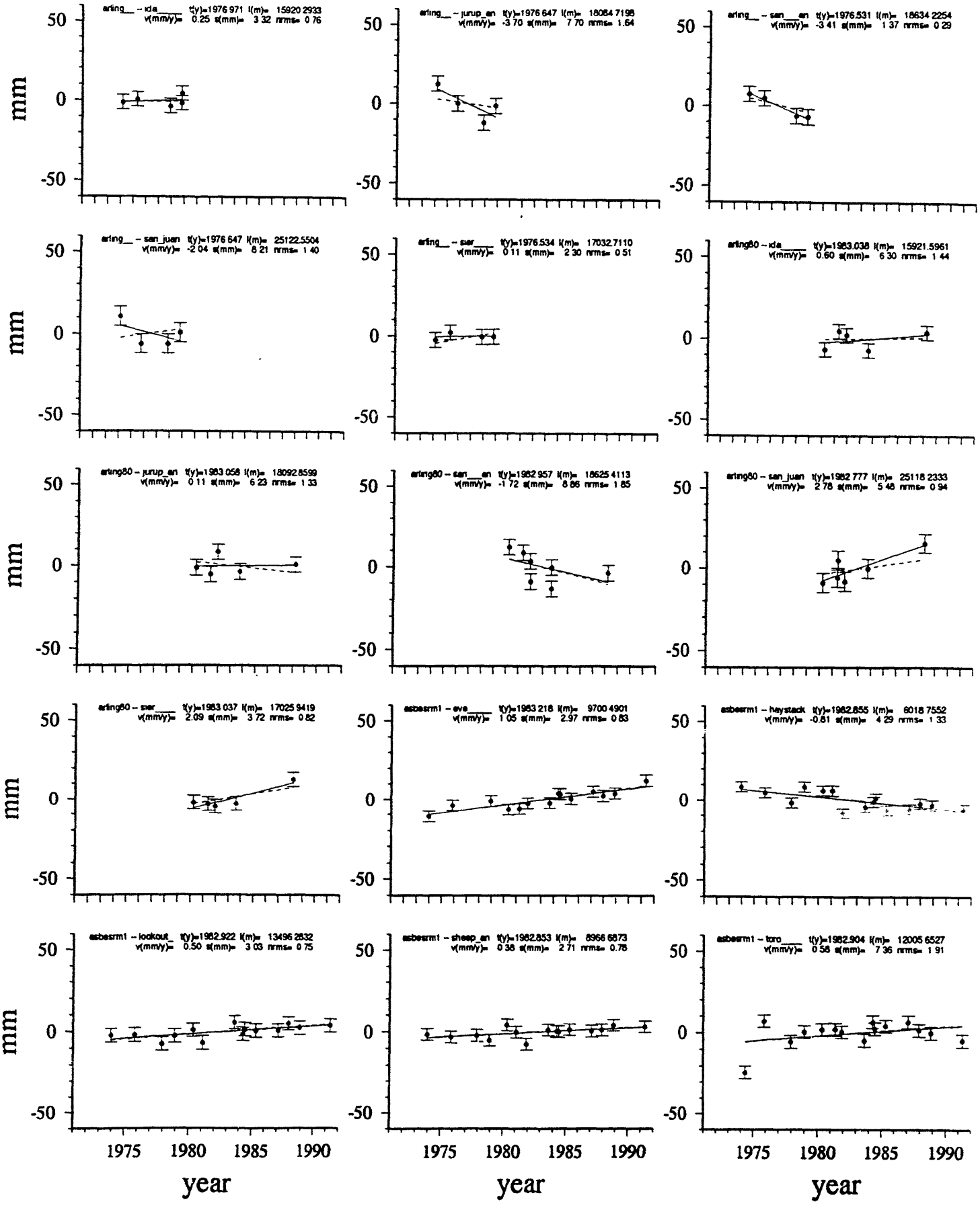
arling__ – ida_____ t(y)=1976.971 l(m)= 15920.2933
v(mm/y)= 0.25 s(mm)= 3.32 nrms= 0.76
arling__ – jurup_an t(y)=1976.647 l(m)= 18084.7198
v(mm/y)= -3.70 s(mm)= 7.70 nrms= 1.64
arling__ – san___an t(y)=1976.531 l(m)= 18634.2254
v(mm/y)= -3.41 s(mm)= 1.37 nrms= 0.29
arling__ – san_juan t(y)=1976.647 l(m)= 25122.5504
v(mm/y)= -2.04 s(mm)= 8.21 nrms= 1.40
arling__ – ser_____ t(y)=1976.534 l(m)= 17032.7110
v(mm/y)= 0.11 s(mm)= 2.30 nrms= 0.51
arling80 – ida_____ t(y)=1983.038 l(m)= 15921.5961
v(mm/y)= 0.60 s(mm)= 6.30 nrms= 1.44
arling80 – jurup_an t(y)=1983.058 l(m)= 18092.8599
v(mm/y)= 0.11 s(mm)= 6.23 nrms= 1.33
arling80 – san___an t(y)=1982.957 l(m)= 18625.4113
v(mm/y)= -1.72 s(mm)= 8.86 nrms= 1.85
arling80 – san_juan t(y)=1982.777 l(m)= 25118.2333
v(mm/y)= 2.78 s(mm)= 5.48 nrms= 0.94
arling80 – ser_____ t(y)=1983.037 l(m)= 17025.9419
v(mm/y)= 2.09 s(mm)= 3.72 nrms= 0.82
asbesrm1 – eve_____ t(y)=1983.218 l(m)= 9700.4901
v(mm/y)= 1.05 s(mm)= 2.97 nrms= 0.83
asbesrm1 – haystack t(y)=1982.855 l(m)= 6018.7552
v(mm/y)= -0.81 s(mm)= 4.29 nrms= 1.33
asbesrm1 – lookout_ t(y)=1982.922 l(m)= 13496.2832
v(mm/y)= 0.50 s(mm)= 3.03 nrms= 0.75
asbesrm1 – sheep_an t(y)=1982.853 l(m)= 8966.6873
v(mm/y)= 0.38 s(mm)= 2.71 nrms= 0.78
asbesrm1 – toro____ t(y)=1982.904 l(m)= 12005.6527
v(mm/y)= 0.58 s(mm)= 7.36 nrms= 1.91
50
0
-50
mm
1975
1980
1985
1990
year

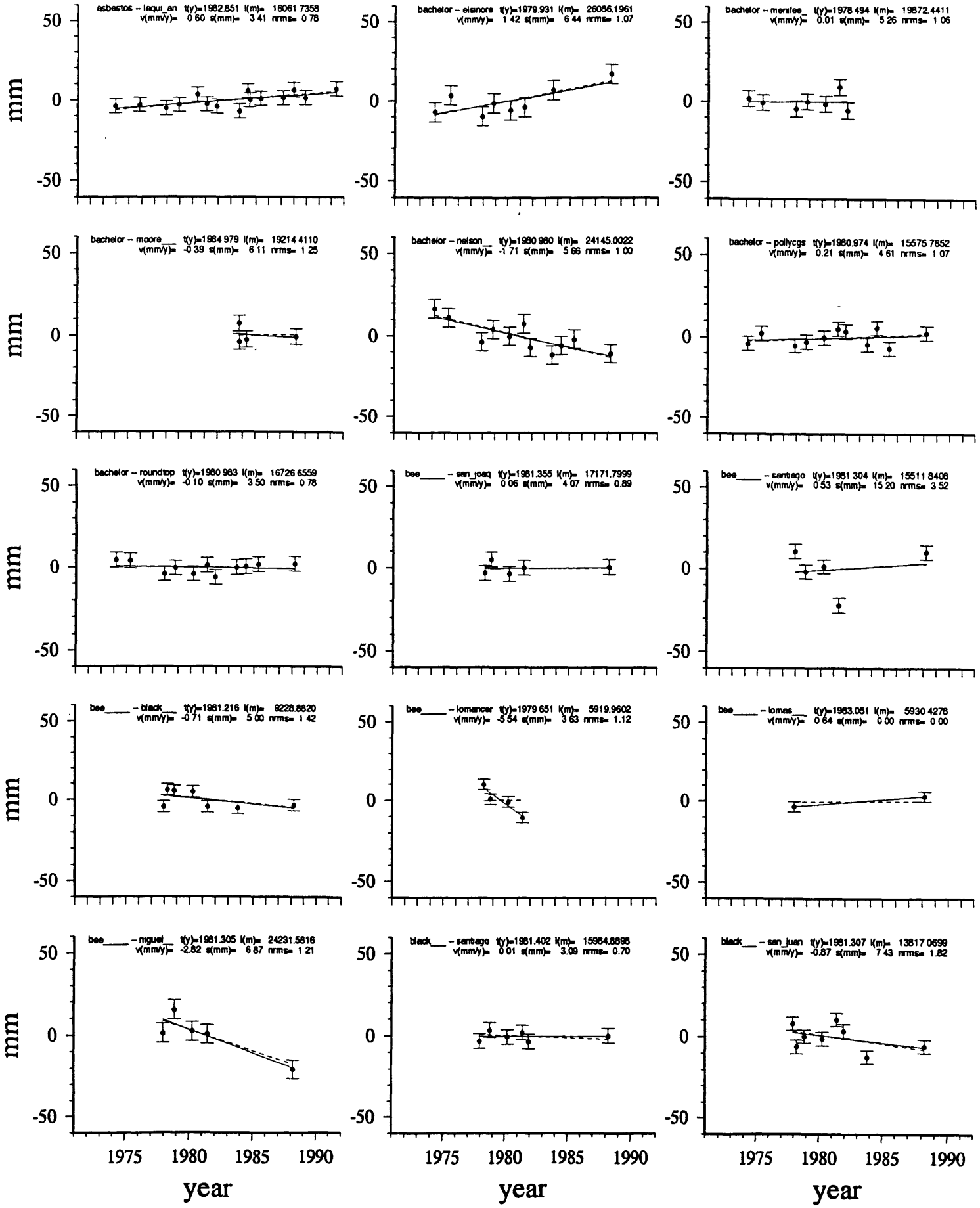
asbestos – laqui_an t(y)=1982.851 l(m)= 16061.7358
v(mm/y)= 0.60 s(mm)= 3.41 nrms= 0.78
bachelor – elsinore t(y)=1979.931 l(m)= 26086.1961
v(mm/y)= 1.42 s(mm)= 6.44 nrms= 1.07
bachelor – mesfee t(y)=1978.494 l(m)= 19872.4411
v(mm/y)= 0.01 s(mm)= 5.26 nrms= 1.06
bachelor – moore t(y)=1984.979 l(m)= 19214.4110
v(mm/y)= -0.39 s(mm)= 6.11 nrms= 1.25
bachelor – nelson t(y)=1980.980 l(m)= 24145.0022
v(mm/y)= -1.71 s(mm)= 5.66 nrms= 1.00
bachelor – pollycgs t(y)=1980.974 l(m)= 15575.7652
v(mm/y)= 0.21 s(mm)= 4.61 nrms= 1.07
bachelor – roundtop t(y)=1980.983 l(m)= 16726.6559
v(mm/y)= -0.10 s(mm)= 3.50 nrms= 0.78
bee – san_joaq t(y)=1981.355 l(m)= 17171.7999
v(mm/y)= 0.06 s(mm)= 4.07 nrms= 0.89
bee – santiago t(y)=1981.304 l(m)= 15511.8408
v(mm/y)= 0.53 s(mm)= 15.20 nrms= 3.52
bee – black t(y)=1981.216 l(m)= 9226.8820
v(mm/y)= -0.71 s(mm)= 5.00 nrms= 1.42
bee – lomancer t(y)=1979.651 l(m)= 5919.9602
v(mm/y)= -5.54 s(mm)= 3.63 nrms= 1.12
bee – lomas t(y)=1983.051 l(m)= 5930.4278
v(mm/y)= 0.64 s(mm)= 0.00 nrms= 0.00
bee – miguel t(y)=1981.305 l(m)= 24231.5616
v(mm/y)= -2.82 s(mm)= 6.87 nrms= 1.21
black – santiago t(y)=1981.402 l(m)= 15984.8898
v(mm/y)= 0.01 s(mm)= 3.09 nrms= 0.70
black – san_juan t(y)=1981.307 l(m)= 13817.0699
v(mm/y)= -0.87 s(mm)= 7.43 nrms= 1.82
mm
50
0
-50
1975
1980
1985
1990
year

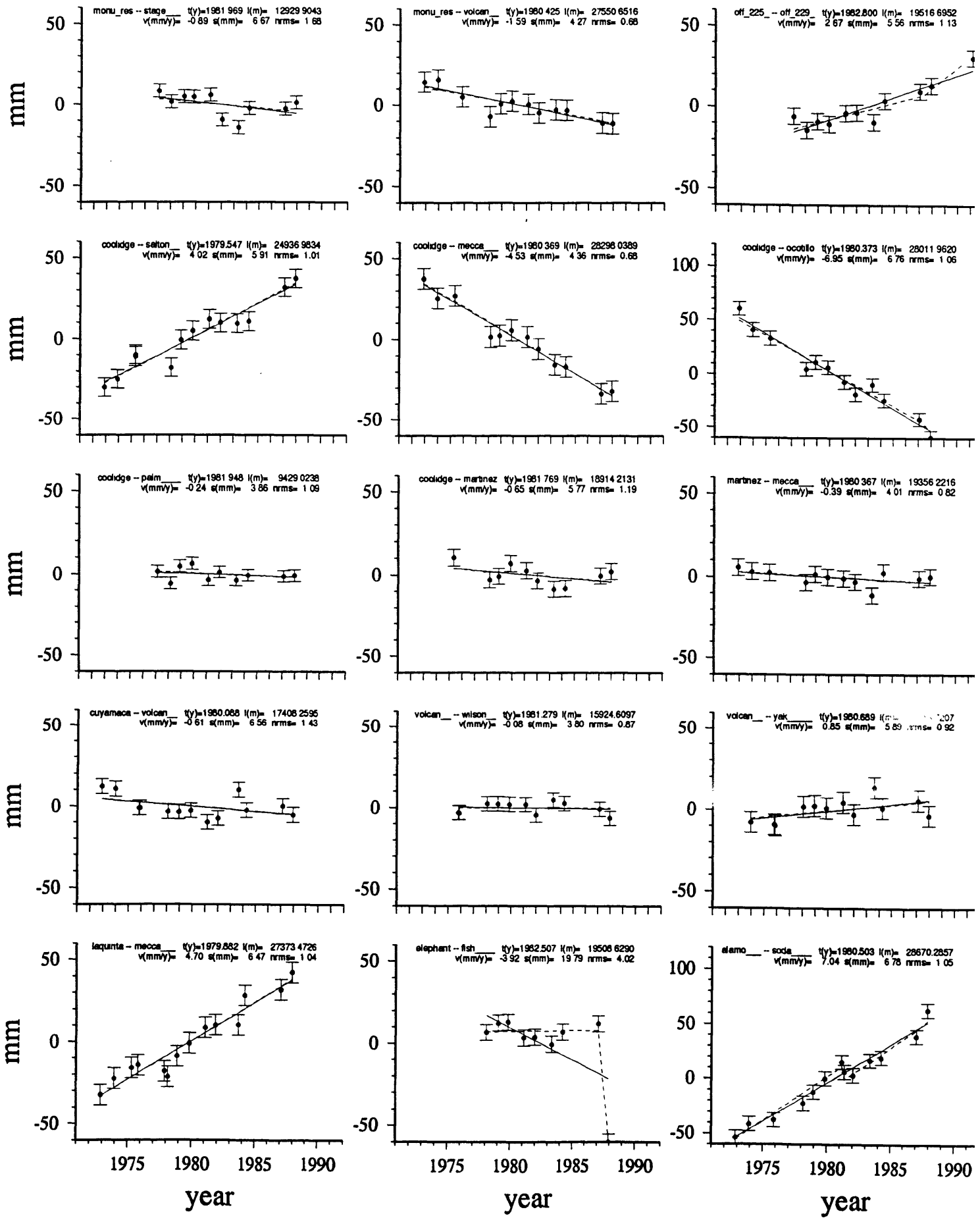
monu_res -- stage___ t(y)=1981.969 l(m)= 12929.9043
v(mm/y)= -0.89 s(mm)= 6.67 nrms= 1.68
monu_res -- volcan__ t(y)=1980.425 l(m)= 27550.6516
v(mm/y)= -1.59 s(mm)= 4.27 nrms= 0.68
off_225_ -- off_229_ t(y)=1982.800 l(m)= 19516.6952
v(mm/y)= 2.67 s(mm)= 5.56 nrms= 1.13
coolidge -- salton__ t(y)=1979.547 l(m)= 24936.9834
v(mm/y)= 4.02 s(mm)= 5.91 nrms= 1.01
coolidge -- mecca___ t(y)=1980.369 l(m)= 28298.0389
v(mm/y)= -4.53 s(mm)= 4.36 nrms= 0.68
coolidge -- ocotillo t(y)=1980.373 l(m)= 28011.9620
v(mm/y)= -6.95 s(mm)= 6.76 nrms= 1.06
coolidge -- palm___ t(y)=1981.948 l(m)= 9429.0238
v(mm/y)= -0.24 s(mm)= 3.86 nrms= 1.09
coolidge -- martinez t(y)=1981.769 l(m)= 18914.2131
v(mm/y)= -0.65 s(mm)= 5.77 nrms= 1.19
martinez -- mecca___ t(y)=1980.367 l(m)= 19356.2216
v(mm/y)= -0.39 s(mm)= 4.01 nrms= 0.82
cuyamaca -- volcan__ t(y)=1980.088 l(m)= 17408.2595
v(mm/y)= -0.61 s(mm)= 6.56 nrms= 1.43
volcan__ -- wilson__ t(y)=1981.279 l(m)= 15924.6097
v(mm/y)= -0.08 s(mm)= 3.80 nrms= 0.87
volcan__ -- yak_____ t(y)=1980.689 l(m)= [illegible]207
v(mm/y)= 0.85 s(mm)= 5.89 [illegible]rms= 0.92
laquinta -- mecca___ t(y)=1979.882 l(m)= 27373.4726
v(mm/y)= 4.70 s(mm)= 6.47 nrms= 1.04
elephant -- fish____ t(y)=1982.507 l(m)= 19508.6290
v(mm/y)= -3.92 s(mm)= 19.79 nrms= 4.02
alamo___ -- soda____ t(y)=1980.503 l(m)= 28670.2857
v(mm/y)= 7.04 s(mm)= 6.78 nrms= 1.05
mm
year
1975
1980
1985
1990

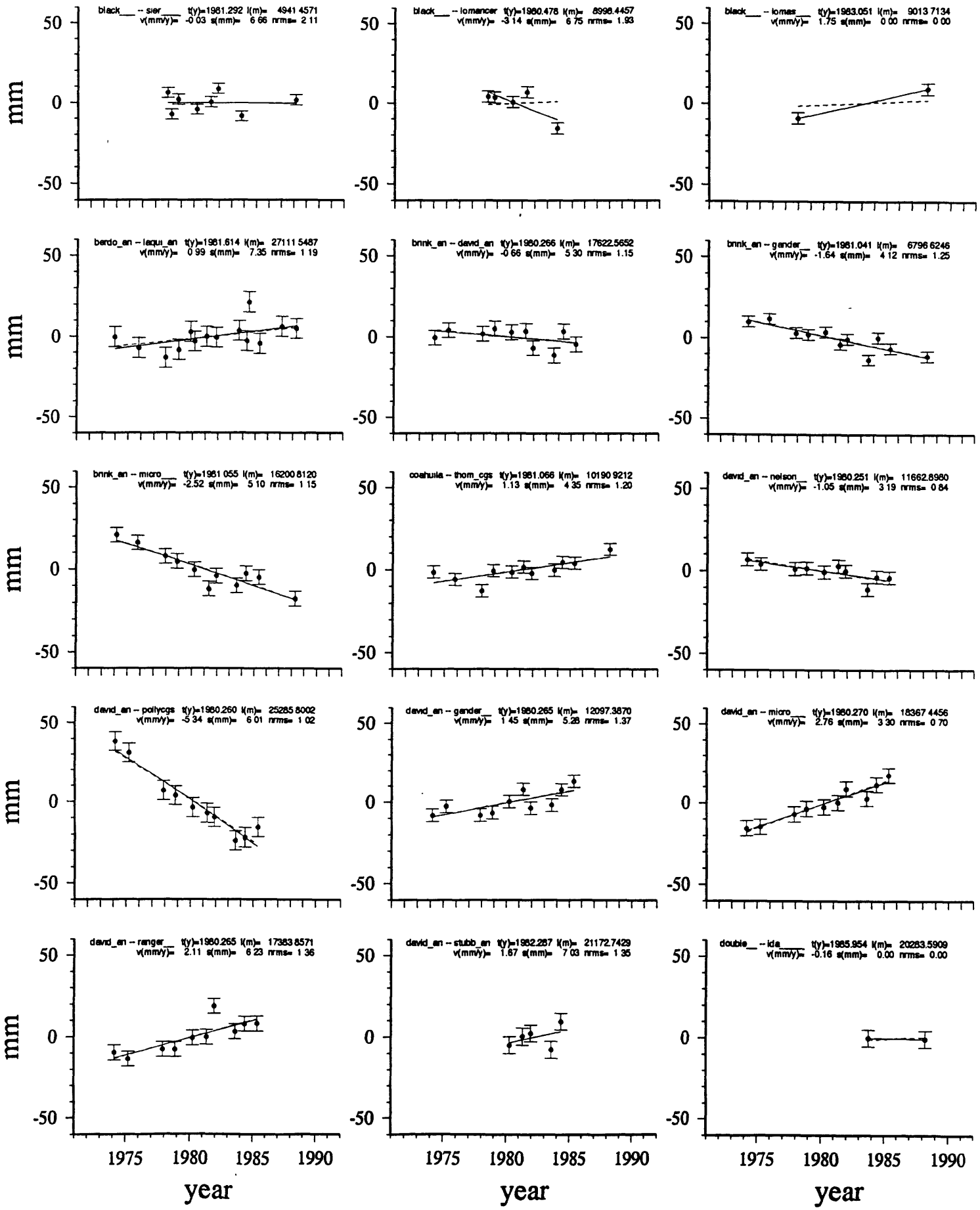
black___ -- sier___ t(y)=1981.292 l(m)= 4941.4571
v(mm/y)= -0.03 s(mm)= 6.66 nrms= 2.11
black___ -- lomancer t(y)=1980.478 l(m)= 8998.4457
v(mm/y)= -3.14 s(mm)= 6.75 nrms= 1.93
black___ -- lomas___ t(y)=1983.051 l(m)= 9013.7134
v(mm/y)= 1.75 s(mm)= 0.00 nrms= 0.00
berdo_en -- laqui_en t(y)=1981.614 l(m)= 27111.5487
v(mm/y)= 0.99 s(mm)= 7.35 nrms= 1.19
brink_en -- david_en t(y)=1980.266 l(m)= 17622.5652
v(mm/y)= -0.66 s(mm)= 5.30 nrms= 1.15
brink_en -- gander___ t(y)=1981.041 l(m)= 6796.6246
v(mm/y)= -1.64 s(mm)= 4.12 nrms= 1.25
brink_en -- micro___ t(y)=1981.055 l(m)= 16200.8120
v(mm/y)= -2.52 s(mm)= 5.10 nrms= 1.15
coahuila -- thorn_cgs t(y)=1981.066 l(m)= 10190.9212
v(mm/y)= 1.13 s(mm)= 4.35 nrms= 1.20
david_en -- nelson___ t(y)=1980.251 l(m)= 11662.8980
v(mm/y)= -1.05 s(mm)= 3.19 nrms= 0.84
david_en -- polycgs t(y)=1980.260 l(m)= 25285.8002
v(mm/y)= -5.34 s(mm)= 6.01 nrms= 1.02
david_en -- gander___ t(y)=1980.265 l(m)= 12097.3870
v(mm/y)= 1.45 s(mm)= 5.28 nrms= 1.37
david_en -- micro___ t(y)=1980.270 l(m)= 18367.4456
v(mm/y)= 2.76 s(mm)= 3.30 nrms= 0.70
david_en -- ranger___ t(y)=1980.265 l(m)= 17383.8571
v(mm/y)= 2.11 s(mm)= 6.23 nrms= 1.36
david_en -- stubb_en t(y)=1982.287 l(m)= 21172.7429
v(mm/y)= 1.87 s(mm)= 7.03 nrms= 1.35
double___ -- ida_____ t(y)=1985.954 l(m)= 20283.5909
v(mm/y)= -0.16 s(mm)= 0.00 nrms= 0.00
50
0
-50
mm
1975
1980
1985
1990
year

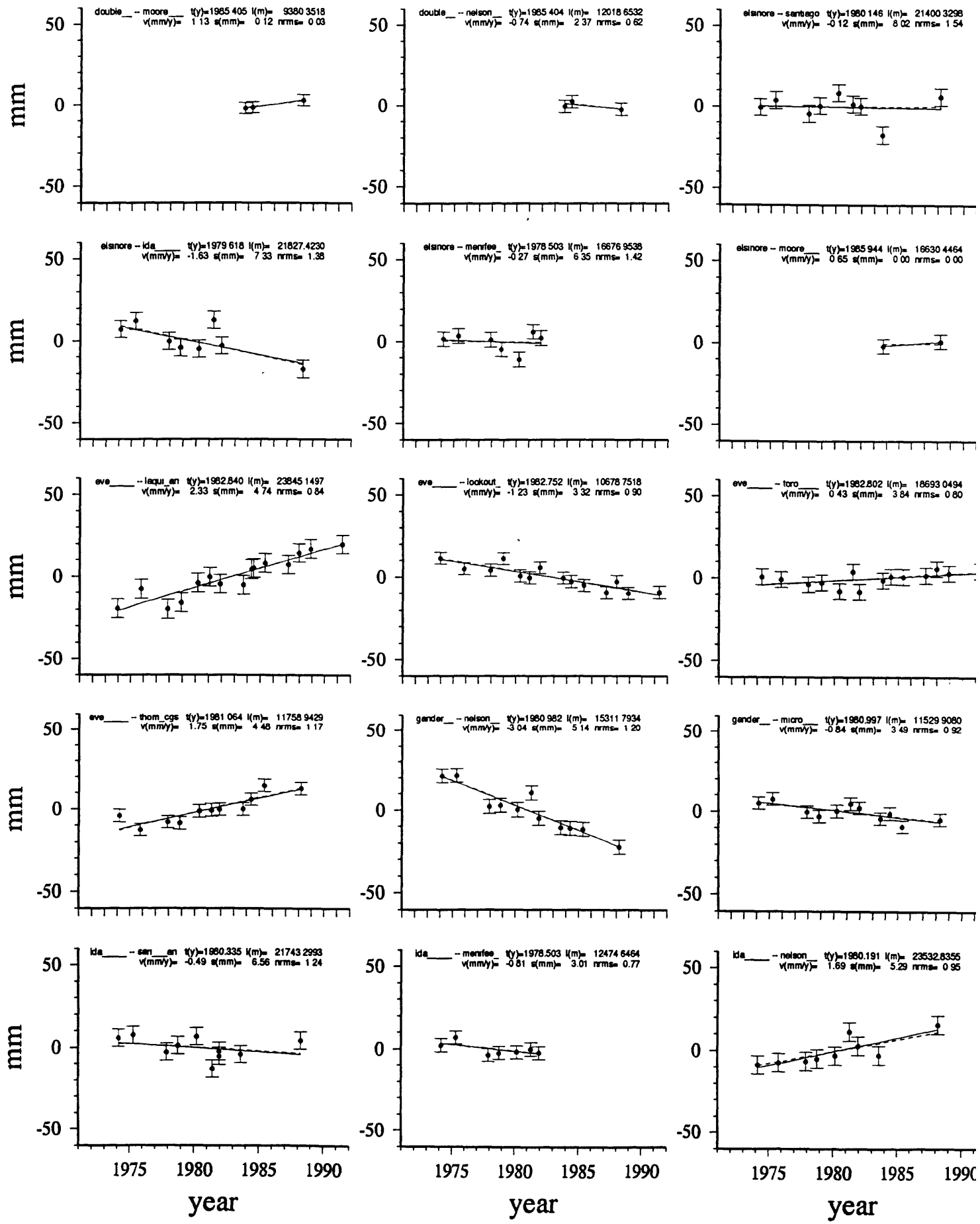
double__ -- moore___ t(y)=1985.405 l(m)= 9380.3518
v(mm/y)= 1.13 s(mm)= 0.12 nrms= 0.03
double__ -- nelson__ t(y)=1985.404 l(m)= 12018.6532
v(mm/y)= -0.74 s(mm)= 2.37 nrms= 0.62
elsinore -- santiago t(y)=1980.146 l(m)= 21400.3298
v(mm/y)= -0.12 s(mm)= 8.02 nrms= 1.54
elsinore -- ida____ t(y)=1979.618 l(m)= 21827.4230
v(mm/y)= -1.63 s(mm)= 7.33 nrms= 1.38
elsinore -- menfee_ t(y)=1978.503 l(m)= 16676.9538
v(mm/y)= -0.27 s(mm)= 6.35 nrms= 1.42
elsinore -- moore___ t(y)=1985.944 l(m)= 16630.4464
v(mm/y)= 0.65 s(mm)= 0.00 nrms= 0.00
eve____ -- laqui_en t(y)=1982.840 l(m)= 23845.1497
v(mm/y)= 2.33 s(mm)= 4.74 nrms= 0.84
eve____ -- lockout_ t(y)=1982.752 l(m)= 10678.7518
v(mm/y)= -1.23 s(mm)= 3.32 nrms= 0.90
eve____ -- toro____ t(y)=1982.802 l(m)= 18693.0494
v(mm/y)= 0.43 s(mm)= 3.84 nrms= 0.80
eve____ -- thom_cgs t(y)=1981.064 l(m)= 11758.9429
v(mm/y)= 1.75 s(mm)= 4.48 nrms= 1.17
gander__ -- nelson__ t(y)=1980.982 l(m)= 15311.7934
v(mm/y)= -3.04 s(mm)= 5.14 nrms= 1.20
gander__ -- micro___ t(y)=1980.997 l(m)= 11529.9080
v(mm/y)= -0.84 s(mm)= 3.49 nrms= 0.92
ida____ -- san__en t(y)=1980.335 l(m)= 21743.2993
v(mm/y)= -0.49 s(mm)= 6.56 nrms= 1.24
ida____ -- menfee_ t(y)=1978.503 l(m)= 12474.6464
v(mm/y)= -0.81 s(mm)= 3.01 nrms= 0.77
ida____ -- nelson__ t(y)=1980.191 l(m)= 23532.8355
v(mm/y)= 1.69 s(mm)= 5.29 nrms= 0.95
mm
50
0
-50
1975
1980
1985
1990
year

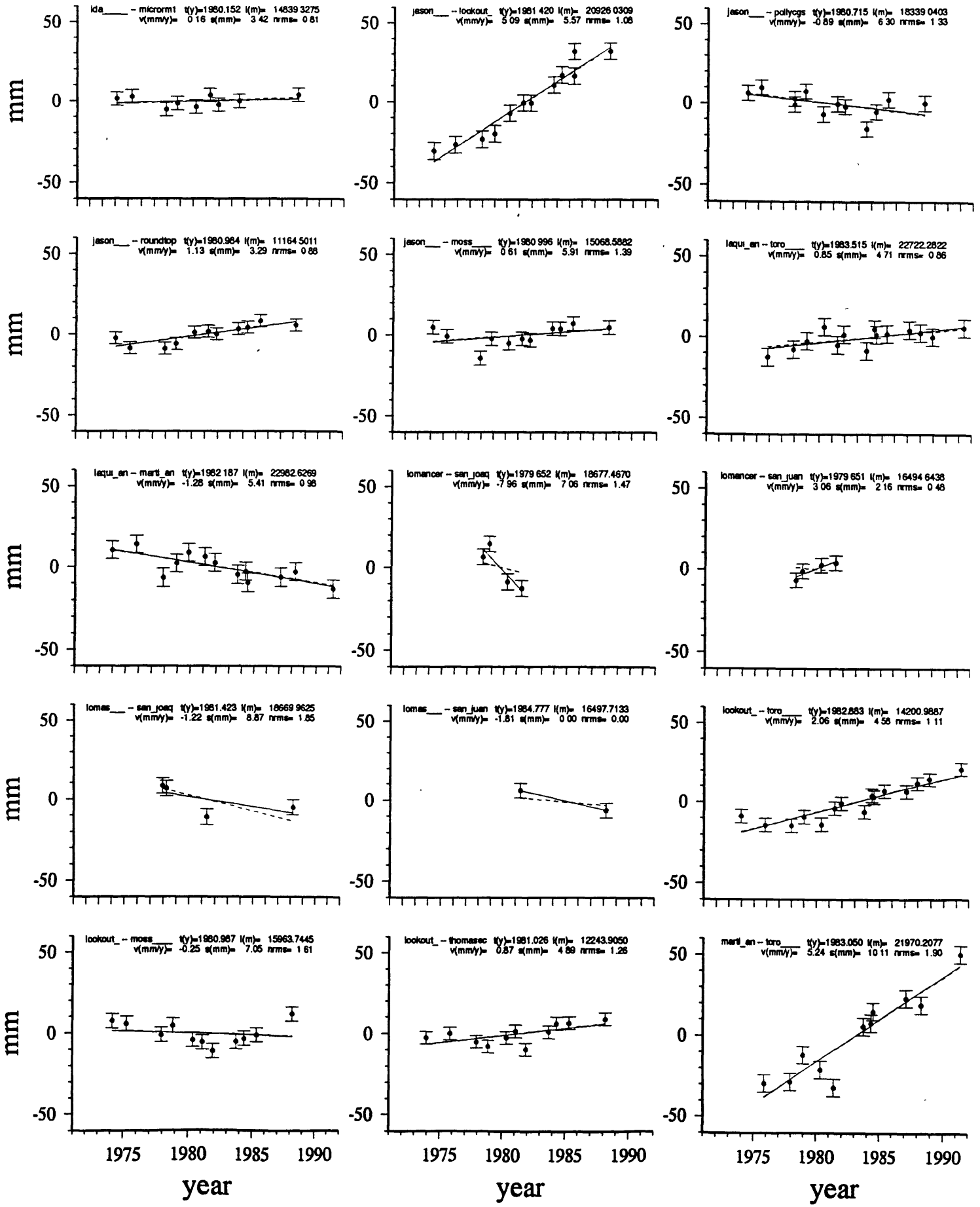
ida____ – microrm1 t(y)=1980.152 l(m)= 14839.3275
v(mm/y)= 0.16 s(mm)= 3.42 nrms= 0.81
jason___ – lookout_ t(y)=1981.420 l(m)= 20926.0309
v(mm/y)= 5.09 s(mm)= 5.57 nrms= 1.08
jason___ – polycgs t(y)=1980.715 l(m)= 18339.0403
v(mm/y)= -0.89 s(mm)= 6.30 nrms= 1.33
jason___ – roundtop t(y)=1980.984 l(m)= 11164.5011
v(mm/y)= 1.13 s(mm)= 3.29 nrms= 0.88
jason___ – moss____ t(y)=1980.996 l(m)= 15068.5882
v(mm/y)= 0.61 s(mm)= 5.91 nrms= 1.39
laqui_en – toro____ t(y)=1983.515 l(m)= 22722.2822
v(mm/y)= 0.85 s(mm)= 4.71 nrms= 0.86
laqui_en – marti_en t(y)=1982.187 l(m)= 22982.6269
v(mm/y)= -1.28 s(mm)= 5.41 nrms= 0.98
lomancer – san_joaq t(y)=1979.652 l(m)= 18677.4670
v(mm/y)= -7.96 s(mm)= 7.06 nrms= 1.47
lomancer – san_juan t(y)=1979.651 l(m)= 16494.6438
v(mm/y)= 3.06 s(mm)= 2.16 nrms= 0.48
lomas___ – san_joaq t(y)=1981.423 l(m)= 18669.9625
v(mm/y)= -1.22 s(mm)= 8.87 nrms= 1.85
lomas___ – san_juan t(y)=1984.777 l(m)= 16497.7133
v(mm/y)= -1.81 s(mm)= 0.00 nrms= 0.00
lookout_ – toro____ t(y)=1982.883 l(m)= 14200.9887
v(mm/y)= 2.06 s(mm)= 4.56 nrms= 1.11
lookout_ – moss____ t(y)=1980.967 l(m)= 15963.7445
v(mm/y)= -0.25 s(mm)= 7.05 nrms= 1.61
lookout_ – thomasec t(y)=1981.026 l(m)= 12243.9050
v(mm/y)= 0.87 s(mm)= 4.89 nrms= 1.26
marti_en – toro____ t(y)=1983.050 l(m)= 21970.2077
v(mm/y)= 5.24 s(mm)= 10.11 nrms= 1.90
50
0
-50
mm
1975
1980
1985
1990
year

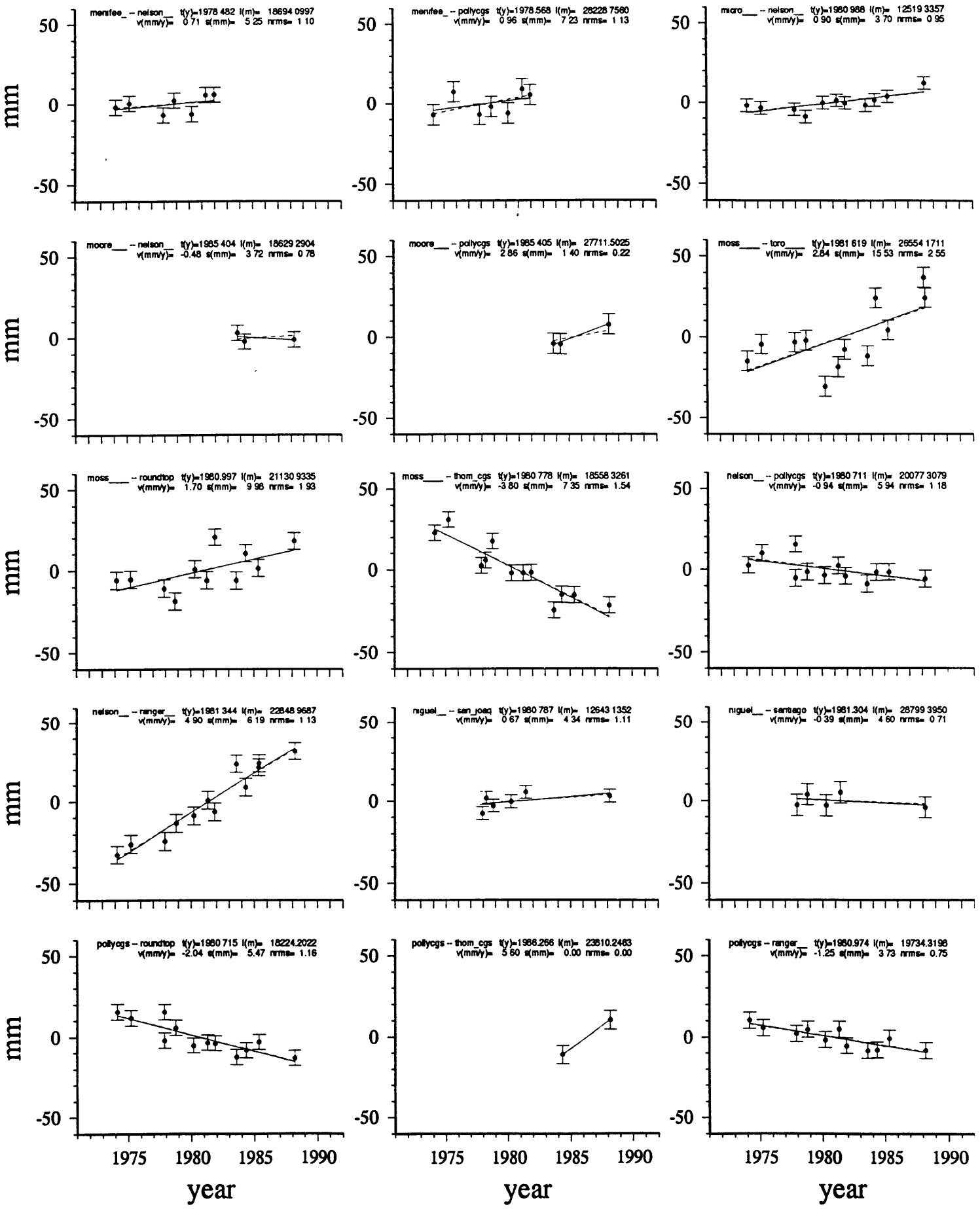
menifee_ -- nelson__ t(y)=1978.482 l(m)= 18694.0997
v(mm/y)= 0.71 s(mm)= 5.25 nrms= 1.10
menifee_ -- polycgs t(y)=1978.568 l(m)= 28228.7560
v(mm/y)= 0.96 s(mm)= 7.23 nrms= 1.13
micro___ -- nelson__ t(y)=1980.988 l(m)= 12519.3357
v(mm/y)= 0.90 s(mm)= 3.70 nrms= 0.95
moore___ -- nelson__ t(y)=1985.404 l(m)= 18629.2904
v(mm/y)= -0.48 s(mm)= 3.72 nrms= 0.78
moore___ -- polycgs t(y)=1985.405 l(m)= 27711.5025
v(mm/y)= 2.86 s(mm)= 1.40 nrms= 0.22
moss____ -- toro___ t(y)=1981.619 l(m)= 26554.1711
v(mm/y)= 2.84 s(mm)= 15.53 nrms= 2.55
moss____ -- roundtop t(y)=1980.997 l(m)= 21130.9335
v(mm/y)= 1.70 s(mm)= 9.98 nrms= 1.93
moss____ -- thorn_cgs t(y)=1980.778 l(m)= 18558.3261
v(mm/y)= -3.80 s(mm)= 7.35 nrms= 1.54
nelson__ -- polycgs t(y)=1980.711 l(m)= 20077.3079
v(mm/y)= -0.94 s(mm)= 5.94 nrms= 1.18
nelson__ -- ranger__ t(y)=1981.344 l(m)= 22848.9687
v(mm/y)= 4.90 s(mm)= 6.19 nrms= 1.13
niguel__ -- san_joaq t(y)=1980.787 l(m)= 12643.1352
v(mm/y)= 0.67 s(mm)= 4.34 nrms= 1.11
niguel__ -- santiago t(y)=1981.304 l(m)= 28799.3950
v(mm/y)= -0.39 s(mm)= 4.60 nrms= 0.71
polycgs -- roundtop t(y)=1980.715 l(m)= 18224.2022
v(mm/y)= -2.04 s(mm)= 5.47 nrms= 1.16
polycgs -- thorn_cgs t(y)=1986.266 l(m)= 23810.2483
v(mm/y)= 5.60 s(mm)= 0.00 nrms= 0.00
polycgs -- ranger__ t(y)=1980.974 l(m)= 19734.3198
v(mm/y)= -1.25 s(mm)= 3.73 nrms= 0.75
50
0
-50
mm
1975
1980
1985
1990
year

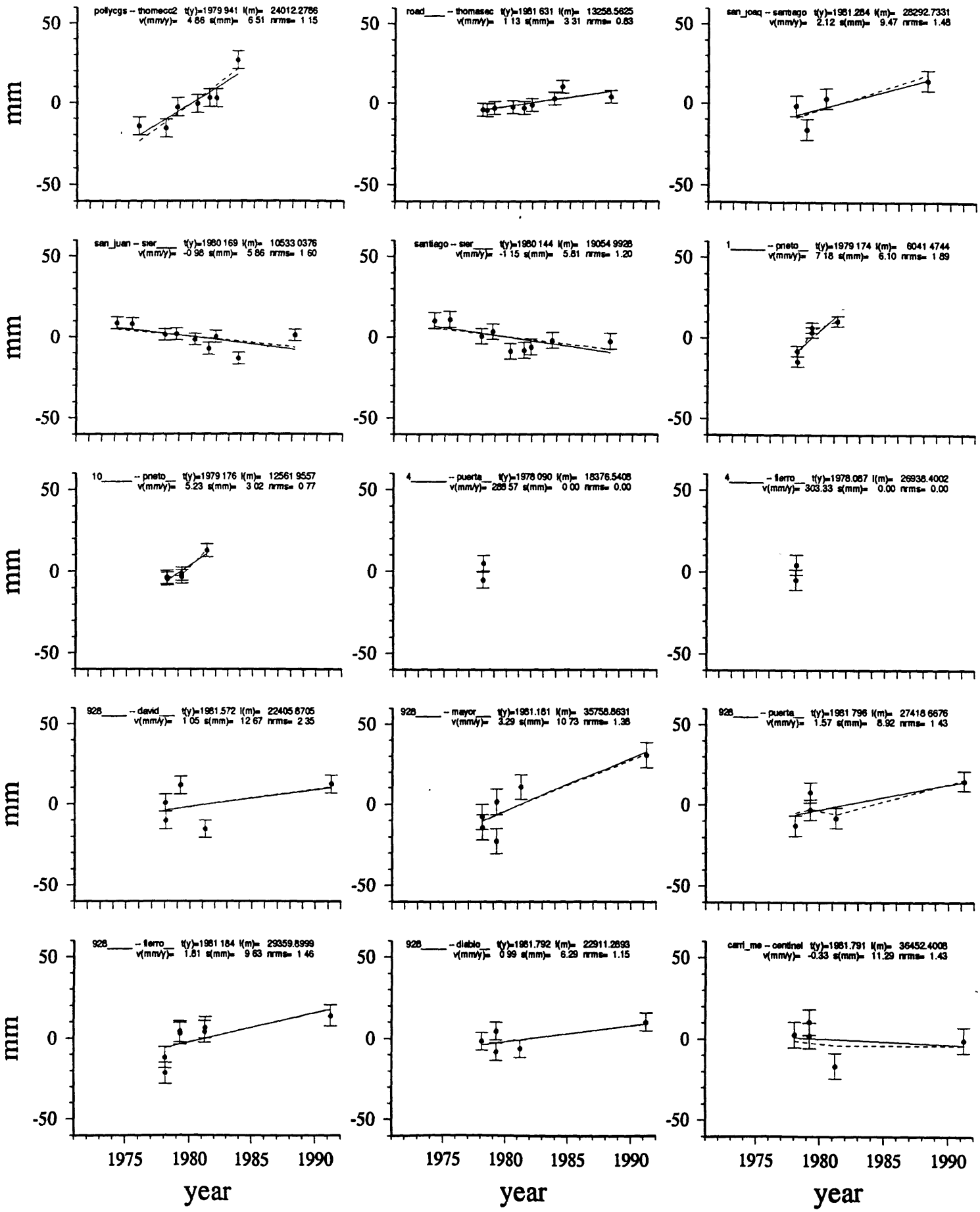
pollycgs -- thomecc2 t(y)=1979.941 l(m)= 24012.2786
v(mm/y)= 4.86 s(mm)= 6.51 nrms= 1.15
road____ -- thomasec t(y)=1981.631 l(m)= 13258.5625
v(mm/y)= 1.13 s(mm)= 3.31 nrms= 0.83
san_joaq -- santiago t(y)=1981.284 l(m)= 28292.7331
v(mm/y)= 2.12 s(mm)= 9.47 nrms= 1.48
san_juan -- sier____ t(y)=1980.169 l(m)= 10533.0376
v(mm/y)= -0.98 s(mm)= 5.86 nrms= 1.60
santiago -- sier____ t(y)=1980.144 l(m)= 19054.9928
v(mm/y)= -1.15 s(mm)= 5.81 nrms= 1.20
1_____ -- pneto__ t(y)=1979.174 l(m)= 6041.4744
v(mm/y)= 7.18 s(mm)= 6.10 nrms= 1.89
10_____ -- pneto__ t(y)=1979.176 l(m)= 12561.9557
v(mm/y)= 5.23 s(mm)= 3.02 nrms= 0.77
4_____ -- puerta__ t(y)=1978.090 l(m)= 18376.5406
v(mm/y)= 288.57 s(mm)= 0.00 nrms= 0.00
4_____ -- fierro__ t(y)=1978.067 l(m)= 26938.4002
v(mm/y)= 303.33 s(mm)= 0.00 nrms= 0.00
928_____ -- david___ t(y)=1981.572 l(m)= 22405.8705
v(mm/y)= 1.05 s(mm)= 12.67 nrms= 2.35
928_____ -- mayor___ t(y)=1981.181 l(m)= 35758.8631
v(mm/y)= 3.29 s(mm)= 10.73 nrms= 1.38
928_____ -- puerta__ t(y)=1981.796 l(m)= 27418.6676
v(mm/y)= 1.57 s(mm)= 8.92 nrms= 1.43
928_____ -- fierro__ t(y)=1981.184 l(m)= 29359.8999
v(mm/y)= 1.81 s(mm)= 9.63 nrms= 1.46
928_____ -- diablo__ t(y)=1981.792 l(m)= 22911.2893
v(mm/y)= 0.99 s(mm)= 6.29 nrms= 1.15
carri_me -- centinel t(y)=1981.791 l(m)= 36452.4008
v(mm/y)= -0.33 s(mm)= 11.29 nrms= 1.43
50
0
-50
mm
1975
1980
1985
1990
year

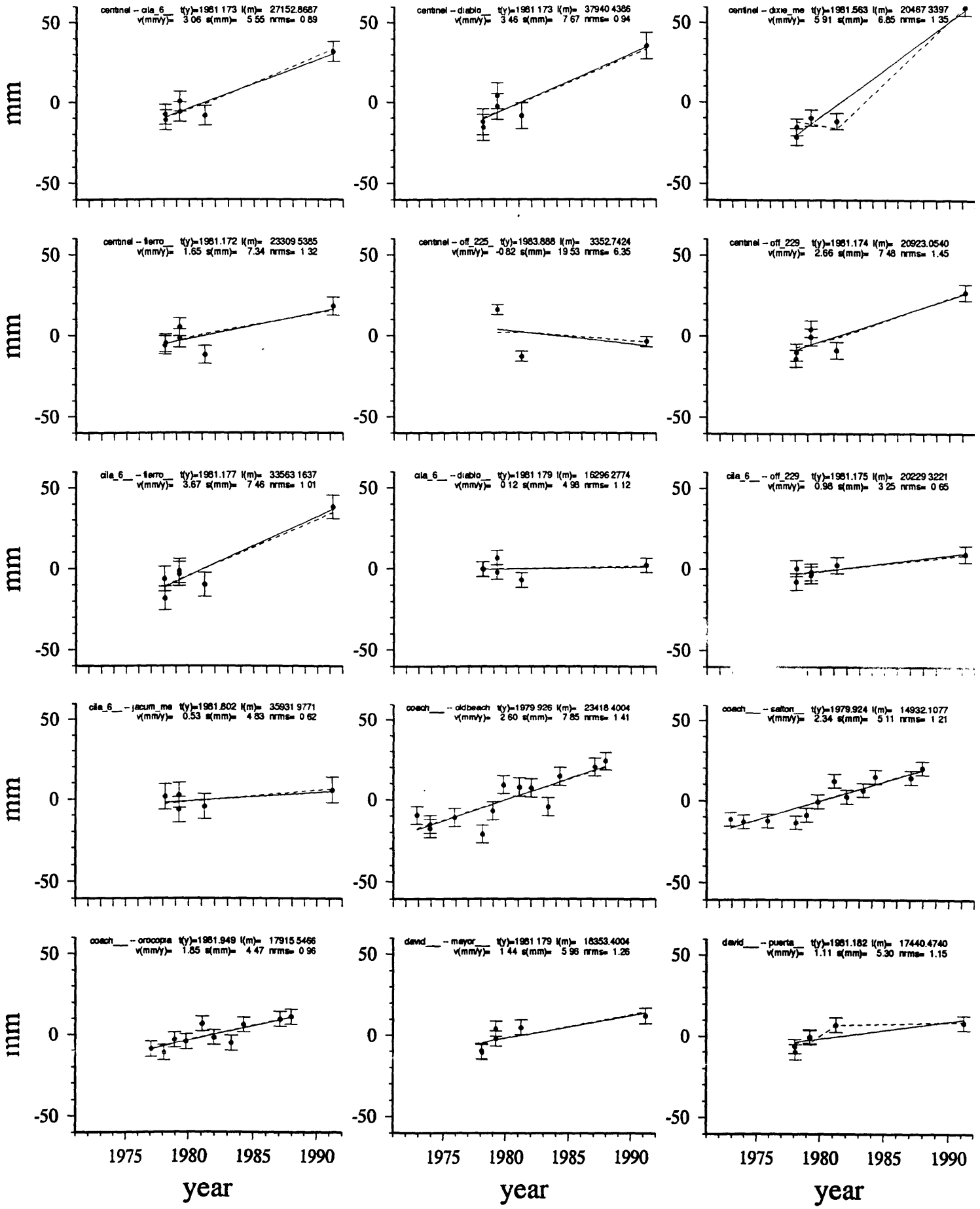
centinel – cia_6__ t(y)=1981.173 l(m)= 27152.8687
v(mm/y)= 3.06 s(mm)= 5.55 nrms= 0.89
centinel – diablo__ t(y)=1981.173 l(m)= 37940.4386
v(mm/y)= 3.46 s(mm)= 7.67 nrms= 0.94
centinel – dixie_me t(y)=1981.563 l(m)= 20467.3397
v(mm/y)= 5.91 s(mm)= 6.85 nrms= 1.35
centinel – tierro__ t(y)=1981.172 l(m)= 23309.5385
v(mm/y)= 1.65 s(mm)= 7.34 nrms= 1.32
centinel – off_225_ t(y)=1983.888 l(m)= 3352.7424
v(mm/y)= -0.82 s(mm)= 19.53 nrms= 6.35
centinel – off_229_ t(y)=1981.174 l(m)= 20923.0540
v(mm/y)= 2.66 s(mm)= 7.48 nrms= 1.45
cia_6__ – tierro__ t(y)=1981.177 l(m)= 33563.1637
v(mm/y)= 3.67 s(mm)= 7.46 nrms= 1.01
cia_6__ – diablo__ t(y)=1981.179 l(m)= 16296.2774
v(mm/y)= 0.12 s(mm)= 4.98 nrms= 1.12
cia_6__ – off_229_ t(y)=1981.175 l(m)= 20229.3221
v(mm/y)= 0.98 s(mm)= 3.25 nrms= 0.65
cia_6__ – jacum_me t(y)=1981.802 l(m)= 35931.9771
v(mm/y)= 0.53 s(mm)= 4.83 nrms= 0.62
coach___ – oldbeach t(y)=1979.926 l(m)= 23418.4004
v(mm/y)= 2.60 s(mm)= 7.85 nrms= 1.41
coach___ – salton__ t(y)=1979.924 l(m)= 14932.1077
v(mm/y)= 2.34 s(mm)= 5.11 nrms= 1.21
coach___ – orocopia t(y)=1981.949 l(m)= 17915.5466
v(mm/y)= 1.85 s(mm)= 4.47 nrms= 0.96
david___ – mayor___ t(y)=1981.179 l(m)= 18353.4004
v(mm/y)= 1.44 s(mm)= 5.96 nrms= 1.26
david___ – puerta__ t(y)=1981.182 l(m)= 17440.4740
v(mm/y)= 1.11 s(mm)= 5.30 nrms= 1.15
50
0
-50
mm
1975
1980
1985
1990
year

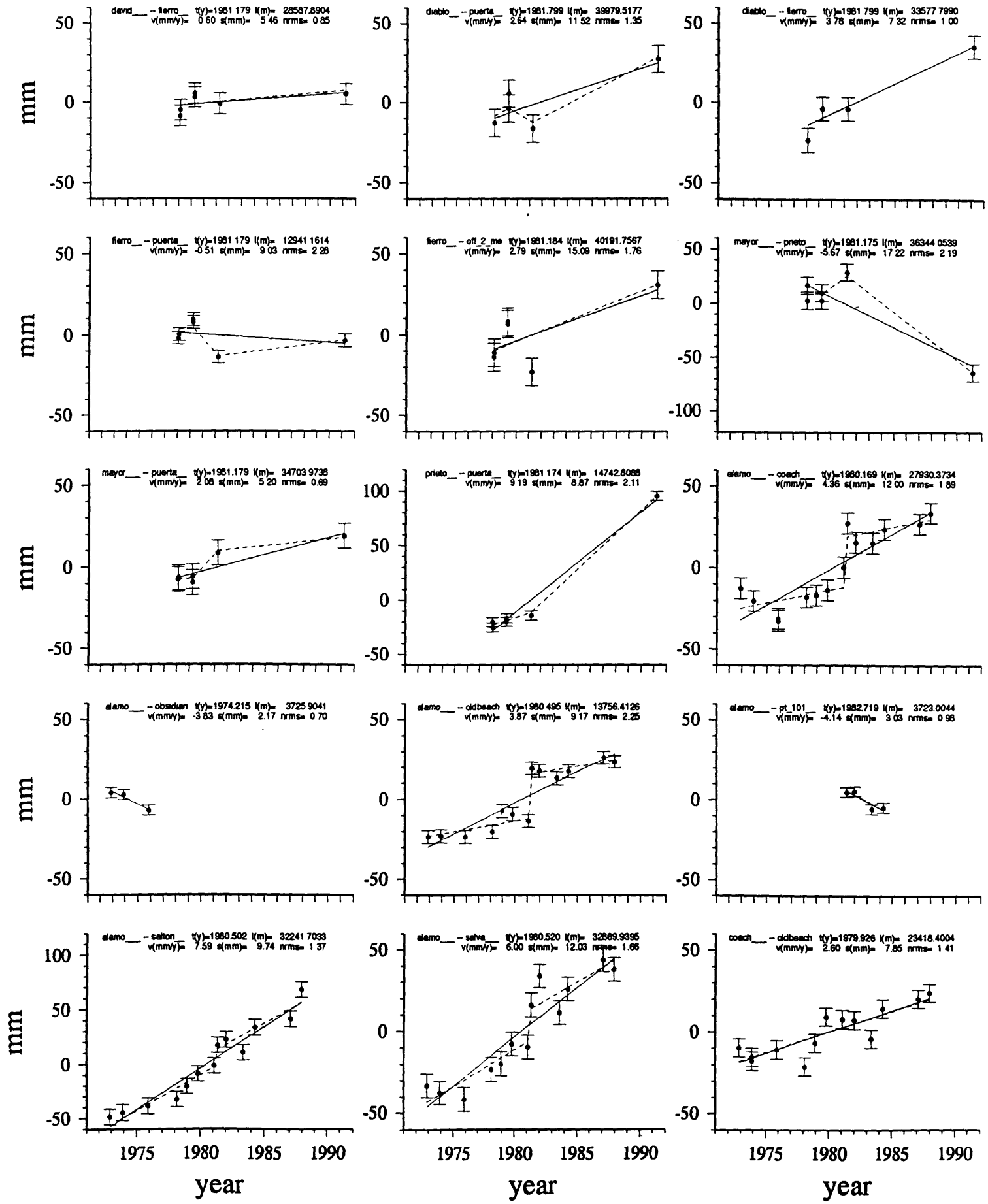
david___ – fierro___ t(y)=1981.179 l(m)= 28587.8904
v(mm/y)= 0.60 s(mm)= 5.46 nrms= 0.85
diablo___ – puerta___ t(y)=1981.799 l(m)= 39979.5177
v(mm/y)= 2.64 s(mm)= 11.52 nrms= 1.35
diablo___ – fierro___ t(y)=1981.799 l(m)= 33577.7990
v(mm/y)= 3.78 s(mm)= 7.32 nrms= 1.00
fierro___ – puerta___ t(y)=1981.179 l(m)= 12941.1614
v(mm/y)= -0.51 s(mm)= 9.03 nrms= 2.28
fierro___ – off_2_me t(y)=1981.184 l(m)= 40191.7567
v(mm/y)= 2.79 s(mm)= 15.09 nrms= 1.76
mayor___ – prieto___ t(y)=1981.175 l(m)= 36344.0539
v(mm/y)= -5.67 s(mm)= 17.22 nrms= 2.19
mayor___ – puerta___ t(y)=1981.179 l(m)= 34703.9738
v(mm/y)= 2.06 s(mm)= 5.20 nrms= 0.69
prieto___ – puerta___ t(y)=1981.174 l(m)= 14742.8088
v(mm/y)= 9.19 s(mm)= 8.87 nrms= 2.11
alamo___ – coach___ t(y)=1980.169 l(m)= 27930.3734
v(mm/y)= 4.36 s(mm)= 12.00 nrms= 1.89
alamo___ – obsidian t(y)=1974.215 l(m)= 3725.9041
v(mm/y)= -3.83 s(mm)= 2.17 nrms= 0.70
alamo___ – oldbeach t(y)=1980.495 l(m)= 13756.4126
v(mm/y)= 3.87 s(mm)= 9.17 nrms= 2.25
alamo___ – pt_101___ t(y)=1982.719 l(m)= 3723.0044
v(mm/y)= -4.14 s(mm)= 3.03 nrms= 0.98
alamo___ – salton___ t(y)=1980.502 l(m)= 32241.7033
v(mm/y)= 7.59 s(mm)= 9.74 nrms= 1.37
alamo___ – salva___ t(y)=1980.520 l(m)= 32569.9395
v(mm/y)= 6.00 s(mm)= 12.03 nrms= 1.66
coach___ – oldbeach t(y)=1979.926 l(m)= 23418.4004
v(mm/y)= 2.60 s(mm)= 7.85 nrms= 1.41
mm
year
1975
1980
1985
1990

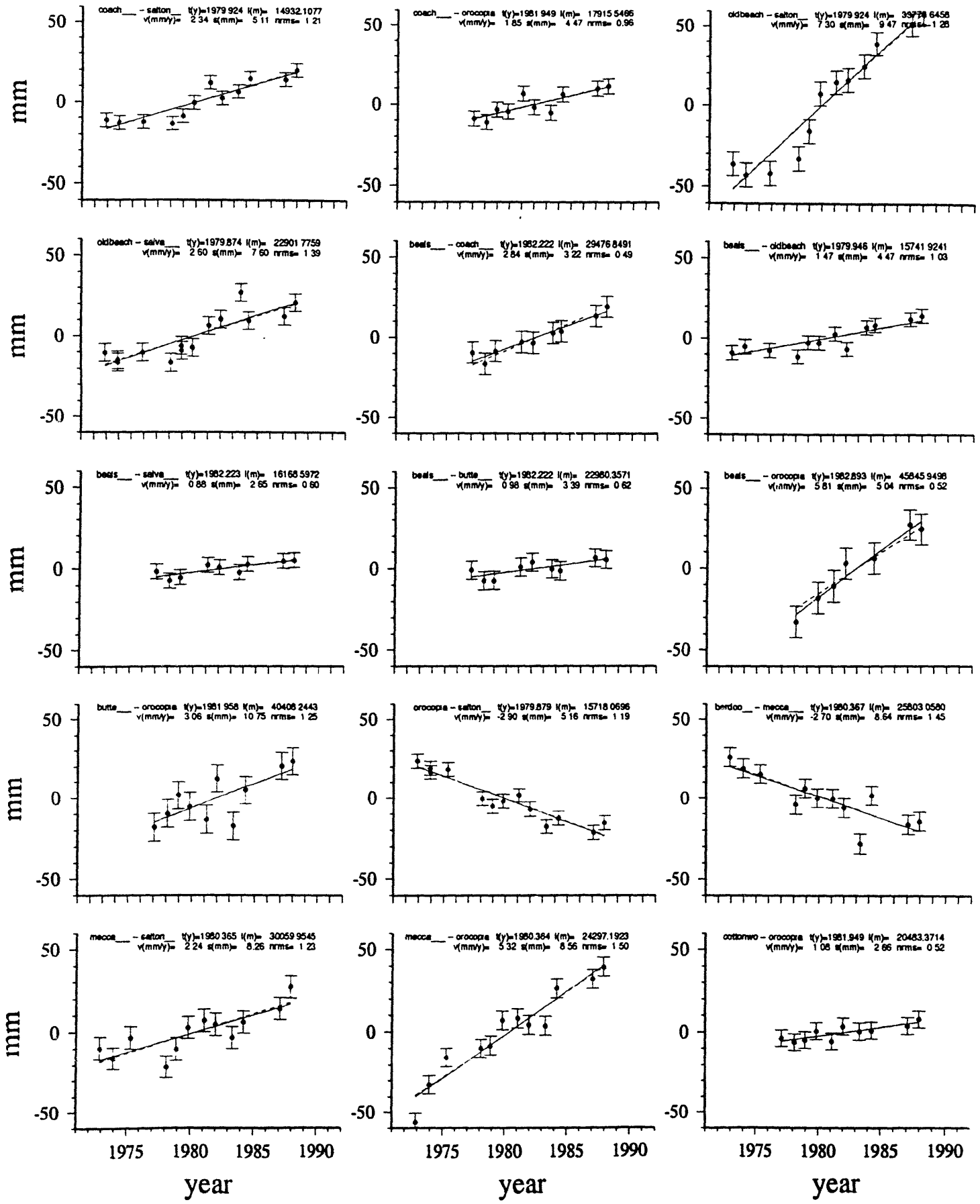
coach___ – salton___ t(y)=1979.924 l(m)= 14932.1077
v(mm/y)= 2.34 s(mm)= 5.11 nrms= 1.21
coach___ – orocopia t(y)=1981.949 l(m)= 17915.5466
v(mm/y)= 1.85 s(mm)= 4.47 nrms= 0.96
oldbeach – salton___ t(y)=1979.924 l(m)= 39778.6458
v(mm/y)= 7.30 s(mm)= 9.47 nrms= 1.26
oldbeach – salva___ t(y)=1979.874 l(m)= 22901.7759
v(mm/y)= 2.60 s(mm)= 7.60 nrms= 1.39
beals___ – coach___ t(y)=1982.222 l(m)= 29476.8491
v(mm/y)= 2.84 s(mm)= 3.22 nrms= 0.49
beals___ – oldbeach t(y)=1979.946 l(m)= 15741.9241
v(mm/y)= 1.47 s(mm)= 4.47 nrms= 1.03
beals___ – salva___ t(y)=1982.223 l(m)= 16168.5972
v(mm/y)= 0.88 s(mm)= 2.65 nrms= 0.80
beals___ – butte___ t(y)=1982.222 l(m)= 22980.3571
v(mm/y)= 0.98 s(mm)= 3.39 nrms= 0.62
beals___ – orocopia t(y)=1982.893 l(m)= 45645.9498
v(mm/y)= 5.81 s(mm)= 5.04 nrms= 0.52
butte___ – orocopia t(y)=1981.958 l(m)= 40406.2443
v(mm/y)= 3.06 s(mm)= 10.75 nrms= 1.25
orocopia – salton___ t(y)=1979.879 l(m)= 15718.0696
v(mm/y)= -2.90 s(mm)= 5.16 nrms= 1.19
berdoo___ – mecca___ t(y)=1980.367 l(m)= 25803.0580
v(mm/y)= -2.70 s(mm)= 8.64 nrms= 1.45
mecca___ – salton___ t(y)=1980.365 l(m)= 30059.9545
v(mm/y)= 2.24 s(mm)= 8.26 nrms= 1.23
mecca___ – orocopia t(y)=1980.364 l(m)= 24297.1923
v(mm/y)= 5.32 s(mm)= 8.56 nrms= 1.50
cottonwo – orocopia t(y)=1981.949 l(m)= 20483.3714
v(mm/y)= 1.08 s(mm)= 2.66 nrms= 0.52
mm
50
0
-50
1975
1980
1985
1990
year

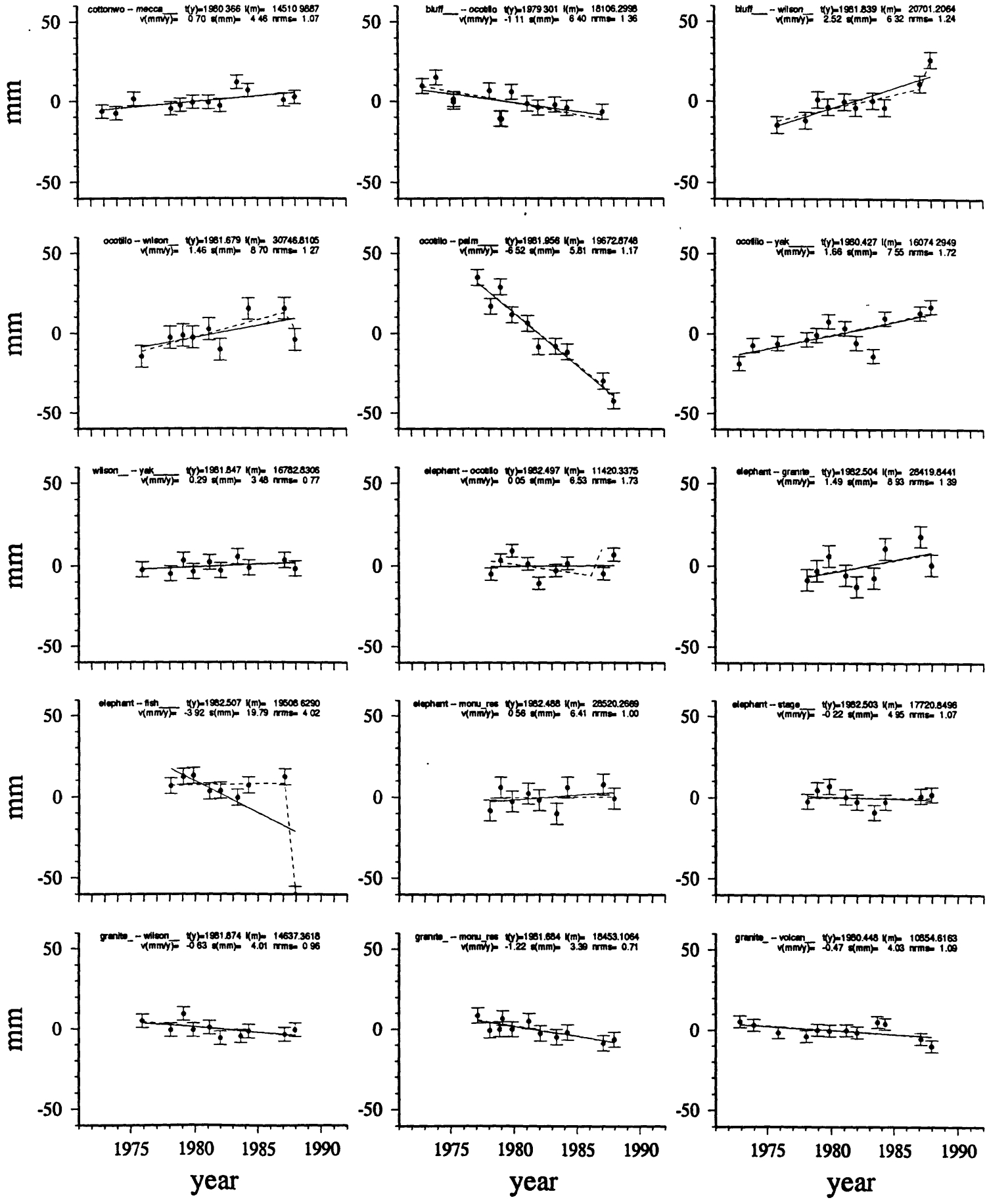
cottonwo – mecca t(y)=1980.366 l(m)= 14510.9857
v(mm/y)= 0.70 s(mm)= 4.46 nrms= 1.07
bluff – ocotillo t(y)=1979.301 l(m)= 18106.2998
v(mm/y)= -1.11 s(mm)= 6.40 nrms= 1.36
bluff – wilson t(y)=1981.839 l(m)= 20701.2064
v(mm/y)= 2.52 s(mm)= 6.32 nrms= 1.24
ocotillo – wilson t(y)=1981.679 l(m)= 30746.8105
v(mm/y)= 1.46 s(mm)= 8.70 nrms= 1.27
ocotillo – palm t(y)=1981.956 l(m)= 19672.8748
v(mm/y)= -6.52 s(mm)= 5.81 nrms= 1.17
ocotillo – yak t(y)=1980.427 l(m)= 16074.2949
v(mm/y)= 1.66 s(mm)= 7.55 nrms= 1.72
wilson – yak t(y)=1981.847 l(m)= 16782.8306
v(mm/y)= 0.29 s(mm)= 3.48 nrms= 0.77
elephant – ocotillo t(y)=1982.497 l(m)= 11420.3375
v(mm/y)= 0.05 s(mm)= 6.53 nrms= 1.73
elephant – granite t(y)=1982.504 l(m)= 28419.8441
v(mm/y)= 1.49 s(mm)= 8.93 nrms= 1.39
elephant – fish t(y)=1982.507 l(m)= 19506.6290
v(mm/y)= -3.92 s(mm)= 19.79 nrms= 4.02
elephant – monu_res t(y)=1982.488 l(m)= 28520.2669
v(mm/y)= 0.56 s(mm)= 6.41 nrms= 1.00
elephant – stage t(y)=1982.503 l(m)= 17720.8496
v(mm/y)= -0.22 s(mm)= 4.95 nrms= 1.07
granite – wilson t(y)=1981.874 l(m)= 14637.3618
v(mm/y)= -0.63 s(mm)= 4.01 nrms= 0.96
granite – monu_res t(y)=1981.684 l(m)= 18453.1064
v(mm/y)= -1.22 s(mm)= 3.39 nrms= 0.71
granite – volcan t(y)=1980.448 l(m)= 10854.6163
v(mm/y)= -0.47 s(mm)= 4.03 nrms= 1.09
50
0
-50
mm
1975
1980
1985
1990
year

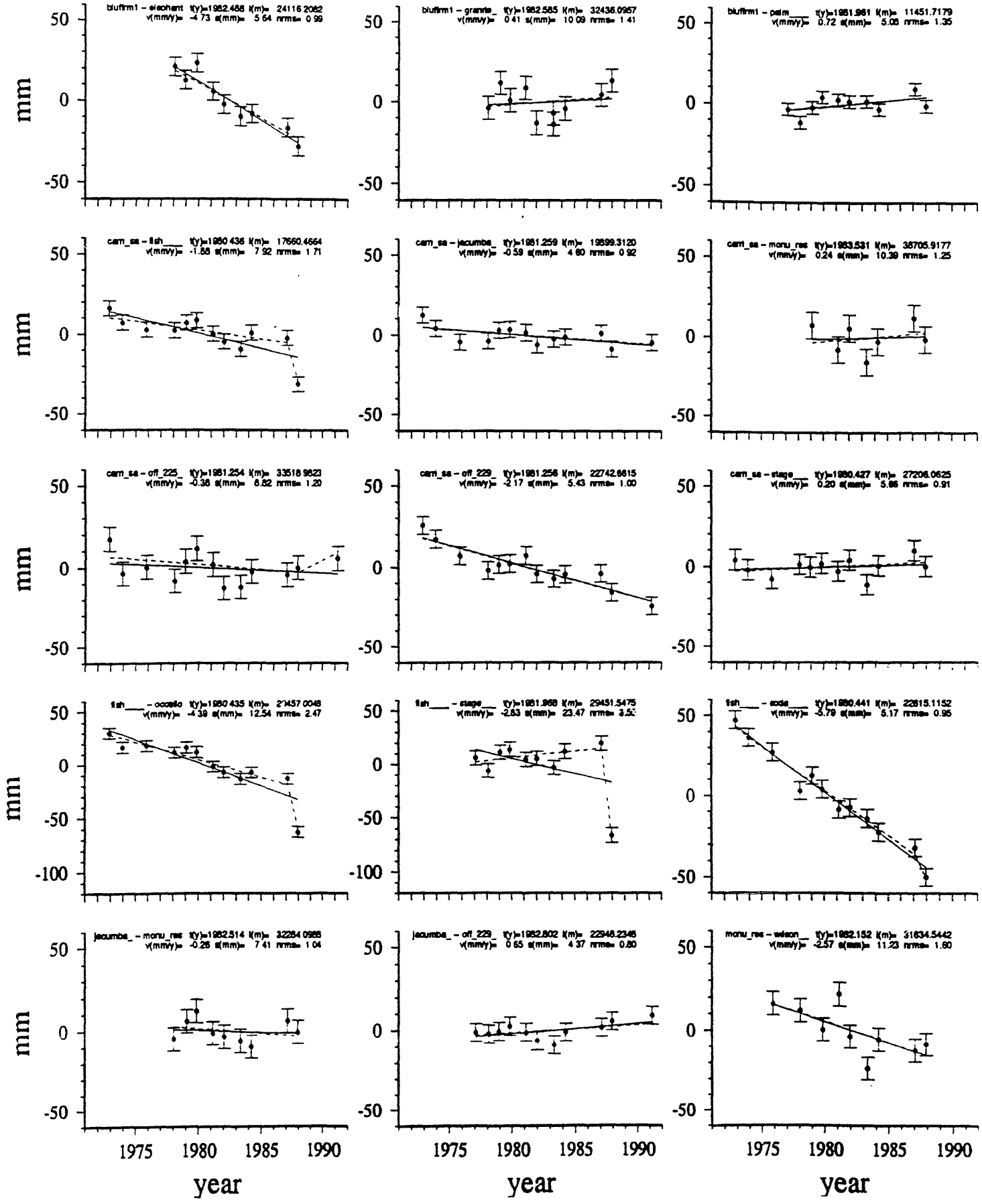
bluffrm1 – elephant t(y)=1982.486 l(m)= 24116.2082
v(mm/y)= -4.73 s(mm)= 5.64 nrms= 0.99
bluffrm1 – granite_ t(y)=1982.585 l(m)= 32436.0957
v(mm/y)= 0.41 s(mm)= 10.09 nrms= 1.41
bluffrm1 – palm___ t(y)=1981.981 l(m)= 11451.7179
v(mm/y)= 0.72 s(mm)= 5.05 nrms= 1.35
cam_sa – fish___ t(y)=1980.436 l(m)= 17660.4664
v(mm/y)= -1.88 s(mm)= 7.92 nrms= 1.71
cam_sa – jacumba_ t(y)=1981.259 l(m)= 19899.3120
v(mm/y)= -0.59 s(mm)= 4.80 nrms= 0.92
cam_sa – monu_nes t(y)=1983.531 l(m)= 38705.9177
v(mm/y)= 0.24 s(mm)= 10.39 nrms= 1.25
cam_sa – off_225_ t(y)=1981.254 l(m)= 33518.9623
v(mm/y)= -0.38 s(mm)= 6.82 nrms= 1.20
cam_sa – off_229_ t(y)=1981.256 l(m)= 22742.6615
v(mm/y)= -2.17 s(mm)= 5.43 nrms= 1.00
cam_sa – stage___ t(y)=1980.427 l(m)= 27206.0625
v(mm/y)= 0.20 s(mm)= 5.66 nrms= 0.91
fish___ – ocotillo t(y)=1980.435 l(m)= 21457.0048
v(mm/y)= -4.39 s(mm)= 12.54 nrms= 2.47
fish___ – stage___ t(y)=1981.968 l(m)= 29451.5475
v(mm/y)= -2.83 s(mm)= 23.47 nrms= 3.5
fish___ – soda___ t(y)=1980.441 l(m)= 22815.1152
v(mm/y)= -5.79 s(mm)= 5.17 nrms= 0.95
jacumba_ – monu_nes t(y)=1982.514 l(m)= 32284.0988
v(mm/y)= -0.26 s(mm)= 7.41 nrms= 1.04
jacumba_ – off_229_ t(y)=1982.802 l(m)= 22948.2346
v(mm/y)= 0.65 s(mm)= 4.37 nrms= 0.80
monu_nes – wilson__ t(y)=1982.152 l(m)= 31634.5442
v(mm/y)= -2.57 s(mm)= 11.23 nrms= 1.60
mm
50
0
-50
-100
1975
1980
1985
1990
year

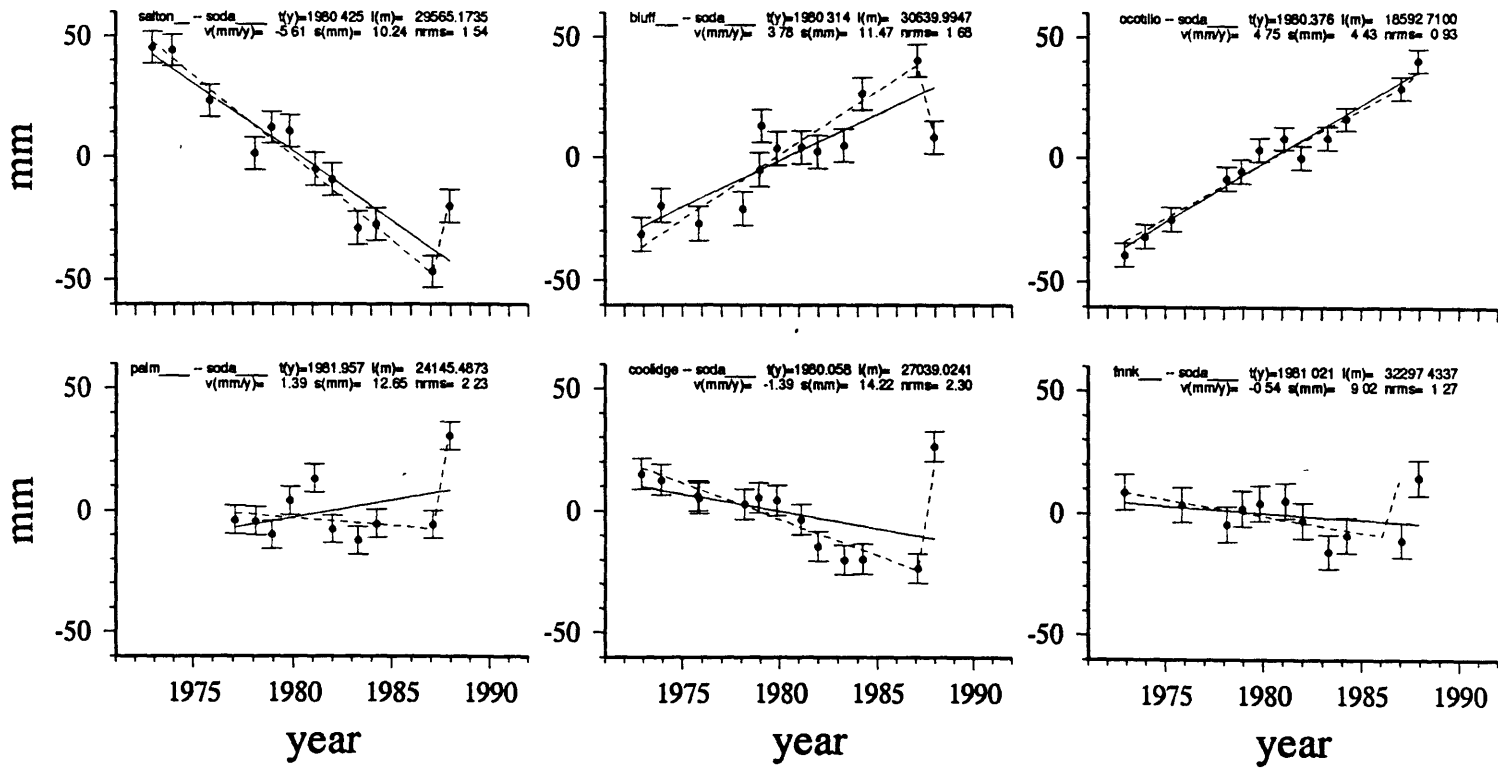
salton__ -- soda____ t(y)=1980.425 l(m)= 29565.1735
v(mm/y)= -5.61 s(mm)= 10.24 nrms= 1.54
bluff___ -- soda____ t(y)=1980.314 l(m)= 30639.9947
v(mm/y)= 3.78 s(mm)= 11.47 nrms= 1.68
ocotillo -- soda____ t(y)=1980.376 l(m)= 18592.7100
v(mm/y)= 4.75 s(mm)= 4.43 nrms= 0.93
palm____ -- soda____ t(y)=1981.957 l(m)= 24145.4873
v(mm/y)= 1.39 s(mm)= 12.65 nrms= 2.23
coolidge -- soda____ t(y)=1980.058 l(m)= 27039.0241
v(mm/y)= -1.39 s(mm)= 14.22 nrms= 2.30
fmk____ -- soda____ t(y)=1981.021 l(m)= 32297.4337
v(mm/y)= -0.54 s(mm)= 9.02 nrms= 1.27
mm
50
0
-50
1975
1980
1985
1990
year

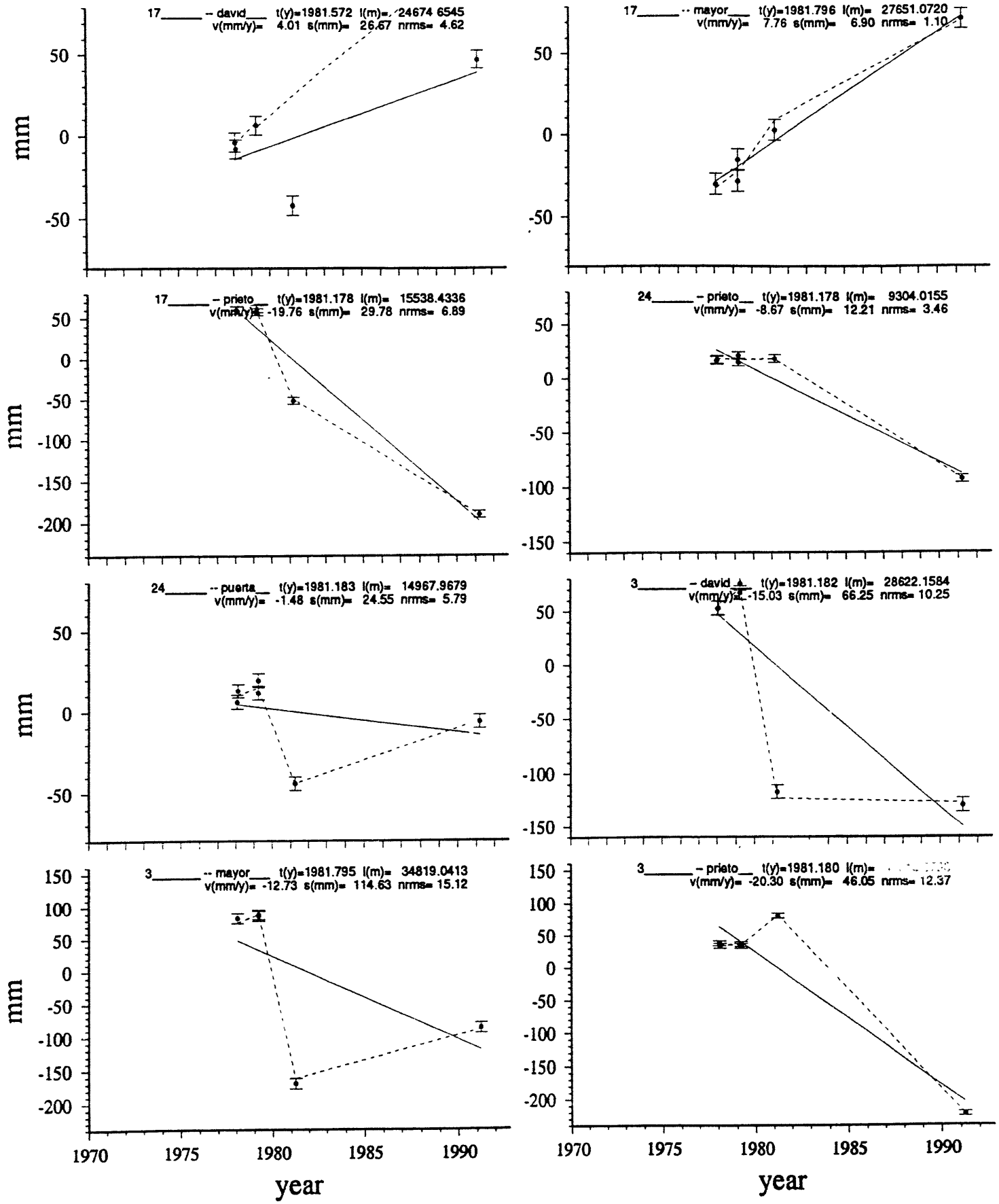
17_____ -- david___ t(y)=1981.572 l(m)= 24674 6545
v(mm/y)= 4.01 s(mm)= 26.67 nrms= 4.62
17_____ -- mayor___ t(y)=1981.796 l(m)= 27651.0720
v(mm/y)= 7.76 s(mm)= 6.90 nrms= 1.10
17_____ -- prieto___ t(y)=1981.178 l(m)= 15538.4336
v(mm/y)= -19.76 s(mm)= 29.78 nrms= 6.89
24_____ -- prieto___ t(y)=1981.178 l(m)= 9304.0155
v(mm/y)= -8.67 s(mm)= 12.21 nrms= 3.46
24_____ -- puerta___ t(y)=1981.183 l(m)= 14967.9679
v(mm/y)= -1.48 s(mm)= 24.55 nrms= 5.79
3_____ -- david___ t(y)=1981.182 l(m)= 28622.1584
v(mm/y)= -15.03 s(mm)= 66.25 nrms= 10.25
3_____ -- mayor___ t(y)=1981.795 l(m)= 34819.0413
v(mm/y)= -12.73 s(mm)= 114.63 nrms= 15.12
3_____ -- prieto___ t(y)=1981.180 l(m)=
v(mm/y)= -20.30 s(mm)= 46.05 nrms= 12.37
mm
year
1970
1975
1980
1985
1990

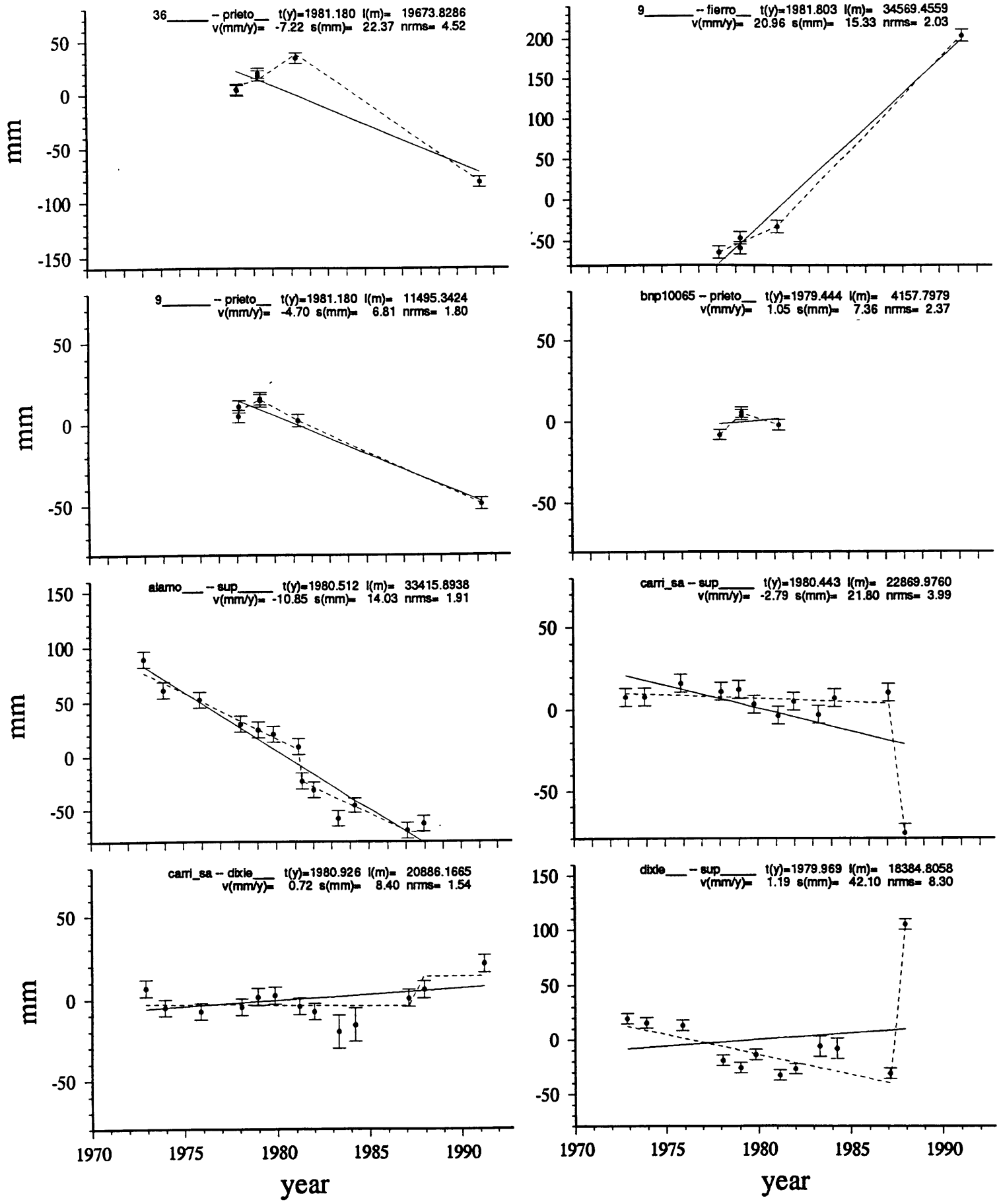
36_____ – prieto___ t(y)=1981.180 l(m)= 19673.8286
v(mm/y)= -7.22 s(mm)= 22.37 nrms= 4.52
9_____ – fierro___ t(y)=1981.803 l(m)= 34569.4559
v(mm/y)= 20.96 s(mm)= 15.33 nrms= 2.03
9_____ – prieto___ t(y)=1981.180 l(m)= 11495.3424
v(mm/y)= -4.70 s(mm)= 6.81 nrms= 1.80
bnp10065 – prieto___ t(y)=1979.444 l(m)= 4157.7979
v(mm/y)= 1.05 s(mm)= 7.36 nrms= 2.37
alamo___ – sup_____ t(y)=1980.512 l(m)= 33415.8938
v(mm/y)= -10.85 s(mm)= 14.03 nrms= 1.91
carri_sa – sup_____ t(y)=1980.443 l(m)= 22869.9760
v(mm/y)= -2.79 s(mm)= 21.80 nrms= 3.99
carri_sa – dixie___ t(y)=1980.926 l(m)= 20886.1665
v(mm/y)= 0.72 s(mm)= 8.40 nrms= 1.54
dixie___ – sup_____ t(y)=1979.969 l(m)= 18384.8058
v(mm/y)= 1.19 s(mm)= 42.10 nrms= 8.30
mm
year
1970
1975
1980
1985
1990

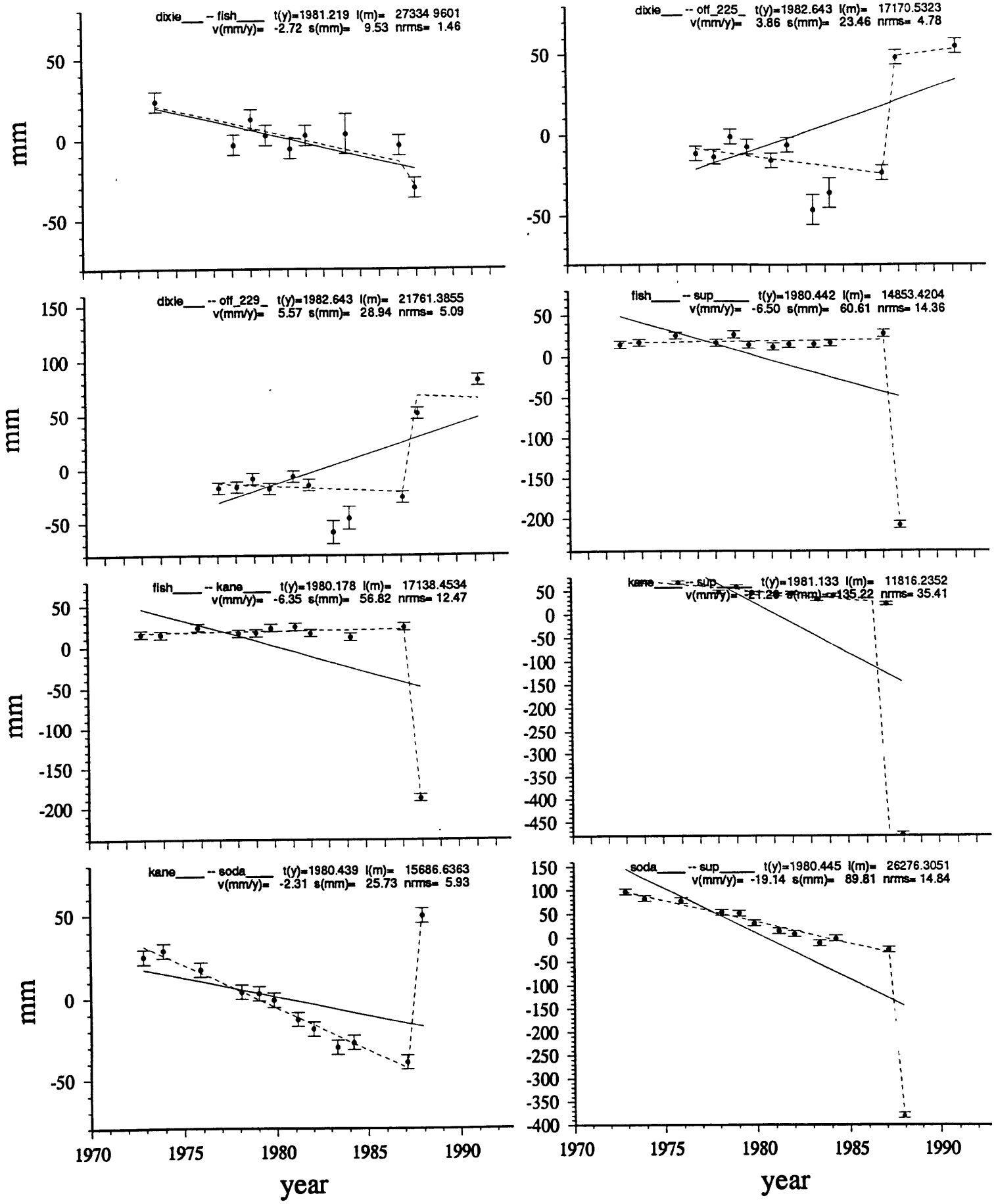
dixie___ -- fish____ t(y)=1981.219 l(m)= 27334.9601
v(mm/y)= -2.72 s(mm)= 9.53 nrms= 1.46
dixie___ -- off_225_ t(y)=1982.643 l(m)= 17170.5323
v(mm/y)= 3.86 s(mm)= 23.46 nrms= 4.78
dixie___ -- off_229_ t(y)=1982.643 l(m)= 21761.3855
v(mm/y)= 5.57 s(mm)= 28.94 nrms= 5.09
fish____ -- sup_____ t(y)=1980.442 l(m)= 14853.4204
v(mm/y)= -6.50 s(mm)= 60.61 nrms= 14.36
fish____ -- kane____ t(y)=1980.178 l(m)= 17138.4534
v(mm/y)= -6.35 s(mm)= 56.82 nrms= 12.47
kane____ -- sup_____ t(y)=1981.133 l(m)= 11816.2352
v(mm/y)= -21.26 s(mm)= 135.22 nrms= 35.41
kane____ -- soda____ t(y)=1980.439 l(m)= 15686.6363
v(mm/y)= -2.31 s(mm)= 25.73 nrms= 5.93
soda____ -- sup_____ t(y)=1980.445 l(m)= 26276.3051
v(mm/y)= -19.14 s(mm)= 89.81 nrms= 14.84
mm
year
1970
1975
1980
1985
1990

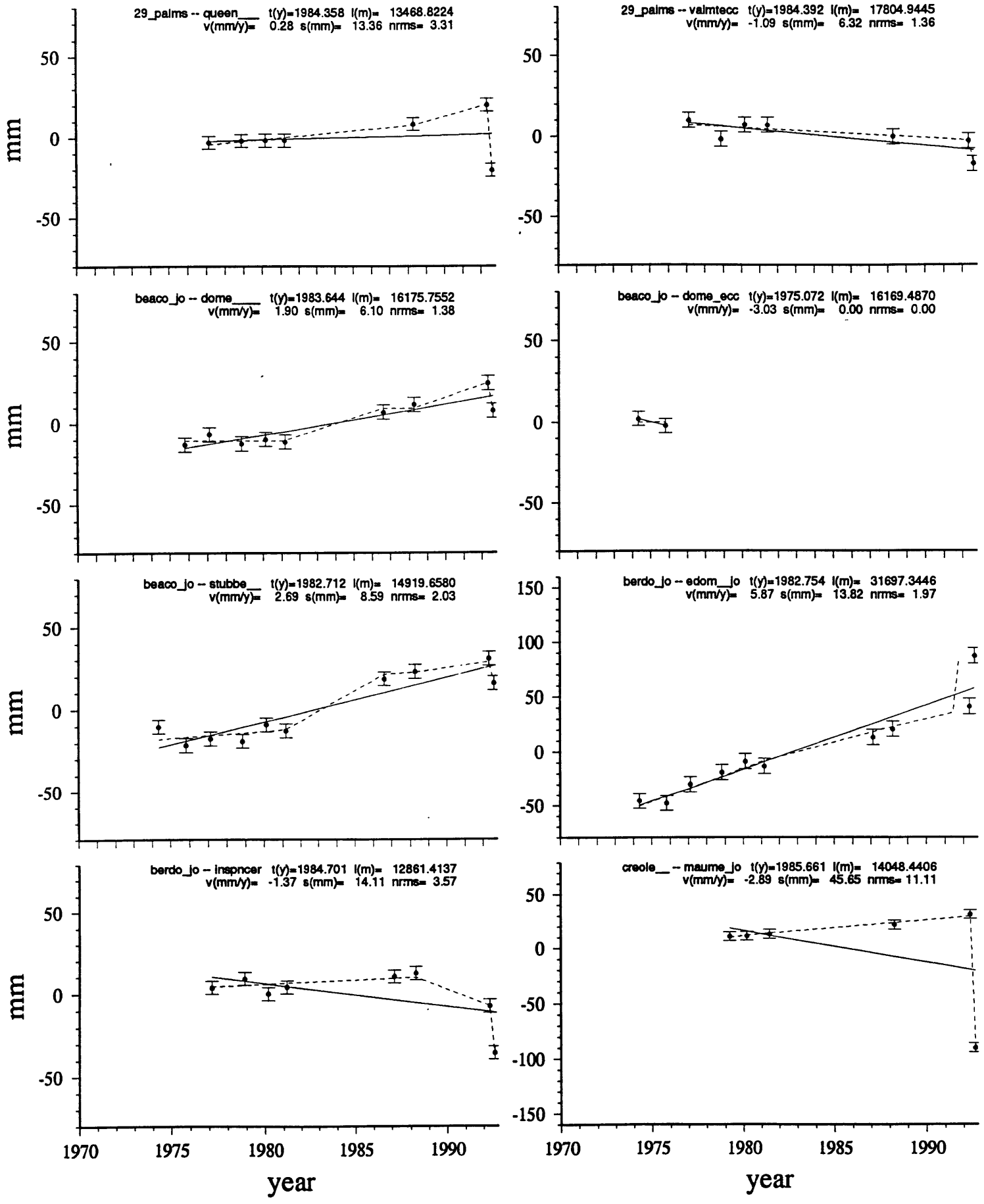
29_palms -- queen___ t(y)=1984.358 l(m)= 13468.8224
v(mm/y)= 0.28 s(mm)= 13.36 nrms= 3.31
29_palms -- valmtecc t(y)=1984.392 l(m)= 17804.9445
v(mm/y)= -1.09 s(mm)= 6.32 nrms= 1.36
beaco_jo -- dome___ t(y)=1983.644 l(m)= 16175.7552
v(mm/y)= 1.90 s(mm)= 6.10 nrms= 1.38
beaco_jo -- dome_ecc t(y)=1975.072 l(m)= 16169.4870
v(mm/y)= -3.03 s(mm)= 0.00 nrms= 0.00
beaco_jo -- stubbe___ t(y)=1982.712 l(m)= 14919.6580
v(mm/y)= 2.69 s(mm)= 8.59 nrms= 2.03
berdo_jo -- edom__jo t(y)=1982.754 l(m)= 31697.3446
v(mm/y)= 5.87 s(mm)= 13.82 nrms= 1.97
berdo_jo -- inspncer t(y)=1984.701 l(m)= 12861.4137
v(mm/y)= -1.37 s(mm)= 14.11 nrms= 3.57
creole__ -- maume_jo t(y)=1985.661 l(m)= 14048.4406
v(mm/y)= -2.89 s(mm)= 45.65 nrms= 11.11
mm
year
1970
1975
1980
1985
1990

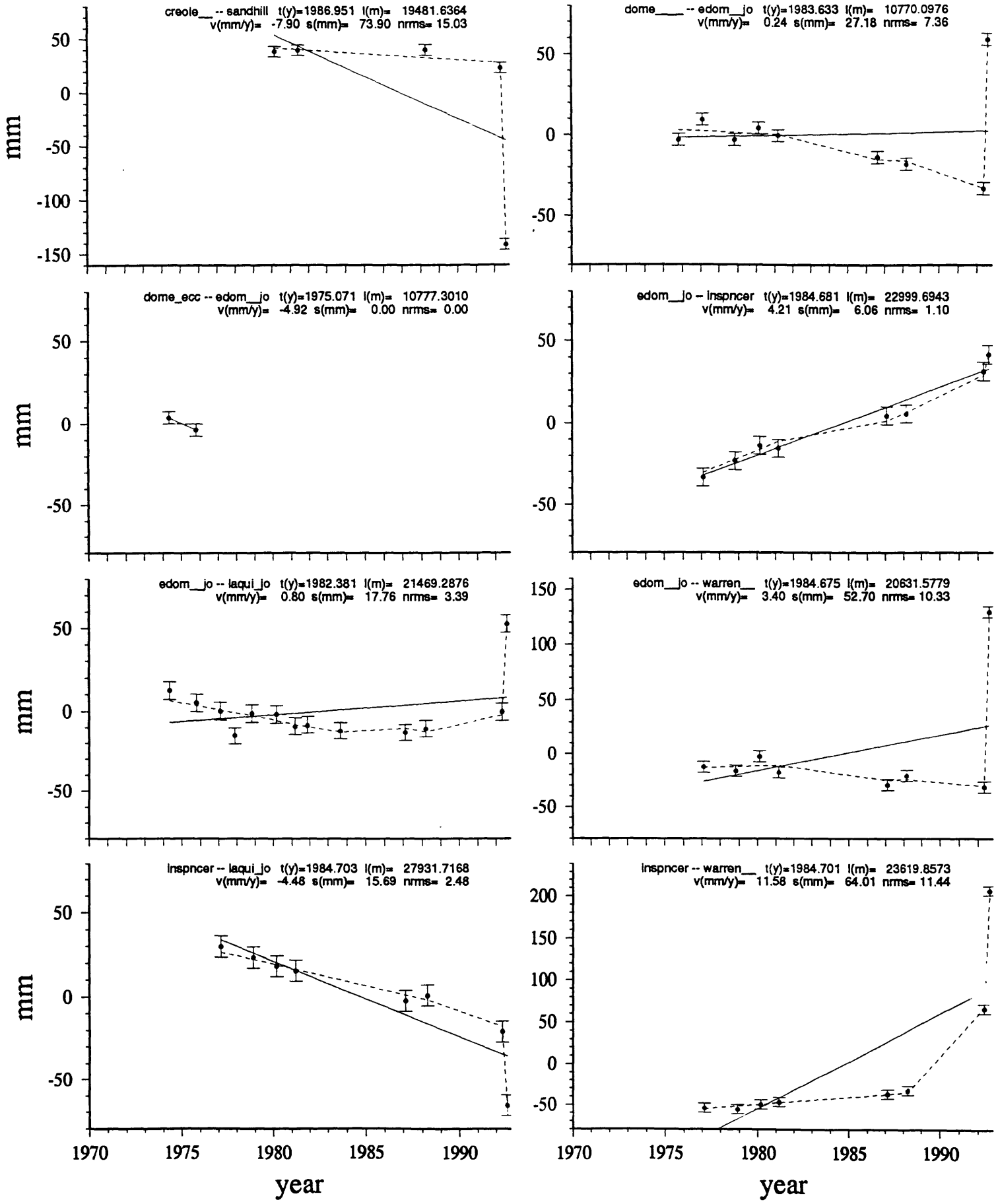
creole__ -- sandhill t(y)=1986.951 l(m)= 19481.6364
v(mm/y)= -7.90 s(mm)= 73.90 nrms= 15.03
dome____ -- edom__jo t(y)=1983.633 l(m)= 10770.0976
v(mm/y)= 0.24 s(mm)= 27.18 nrms= 7.36
dome_ecc -- edom__jo t(y)=1975.071 l(m)= 10777.3010
v(mm/y)= -4.92 s(mm)= 0.00 nrms= 0.00
edom__jo -- inspncer t(y)=1984.681 l(m)= 22999.6943
v(mm/y)= 4.21 s(mm)= 6.06 nrms= 1.10
edom__jo -- laqui_jo t(y)=1982.381 l(m)= 21469.2876
v(mm/y)= 0.80 s(mm)= 17.76 nrms= 3.39
edom__jo -- warren__ t(y)=1984.675 l(m)= 20631.5779
v(mm/y)= 3.40 s(mm)= 52.70 nrms= 10.33
inspncer -- laqui_jo t(y)=1984.703 l(m)= 27931.7168
v(mm/y)= -4.48 s(mm)= 15.69 nrms= 2.48
inspncer -- warren__ t(y)=1984.701 l(m)= 23619.8573
v(mm/y)= 11.58 s(mm)= 64.01 nrms= 11.44
mm
year
1970
1975
1980
1985
1990

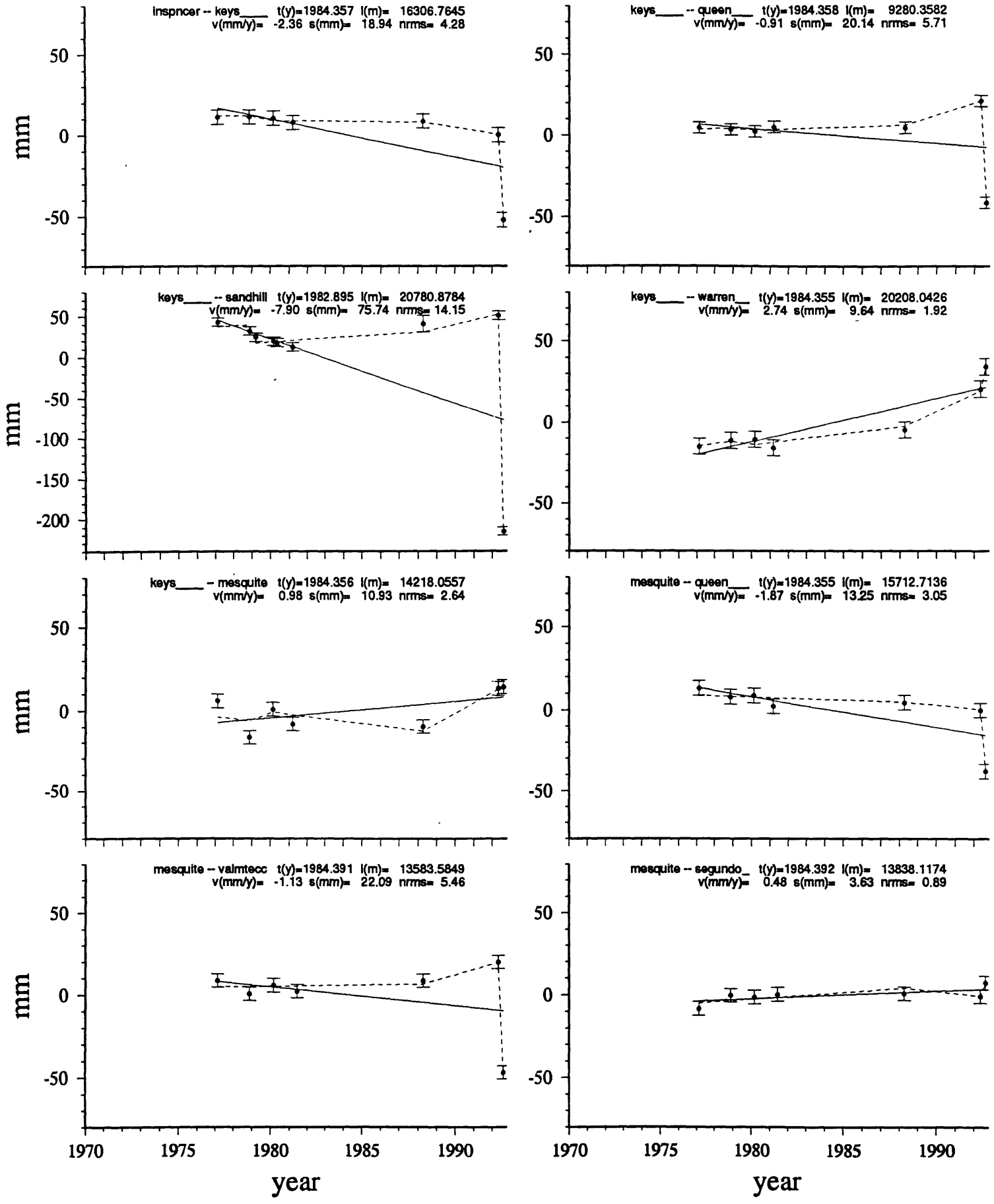
inspncer -- keys____ t(y)=1984.357 l(m)= 16306.7645
v(mm/y)= -2.36 s(mm)= 18.94 nrms= 4.28
keys____ -- queen___ t(y)=1984.358 l(m)= 9280.3582
v(mm/y)= -0.91 s(mm)= 20.14 nrms= 5.71
keys____ -- sandhill t(y)=1982.895 l(m)= 20780.8784
v(mm/y)= -7.90 s(mm)= 75.74 nrms= 14.15
keys____ -- warren__ t(y)=1984.355 l(m)= 20208.0426
v(mm/y)= 2.74 s(mm)= 9.64 nrms= 1.92
keys____ -- mesquite t(y)=1984.356 l(m)= 14218.0557
v(mm/y)= 0.98 s(mm)= 10.93 nrms= 2.64
mesquite -- queen___ t(y)=1984.355 l(m)= 15712.7136
v(mm/y)= -1.87 s(mm)= 13.25 nrms= 3.05
mesquite -- valmtecc t(y)=1984.391 l(m)= 13583.5849
v(mm/y)= -1.13 s(mm)= 22.09 nrms= 5.46
mesquite -- segundo_ t(y)=1984.392 l(m)= 13838.1174
v(mm/y)= 0.48 s(mm)= 3.63 nrms= 0.89
mm
year
1970
1975
1980
1985
1990

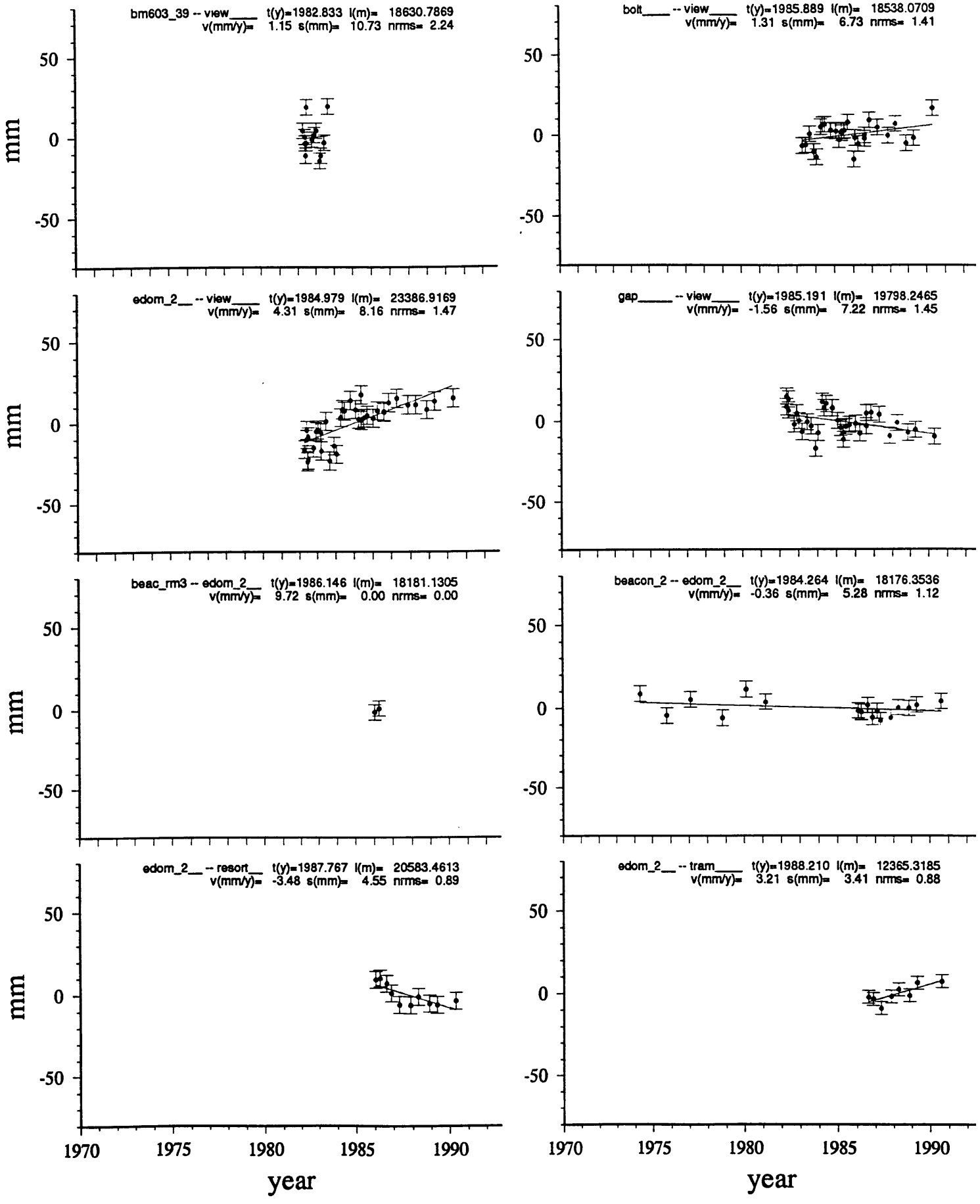
bm603_39 -- view____ t(y)=1982.833 l(m)= 18630.7869
v(mm/y)= 1.15 s(mm)= 10.73 nrms= 2.24
bolt____ -- view____ t(y)=1985.889 l(m)= 18538.0709
v(mm/y)= 1.31 s(mm)= 6.73 nrms= 1.41
edom_2__ -- view____ t(y)=1984.979 l(m)= 23386.9169
v(mm/y)= 4.31 s(mm)= 8.16 nrms= 1.47
gap_____ -- view____ t(y)=1985.191 l(m)= 19798.2465
v(mm/y)= -1.56 s(mm)= 7.22 nrms= 1.45
beac_rm3 -- edom_2__ t(y)=1986.146 l(m)= 18181.1305
v(mm/y)= 9.72 s(mm)= 0.00 nrms= 0.00
beacon_2 -- edom_2__ t(y)=1984.264 l(m)= 18176.3536
v(mm/y)= -0.36 s(mm)= 5.28 nrms= 1.12
edom_2__ -- resort__ t(y)=1987.767 l(m)= 20583.4613
v(mm/y)= -3.48 s(mm)= 4.55 nrms= 0.89
edom_2__ -- tram____ t(y)=1988.210 l(m)= 12365.3185
v(mm/y)= 3.21 s(mm)= 3.41 nrms= 0.88
mm
50
0
-50
1970
1975
1980
1985
1990
year

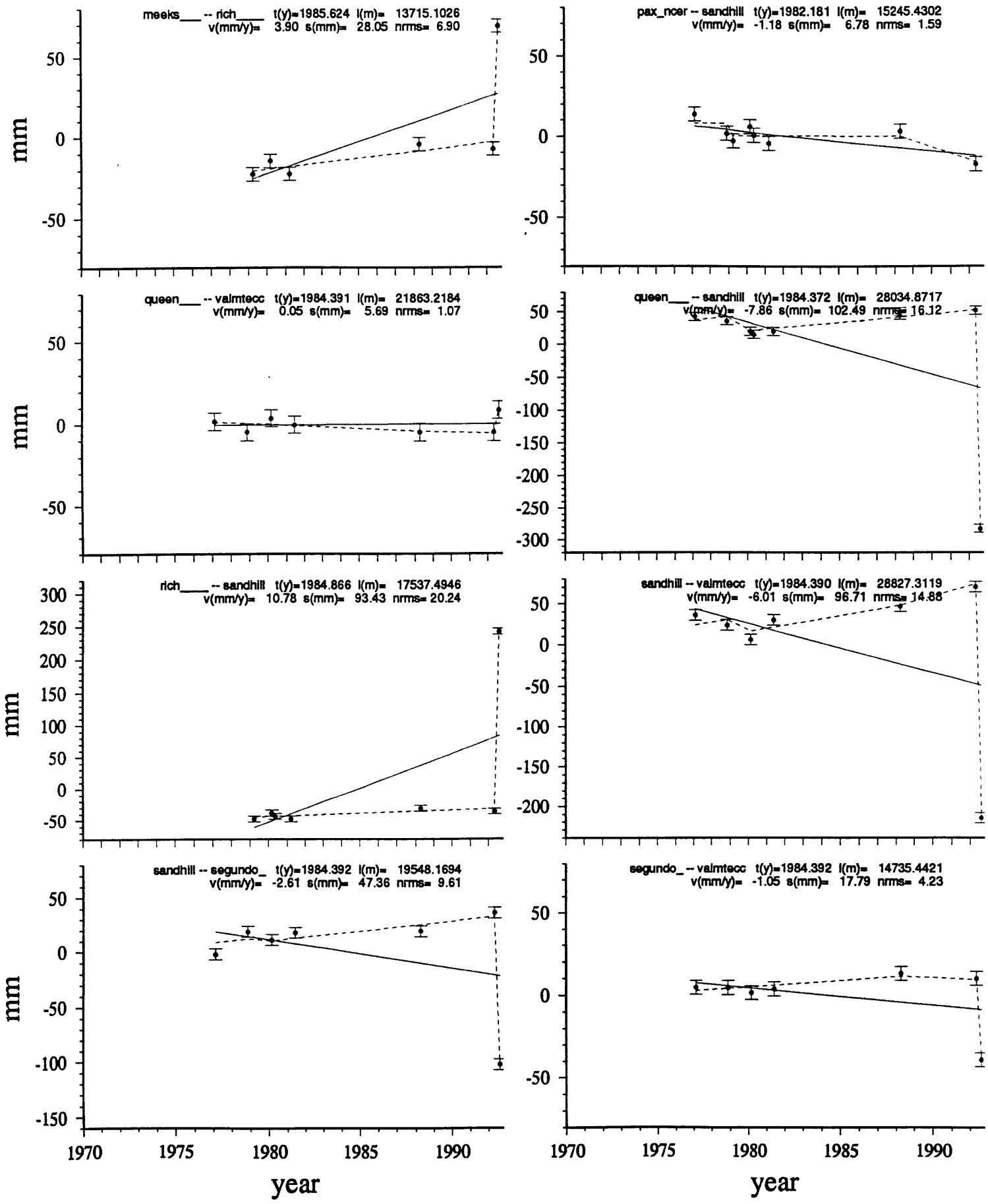
meeks___ -- rich____ t(y)=1985.624 l(m)= 13715.1026
v(mm/y)= 3.90 s(mm)= 28.05 nrms= 6.90
pax_ncer -- sandhill t(y)=1982.181 l(m)= 15245.4302
v(mm/y)= -1.18 s(mm)= 6.78 nrms= 1.59
queen___ -- valmtecc t(y)=1984.391 l(m)= 21863.2184
v(mm/y)= 0.05 s(mm)= 5.69 nrms= 1.07
queen___ -- sandhill t(y)=1984.372 l(m)= 28034.8717
v(mm/y)= -7.86 s(mm)= 102.49 nrms= 16.12
rich____ -- sandhill t(y)=1984.866 l(m)= 17537.4946
v(mm/y)= 10.78 s(mm)= 93.43 nrms= 20.24
sandhill -- valmtecc t(y)=1984.390 l(m)= 28827.3119
v(mm/y)= -6.01 s(mm)= 96.71 nrms= 14.88
sandhill -- segundo_ t(y)=1984.392 l(m)= 19548.1694
v(mm/y)= -2.61 s(mm)= 47.36 nrms= 9.61
segundo_ -- valmtecc t(y)=1984.392 l(m)= 14735.4421
v(mm/y)= -1.05 s(mm)= 17.79 nrms= 4.23
mm
year
1970
1975
1980
1985
1990

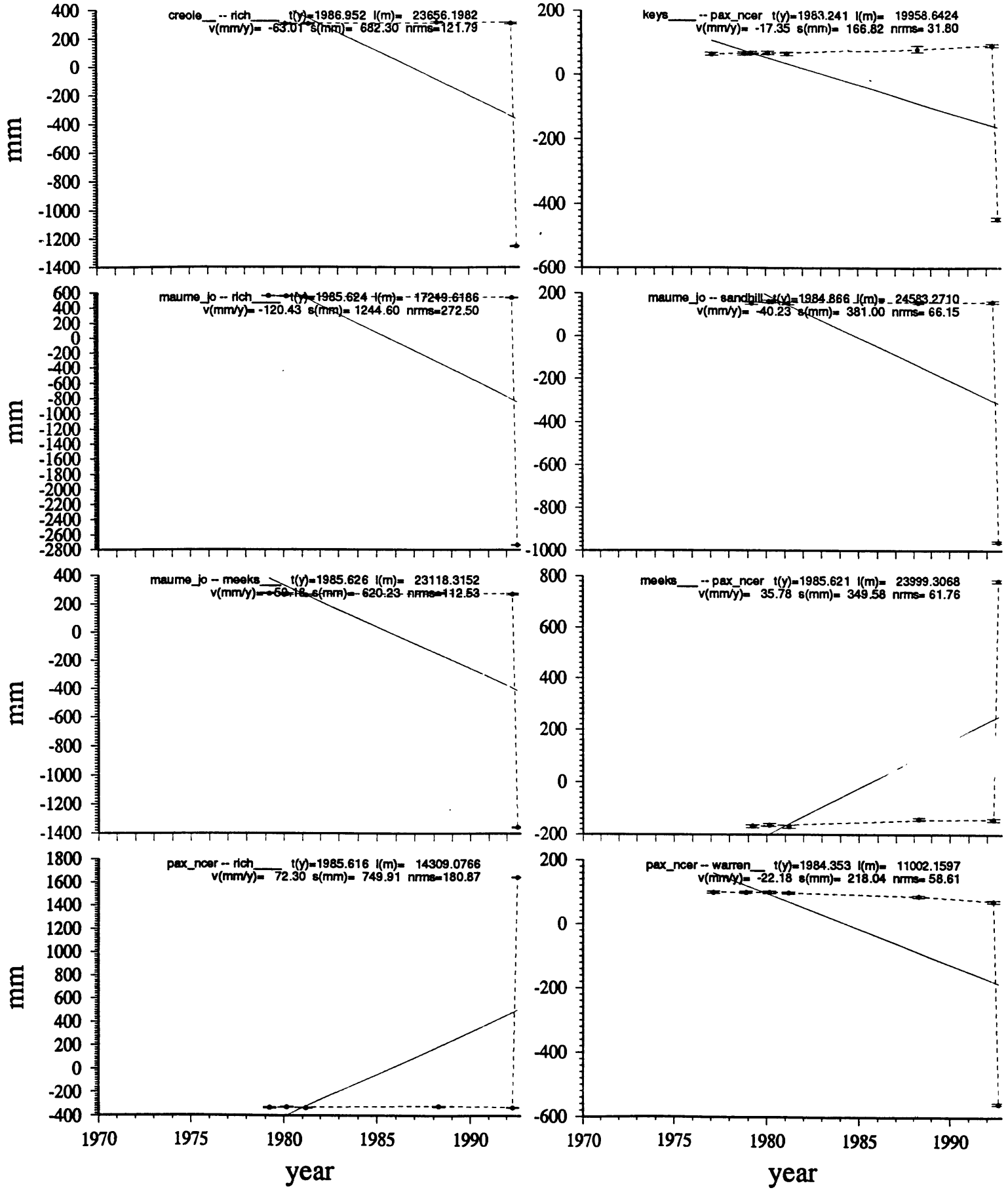
creole__ -- rich____ t(y)=1986.952 l(m)= 23656.1982
v(mm/y)= -63.01 s(mm)= 682.30 nrms=121.79
keys____ -- pax_ncer t(y)=1983.241 l(m)= 19958.6424
v(mm/y)= -17.35 s(mm)= 166.82 nrms= 31.80
maume_jo -- rich____ t(y)=1985.624 l(m)= 17249.6186
v(mm/y)= -120.43 s(mm)= 1244.60 nrms=272.50
maume_jo -- sandhill t(y)=1984.866 l(m)= 24583.2710
v(mm/y)= -40.23 s(mm)= 381.00 nrms= 66.15
maume_jo -- meeks___ t(y)=1985.626 l(m)= 23118.3152
v(mm/y)= -69.18 s(mm)= 620.23 nrms=112.53
meeks___ -- pax_ncer t(y)=1985.621 l(m)= 23999.3068
v(mm/y)= 35.78 s(mm)= 349.58 nrms= 61.76
pax_ncer -- rich____ t(y)=1985.616 l(m)= 14309.0766
v(mm/y)= 72.30 s(mm)= 749.91 nrms=180.87
pax_ncer -- warren__ t(y)=1984.353 l(m)= 11002.1597
v(mm/y)= -22.18 s(mm)= 218.04 nrms= 58.61
mm
year
1970
1975
1980
1985
1990

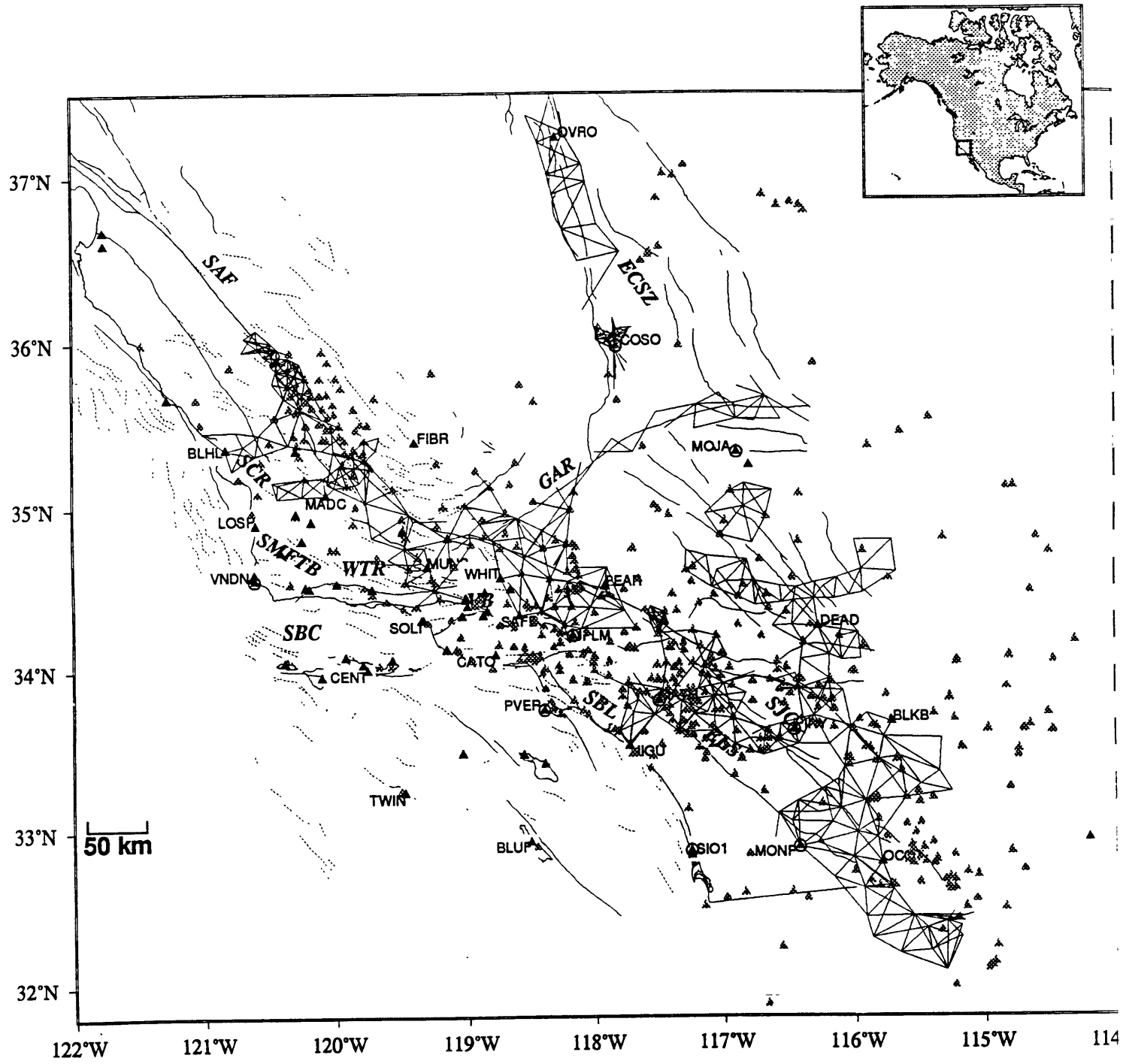

Figure 17. Map of southern California showing the VLBI/GPS (VG) stations (triangles) and USGS trilateration network (linked with solid lines). All the tectonic features and plotting conventions are the same as in Figure 1. The gray triangles represent the recent GPS sites. Most of the new GPS sites are from SCEC and Caltrans GPS experiments. The gray sites at the southeast corner are part of the Salton Trough and Riverside County (STRC) network (R. Reilinger, personal communication, 1993, and those in the northeast corner are part of the Death Valley network (B. Wernicke, personal communication, 1993).

Table 1 :

measurement	span	accuracy	reference
1-st order direction		0.6 arc seconds	*Snay* [1990]
2-nd order direction		0.7 arc seconds	*Snay* [1990]
3-rd order direction		1.2 arc seconds	*Snay* [1990]
4-th order direction		3.0 arc seconds	*Snay* [1990]
1-st order azimuth		1.4 arc seconds	*Snay* [1990]
Taped distances		10 mm + 1.0 ppm	*Snay* [1990]
EDM[a] (NGS[b])		15 mm + 1.0 ppm	*Snay et al.* [1987]
EDM (USGS[c])	1972-1992	3 mm + 0.2 ppm	*Savage, Prescott* [1973]
EDM (CDWR[d])[g]	1959-1969	10 mm + 1.0 ppm	*King et al.* [1987]
EDM (CDMG[e])	1970-1979	6 mm + 0.7 ppm	*King et al.* [1987]
HP[f] (USGS)		3 mm + 2.0 ppm	*Lisowski* [personal communication,1993]

a. Electronic Distance Measurement

b. National Geodetic Survey

c. United States Geological Survey

d. California Department of Water Resources

e. California Division of Mines and Geology

f. Hewlett-Packard

g. There are offsets between CDWR and CDMG measurements due to the changes of instrument and the procedures for correcting atmospheric refraction effects [*King et al.*, 1987].

Table 2:

data	span	north	east	up	reference
GPS	1986-1992	3.4mm+0 ppb	6.9mm+15ppb	21.6mm-12ppb	*Feigl et al.*,1993
VLBI	1984-1991	7.1mm-1 ppb	5.5mm+2 ppb	38.4mm ppb	*Feigl et al.*,1993

Table 3: USGS EDM site used in this analysis

```
* frame:  WGS84
*  u = V(east)  v = V(north)  w = V(up),  unit: m/year
*  uncertainty of coordinates: Sn = north, Se = east, Su = up,  unit: meter
*
*  site     full-name      latitude          longitude          height      u        v        w      epoch       Sn       Se       Su
 apache__ lospa_net    N34 45 25.61230 W119 19  0.30178    1451.1121 -0.0241  0.0236  0.0000 1983.000   0.2219   0.1099  3.8080
 fraz_rm2 lospa_net    N34 46 30.72961 W118 58  8.53902    2410.7462 -0.0241  0.0222  0.0000 1992.900  18.9788   4.9456  0.0000
 frazier_ lospa_net    N34 46 29.89344 W118 58  8.83236    2411.8389 -0.0224  0.0202  0.0000 1983.000   0.1560   0.0449  0.1000
 kitchen_ lospa_net    N34 55 16.76401 W119  9  4.43015    1523.8605  0.0000  0.0000  0.0000 1983.000  19.6105   0.1466  4.9937
 madulce2 lospa_net    N34 41 27.51573 W119 35 28.04845    1958.3607 -0.0290  0.0330  0.0000 1983.000   0.3673   0.2002  4.9937
 monte___ lospa_net    N34 32 21.75213 W119 28  0.48607    1792.9904 -0.0315  0.0291  0.0000 1983.000   0.1730   0.1225  3.8502
 mt_pinos lospa_net    N34 48 46.17056 W119  8 43.47847    2662.5981 -0.0217  0.0219  0.0290 1983.000   0.0199   0.0198  0.0100
 nordhoff lospa_net    N34 29 53.92406 W119 14 31.53176    1332.7173 -0.0303  0.0252  0.0000 1983.000   0.3203   0.1156  4.7558
 paa-1___ lospa_net    N34 22 20.86752 W119 25 13.30220     624.3609  0.0000  0.0000  0.0000 1983.000  14.9109  12.7279  4.9936
 patti_lo lospa_net    N34 57 35.04883 W119 25 56.43958     983.8125 -0.0180  0.0231  0.0000 1983.000   0.1965   0.1316  0.9001
 pelat_lo lospa_net    N34 55 12.63994 W119 24 19.57132    1334.4679 -0.0201  0.0234  0.0000 1983.000   0.1761   0.1135  1.1216
 pinosecc lospa_net    N34 48 43.62711 W119  8 54.89266    2655.0005 -0.0222  0.0215  0.0290 1983.000  16.5692  10.4956  4.9932
 poison__ lospa_net    N34 24 35.84206 W119 12 14.09952     797.3545  0.0000  0.0000  0.0000 1983.000   6.6098  18.4545  4.9933
 police__ lospa_net    N34 54 10.92070 W118 54 16.16366    1441.4478 -0.0177  0.0187  0.0000 1983.000   0.1939   0.0917  2.5719
 reyes___ lospa_net    N34 37 51.01883 W119 16 53.79341    2260.4178 -0.0280  0.0245  0.0000 1983.000   0.0939   0.1546  2.8245
 santapau lospa_net    N34 26 25.26217 W119  0 34.72667    1476.6904 -0.0242  0.0231 -0.0009 1983.000   0.0200   0.0200  0.0100
 seco____ lospa_net    N34 37 31.69263 W119 26 29.78824    1642.9545 -0.0302  0.0282  0.0000 1983.000   0.2018   0.2319  3.6211
 sulpher_ lospa_net    N34 24 35.61772 W119 12 13.70619     797.3679  0.0000  0.0000  0.0000 1983.000   6.6176  18.4488  4.9933
 sulphrm2 lospa_net    N34 24 35.44595 W119 12 13.83852     797.3600  0.0000  0.0000  0.0000 1983.000   6.6153  18.4649  4.9933
 tecuy_lo lospa_net    N34 50 32.95040 W118 58 53.78244    2144.7793 -0.0204  0.0198  0.0000 1983.000   0.1912   0.0833  3.0297
 tejon_41 lospa_net    N34 48 13.08161 W118 48 56.01569    1450.3935 -0.0181  0.0206  0.0000 1983.000   0.2006   0.0822  2.6484
 temb__lo lospa_net    N35  6 45.42802 W119 33 17.31278    1050.2923 -0.0144  0.0231  0.0000 1983.000   1.8919   2.8944  3.4225
 tembl_lo lospa_net    N35  6 46.02261 W119 33 18.03093    1052.6130 -0.0143  0.0223  0.0000 1983.000   0.1392   0.1204  0.1000
 thorn___ lospa_net    N34 36 23.01770 W119  7 39.74730    2076.4345 -0.0294  0.0244  0.0000 1983.000   0.1089   0.2177  4.4957
 wh2_r_lo lospa_net    N35  0 38.48728 W119  0 51.44161     619.1405 -0.0162  0.0175  0.0000 1983.000   9.4144  17.2087  4.9927
 yam___lo lospa_net    N34 45 14.66608 W119 28 30.84604    1759.1000 -0.0260  0.0282  0.0000 1983.000   0.2259   0.0607  0.9705
 avenue__ tehac_net    N34 46 36.41672 W118 13 12.45679     686.6644 -0.0101  0.0175  0.0000 1983.000   0.1188   0.0959  1.0786
 bald____ tehac_net    N35 16 20.87108 W118  5 42.62243    1497.0305  0.0000  0.0000  0.0000 1983.000   5.0412  18.9525  4.9937
 black_bu tehac_net    N34 31 42.81593 W117 45 45.84838     909.4605  0.0000  0.0000  0.0000 1983.000  19.5600  13.9402  4.9938
 bull____ tehac_net    N34 49  6.07655 W118 33 12.04428     840.0742 -0.0133  0.0186  0.0000 1983.000   0.4324   0.2672  3.3789
 denis___ tehac_net    N34 37 52.47653 W118  8 36.28931     757.2185  0.0000  0.0000  0.0000 1983.000  19.6101   0.4339  4.9938
 diorite_ tehac_net    N34 56  4.30280 W118 36 54.77835    2003.3791 -0.0117  0.0167  0.0000 1983.000   0.1534   0.1097  1.6488
 doub_rm1 tehac_net    N35  1 59.95584 W118 29 12.39881    2403.7848  0.0000  0.0000  0.0000 1983.000   0.1974   0.1246  0.1000
 fairmont tehac_net    N34 44 56.77672 W118 24 26.66490     932.1150 -0.0140  0.0196  0.0000 1983.000   0.1095   0.0926  0.0991
 gneiss__ tehac_net    N34 57 33.31202 W118 42 11.38772    1765.8394 -0.0135  0.0165  0.0000 1983.000   0.1546   0.1915  4.3808
 leona___ tehac_net    N34 38 39.26642 W118 19 27.53673    1181.5605  0.0000  0.0000  0.0000 1983.000  10.6684  16.4519  4.9936
 lit_rock tehac_net    N34 30 48.36311 W117 56 18.82555     896.6805  0.0000  0.0000  0.0000 1983.000  19.5583  13.9426  4.9938
 pajuela_ tehac_net    N35  7 14.69928 W118 17 40.45406    1705.4005  0.0000  0.0000  0.0000 1983.000  10.4510  16.5959  4.9936
 pelona__ tehac_net    N34 33 39.51892 W118 21 21.81899    1446.7732 -0.0201  0.0215  0.0000 1983.000   0.1089   0.1349  0.0998
 police__ tehac_net    N34 54 10.92070 W118 54 16.16366    1441.4478 -0.0177  0.0187  0.0000 1983.000   0.1939   0.0917  2.5719
 rit_rid_ tehac_net    N34 36 23.85883 W118 12 52.93049     991.6605  0.0000  0.0000  0.0000 1983.000   0.5370  19.6040  4.9937
 saw_ecc_ tehac_net    N34 41 35.33391 W118 33 41.25343    1648.1312 -0.0183  0.0208  0.0000 1983.000   0.1349   0.1000  0.4833
 sawmill_ tehac_net    N34 41 35.35890 W118 33 41.08149    1646.6612 -0.0182  0.0234  0.0000 1983.000   0.2391   0.1118  4.9935
 soledad_ tehac_net    N34 58 57.04194 W118 11 19.83701    1245.7883 -0.0083  0.0160  0.0000 1983.000   0.1231   0.1149  0.0999
 tecuyrm1 tehac_net    N34 50 32.95040 W118 58 53.78244    2144.7793 -0.0204  0.0198  0.0000 1983.000   0.1912   0.0833  3.0297
 tej32rm2 tehac_net    N35  7 25.28572 W118 49 20.82011     291.9585 -0.0148  0.0136  0.0000 1983.000  10.0647  16.8372  4.9930
 tejon_32 tehac_net    N35  7 25.62617 W118 49 21.33954     293.2910 -0.0148  0.0136  0.0000 1983.000   0.1774   0.1530  0.1000
 tejon_41 tehac_net    N34 48 13.08161 W118 48 56.01569    1450.3935 -0.0181  0.0206  0.0000 1983.000   0.2006   0.0822  2.6484
 thumb___ tehac_net    N34 51 45.72622 W118 25  8.68421     807.1821 -0.0089  0.0152  0.0000 1983.000   0.1106   0.0955  0.7215
 tom_____ tehac_net    N34 37 51.79210 W117 53 55.05163     960.0292 -0.0111  0.0162  0.0000 1983.000   0.8730   0.4292  3.4393
 tom_rm3_ tehac_net    N34 37 52.23434 W117 53 54.76137     960.1605 -0.0097  0.0162  0.0000 1983.000  19.6113   0.4371  4.9937
 weed_rm1 tehac_net    N35 13 22.37498 W118 55 56.43419      74.8279  0.0000  0.0000  0.0000 1992.900  13.1967  14.5082  0.0000
 wheeler2 tehac_net    N35  0 38.11203 W119  0 51.49925     619.6983 -0.0162  0.0175  0.0000 1983.000   0.1248   0.1161  0.1000
 alderaux sanga_net    N34 22 58.49014 W118  2  2.56892    2137.3552 -0.0202  0.0201  0.0000 1983.000  29.0789  64.4598  9.9502
 ant_aux_ sanga_net    N34 14 54.64678 W117 40 30.66125    2042.5188 -0.0179  0.0208  0.0000 1983.000   1.3289   0.6792  4.9871
 bad_pow_ sanga_net    N34 21 29.93964 W117 45 52.91081    2831.4394 -0.0182  0.0184  0.0000 1983.000   1.0799   0.4721  3.3992
 bull____ sanga_net    N34 49  6.07655 W118 33 12.04428     840.0742 -0.0133  0.0186  0.0000 1983.000   0.4324   0.2672  3.3789
 camp_9__ sanga_net    N34 21 11.55058 W118 25  5.05922    1190.4235 -0.0238  0.0226  0.0000 1983.000   0.1512   0.4579  2.7286
 dispoint sanga_net    N34 14 47.60739 W118  6 18.62599    1789.1679 -0.0224  0.0205  0.0000 1983.000   0.4629   0.6812  4.9905
 dugo____ sanga_net    N34 12 55.29996 W118 16 36.51791     898.3405 -0.0214  0.0223  0.0000 1983.000   0.6347   0.7781  4.9912
 flint___ sanga_net    N34  9 48.84302 W118 11 48.55053     542.3022 -0.0223  0.0219  0.0000 1983.000   0.6588   0.9350  4.9901
 gln_ncer sanga_net    N34 23 12.73038 W118 11  5.58283    1895.4488 -0.0214  0.0213  0.0000 1983.000   0.3234   0.4115  3.4159
 handle__ sanga_net    N34 14 49.29782 W118  6 23.03838    1789.0705  0.0000  0.0000  0.0000 1983.000  13.1413  14.5781  4.9921
 hau_ecc1 sanga_net    N34 32 51.18533 W118 12 55.91141    1547.6790 -0.0182  0.0210  0.0000 1983.000   0.2868   0.3129  4.4738
 hauser__ sanga_net    N34 32 51.79688 W118 12 55.98116    1546.7605 -0.0182  0.0210  0.0000 1983.000  19.4837   2.2398  4.9937
 jpll_rm1 sanga_net    N34 12 17.06896 W118 10 15.45801     441.2933 -0.0190  0.0161  0.0123 1983.000   0.7752   0.9002  4.9933
 littejon sanga_net    N34 48  2.27059 W118 48  9.63516    1412.5494 -0.0192  0.0214  0.0000 1983.000   0.6118   0.3279  0.0000
 may_____ sanga_net    N34 21  8.13934 W118 25 46.71126    1169.6830 -0.0238  0.0226  0.0000 1983.000   0.1651   0.4595  2.7561
 mtgleasn sanga_net    N34 23 12.55435 W118 11  5.29922    1896.5622 -0.0214  0.0213  0.0000 1983.000   0.3235   0.4114  3.3941
 nbaldaux sanga_net    N34 21 30.73482 W117 45 52.87044    2830.3239 -0.0197  0.0173  0.0000 1983.000   1.0799   0.4718  3.4041
 pac_unk_ sanga_net    N34 22 54.87700 W118  2  4.76932    2140.3605 -0.0224  0.0216  0.0000 1983.000   0.6683   0.4205  4.9937
 pac1ncer sanga_net    N34 22 58.29141 W118  2  2.67636    2137.3611 -0.0202  0.0201  0.0000 1983.000   0.6194   1.0624  4.9908
 pac2ncer sanga_net    N34 22 54.31056 W118  2  4.72927    2137.2076 -0.0202  0.0201  0.0000 1983.000   0.5896   0.4381  4.9888
 pacifico sanga_net    N34 22 54.46355 W118  2  4.77896    2141.0542 -0.0202  0.0201  0.0000 1983.000   0.6678   0.4207  4.9812
 parkaux2 sanga_net    N34 27 35.01351 W118 13  7.64696    1225.3305 -0.0196  0.0215  0.0000 1983.000   7.0756  18.2978  4.9928
 park_rm3 sanga_net    N34 27 35.04242 W118 13  7.66270    1225.0005 -0.0196  0.0215  0.0000 1983.000   7.0757  18.2977  4.9928
 parker__ sanga_net    N34 27 35.21521 W118 13  7.81361    1224.8970 -0.0196  0.0215  0.0000 1983.000   0.3275   0.3492  2.3477
 pelon_sa sanga_net    N34 33 39.51892 W118 21 21.81899    1446.7732 -0.0201  0.0215  0.0000 1983.000   0.1089   0.1349  0.0998
 piconcer sanga_net    N34 19 50.44537 W118 36  4.84526    1101.2861 -0.0256  0.0253  0.0137 1983.000   0.4244   0.5010  4.9133
 port____ sanga_net    N34 23 10.86265 W118 19 47.36705    1446.8605 -0.0226  0.0226  0.0000 1983.000  10.5950  16.5042  4.9938
```

port_rml	sanga_net	N34	23	11.59581	W118	19	47.43639	1439.1396	-0.0226	0.0226	0.0000	1983.000	0.1179	0.4017	2.8351
saw_e_sa	sanga_net	N34	41	35.32136	W118	33	41.23451	1647.9615	-0.0182	0.0234	0.0000	1983.000	0.1731	0.1435	0.0000
sawmi_sa	sanga_net	N34	41	35.36000	W118	33	41.08153	1646.6605	-0.0182	0.0234	0.0000	1983.000	0.1347	0.1000	0.0000
siselsie	sanga_net	N34	16	8.33520	W118	14	20.76853	1515.2357	-0.0242	0.0224	0.0000	1983.000	0.2326	0.6353	4.7917
tank____	sanga_net	N34	30	0.21537	W117	55	20.70144	974.7580	-0.0144	0.0191	0.0000	1983.000	0.8290	0.3811	2.0108
tom___sa	sanga_net	N34	37	51.79210	W117	53	55.05163	960.0292	-0.0111	0.0162	0.0000	1983.000	0 8730	0.4292	3.4393
allen___	carri_net	N35	11	6.88854	W120	5	6.02339	1115.2046	-0.0252	0.0304	0.0000	1983.000	0.0390	0.1921	2.9426
berros__	carri_net	N35	3	37.54265	W120	26	12.16836	516.1257	-0.0278	0.0336	0.0000	1983.000	0.6411	0.0674	4.9904
biddle__	carri_net	N35	9	40.45222	W120	28	29.91351	525.5343	-0.0273	0.0333	0.0000	1983.000	0.7079	0.1861	4.9917
calie_ca	carri_net	N35	2	10.93662	W119	45	37.08083	1522.1080	-0.0225	0.0288	0.0000	1983.000	0.2123	0.0989	0.9573
carrizo_	carri_net	N35	15	0.07093	W119	50	52.24985	561.4921	-0.0226	0.0283	0.0000	1983.000	0.1355	0.2650	2.1534
cauvel__	carri_net	N35	21	28.98992	W119	51	3.30419	1164.9491	-0.0192	0.0244	0.0000	1983.000	0.1404	0.1904	4.7372
crock_88	carri_net	N35	14	31.84919	W119	43	28.72277	1171.5273	-0.0192	0.0242	0.0000	1983.000	0.1844	0.2605	2.5056
crocker_	carri_net	N35	14	31.65193	W119	43	28.68514	1172.1354	-0.0192	0.0242	0.0000	1983.000	0.1844	0.2598	2.4999
glo_13__	carri_net	N35	26	28.36477	W119	39	14.21136	93.2105	-0.0118	0.0185	0.0000	1983.000	0.9873	0.9723	4.9936
gould___	carri_net	N35	24	49.05892	W119	45	58.51299	393.6905	-0.0143	0.0214	0.0000	1983.000	0.4476	0.7803	4.9924
hath_2__	carri_net	N35	10	56.17290	W120	14	8.94614	797.0462	-0.0262	0.0319	0.0000	1983.000	0.2878	0.2175	3.6243
kittncer	carri_net	N35	17	27.67382	W119	45	47.99317	1285.5180	-0.0183	0.0242	0.0000	1983.000	0.3411	0.6408	4.9919
madre_80	carri_net	N35	4	32.23361	W120	4	1.66672	958.0797	-0.0250	0.0306	0.0065	1983.000	0.0200	0.0200	0.0100
madreecc	carri_net	N35	4	32.24268	W120	4	1.65634	958.4841	-0.0250	0.0306	0.0065	1983.000	0.0203	0.0203	0.1684
mcktt_ca	carri_net	N35	17	26.52770	W119	45	50.37258	1287.0524	-0.0183	0.0242	0.0000	1983.000	0.2069	0.2627	2.2969
painted_	carri_net	N35	9	12.78211	W119	48	29.59607	584.5460	-0.0219	0.0307	0.0000	1983.000	0.1299	0.3407	3.9418
saltos__	carri_net	N35	8	0.17236	W119	54	7.04544	1070.6750	-0.0233	0.0303	0.0000	1983.000	0.2039	0.1462	4.0695
stanley2	carri_net	N35	4	22.60360	W120	15	4.74334	724.9126	-0.0267	0.0327	0.0000	1983.000	0.3239	0.0536	4.1218
sycamore	carri_net	N35	7	31.89316	W119	59	55.77911	856.8253	-0.0238	0.0310	0.0000	1983.000	0.0864	0.1018	3.2045
turkey__	carri_net	N35	15	40.46411	W119	57	19.19469	825.8122	-0.0236	0.0293	0.0000	1983.000	0.1178	0.2199	4.6663
welport_	carri_net	N35	21	31.69290	W119	40	53.80225	252.5701	-0.0099	0.0212	0.0000	1983.000	0.8242	0.5289	4.9913
airway__	sanlu_net	N35	19	30.36093	W120	36	17.88046	751.7595	-0.0278	0.0334	0.0000	1983.000	0.2034	0.1911	4.4303
almond__	sanlu_net	N35	33	6.36975	W120	27	11.12835	487.2419	-0.0239	0.0325	0.0000	1983.000	0.1578	0.2131	0.4961
barren__	sanlu_net	N35	27	20.45438	W120	34	23.40613	556.5579	-0.0254	0.0327	0.0000	1983.000	0.2433	0.2892	4.9929
bench___	sanlu_net	N35	44	44.32084	W120	21	4.70466	617.5007	-0.0198	0.0301	0.0000	1983.000	0.1345	0.1309	0.3015
blackhll	sanlu_net	N35	21	31.35894	W120	49	54.22538	166.4238	-0.0267	0.0355	0.0071	1983.000	0.0200	0.0200	0.0100
blhllres	sanlu_net	N35	21	30.83391	W120	49	54.07629	166.1144	-0.0264	0.0356	0.0071	1983.000	0.3012	0.2315	4.3400
bonnie__	sanlu_net	N35	52	39.51765	W120	15	49.83476	756.1034	-0.0095	0.0212	0.0000	1983.000	0.1396	0.1618	0.2836
break___	sanlu_net	N35	53	15.87064	W120	27	44.90664	562.7113	-0.0194	0.0330	0.0000	1983.000	0.2350	0.1840	0.4907
buck_ecc	sanlu_net	N35	55	29.89134	W120	32	14.76649	793.4792	-0.0192	0.0380	0.0000	1983.000	0.2497	0.3147	4.9935
buckhill	sanlu_net	N35	55	29.96787	W120	32	14.09124	789.5408	-0.0192	0.0380	0.0000	1983.000	0.2700	0.1637	0.4994
caliente	sanlu_net	N35	2	10.93662	W119	45	37.08083	1522.1080	-0.0225	0.0288	0.0000	1983.000	0.2123	0.0989	0.9573
car_____	sanlu_net	N35	53	17.24149	W120	25	50.06793	479.7071	-0.0187	0.0312	0.0000	1983.000	0.2590	0.3161	0.4942
car_rml_	sanlu_net	N35	53	18.70575	W120	25	47.98076	479.3405	-0.0269	0.0287	0.0000	1983.000	13.4921	14.2324	4.9938
car_rm2_	sanlu_net	N35	53	16.95060	W120	25	50.19710	479.3405	-0.0187	0.0312	0.0000	1983.000	18.3267	6.9574	4.9932
castle__	sanlu_net	N35	56	20.73621	W120	20	25.03502	1291.5605	0.0000	0.0000	0.0000	1993.000	18.6341	6.1132	4.9937
chi2_no1	sanlu_net	N35	23	33.10078	W120	21	7.71435	1070.5015	-0.0247	0.0319	0.0000	1983.000	18.6562	6.0493	4.9937
chiches2	sanlu_net	N35	23	33.32111	W120	21	7.27410	1070.2821	-0.0247	0.0319	0.0000	1983.000	0.1766	0.3383	4.9292
cholame_	sanlu_net	N35	58	16.41121	W120	34	54.79608	762.2697	-0.0199	0.0403	0.0000	1993.000	0.2747	0.2538	0.5369
cobra___	sanlu_net	N35	50	6.84484	W120	26	16.45064	701.8680	-0.0203	0.0320	0.0000	1993.000	0.1664	0.1896	3.7228
cotton__	sanlu_net	N35	47	15.90678	W120	13	20.85269	735.9345	-0.0121	0.0222	0.0000	1993.000	0.1499	0.1324	0.3513
davis___	sanlu_net	N35	13	58.42541	W120	47	3.99956	513.2179	-0.0285	0.0349	0.0000	1983.000	0.2157	0.1946	4.8070
flattop_	sanlu_net	N35	51	51.73209	W120	28	25.17848	758.3563	-0.0214	0.0331	0.0000	1993.000	0.2814	0.3064	4.8440
gastro__	sanlu_net	N36	0	2.91211	W120	28	39.94246	1164.6301	-0.0036	0.0268	0.0000	1993.000	0.2218	0.2771	1.1118
gifford_	sanlu_net	N35	8	57.80267	W120	3	15.40070	1007.3954	-0.0252	0.0304	0.0000	1993.000	0.4178	0.1369	4.0033
gold____	sanlu_net	N35	49	50.62846	W120	21	0.58404	472.5891	-0.0129	0.0241	0.0000	1993.000	0.1345	0.1427	0.1961
hatch___	sanlu_net	N35	41	9.29999	W120	10	40.85461	732.3205	-0.0161	0.0219	0.0000	1993.000	0.1681	0.1467	4.9937
hatchrml	sanlu_net	N35	41	9.75507	W120	10	41.01843	732.0159	-0.0161	0.0219	0.0000	1993.000	0.1656	0.1435	0.993
hearst__	sanlu_net	N35	45	20.21852	W120	16	3.81932	371.8614	-0.0133	0.0224	0.0000	1993.000	0.1938	0.3610	9.9500
hopp_rm3	sanlu_net	N35	40	26.69809	W120	22	53.36402	471.7205	-0.0339	0.0308	0.0000	1993.000	19.3021	40.3404	9.9504
hopper__	sanlu_net	N35	40	26.59321	W120	22	53.74809	471.4363	-0.0195	0.0319	0.0000	1993.000	0.1385	0.1477	0.3295
kenger__	sanlu_net	N35	54	49.46123	W120	20	49.99094	951.3886	-0.0089	0.0216	0.0000	1993.000	0.1344	0.1809	0.3015
kerr____	sanlu_net	N35	45	57.71263	W120	21	27.53516	552.8520	-0.0198	0.0301	0.0000	1993.000	0.1352	0.1307	0.3325
kitchen_	sanlu_net	N34	55	16.76401	W119	9	4.43015	1523.8605	0.0000	0.0000	0.0000	1993.000	19.6105	0.1466	4.9937
l_yeguas	sanlu_net	N35	26	27.90522	W119	57	24.37811	985.3105	0.0000	0.0000	0.0000	1993.000	16.0104	12.0467	4.9937
mason___	sanlu_net	N35	49	57.32600	W120	26	34.73120	711.9869	-0.0201	0.0332	0.0000	1993.000	0.1544	0.1432	0.3690
mcdonrm2	sanlu_net	N35	21	29.87968	W120	5	41.37832	708.9005	-0.0137	0.0784	0.0000	1993.000	5.3395	1.2277	4.9622
mckttrck	sanlu_net	N35	17	26.52770	W119	45	50.37258	1287.0524	-0.0183	0.0242	0.0000	1983.000	0.2069	0.2627	2.2969
mel_ecc_	sanlu_net	N35	52	12.78806	W120	22	29.39129	517.5957	-0.0162	0.0251	0.0000	1983.000	0.1375	0.1595	0.4500
melville	sanlu_net	N35	52	12.44325	W120	22	29.25871	518.1186	-0.0162	0.0251	0.0000	1993.000	0.3959	1702	9.9502
mid_e_sa	sanlu_net	N35	56	58.72126	W120	29	53.81628	749.3444	-0.0160	0.0264	0.0000	1992.800	0.1412	0.0421	0.0000
mid_f___	sanlu_net	N35	55	12.58428	W120	31	14.85516	661.3114	-0.0181	0.0346	0.0000	1993.000	0.4990	0.1960	4.9934
mine_mt_	sanlu_net	N35	58	9.81038	W120	26	5.60180	1069.4826	-0.0049	0.0231	0.0000	1983.000	0.2469	0.2529	0.4342
mine_rm2	sanlu_net	N35	58	9.79433	W120	26	5.35476	1065.7059	-0.0049	0.0231	0.0000	1983.000	0.2790	3.7440	4.9614
mith____	sanlu_net	N36	4	43.99012	W120	35	45.61473	1169.9022	-0.0027	0.0228	0.0000	1983.000	0.3150	0.4355	0.9998
montosa_	sanlu_net	N35	56	56.15735	W120	42	27.22983	587.9599	-0.0197	0.0417	0.0000	1983.000	0.4827	0.2503	0.9992
moose___	sanlu_net	N35	48	56.57241	W120	17	25.13828	534.6937	-0.0126	0.0221	0.0000	1983.000	0.1355	0.1382	0.2258
napoleon	sanlu_net	N35	30	12.55765	W119	57	33.53796	854.5505	0.0000	0.0000	0.0000	1983.000	18.1206	7.5017	4.9938
park____	sanlu_net	N35	53	43.97654	W120	18	21.82772	786.0270	-0.0088	0.0230	0.0000	1983.000	0.1341	0.1708	0.2547
pelato__	sanlu_net	N34	55	12.63994	W119	24	19.57132	1334.4679	-0.0201	0.0234	0.0000	1983.000	0.1761	0.1135	1.0
pfl_____	sanlu_net	N35	53	17.06149	W120	25	49.79463	480.0138	-0.0187	0.0312	0.0000	1983.000	0.156	0.1692	1
pitt____	sanlu_net	N35	55	28.69651	W120	28	36.01730	668.8587	-0.0216	0.0306	0.0000	1983.000	0.4530	0.5961	9
prospect	sanlu_net	N35	28	20.30440	W120	45	1.83441	632.3530	-0.0262	0.0359	0.0000	1983.000	0.2859	0.3267	4.9928
ranchito	sanlu_net	N35	54	0.78050	W120	31	29.93330	838.3905	0.0000	0.0000	0.0000	1983.000	14.2504	1.4669	4.9937
red_hill	sanlu_net	N35	36	17.82784	W120	15	38.13719	751.3333	-0.0211	0.0286	0.0000	1983.000	0.1402	0.1808	0.4267
shade___	sanlu_net	N36	1	46.93962	W120	40	56.90183	706.7221	-0.0195	0.0409	0.0000	1983.000	0.4384	0.3167	2.1497
simmler_	sanlu_net	N35	21	5.49087	W120	0	18.56551	578.1675	-0.0244	0.0278	0.0000	1983.000	0.3641	0.3138	3.4178
smithecc	sanlu_net	N36	4	43.42821	W120	35	45.22760	1173.2348	-0.0027	0.0228	0.0000	1983.000	0.3153	0.4081	3.3403
table___	sanlu_net	N35	56	10.77188	W120	24	32.01459	838.0615	-0.0084	0.0233	0.0000	1983.000	0.3736	0.3112	4.9932
temb_rml	sanlu_net	N35	6	45.42802	W119	33	17.31278	1050.2923	-0.0143	0.0223	0.0000	1983.000	1.8919	2.8944	3.4225
temblor_	sanlu_net	N35	6	46.02261	W119	33	18.03093	1052.6130	-0.0144	0.0231	0.0000	1983.000	0.1392	0.1204	0.1000
tess____	sanlu_net	N35	23	8.69911	W120	41	51.47182	807.3516	-0.0268	0.0351	0.0000	1983.000	0.1806	0.2397	3.6375

towers__	sanlu_net	N35	47	20.49570	W120	25	13.27121	671.9138	-0.0222	0.0326	0.0000	1983.000	0.1612	0.1660	4.8871
twis_rm2	sanlu_net	N35	29	15.72047	W120	1	5.31412	876.3548	-0.0195	0.0236	0.0000	1983.000	0.2432	0.2563	0.5000
twissel_	sanlu_net	N35	29	15.24037	W120	1	5.30391	877.1005	-0.0195	0.0236	0.0000	1983.000	1.5700	19.5520	4.9937
two_oaks	sanlu_net	N35	51	31.56240	W120	19	9.91966	524.9454	-0.0090	0.0201	0.0000	1983.000	0.1336	0.1533	0.2099
vill2rm2	sanlu_net	N35	28	3.03001	W121	0	22.44634	122.4205	-0.0284	0 0343	0.0000	1983.000	0.4819	0.3664	4.9936
villa_2_	sanlu_net	N35	28	3 37969	W121	0	22.69944	122.4210	-0.0284	0.0343	0.0000	1983.000	0.4820	0.3666	4.9936
wild____	sanlu_net	N35	45	47.84540	W120	28	8.97252	587.8591	-0.0211	0.0343	0.0000	1983.000	0.1639	0.1304	0.4840
almon_mo	monit_net	N35	33	6.36975	W120	27	11.12835	487.2419	-0.0239	0.0325	0.0000	1983.000	0.1578	0.2131	0.4961
beacon_2	monit_net	N33	55	25.57708	W116	37	0.79903	494.1899	0.0000	0.0000	0.0000	1983.000	14.1488	4.8885	19.6012
bm603_39	monit_net	N33	46	53.43491	W116	17	17.10492	11.2441	0.0000	0.0000	0.0000	1983.002	9.9000	17.0000	19.5000
bolt____	monit_net	N33	46	56.01886	W116	17	15.24092	12.4241	0.0000	0.0000	0.0000	1983.000	9.9000	17.0000	19.5000
bull__mo	monit_net	N34	49	6.06813	W118	33	12.05145	840.0742	-0.0133	0.0186	0.0000	1983.000	0.4324	0.2672	3.3789
cajon___	monit_net	N34	20	49.94303	W117	27	3.91896	1309.4025	0.0000	0.0000	0.0000	1992.800	0.0050	0.0050	0.0000
calie_mo	monit_net	N35	2	10.93662	W119	45	37.08083	1522.1080	-0.0225	0.0288	0.0000	1983.000	0.2123	0.0989	0.9573
car__mo	monit_net	N35	53	17.24149	W120	25	50.06793	479.7071	-0.0187	0.0312	0.0000	1983.000	0.2590	0.3161	0.4942
chola_mo	monit_net	N35	58	16.41121	W120	34	54.79608	762.2697	-0.0199	0.0403	0.0000	1983.000	0.2747	0.2538	0.5369
cotto_mo	monit_net	N35	47	15.90678	W120	13	20.85269	735.9345	-0.0121	0.0222	0.0000	1983.000	0.1499	0.1324	0.3513
edom_2__	monit_net	N33	52	13.51980	W116	25	51.98386	453.1565	-0.0139	0.0155	0.0000	1983.000	0.8679	1.0526	15.3614
gap_____	monit_net	N33	44	56.36615	W116	10	16.17828	32.1904	0.0000	0.0000	0.0000	1983.002	0.5000	0.5000	1.0000
gastr_mo	monit_net	N36	0	2.91211	W120	28	39.94246	1164.6301	-0.0036	0.0268	0.0000	1983.000	0.2218	0.2771	1.1118
lgo_70__	monit_net	N35	2	10.73410	W119	45	37.43825	1521.7460	-0.0225	0.0288	0.0000	1983.000	0.6555	2.9513	0.9999
litte_mo	monit_net	N34	48	2.26770	W118	48	9.63656	1412.5494	-0.0189	0.0192	0.0000	1983.000	0.6111	0.3275	0.9995
mid_ecc_	monit_net	N35	56	58.71502	W120	29	53.81744	749.3190	-0.0181	0.0346	0.0000	1983.000	0.2139	0.2502	0.4112
mine__mo	monit_net	N35	58	9.81038	W120	26	5.60180	1069.4826	-0.0049	0.0231	0.0000	1983.000	0.2469	0.2529	0.4342
park__mo	monit_net	N35	53	43.97654	W120	18	21.82772	786.0270	-0.0088	0.0230	0.0000	1983.000	0.1341	0.1708	0.2547
pattiway	monit_net	N34	57	35.04883	W119	25	56.43958	983.8125	-0.0180	0.0231	0.0000	1983.000	0.1965	0.1316	0.9001
red_h_mo	monit_net	N35	36	17.82784	W120	15	38.13719	751.3333	-0.0211	0.0286	0.0000	1983.000	0.1402	0.1808	0.4267
resort__	monit_net	N33	41	16.22738	W116	23	29.48837	188.1576	0.0000	0.0000	0.0000	1992.802	0.5000	0.5000	1.0000
salisbur	monit_net	N34	49	22.49898	W119	42	48.46660	1545.9185	-0.0268	0.0327	0.0000	1983.000	0.3929	0.0352	0.9999
sal_rm__	monit_net	N34	49	23.36478	W119	42	47.12138	1545.8605	-0.0268	0.0327	0.0000	1983.000	38.4783	22.7927	9.9503
saw_e_mo	monit_net	N34	41	35.33391	W118	33	41.25343	1648.1312	-0.0183	0.0208	0.0000	1983.000	0.1349	0.1000	0.4833
sawmi_mo	monit_net	N34	41	35.36000	W118	33	41.08153	1646.6605	-0.0182	0.0234	0.0000	1983.000	0.1347	0.1000	0.0000
tejon_41	monit_net	N34	48	13.08161	W118	48	56.01569	1450.3935	-0.0181	0.0206	0.0000	1983.000	0.2006	0.0822	2.6484
tram____	monit_net	N33	52	12.03733	W116	33	52.94809	173.7541	0.0000	0.0000	0.0000	1983.000	19.6000	0.6000	19.6000
view_2__	monit_net	N33	55	35.05737	W116	11	15.56683	1545.7990	0.0084	-0.0062	0.0000	1983.002	1.6000	0.7000	19.5000
whita_mo	monit_net	N34	34	3.37897	W118	44	34.16316	1221.9767	-0.0243	0.0211	0.0014	1983.000	0.4709	0.4484	3.5321
17______	mexic_net	N32	19	7.36525	W115	11	28.78539	-21.5440	-0.0149	0.0365	0.0000	1983.000	1.0996	1.5824	11.4889
24______	mexic_net	N32	20	3.83206	W115	18	21.95877	-22.3993	-0.0186	0.0328	0.0000	1983.000	1.1107	2.1024	19.5623
3_______	mexic_net	N32	23	21.13506	W115	11	44.04538	-18.9723	-0.0168	0.0406	0.0000	1983.000	1.0934	1.4833	11.3582
36______	mexic_net	N32	27	56.68392	W115	6	21.30806	-10.4459	0.0000	0.0000	0.0000	1983.000	18.9058	5.4450	19.6109
4_______	mexic_net	N32	26	14.33475	W115	16	28.36779	-25.2576	0.0000	0.0000	0.0000	1982.900	1.3106	1.5253	9.8182
8_______	mexic_net	N32	28	46.44733	W115	15	14.82809	-16.2459	0.0000	0.0000	0.0000	1983.000	11.7180	15.8023	19.6062
9_______	mexic_net	N32	27	13.48933	W115	11	33.56743	-14.2683	-0.0130	0.0317	0.0000	1983.000	1.1995	1.7068	44.7093
928_____	mexic_net	N32	12	15.88267	W115	39	49.84410	-26.8555	-0.0263	0.0320	0.0000	1983.000	0.8313	1.7546	9.7520
bnp10065	mexic_net	N32	25	45.21290	W115	15	54.97659	-21.2459	0.0000	0.0000	0.0000	1983.000	19.6116	19.6116	19.6116
carri_me	mexic_net	N32	49	30.77047	W116	0	54.49878	701.7696	-0.0268	0.0308	0.0000	1983.000	0.4426	0.8925	6.0612
centinel	mexic_net	N32	37	17.40960	W115	42	36.08916	743.3144	-0.0250	0.0343	-0.0004	1983.000	0.5241	1.1757	6.1394
cila_6__	mexic_net	N32	27	2.90914	W115	55	1.00690	1661.6177	-0.0270	0.0322	0.0000	1983.000	0.5300	1.4586	8.8136
david___	mexic_net	N32	13	20.12606	W115	25	38.00354	640.0622	-0.0250	0.0314	0.0000	1983.000	0.8092	1.7213	8.8540
diablo__	mexic_net	N32	18	31.27523	W115	52	23.16826	1488.7082	-0.0274	0.0320	0.0000	1983.000	0.5338	1.6570	13.2263
dixie_me	mexic_net	N32	47	27.55835	W115	47	45.57767	-36.6410	-0.0267	0.0319	0.0000	1983.000	0.4581	0.9291	6.1495
fierro__	mexic_net	N32	27	14.35180	W115	33	36.69983	809.1525	-0.0235	0.0329	0.0000	1983.000	0.6828	1.4153	8.9555
jacum_me	mexic_net	N32	41	52.07728	W116	9	52.05495	1345.7927	-0.0278	0.0325	0.0000	1983.000	0.5526	1.0640	10.1945
mayor___	mexic_net	N32	5	26.23844	W115	18	33.70314	923.7605	-0.0232	0.0309	0.0000	1983.000	0.9179	1.9110	15.2111
off_225m	mexic_net	N32	38	53.18203	W115	43	31.64183	81.0491	-0.0059	0.0169	0.0003	1983.000	0.4972	1.1288	5.9615
off_2_me	mexic_net	N32	37	56.67688	W115	55	57.24961	498.0631	-0.0270	0.0330	0.0000	1983.000	0.4274	1.1523	5.3514
prieto__	mexic_net	N32	25	5.76364	W115	18	26.95583	188.0666	-0.0196	0.0316	0.0000	1983.000	0.9619	1.4420	8.9259
puerta__	mexic_net	N32	22	39.03035	W115	27	22.81971	1058.1591	-0.0230	0.0319	0.0000	1983.000	0.7599	1.5289	6.7192
7-8-28__	anza__net	N33	32	1.14609	W117	43	48.85747	175.0786	0.0000	0.0000	0.0000	1967.426	11.8312	19.1518	0.0000
arling__	anza__net	N33	52	15.91418	W117	28	17.10731	530.2309	-0.0266	0.0266	0.0000	1983.000	0.4582	0.1076	12.4643
arling80	anza__net	N33	52	15.67492	W117	28	17.33416	530.4337	-0.0266	0.0266	0.0000	1983.000	0.4583	0.1076	12.4661
asbesrm1	anza__net	N33	37	39.67516	W116	27	32.87475	1567.8805	-0.0170	0.0205	0.0000	1983.000	1.1925	0.7370	7.0619
asbestos	anza__net	N33	37	39.42444	W116	27	33.04111	1572.1398	-0.0170	0.0205	0.0000	1983.000	9.4406	7.4517	16.0421
bachelor	anza__net	N33	36	19.61120	W117	3	44.38534	719.2156	-0.0266	0.0275	0.0000	1983.000	0.5181	0.4361	11.7824
bee_____	anza__net	N33	43	44.39257	W117	41	58.43490	507.7101	-0.0285	0.0281	0.0000	1983.000	0.0873	0.5007	4.9100
berdo_an	anza__net	N33	51	40.52367	W116	5	20.36316	1577.6169	-0.0079	0.0115	0.0000	1983.000	0.6062	0.8602	9.5720
black___	anza__net	N33	48	22.56058	W117	39	45.97021	794.7609	-0.0287	0.0275	0.0000	1983.000	0.1215	0.2145	3.0721
brink_an	anza__net	N34	0	49.62429	W117	8	21.13025	663.9043	-0.0216	0.0218	0.0000	1983.000	0.4647	0.4558	0.9976
brinkrma	anza__net	N34	0	49.29734	W117	8	19.97527	662.3584	-0.0006	0.0077	0.0000	1983.000	0.7577	0.8940	13.8333
coahuila	anza__net	N33	35	0.16606	W116	46	57.61770	1674.5843	0.0000	0.0000	0.0000	1983.000	17.8585	8.1802	19.6000
david_an	anza__net	N33	54	29.38891	W116	59	48.58947	910.8104	-0.0222	0.0221	0.0000	1983.000	0.5536	0.4499	12.3107
davis___	anza__net	N33	56	29.60497	W116	59	48.23438	898.6569	-0.0285	0.0349	0.0000	1983.000	8.7980	2.9988	70.1550
double__	anza__net	N33	43	26.12393	W117	7	23.59382	765.0032	-0.0261	0.0270	0.0000	1983.000	0.4792	0.3806	6.3147
elsinore	anza__net	N33	36	8.70462	W117	20	35.93141	1032.8638	-0.0282	0.0281	0.0000	1983.000	0.4398	0.5152	10.6425
eve_____	anza__net	N33	38	55.56498	W116	33	37.45588	2114.1003	-0.0176	0.0216	0.0010	1983.000	1.5605	0.9133	11.4774
eve_rm1_	anza__net	N33	38	55.50174	W116	33	37.50194	2116.7029	0.0000	0.0000	0.0000	1982.882	1.8787	2.2576	19.5424
gander__	anza__net	N33	57	22.11212	W117	6	51.48114	755.3225	-0.0235	0.0229	0.0000	1983.000	0.4775	0.4103	3.6169
hay_rm1_	anza__net	N33	40	55.43459	W116	27	38.15799	1126.9869	0.0000	0.0000	0.0000	1983.000	3.6437	44.7100	44.6065
haystack	anza__net	N33	40	54.41405	W116	27	37.98518	1127.4409	0.0000	0.0000	0.0000	1983.000	2.0064	19.6069	19.5603
ida_____	anza__net	N33	47	54.40246	W117	19	23.27089	808.2544	-0.0267	0.0263	0.0000	1983.000	0.4305	0.3678	12.0433
jason___	anza__net	N33	33	41.54072	W116	47	57.09115	1376.6506	-0.0248	0.0286	0.0000	1983.000	0.7155	0.7818	11.2037
jurup_an	anza__net	N34	1	56.46646	W117	26	33.96287	642.4252	0.0000	0.0000	0.0000	1982.999	0.4727	0.4994	0.9999
kitching	anza__net	N33	58	31.10829	W116	45	32.12235	1215.9169	0.0000	0.0000	0.0000	1983.002	0.0000	0.0000	0.0000
kitchrm2	anza__net	N33	58	31.10829	W116	45	32.12235	1211.3469	0.0000	0.0000	0.0000	1983.000	44.7213	44.7214	44.7214
laqui_an	anza__net	N33	42	14.54143	W116	18	45.67968	361.5385	-0.0142	0.0177	0.0000	1983.000	0.6364	0.7532	8.8085
lomancer	anza__net	N33	45	54.83638	W117	44	47.20368	367.1637	-0.0291	0.0275	0.0000	1983.000	0.0734	0.6306	10.6449
lomas___	anza__net	N33	45	54.76166	W117	44	47.83939	366.8923	-0.0291	0.0275	0.0000	1983.000	0.0736	0.6311	10.6720
lookout_	anza__net	N33	33	11.85937	W116	34	26.88115	1659.0607	-0.0199	0.0233	0.0002	1983.000	1.3794	0.7260	9.9819

martı_an	anza__net	N33	31	25.17296	W116	11	27.05689	174.5166	-0.0143	0.0191	0.0000	1983.000	0.4957	0.7469	8.0709
menifee_	anza__net	N33	43	5.67666	W117	13	43.56507	675.5441	-0.0270	0.0270	0.0000	1983.000	0.4532	0.3950	5.9409
micro___	anza__net	N33	52	27.53044	W117	11	28.19138	735.3603	-0.0260	0.0258	0.0000	1983.000	0.4547	0.3669	11.8795
microrml	anza__net	N33	52	27.29490	W117	11	27.80000	750.6413	-0.0260	0.0258	0.0000	1983.000	16.1684	11.1110	19.6115
moore___	anza__net	N33	42	50.52691	W117	13	25.35194	633.8399	-0.0270	0.0270	0.0000	1983.000	0.4617	0.4003	5.5305
moss____	anza__net	N33	27	16.77916	W116	41	57.08869	1691.4830	-0.0243	0.0282	0.0000	1983.000	0.8140	0.9282	16.2555
nelson__	anza__net	N33	49	22.77018	W117	4	14.54176	818.7602	-0.0251	0.0256	0.0000	1983.000	0.5032	0.3935	11.4267
niguel__	anza__net	N33	30	44.93827	W117	44	3.12804	279.5533	-0.0298	0.0309	0.0000	1983.000	0.0584	1.0480	10.4976
niguel_a	anza__net	N33	30	52.32339	W117	43	49.13396	264.1502	0.0000	0.0000	0.0000	1983.000	0.0628	1.0430	10.3660
pollycgs	anza__net	N33	41	16.53271	W116	55	35.37100	975.7916	-0.0256	0.0266	0.0000	1983.000	0.6102	0.3838	12.0366
pollydmg	anza__net	N33	41	16.19149	W116	55	35.44404	985.6069	-0.0256	0.0266	0.0000	1983.000	42.5292	13.9703	44.6814
ranger__	anza__net	N33	50	39.81959	W116	49	31.34687	1558.7196	-0.0198	0.0222	0.0000	1983.000	0.8092	0.6920	15.3972
road____	anza__net	N33	31	36.56151	W116	35	21.05348	1485.5569	0.0000	0.0000	0.0000	1983.000	44.7213	44.7214	44.7214
roundtop	anza__net	N33	31	27.09017	W116	54	38.15534	757.5660	-0.0260	0.0286	0.0000	1983.000	0.7350	0.6509	15.8009
san___an	anza__net	N33	42	41.75636	W117	31	59.72667	1695.9569	-0.0277	0.0289	0.0000	1983.000	2.9512	1.3498	44.1436
san_joaq	anza__net	N33	36	21.66973	W117	48	43.22220	343.8264	-0.0314	0.0304	0.0000	1983.000	0.2701	0.7457	9.0233
san_juan	anza__net	N33	54	49.54550	W117	44	17.24583	508.7473	-0.0278	0.0268	0.0002	1983.000	0.0498	0.0498	0.1000
santiago	anza__net	N33	42	37.98038	W117	32	3.11784	1700.4236	-0.0277	0.0289	0.0000	1983.000	0.2977	0.3890	0.9897
sheep_an	anza__net	N33	35	9.03977	W116	22	35.37631	1533.6569	0.0000	0.0000	0.0000	1983.000	38.2536	23.1797	44.7211
sier____	anza__net	N33	51	0.55692	W117	39	13.33651	893.8610	-0.0282	0.0275	0.0000	1983.000	0.1282	0.2309	4.3874
stubb_an	anza__net	N33	57	11.18945	W116	46	27.51112	894.8569	-0.0163	0.0049	0.0000	1983.000	4.4824	1.1046	31.5552
thom_cgs	anza__net	N33	37	16.82519	W116	40	58.03120	2031.1650	-0.0203	0.0242	0.0000	1983.000	1.0058	1.0034	15.2931
thom2asu	anza__net	N33	37	14.31260	W116	40	50.59013	2048.2469	-0.0203	0.0242	0.0000	1983.000	42.4911	14.1118	44.6733
thomasec	anza__net	N33	37	7.45132	W116	40	48.81831	2040.0469	-0.0203	0.0242	0.0000	1983.000	44.7213	44.7214	44.7214
thomecc2	anza__net	N33	37	14.36368	W116	40	50.78569	2050.1469	-0.0203	0.0242	0.0000	1983.000	42.4908	14.1124	44.6731
toro____	anza__net	N33	31	24.82421	W116	25	32.99043	2617.9271	-0.0190	0.0199	0.0003	1983.000	1.7781	0.8170	7.4362
toro_80_	anza__net	N33	31	24.82551	W116	25	32.98888	2617.9688	-0.0024	0.0007	0.0003	1983.000	19.6116	2.5711	19.4869
29_palms	joshu_net	N34	3	30.85252	W115	57	5.24174	1357.1830	-0.0052	0.0084	0.0000	1983.000	1.5573	0.8718	19.5899
beaco_jo	joshu_net	N33	55	25.57708	W116	37	0.79903	494.1899	0.0000	0.0000	0.0000	1983.000	14.1488	4.8885	19.6012
berdo_jo	joshu_net	N33	51	40.55881	W116	5	20.33033	1577.6169	-0.0079	0.0115	0.0000	1983.000	0.6062	0.8602	9.5720
creole__	joshu_net	N34	25	44.70369	W116	18	21.77680	1316.4556	-0.0083	0.0146	0.0000	1983.000	0.4031	1.0297	9.3146
creolrm1	joshu_net	N34	25	44.41606	W116	18	21.93814	1315.3689	0.0062	-0.0050	0.0000	1983.000	0.4028	1.0293	9.3135
creolrm2	joshu_net	N34	25	44.84757	W116	18	22.17192	1315.4187	0.0062	-0.0050	0.0000	1983.000	0.4027	1.0298	9.3173
creolrm3	joshu_net	N34	25	44.40945	W116	18	21.91345	1317.2659	0.0062	-0.0050	0.0000	1983.000	4.5855	3.9433	19.5332
dome____	joshu_net	N33	57	58.62884	W116	26	58.30997	585.5819	-0.0106	0.0156	0.0000	1983.000	1.5891	8.7470	19.6097
dome_ecc	joshu_net	N33	57	58.82263	W116	26	58.63459	583.9569	-0.0106	0.0156	0.0000	1983.000	1.6834	8.7521	44.6991
edom__jo	joshu_net	N33	52	13.51980	W116	25	51.98386	453.1565	-0.0139	0.0155	0.0000	1983.000	0.8679	1.0526	15.3614
insp_rm2	joshu_net	N33	56	8.10710	W116	11	43.12673	1664.3903	0.0084	-0.0062	0.0000	1983.000	18.6282	6.2933	19.5826
inspncer	joshu_net	N33	56	8.68389	W116	11	43.80460	1677.4028	-0.0079	0.0122	0.0000	1983.000	0.4892	0.9764	8.3447
keys____	joshu_net	N34	4	57.49099	W116	11	26.97478	1330.5187	-0.0061	0.0118	0.0000	1983.000	0.6677	0.5646	13.2275
laqui_jo	joshu_net	N33	42	14.54143	W116	18	45.67968	361.5385	-0.0142	0.0177	0.0000	1983.000	0.6364	0.7532	8.8085
mauma_jo	joshu_net	N34	25	8.61109	W116	27	30.11188	1232.5279	-0.0097	0.0131	0.0000	1983.000	0.5255	0.9907	11.4372
meeks___	joshu_net	N34	15	28.45705	W116	37	2.72757	1880.5352	-0.0102	0.0132	0.0000	1983.000	0.9928	0.8487	18.3081
mesquite	joshu_net	N34	11	35.77336	W116	6	48.32663	609.5764	-0.0047	0.0100	0.0000	1983.000	0.9166	0.4324	8.3449
pax_ncer	joshu_net	N34	9	11.22174	W116	23	23.34968	1127.4446	-0.0068	0.0138	0.0000	1983.000	0.3785	0.3845	0.9987
queen___	joshu_net	N34	3	9.49104	W116	5	49.51247	1694.1966	-0.0064	0.0099	0.0000	1983.000	1.0152	0.6862	14.3939
rich____	joshu_net	N34	15	50.75451	W116	28	7.96690	1276.3215	-0.0088	0.0142	0.0000	1983.000	0.5529	0.4706	6.5695
sandhill	joshu_net	N34	15	17.99092	W116	16	43.95406	833.1388	-0.0066	0.0148	0.0000	1983.000	0.3755	0.4155	0.9984
segreset	joshu_net	N34	18	52.75860	W116	4	44.93740	1028.4080	0.0096	-0.0079	0.0000	1983.000	1.2714	0.6418	13.8856
segundo_	joshu_net	N34	18	52.75883	W116	4	44.93738	1028.1835	-0.0025	0.0103	0.0000	1983.000	1.2728	0.6418	13.9302
stubbe__	joshu_net	N33	57	11.22046	W116	46	27.51632	894.8569	-0.0163	0.0049	0.0000	1983.000	4.4824	1.1046	31.5552
valmtecc	joshu_net	N34	13	5.74562	W115	58	8.95406	672.1009	-0.0040	0.0078	0.0000	1983.000	1.3885	0.3846	17.6503
warren__	joshu_net	N34	3	18.25815	W116	24	25.77798	1527.1370	-0.0079	0.0155	0.0000	1983.000	0.3811	0.6954	10.9344
alamo___	salto_net	N33	11	46.91194	W115	36	40.22378	-72.8375	-0.0082	0.0049	0.0000	1983.000	0.5824	0.5099	14.8055
beals___	salto_net	N33	21	16.65146	W115	21	29.89235	748.5412	-0.0035	0.0037	0.0000	1983.000	1.2865	0.7187	19.0933
berdoo__	salto_net	N33	51	40.55881	W116	5	20.33033	1577.6169	-0.0079	0.0115	0.0000	1983.000	0.6062	0.8602	9.5720
blbuvlbi	salto_net	N33	39	49.46633	W115	43	11.38318	485.6569	0.0000	0.0000	0.0000	1983.000	2.3941	2.8656	44.2567
bluff___	salto_net	N33	15	24.27507	W116	13	59.18833	362.1046	-0.0211	0.0265	0.0003	1983.000	0.6209	0.5022	6.4767
bluffres	salto_net	N33	15	24.27198	W116	13	59.18760	360.7130	-0.0211	0.0265	0.0003	1983.000	0.6211	0.5021	6.4661
bluffrm1	salto_net	N33	15	25.17957	W116	13	58.98167	359.3074	-0.0211	0.0265	0.0003	1983.000	0.6211	0.5020	6.4689
butte___	salto_net	N33	33	41.06371	W115	20	41.28449	1340.4277	-0.0035	0.0047	0.0000	1983.000	1.1949	0.8544	19.6036
carrizo_	salto_net	N32	49	30.77047	W116	0	54.49878	701.7696	-0.0226	0.0283	0.0000	1983.000	0.4426	0.8925	6.0612
coach___	salto_net	N33	26	42.89474	W115	39	22.07239	663.8995	-0.0060	0.0065	0.0000	1983.000	0.7100	0.6381	7.4649
coolidge	salto_net	N33	22	56.17818	W116	4	38.07997	652.6819	-0.0152	0.0193	0.0000	1983.000	0.4551	0.5795	7.3242
cottonwo	salto_net	N33	43	5.52576	W115	54	35.82897	1300.5255	-0.0063	0.0100	0.0000	1983.000	0.7043	1.3302	19.5302
cuyamaca	salto_net	N32	56	48.24979	W116	36	24.24881	1951.4914	0.0000	0.0000	0.0000	1983.000	3.0911	19.3888	19.6003
dixie___	salto_net	N32	47	27.55835	W115	47	45.57767	-36.6410	-0.0267	0.0319	0.0000	1983.000	0.4581	0.9291	6.1495
elephant	salto_net	N33	2	42.40424	W116	10	31.74216	1000.1433	-0.0254	0.0298	0.0003	1983.000	0.5074	0.6766	5.1562
fish____	salto_net	N32	58	54.39550	W115	58	50.74524	676.2472	-0.0254	0.0295	0.0000	1983.000	0.4349	0.7163	4.9837
frink___	salto_net	N33	21	37.10011	W115	38	49.16916	-85.5989	0.0000	0.0000	0.0000	1983.000	0.4915	0.4865	0.9999
frinkrm1	salto_net	N33	21	37.00149	W115	38	49.28217	-85.1377	0.0000	0.0000	0.0000	1983.000	15.3443	12.2226	19.6116
granite_	salto_net	N33	3	4.04912	W116	28	46.27907	1682.1796	-0.0267	0.0311	0.0001	1983.000	0.8154	0.7017	7.0324
jacumba_	salto_net	N32	41	52.07728	W116	9	52.05495	1345.7927	-0.0278	0.0325	0.0000	1983.000	0.5526	1.0640	10.1945
kane____	salto_net	N33	3	41.13981	W115	49	25.48262	7.7220	-0.0220	0.0245	0.0000	1983.000	0.4332	0.6220	6.1959
laquinta	salto_net	N33	42	14.54143	W116	18	45.67968	361.5385	-0.0142	0.0177	0.0000	1983.000	0.6364	0.7532	8.8085
martinez	salto_net	N33	31	25.17296	W116	11	27.05689	174.5166	-0.0143	0.0191	0.0000	1983.000	0.4957	0.7469	8.0709
mecca___	salto_net	N33	38	3.25937	W116	1	46.55768	479.0259	-0.0104	0.0139	0.0000	1983.000	0.4377	0.6766	11.6957
monu_res	salto_net	N32	53	32.52460	W116	25	14.33672	1879.6353	-0.0276	0.0321	-0.0064	1986.573	0.7256	0.9884	12.0354
obsidian	salto_net	N33	10	16.42733	W115	38	15.65288	-71.7596	0.0000	0.0000	0.0000	1983.000	13.1000	14.7007	2.0000
oco_rm1_	salto_net	N33	7	52.32674	W116	6	32.27763	104.7767	-0.0060	0.0088	0.0002	1983.000	0.5095	0.5577	3.7343
ocotillo	salto_net	N33	7	52.26759	W116	6	32.56174	105.3077	-0.0232	0.0267	0.0002	1983.000	0.5096	0.5577	3.7342
off_225_	salto_net	N32	38	53.18203	W115	43	31.64183	81.0491	-0.0250	0.0343	0.0003	1983.000	0.4972	1.1288	5.9615
off_229_	salto_net	N32	37	56.67688	W115	55	57.24961	498.0631	-0.0270	0.0330	0.0000	1983.000	0.4274	1.1523	5.3514
oldbeach	salto_net	N33	16	44.53534	W115	30	4.11555	-15.1996	-0.0053	0.0040	-0.0001	1983.000	0.6927	0.4805	8.3771
orocopia	salto_net	N33	34	8.65568	W115	46	47.28806	1137.9786	-0.0065	0.0086	0.0000	1983.000	0.9684	0.8619	12.5117
palm____	salto_net	N33	18	28.29139	W116	7	34.25420	790.3725	-0.0169	0.0206	0.0000	1983.000	0.4861	0.5424	6.1951
pt_101__	salto_net	N33	10	16.12410	W115	38	15.10583	-71.7558	0.0000	0.0000	0.0000	1983.000	12.9495	14.7408	19.6116
salton__	salto_net	N33	25	51.47342	W115	48	56.29714	2.5901	-0.0091	0.0118	0.0002	1983.000	0.4392	0.5157	7.8093

salva___	salto_net	N33	14	1.15601	W115	15	41.32205	594.0476	-0.0030	0.0029	0.0001	1983.000	1.0148	0.6815	17.4032
soda____	salto_net	N33	10	42.96416	W115	55	4.38765	31.9068	-0.0171	0.0215	0.0001	1983.000	0.4096	0.5212	5.0317
stage___	salto_net	N32	54	54.26926	W116	17	8.11664	824.8944	-0.0272	0.0311	0.0004	1983.000	0.6041	0.8009	8.4216
sup_____	salto_net	N32	57	17.65786	W115	49	30.74694	191.8180	-0.0253	0.0283	0.0001	1983.000	0.4424	0.7456	6.8293
volcan__	salto_net	N33	6	6.73003	W116	34	43.99499	1594.2916	-0.0259	0.0316	0.0000	1983.000	1.0083	0.6408	10.0317
volcan_2	salto_net	N33	6	6.73013	W116	34	43.99481	1594.3875	-0.0083	0.0107	0.0000	1983.000	1.0083	0.6408	10.0341
wilson__	salto_net	N33	10	38.22493	W116	26	1.39365	1363.8983	-0.0247	0.0298	0.0001	1983.000	0.7782	0.5624	6.2821
yak_____	salto_net	N33	6	8.57596	W116	16	39.00044	1081.2583	-0.0251	0.0285	0.0002	1983.000	0.5981	0.6180	4.7886

Table 4: VLBI/GPS sites used in this analysis

```
* frame: WGS84
*  u = V(east)  v = V(north)  w = V(up),  unit: m/year
*  uncertainty of coordinates: Sn = north, Se = east, Su = up,  unit: meter
*
*  site    full-name      latitude        longitude         height      u        v        w       epoch      Sn      Se      Su
 YUMA7894 glbk_sln     N32 56 20.89178 W114 12 11.30341     238.4184  0.0004  0.0002  0.0105 1987.353  0.0657  0.0647  0.0653
 BLKB7269 glbk_sln     N33 39 49.49969 W115 43 11.33474     489.3921 -0.0054  0.0010 -0.0031 1987.079  0.0658  0.0649  0.0654
 DEAD7267 glbk_sln     N34 15 17.99416 W116 16 43.97113     833.0976 -0.0040 -0.0002  0.0541 1987.642  0.0659  0.0651  0.0655
 MONP7274 glbk_sln     N32 53 30.35936 W116 25 22.14310    1838.7331 -0.0317  0.0253 -0.0064 1987.544  0.0657  0.0646  0.0653
 PINY_GPS glbk_sln     N33 36 33.29567 W116 27 31.68935    1235.5440 -0.0165  0.0212 -0.0018 1986.480  0.0636  0.0332  0.0102
 GOLDVENU glbk_sln     N35 14 51.72318 W116 47 41.60213    1062.8826 -0.0024  0.0082 -0.0081 1989.506  0 0658  0.0647  0.0653
 MOJA_GPS glbk_sln     N35 19 53.60277 W116 53 17.35055     904.5336 -0.0039  0.0077 -0.0032 1991.161  0.0619  0.0317  0.0075
 SIO1_GPS glbk_sln     N32 52  3.98589 W117 15  8.39604       7.5681 -0.0322  0.0299  0.0153 1991.876  0.0635  0.0327  0.0069
 SOLJ_GPS glbk_sln     N32 50 23.52199 W117 15  8.99042     215.4982 -0.0323  0.0285  0.0069 1988.170  0.0636  0.0331  0.0078
 NIGU_GPS glbk_sln     N33 30 52.32750 W117 43 49.05408     235.7494 -0.0314  0.0307  0.0011 1989.787  0.0628  0.0331  0.0072
 PEAR7254 glbk_sln     N34 30 43.67421 W117 55 20.61791     890.9723 -0.0150  0.0205 -0.0158 1986.877  0.0659  0.0651  0.0656
 JPLM_GPS glbk_sln     N34 12 17.35069 W118 10 23.59868     423.9774 -0.0270  0.0242  0.0126 1991.901  0.0620  0.0332  0.0067
 OVRO_GPS glbk_sln     N37 13 57.22076 W118 17 37.65250    1178.0603 -0.0058  0.0076 -0.0010 1989.908  0.0597  0.0323  0.0069
 PVER_GPS glbk_sln     N33 44 37.54758 W118 24 12.78565      69.4543 -0.0291  0.0301  0.0092 1990.778  0.0622  0.0337  0.0069
 BRSH_GPS glbk_sln     N33 24 25.25418 W118 24 17.47350     448.5902 -0.0307  0.0333  0.0088 1989.508  0.0625  0.0339  0.0072
 BLUF_GPS glbk_sln     N32 55 36.40844 W118 31  6.75401     297.3293 -0.0306  0.0359  0.0070 1989.313  0.0627  0.0343  0.0073
 SAFE_GPS glbk_sln     N34 19 49.57244 W118 36  4.85026    1102.9961 -0.0261  0.0255  0.0094 1991.498  0.0617  0.0337  0.0069
 LOVE_GPS glbk_sln     N34 29 46.75128 W118 40  7.17291     727.0558 -0.0248  0.0218  0.0068 1991.749  0.0615  0.0337  0.0070
 WHIT_GPS glbk_sln     N34 34  2.77603 W118 44 34.00343    1221.3702 -0.0121  0.0251  0.0009 1990.550  0.0615  0.0340  0.0076
 CATO_GPS glbk_sln     N34  5  8.92891 W118 47  8.75839     825.5900 -0.0291  0.0291  0.0014 1991.589  0.0618  0.0340  0.0070
 HAPY_GPS glbk_sln     N34 21 28.70043 W118 51  0.52712     669.0879 -0.0248  0.0296  0.0144 1991.762  0.0615  0.0340  0.0071
 HOPP_GPS glbk_sln     N34 28 39.80814 W118 51 55.96788    1344.9731 -0.0227  0.0236  0.0123 1991.881  0.0614  0.0339  0.0069
 SNPA_GPS glbk_sln     N34 23 16.33306 W118 59 55.65153     184.7995 -0.0272  0.0270  0.0062 1990.597  0.0614  0.0341  0.0069
 SNP2_GPS glbk_sln     N34 26 25.26217 W119  0 34.72668    1476.6934 -0.0242  0.0231 -0.0023 1992.127  0.0614  0.0341  0.0069
 SCLA_GPS glbk_sln     N34 19 32.44823 W119  2 21.12539     655.3611 -0.0264  0 0286  0.0195 1990.215  0.0615  0.0344  0.0076
 MPNS_GPS glbk_sln     N34 48 46.17029 W119  8 43.47866    2662.6006 -0.0223  0.0198  0.0233 1991.705  0.0610  0.0341  0.0071
 COTR_GPS glbk_sln     N34  7 12.68080 W119  9 14.39109     -34.0748 -0.0289  0.0340 -0.0271 1989.603  0.0616  0.0346  0.0078
 MUNS_GPS glbk_sln     N34 38  8.81283 W119 18  1.94763    2107.5871 -0.0280  0.0249  0.0044 1991.396  0.0611  0.0343  0.0070
 SOLI_GPS glbk_sln     N34 17 54.02647 W119 20 33.67371     -11.6259 -0.0292  0.0281  0.0046 1991.471  0.0613  0.0345  0.0069
 FIBR_GPS glbk_sln     N35 23 54.58928 W119 23 38.45561      54.7118 -0.0088  0.0127  0.0040 1989.906  0.0604  0.0341  0.0070
 TWIN_GPS glbk_sln     N33 13 54.29920 W119 28 44.25935     200.1605 -0.0324  0.0355 -0.0026 1989.613  0.0620  0.0352  0.0073
 YAM2_GPS glbk_sln     N34 51  9.16981 W119 29  3.89002     806.6027 -0.0280  0.0284  0.0010 1990.462  0.0608  0.0345  0.0072
 LACU_GPS glbk_sln     N34 29 39.87590 W119 42 50.01706    1164.8576 -0.0298  0.0301  0.0036 1991.061  0.0609  0.0348  0.0069
 CENT_GPS glbk_sln     N33 59 41.43538 W119 45 10.51788     389.5322 -0.0278  0.0342  0.0065 1989.853  0.0612  0.0351  0.0070
 MADC_GPS glbk_sln     N35  4 32.23428 W120  4  1.66736     958.0918 -0.0248  0.0306  0.0040 1990.801  0.0603  0.0349  0.0069
 GAVI_GPS glbk_sln     N34 30  6.52010 W120 11 55.65845     713.3918 -0.0323  0.0344 -0.0098 1989.950  0.0606  0.0354  0.0073
 ALAM_GPS glbk_sln     N34 47 54.60789 W120 15 24.47970     457.2234 -0.0312  0.0347  0.0282 1991.478  0.0604  0.0353  0.0069
 POZO_GPS glbk_sln     N35 20 45.59111 W120 17 55.29107     728.6537 -0.0242  0.0316  0.0144 1989.899  0.0600  0.0352  0.0072
 GRAS_GPS glbk_sln     N34 43 50.04385 W120 24 50.64455     331.1783 -0.0286  0 0369  0.0165 1991.231  0.0603  0.0354  0.0069
 LOSP_GPS glbk_sln     N34 53 37.47457 W120 36 22.28021     463.1409 -0.0279  0.0347  0.0050 1990.706  0.0601  0.0356  0.0069
 VNDN_GPS glbk_sln     N34 33 22.55601 W120 36 58.31329     -11.4871 -0.0302  0.0363  0.0030 1991.399  0.0603  0.0357  0.0068
 BLHL_GPS glbk_sln     N35 21 31.36183 W120 49 54.22078     166.4970 -0.0264  0.0357  0.0068 1989.712  0.0596  0.0356  0.0070
 BLAN_GPS glbk_sln     N35 39 52.44917 W121 17  4.04932     -24.8115 -0.0246  0.0359 -0.0089 1989.960  0.0591  0.0360  0.0071
```

Table 5: USGS trilateration subnetworks

subnetwork	site[a]	min. vel. direction	scatters
San Gabriel - Tehachapi	52	N25°E	5.70 mm, 0.17 ppm
Los Padres - Tehachapi	35	N30°E	4.23 mm, 0.20 ppm
Carrizo - San Luis	26	N50°E	3.07 mm, 0.22 ppm
San Luis - Parkfield	67	N50°E	4.84 mm, 0.25 ppm
Salton - Mexicali	63	N50°E	3.35 mm, 0.22 ppm
Anza - Joshua	83	N50°E	3.64 mm, 0.22 ppm

a. Some sites are used by two subnetworks. The total number of sites is 323

Table 6: imposed constraints for minimum constrained solutions

section	constraint	function
southern	V(Mecca) = 0	control section translation
	V(Salva) towards N135°E	control section rotation
northern	V(Pattiway) = 0	control section translation
	V(Tank) towards N115°E	control section rotation
	V(Red hill) towards N40°W	remedy connection defect between San Luis and Carrizo subnetworks
	V(Gifford) = V(Allen)	stabilize Carrizo subnetwork

Table 7: Velocity constraints

VG site	EDM site	distance	final status
DEAD7267	Sandhill	0 km	used
NIGU_GPS	Niguel	0.43 km	used
PINY_GPS	Asbestos	2.07 km	used
MONP7274	Monu_res	0.22 km	not used
BLHL_GPS	Blhllres	0.02 km	used
SAFE_GPS	Piconcer	0.03 km	used
MPNS_GPS	Mt_pinos	0 km	used
SNP2_GPS	Santapau	0 km	not used
JPLM_GPS	Jpl1_rm1	0.21 km	not used
PEAR7254	Tank	1.34 km	used
WHIT_GPS	whitaker	0.02 km	not used
MUNS_GPS	Reyes	1.83 km	used

Table 8a: Compatibility test: formal uncertaities of VG solution scaled by a factor of 2

```
**********************************************************************************************
*          Compatibility test:  using VG final combined sites, 2 sigma scaling
**********************************************************************************************
* dif. between: ../net_mid/solvem_scum.map.2sig and solvem_comb.map.2sig  time: 1993/ 6/19    9:11:10
*
*  symbol ! means failed to pass compatibility criterion (95 % confidence level)
*     lon            lat            dVe            dVn          Cve       Cvn      corr      site
   245.79686014   32.93913660    0.00136413     0.02452755    0.010     0.060    0.0002   YUMA7894
   244.28018503   33.66374988   -0.01315690     0.01159851    0.010     0.010    0.0001   BLKB7269
!  243.72111933   34.25499839    0.45676708   -14.35719731    1.874     4.865    0.4458   DEAD7267
   243.57718401   32.89176545   -0.00700461     0.00997472    0.010     0.075    0.0009   MONP7274
!  243.54119793   33.60924826    0.29972965     0.56813894    0.329     0.210   -0.2082   PINY_GPS
   243.20511069   35.24770040   -0.00629703     0.00881368    0.010     0.059    0.0000   GOLDVENU
   243.11184743   35.33155577   -0.00265779     0.01103823    0.010     0.068    0.0118   MOJA_GPS
!  242.74767081   32.86777149    0.12466139     0.34017860    0.158     0.112   -0.0327   SIO1_GPS
   242.74750448   32.83986590   -0.62119023    -0.05496714    0.351     0.082    0.2946   SOLJ_GPS
   242.26970952   33.51453355   -0.93363227    -0.09740505    0.558     0.090    0.3535   NIGU_GPS
   242.07760677   34.51213101   -0.35341706     0.94341074    1.139     1.503    0.1356   PEAR7254
!  241.82678075   34.20481771    0.02744370     0.23830264    0.066     0.087    0.1238   JPLM_GPS
   241.70620810   37.23256085    0.00185869     0.00768912    0.032     0.058    0.5619   OVRO_GPS
   241.59645089   33.74376112   -0.15998870    -0.00620707    0.099     0.065    0.1891   PVER_GPS
   241.59514843   33.40701310   -0.23408981    -0.02840351    0.145     0.059    0.3541   BRSH_GPS
   241.48145932   32.92677808   -0.28616706    -0.02482963    0.173     0.074    0.3831   BLUF_GPS
   241.39865512   34.33043485   -0.27162688     0.09311457    0.258     0.151   -0.1215   SAFE_GPS
   241.33134321   34.49631810   -0.15725304    -0.05568800    0.154     0.087    0.0174   LOVE_GPS
!  241.25722227   34.56743609   -0.05806882     0.04037959    0.099     0.010    0.0002   WHIT_GPS
   241.21423648   34.08581136   -0.10485400     0.02804152    0.125     0.087    0.1354   CATO_GPS
   241.14985593   34.35797001   -0.07133113     0.03383853    0.126     0.064   -0.0114   HAPY_GPS
   241.13445555   34.47772261   -0.06852287     0.03997701    0.123     0.085    0.0217   HOPP_GPS
   241.00121016   34.38786845   -0.07769973     0.02264104    0.088     0.092    0.1770   SNPA_GPS
   240.99035625   34.44034866   -0.06183294     0.03334909    0.133     0.079    0.0035   SNP2_GPS
   240.96080051   34.32567828   -0.00853319     0.11668614    0.166     0.089    0.0079   SCLA_GPS
   240.85459139   34.81282355   -0.53368052    -1.89414712    1.084     0.972    0.0442   MPNS_GPS
   240.84600455   34.12018709   -0.01927014     0.04762380    0.075     0.079    0.2635   COTR_GPS
   240.69946154   34.63577947    0.11105169     0.39055221    0.376     0.289   -0.2492   MUNS_GPS
   240.65731550   34.29833854   -0.07910686    -0.01003713    0.071     0.083    0.4248   SOLI_GPS
   240.60598525   35.39849624    0.01268432    -0.00574471    0.088     0.052    0.2558   FIBR_GPS
   240.52104141   33.23174766   -0.22896639    -0.01672173    0.128     0.078    0.2807   TWIN_GPS
   240.51558838   34.85254527    0.08541753     0.16629373    0.389     0.118   -0.1298   YAM2_GPS
   240.28610896   34.49440779   -0.04608349     0.00924951    0.051     0.067    0.6352   LACU_GPS
   240.24708046   33.99484105   -0.08073921     0.00144013    0.071     0.073    0.3680   CENT_GPS
   239.93287233   35.07561848    0.08124144    -0.02023866    0.183     0.101   -0.2460   MADC_GPS
   239.80120849   34.50180898   -0.03119595     0.01093596    0.053     0.065    0.3211   GAVI_GPS
   239.74320302   34.79849954   -0.01240376     0.00230387    0.010     0.066    0.0012   ALAM_GPS
   239.70130990   35.34599556   -0.00357143     0.01445015    0.048     0.053    0.5409   POZO_GPS
   239.58593468   34.73056499   -0.00905166     0.00600201    0.039     0.064    0.6166   GRAS_GPS
   239.39381344   34.89374052   -0.00955126     0.00769894    0.037     0.047    0.5056   LOSP_GPS
   239.38380469   34.55626281   -0.00583750     0.01671035    0.027     0.073    1.0641   VNDN_GPS
   239.16827399   35.35870946    0.03555383     0.01247149    0.115     0.080    0.4527   BLHL_GPS
   238.71554378   35.66456696    0.06122698     0.02540618    0.050     0.059    0.3777   BLAN_GPS
```

Table 8b: Compatibility test: formal uncertaities of VG solution scaled by a factor of 3

```
*****************************************************************************************************
*           Compatibility test:  using VG final combined sites, 3 sigma scaling
*****************************************************************************************************
* dif. between: solvem_scum.map and solvem_comb.map  time: 1993/ 6/18   10:38: 8
*
*  symbol ! means failed to pass compatibility criterion (95 % confidence level)
*     lon           lat           dVe          dVn          Cve       Cvn      corr      site
   245.79686014   32.93913660   0.00110082   0.04783318   0.010     0.128    0.0002   YUMA7894
   244.28018503   33.66374988  -0.01423932   0.03626075   0.010     0.115    0.0001   BLKB7269
   243.72111933   34.25499839   2.57709513 -14.92675860   3.493     7.405    0.3441   DEAD7267
   243.57718401   32.89176545  -0.00925721   0.02890729   0.046     0.106    0.3424   MONP7274
   243.54119793   33.60924826   0.44382895   0.72407307   0.622     0.349   -0.1914   PINY_GPS
   243.20511069   35.24770040  -0.01169488   0.02355854   0.010     0.072    0.0000   GOLDVENU
   243.11184743   35.33155577  -0.00284685   0.03034332   0.026     0.105    0.9018   MOJA_GPS
   242.74767081   32.86777149   0.17561412   0.44715790   0.306     0.185   -0.0492   SIO1_GPS
   242.74750448   32.83986590  -1.04459018  -0.07692382   0.668     0.143    0.2982   SOLJ_GPS
   242.26970952   33.51453355  -1.55243931  -0.14888767   1.048     0.164    0.3662   NIGU_GPS
   242.07760677   34.51213101  -0.59677372   1.32770323   1.932     2.655    0.0898   PEAR7254
   241.82678075   34.20481771   0.03755696   0.31948650   0.115     0.150    0.1054   JPLM_GPS
   241.70620810   37.23256085   0.00716116   0.01687425   0.055     0.091    0.5763   OVRO_GPS
   241.59645089   33.74376112  -0.27230285  -0.00086074   0.176     0.113    0.1705   PVER_GPS
   241.59514843   33.40701310  -0.39212608  -0.03529394   0.266     0.103    0.3356   BRSH_GPS
   241.48145932   32.92677808  -0.47673354  -0.02852606   0.317     0.128    0.3683   BLUF_GPS
   241.39865512   34.33043485  -0.49641544   0.21086890   0.463     0.295   -0.2375   SAFE_GPS
   241.33134321   34.49631810  -0.25995412  -0.02756850   0.272     0.141   -0.0483   LOVE_GPS
   241.25722227   34.56743609  -0.12751644   0.07081243   0.210     0.125   -0.0854   WHIT_GPS
   241.21423648   34.08581136  -0.20485314   0.05775850   0.228     0.142    0.0614   CATO_GPS
   241.14985593   34.35797001  -0.15432592   0.05655611   0.227     0.125   -0.1042   HAPY_GPS
   241.13445555   34.47772261  -0.15316821   0.06726543   0.236     0.139   -0.0741   HOPP_GPS
   241.00121016   34.38786845  -0.14941471   0.04121216   0.159     0.154    0.1368   SNPA_GPS
   240.99035625   34.44034866  -0.13929515   0.05770642   0.247     0.157   -0.1161   SNP2_GPS
   240.96080051   34.32567828  -0.07261411   0.13980394   0.288     0.172   -0.1224   SCLA_GPS
   240.85459139   34.81282355  -0.56636179  -2.05712972   1.725     1.534   -0.0090   MPNS_GPS
   240.84600455   34.12018709  -0.03382335   0.06308288   0.130     0.138    0.2363   COTR_GPS
   240.69946154   34.63577947   0.03599830   0.40834621   0.685     0.507   -0.3795   MUNS_GPS
   240.65731550   34.29833854  -0.12692127   0.01022904   0.134     0.129    0.3762   SOLI_GPS
   240.60598525   35.39849624   0.05412186  -0.00156087   0.187     0.110    0.2489   FIBR_GPS
   240.52104141   33.23174766  -0.37961713  -0.01427152   0.243     0.135    0.2550   TWIN_GPS
   240.51558838   34.85254527  -0.04306524   0.20396856   0.662     0.214   -0.2316   YAM2_GPS
   240.28610896   34.49440779  -0.07326673   0.02745191   0.099     0.123    0.4817   LACU_GPS
   240.24708046   33.99484105  -0.12629734   0.01161305   0.124     0.127    0.3309   CENT_GPS
   239.93287233   35.07561848   0.19091242  -0.02636650   0.365     0.186   -0.2492   MADC_GPS
   239.80120849   34.50180898  -0.04346573   0.03291356   0.064     0.125    0.3208   GAVI_GPS
   239.74320302   34.79849954  -0.01514391   0.02141486   0.058     0.127    0.5712   ALAM_GPS
   239.70130990   35.34599556   0.00567670   0.02951935   0.083     0.103    0.4656   P[illegible]
   239.58593468   34.73056499  -0.00773401   0.02124843   0.068     0.101    0.6476   GRAS[illegible]
   239.39381344   34.89374052  -0.00298646   0.02103266   0.078     0.081    0.3805   LOSP_GPS
   239.38380469   34.55626281  -0.00369599   0.03898145   0.058     0.126    0.8062   VNDN_GPS
   239.16827399   35.35870946   0.07398258   0.02387236   0.243     0.139    0.4297   BLHL_GPS
   238.71554378   35.66456696   0.12775462   0.05067990   0.137     0.103    0.2276   BLAN_GPS
```

Table 8c: Compatibility test: add constraint on site SNP2 with scaling factor of 3

```
**********************************************************************************************
*          Compatibility test:  using VG final combined sites + SNP2, 3 sigma scaling
**********************************************************************************************
* dif. between: solvem_scum.map and ../comb/solvem_comb.map.snp2  time: 1993/ 6/18   18:56:46
*
*  symbol ! means failed to pass compatibility criterion (95 % confidence level)
*     lon           lat           dVe           dVn          Cve      Cvn      corr      site
   245.79686014  32.93913660   0.00062210   0.04638422   0.010    0.128    0.0002   YUMA7894
   244.28018503  33.66374988  -0.01679431   0.03640911   0.010    0.115    0.0001   BLKB7269
   243.72111933  34.25499839   2.57623295 -14.93775455   3.493    7.405    0.3441   DEAD7267
   243.57718401  32.89176545  -0.01086821   0.02956983   0.046    0.106    0.3424   MONP7274
   243.54119793  33.60924826   0.44445764   0.71270209   0.622    0.349   -0.1906   PINY_GPS
   243.20511069  35.24770040  -0.01186425   0.02188190   0.010    0.072    0.0000   GOLDVENU
   243.11184743  35.33155577  -0.00252674   0.02949113   0.026    0.110    0.8924   MOJA_GPS
   242.74767081  32.86777149   0.18070759   0.42883385   0.306    0.185   -0.0492   SIO1_GPS
   242.74750448  32.83986590  -1.05818341  -0.10910137   0.668    0.143    0.2982   SOLJ_GPS
   242.26970952  33.51453355  -1.56120081  -0.16316473   1.048    0.164    0.3662   NIGU_GPS
   242.07760677  34.51213101  -0.68450200   1.39049791   1.933    2.655    0.0897   PEAR7254
   241.82678075  34.20481771   0.03297855   0.30765412   0.115    0.150    0.1188   JPLM_GPS
   241.70620810  37.23256085   0.00573141   0.03056316   0.055    0.091    0.5889   OVRO_GPS
   241.59645089  33.74376112  -0.29150033  -0.01424201   0.176    0.113    0.1777   PVER_GPS
   241.59514843  33.40701310  -0.40689957  -0.04980978   0.266    0.103    0.3356   BRSH_GPS
   241.48145932  32.92677808  -0.49282079  -0.04595694   0.317    0.128    0.3745   BLUF_GPS
   241.39865512  34.33043485  -0.54412173   0.08908248   0.465    0.298   -0.2268   SAFE_GPS
   241.33134321  34.49631810  -0.30436696  -0.07761282   0.272    0.141   -0.0365   LOVE_GPS
   241.25722227  34.56743609   0.24790731  -0.07170299   0.243    0.177   -0.2767   WHIT_GPS
   241.21423648  34.08581136  -0.23940957   0.00967397   0.228    0.142    0.0748   CATO_GPS
   241.14985593  34.35797001   0.56825584  -0.12866179   0.355    0.148   -0.4187   HAPY_GPS
   241.13445555  34.47772261   0.03986010  -0.02630640   0.246    0.147   -0.1409   HOPP_GPS
   241.00121016  34.38786845  -0.20397400   0.02924975   0.159    0.160    0.1335   SNPA_GPS
!  240.99035625  34.44034866   3.31178821  -1.16591662   1.308    0.495   -0.9223   SNP2_GPS
   240.96080051  34.32567828   1.43123129  -0.20789753   0.637    0.218   -0.6096   SCLA_GPS
   240.85459139  34.81282355  -1.09346625  -2.02486192   1.736    1.534   -0.0097   MPWS_GPS
   240.84600455  34.12018709  -0.03237065   0.06869857   0.130    0.138    0.2363   COTR_GPS
   240.69946154  34.63577947  -0.97691006   0.73009727   0.781    0.521   -0.4340   MUNS_GPS
   240.65731550  34.29833854  -0.15482160  -0.01342988   0.134    0.137    0.3743   SOLI_GPS
   240.60598525  35.39849624   0.03997369   0.01125985   0.187    0.110    0.2489   FIBR_GPS
   240.52104141  33.23174766  -0.39738183  -0.02148697   0.243    0.135    0.2550   TWIN_GPS
   240.51558838  34.85254527  -0.47665767   0.25139274   0.678    0.214   -0.2417   YAM2_GPS
   240.28610896  34.49440779  -0.09003169   0.02136957   0.099    0.123    0.5017   LACU_GPS
   240.24708046  33.99484105  -0.14598127   0.01043949   0.124    0.127    0.3390   CENT_GPS
   239.93287233  35.07561848   0.17639476   0.06861393   0.365    0.191   -0.2433   MADC_GPS
   239.80120849  34.50180898  -0.05299823   0.03557993   0.064    0.125    0.3609   GAVI_GPS
   239.74320302  34.79849954  -0.02052562   0.01754592   0.058    0.127    0.5712   ALAM_GPS
   239.70130990  35.34599556  -0.01205101   0.04022318   0.083    0.103    0.4656   POZO_GPS
   239.58593468  34.73056499  -0.01742585   0.01944794   0.068    0.101    0.6817   GRAS_GPS
   239.39381344  34.89374052  -0.01451327   0.02660506   0.078    0.090    0.3595   LOSP_GPS
   239.38380469  34.55626281  -0.00831644   0.04127723   0.058    0.131    0.7991   VNDN_GPS
   239.16827399  35.35870946   0.04858753   0.04153991   0.243    0.139    0.4332   BLHL_GPS
   238.71554378  35.66456696   0.11046139   0.07797983   0.137    0.103    0.2276   BLAN_GPS
```